The regulatory function of Hsp90 and its cochaperone in DNA double strand break repair pathway

 $\mathbf{B}\mathbf{y}$

Nupur Fangaria

(16LTPH11)

Under the supervision of

Dr. Sunanda Bhattacharyya





Department of Biotechnology and Bioinformatics

School of Life Sciences

University of Hyderabad

Gachibowli

Hyderabad: 500046

Telangana, India

December 2022





University of Hyderabad

School of Life Sciences

Department of Biotechnology and Bioinformatics

DECLARATION

I, Nupur Fangaria, hereby declare that this thesis entitled, "The regulatory function of Hsp90 and its cochaperone in DNA double strand break repair pathway" submitted by me under the guidance and supervision of Dr. Sunanda Bhattacharyya, is an original and independent research work. I also declare that it has not been submitted previously in part or in full to this University or any other University or Institution for the award of any degree or diploma.

Dr. Sunanda Bhattacharyya (Research Supervisor)

Dr. SUNANDA BHATTACHARYYA
Associate Professor
Dept. of Biotechnology & Bioinformatics
School of Life Sciences
University of Hyderabad
Gachibowli, Hyderabad-500 046.

Nupur Fangaria (16LTPH11) (Research Scholar)





University of Hyderabad

School of Life Sciences

Department of Biotechnology and Bioinformatics

CERTIFICATE

This is to certify that this thesis entitled, "The regulatory function of Hsp90 and its cochaperone in DNA double strand break repair pathway" is a record of bona fide work done by Nupur Fangaria, a research scholar for the Ph.D. program in Department of Biotechnology and Bioinformatics, School of Life Sciences, University of Hyderabad under my guidance and supervision. The thesis is free from plagiarism and has not been submitted previously in part or in full to this or any other University or Institution for the award of any degree or diploma.

- **A.** Part of this thesis has been published in the following journals:
- Suhane, T., Bindumadhavan, V., Fangaria, N., Nair, A. S., Tabassum, W., Muley, P., Bhattacharyya, M. K., and Bhattacharyya, S. (2019) Glu-108 in Saccharomyces cerevisiae Rad51 Is Critical for DNA Damage-Induced Nuclear Function. *mSphere*. 10.1128/mSphere.00082-19

2. Fangaria, N., Rani, K., Singh, P., Dey, S., Kumar, K. A., and Bhattacharyya, S., (2022) DNA damage induced nuclear import of HSP90α is promoted by Aha1. *MBoC*. 10.1091/mbc.E21-11-0554

B. Part of the work has been presented in the following conferences:

1. 10th Conference on Yeast Biology (CYB), 2018. Held at Jawaharlal Nehru University.
 Poster presentation.

2. Bioquest, 2019. Held at University of Hyderabad. Poster presentation.

3. BioAnveshana, 2022. Held at University of Hyderabad. Oral presentation.

C. Publications from other projects:

Singh, P., Tabassum, W., Fangaria, N., Dey, S., Padhi, S., Bhattacharyya, M. K., Kumar, K. A., Roy, A., and Bhattacharyya, S., Plasmodium Topoisomerase VIB and Spo11 constitute functional type IIB topoisomerase in malaria parasite and its possible role in mitochondrial DNA segregation. (MS submitted)

In - change Head of Department (DOBB)

Growaled

HEAD
Dept. of Biotechnology & Bioinformatics
University of Hyderabad
Hyderabad.

Dr. SUNANDASBPATTACHARYYA

Associate Professor
Dept. of Biotechnology & Bioinformatics
School of Life Sciences
University of Hyderabad
Gachibowli, Hyderabad-500 046.

Dean

(School of Life Science)

School of Life Sciences University of Hyderabad Hyderabad-500 046.

Dean 15/5/2011

Dedicated to my loved ones

ACKNOWLEDGEMENTS

I would like to extend my sincere gratitude to my supervisor, **Dr. Sunanda Bhattacharyya** for her guidance, support, and encouragement during the course of my PhD.

I offer my sincere thanks to my doctoral committee members, **Prof. Mrinal Bhattacharyya** and **Dr. Vaibhav Vindal** for their valuable inputs.

I offer my sincere thanks to the present and former Heads of Dept. of Biotechnology & Bioinformatics, Prof. J.S.S. Prakash, Prof. K.P.M.S.V Padmasree, Prof. Anand Kondapi and Prof. Niyaz Ahmed for allowing me to use all research facilities available in the department during my work.

I am thankful to the present and former Deans of the School of Life sciences, **Prof. N. Siva Kumar,Prof. S. Dayananda**, **Prof. K.V.A Ramaiah**, **Prof. P. Reddanna**, for providing the necessary facilities in SLS during my work.

I would like to extend special thanks to **Prof. Kota Arun Kumar** and **Sandeep Dey** for their help and support during a critical time of publication of my manuscript.

I thank all the teaching and non-teaching staff of Biotechnology department and life sciences for their extended help during my work.

I would like to thank **Mr. Ramesh** for his help in the lab.

I would like to thank **CSIR** for providing me Fellowship during my work.

Sincere thanks to the funding bodies ICMR, DBT, DST, UGC SAP, DST FIST, and DBT Builder for providing funds to our lab during my work.

I thank the Bhattacharyya laboratories family including all my present and former lab mates from the lab of Dr. Sunanda Bhattacharyya and Prof. Mrinal K. Bhattacharyya for their help, support, and encouragement throughout my PhD journey.

I thank all my friends from HCU, Capstone Church and my friends back at home for brightening up my PhD journey.

I am grateful to my parents, **Mr. Pawan Fangaria** Mrs. **SmitaFangaria**; my sister, **ManyaFangaria**; and my husband, **Mr. ChukhuMuj** for their unconditional love and support.

Finally I thank **God Almighty** with all my heart, whose blessings gave me the strength to complete this journey.

Nupur Fangaría

Table of Contents

INTRODUCTION1		18
1.1 Hs _l	p90 among other molecular chaperones	18
1.2 Hs _l	p90 structure	19
1.2.1	N-Terminal domain (NTD)	21
1.2.2	Charged Linker Region (CL)	21
1.2.3	Middle Domain (MD)	22
1.2.4	C-Terminal Domain (CTD)	22
1.2.5	Hsp90 isoforms	22
1.3 Hs ₁	p90 Chaperone cycle	23
1.4 Hs _]	p90 Co-chaperones	26
1.4.1	Remodelling co-chaperones	26
1.4.2	Client recruiter co-chaperones	26
1.4.3	Late acting co-chaperones	27
1.4.4	Co-chaperones with a TPR motif	27
1.5 Hs _l	p90 co-chaperones: functions other than the Hsp90 chaperone cycle	27
1.6 The	e cellular roles of Aha1, Sba1 and Cdc37	28
1.6.1	The unique relationship between Aha1 and Hsp90 conformational dynamics	28
1.6.2	Cdc37: linkng Hsp90 with signal transduction	30

1.6.3	Sba1: expanding the Hsp90 chaperone network	31
1.7 Hs ₁	990 in disease: a novel target	32
1.7.1	Hsp90 in Cancer	32
1.7.2	Hsp90 role in neurodegenerative disorders	33
1.7.3	Hsp90 in infectious diseases	34
1.7.4	Hsp90 in Cystic fibrosis	35
1.8 Noi	n canonical roles of Hsp90	36
1.8.1	Hsp90 in Telomere maintenance	36
1.8.2	Hsp90 in Transcription regulation	36
1.8.3	Hsp90 in Chromatin remodelling	37
1.8.4	Hsp90 in multimeric protein complex assembly	38
1.8.5	Hsp90 and Protein transport	39
1.8.6	Hsp90 in DNA repair	40
1.9 Pos	t translational modifications of Hsp90	40
1.10 DN	A repair by Homologous recombination	47
1.11 Hs _I	990 in homologous recombination mediated DNA repair	49
1.12 Ob	jectives of the study	51
1.13 Spe	ecific Aims	52
MATER	IALS AND METHODS	53

2.1 Mo	lecular Biology Techniques	53
2.1.1	Bacterial competent cell preparation	53
2.1.2	Bacterial transformation	53
2.1.3	Bacterial plasmid DNA isolation by alkaline lysis method	54
2.1.4	Site-directed mutagenesis	54
2.1.5	Plasmid DNA subcloning	55
2.2 Me	thods in yeast genetics	56
2.2.1	Yeast transformation	56
2.2.2	Gene tagging and gene knockout	57
2.2.3	Real-time RT-PCR	58
2.3 Yea	st Cell biology methods	58
2.3.1	Fluorescence imaging	59
2.3.2	Indirect immunofluorescence assay	59
2.4 Bio	chemical methods	61
2.4.1	Protein isolation	61
2.4.2	Cellular Fractionation	61
2.4.3	Coimmunoprecipitation	63
2.4.4	Western blotting	64
2.4.5	MMS sensitivity assays	64
2.4.6	Repair Kinetics of a single double strand DNA break	65

2.4.7	Chromatin immunoprecipitation65
SPECIF	TIC AIM 1: TO STUDY WHETHER yHSP90A REGULATES THE NUCLEAR
FUNCT	ION OF RAD51 DURING DNA REPAIR74
3.1 Int	roduction74
3.2 Res	sults75
3.2.1	yHsp90α exists in a dynamic physical association with Rad51 ^{WT} 75
3.2.2	The dynamic physical association of yHsp90 α with Rad51 WT is lost in the case of the
mutan	t Rad51 ^{E108L} 77
3.2.3	Quantitative analysis shows stronger association of yHsp90α with Rad51 ^{E108L} as
compa	ared to Rad51 ^{WT} 79
	TIC AIM 2: TO STUDY WHETHER $yHSP90\alpha$ IS IMPORTED TO THE
CHRON	MATIN
4.1 Int	roduction81
4.2 Res	sults84
4.2.1	Nuclear accumulation of yHSP90α during DNA damage
4.2.2	The nuclear import of HsHsp90α during genotoxic stress is independent of Thr7
phosp	horylation88
4.2.3	Nuclear accumulation of yHSP90α upon induction of a single double strand break90

4.2.4	Extent and kinetics of occupancy of yHSP90α at DSB ends
CDE CU	
SPECI	FIC AIM 3: TO STUDY THE MECHANISM OF OF yHSP90α NUCLEAR
IMPOI	RT DURING DNA REPAIR97
5.1 In	troduction97
5.2 Re	esults99
5.2.1	Increased nuclear localization of Aha1 in response to DNA damage99
5.2.2	y $Hsp90\alpha$ transport to the nucleus upon DNA damage is independent of Cdc37 and
Sba1	104
5.2.3	yHsp90α transport to the nucleus upon DNA damage is dependent on Aha1107
5.2.4	The Aha1 dependent nuclear import of yHsp90α is independent of genotypic
back	ground
5.2.5	The charged linker domain of $yHsp90\alpha$ is essential for its nuclear translocation upon
DNA	damage
5.2.6	Loss of nuclear translocation of yHsp 90α is correlated with increased sensitivity to
MMS	S 119
DISCUS	SSION 121
REFER	ENCES
APPEN	DIX-I I
6.1 Cl	oning GFP tagged yHsp90 $lpha$, yHsp90 $lpha^{\Delta 211 ext{-}259}$ and yHsp90 $lpha^{\Delta 211 ext{-}259}$ in <i>pHCA</i> vector i

6.2	Cloning of FLAG tagged HsHSP90 α , Hshsp90 α T7A and Hshsp90 α Δ (224-279) into
pН(CA vector iii
6.3	Subcloning AHA1 into pBEVYT vectoriv
API	PENDIX-II
7.1	Synopsisi
Lis	st of Figures:
Fig.	1. Hsp90 consists of 3 domains; N-terminal domain, Middle domain and C-terminal
	domain20
Fig.	2. Schematic diagram of the Hsp90 chaperone cycle showing its different
	conformational changes25
Fig.	3. Western blot showing coimmunoprecipitation of Rad 51^{WT} with yHsp 90α from whole
	cell extracts of wild-type strain in conditions of cells untreated and treated with 0.15%
	MMS for 2 hrs76
Fig.	4. Western blot showing coimmunoprecipitation of Rad51 $^{\rm E108L}$ with yHsp90 α from
	whole cell extracts of $E108Lrad51$ mutant strain in conditions of cells untreated and
	treated with 0.15% MMS for 2 hrs
Fig.	5. Relative association of yHsp90 α with Rad51 is calculated from at least three
	independent coimmunoprecipitation experiments and standard deviations are plotted
	for both wild type RAD51 and mutant E108Lrad51 strain80
Fig.	6. The pairwise sequence alignment between human Hsp90α and yeast Hsp82 shows
	that the first 14 amino acids are absent in Hsp8283

Fig.	7. Accumulation of yHsp90 α in the nucleus in response to MMS induced DNA damage
Fig.	8. Accumulation of Hs Hsp90 α in the nucleus in response to MMS induced DNA
	damage89
Fig.	9. Nuclear accumulation of yHSP90 α upon induction of a single double strand break 91
Fig.	10. Extent and kinetics of occupancy of yHSP90α at DSB ends95
Fig.	11. Increased nuclear presence of Aha1 during the conditions of DNA damage102
Fig.	12. Expression of AHA1 and SBA1 in response to MMS103
Fig.	13. yHsp90α transport to the nucleus upon DNA damage is independent of Cdc37 and
	Sba1105
Fig.	14. yHsp90α transport to the nucleus upon DNA damage is dependent on Aha1108
Fig.	15. yHsp90α transport to the nucleus upon DNA damage is dependent on Aha1 in
	BY4741 strain111
Fig.	16. The domain responsible for the conformational flexibility between the NTD and the
	MD of yHsp90α is essential for its nuclear translocation upon DNA damage)113
Fig.	17. The subcellular fractionation of various mutants of yHSP90α in response to DNA
	damage117
Fig.	18. Loss of nuclear translocation of yHSP90α is correlated with increased sensitivity to
	MMS
Fig.	19. Schematic diagram showing a representative model of the study126
Fig.	20. Cloning of <i>HSP82</i> , <i>hsp82</i> Δ(211-259) and <i>hsp82</i> Δ(211-242) into <i>pHCA</i> vectors ii
Fig.	21. GFP tagging of pHCA-HSP82, pHCA-hsp82\(\Delta(211-259)\) and pHCA-hsp82\(\Delta(211-242)\)
	ii

Fig. 22. Cloning of $FLAG$ tagged $HsHSP90\alpha$, $Hshsp90\alpha T/A$ and $Hshsp90\alpha\Delta(224-279)$ into	
pHCA vector	iv
Fig. 23. Cloning of AHA1 into pTA vector	V
<u>List of Tables:</u>	
Table 1. Hsp90 post-translational modifications and their effects	41
Table 2. Yeast strains used in this study	66
Table 3. Primers used in this study	69
Abbreviations:	
NTD: N-terminal domain	
MD: Middle domain	
CL: Charged linker	
CTD: C-terminal domain	
Hsp90: Heat shock protein 90	
HSF1: Heat shock factor 1	
SUMO: Small Ubiquitin-like Modifier	
CFTR: Cystic fibrosis transmembrane conductance regulator	
UV: Ultraviolet radiation	
MMS: Methylmethane sulfonate	

EGFR: Epidermal growth factor receptor

CDK: Cell Division Kinase

LCK: Lymphocyte-specific protein tyrosine kinase

Src: Sarcoma

UHRF1: Ubiquitin-like protein TOCcontaining PHD and RING finger domains 1

HIF1α: Hypoxia inducible factor 1α

NF-κB: Nuclear factor kappa light chain enhancer of activated B cells

STAT: Signal transducer and activator of transcription

NLS: Nuclear localization signal

R2TP: Rvb1-Rvb2-Tah1-Pih1

PIKKs: Phosphatidylinositol-3 kinase-related protein kinase family proteins

DNA PKcs: DNA dependent protein kinase, catalytic subunit

ATR: Ataxia telangiectasia and Rad3-related

ATM: Ataxia telangiectasia mutated

TORC1: TOR complex 1

TORC2: TOR complex 2

CBF3: Centromere Binding Complex 3

RISC: RNA induced silencing complex

TOC: Translocon of the outer envelope of chloroplasts

TOM: Translocase of the mitochondrial outer membrane

BER: Base excision repair

HR: Homologous recombination

NHEJ: Non homologous end joining

NER: Nucleotide excision repair

DSBs: Double strand DNA breaks

MRX: Mre11-Rad50-Xrs2

MRN: Mre11-Rad50-Nbs1

PCIA: Phenol, Chloroform, Isoamyl alcohol mixture

RT-PCR: Reverse transcription-Polymerase chain reaction

FP: Forward primer

RP: Reverse primer

Introduction

1.1 Hsp90 among other molecular chaperones

Maintaining homeostasis in the cell is vital for the growth and proper functioning of any living organism. Molecular chaperones play a large role in maintaining cellular homeostasis by aiding proteins to attain a stable folded state and hence prevent their aggregation in a constantly changing cellular environment (1). There are a wide variety of molecular chaperones and protein-remodelling factors present in the cell which are primarily involved in the correct folding and maturation of newly synthesized proteins. The eukaryotic heat shock response involves an upregulation of these molecular chaperones so as to keep the cellular proteins in a stable, functional state during stress. This enables the cell to maintain proteostasis at all times and cope with the environmental stress (2–4).

The major class of molecular chaperones which are involved in the stabilization of proteins and helping them to attain a conformation which is functionally active are termed as "heat shock proteins" due to their unique feature of being upregulated in response to cellular stresses such as high temperature. Among these, the Heat Shock Proteins, Hsp70s and Hsp90s utilize ATP and co-chaperone mediated chaperone cycles for the folding and maturation of client proteins. Both Hsp70 and Hsp90 molecular chaperones consist of constitutive and stress inducible isoforms (4).

Hsp90 is a unique molecular chaperone which interacts with a select subset of proteins known as its clients which constitute proteins involved in signal transduction pathways such as transcription factors, protein kinases, DNA repair proteins, steroid hormone receptors etc. (5–10). Along with ensuring their stability and maturation, Hsp90 also mediates the transport of its

client proteins into various cellular compartments and their activation in accordance with cellular signals (11, 12). Due to such a diverse clientele, Hsp90 is an integral part of various essential pathways in the cell such as telomere maintenance, DNA repair, cell cycle progression, apoptosis, etc. (13). Hsp90 is found to be evolutionary conserved across all forms of life except archaebacteria (14, 15).

1.2 Hsp90 structure

The molecular structure of the Hsp90 protomer is comprised of three basic domains, namely; the N-terminal domain, the Middle domain and the C-terminal domain (Fig.1). The functional form of Hsp90 exists as a dimer wherein each protomer of Hsp90 is linked via the C-terminal domain. The N-terminal domain and the Middle domain are connected with a highly charged linker region in eukaryotes. Each of these domains carry out specific functions which are essential to the Hsp90 chaperonic cycle (16, 17).

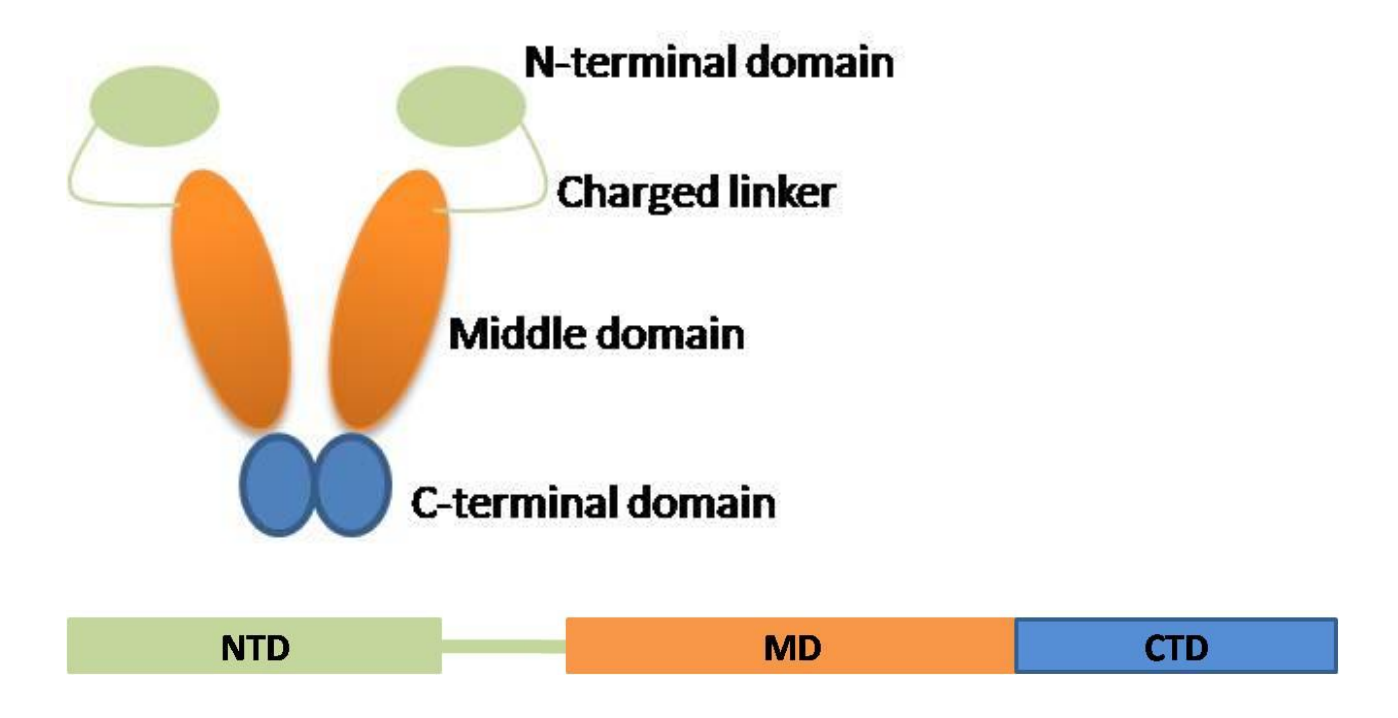


Fig. 1. Hsp90 consists of 3 domains; N-terminal domain, Middle domain and C-terminal domain. The NTD and MD are linked together via a highly charged, flexible linker region. Hsp90 exists as a dimer in the cell.

1.2.1 N-Terminal domain (NTD)

The N-terminal domain consists of a highly conserved ATP binding site consisting of a unique αβ sandwich motif known as the Bergerat fold which is distinctly different from the more common P-loop NTPase fold which forms the ATP binding pocket of most ATPases (18, 19). This Bergerat fold is also found in the ATP binding pockets of GyrB, MutL and histidine kinases prompting scientists to combine these proteins into the GHKL family (18, 19). This Bergerat fold comprises the catalytic site in the Hsp90 NTD wherein ATP binds and is hydrolysed to ADP. This ATPase activity of Hsp90 fuels the Hsp90 chaperonic cycle which is essential for client maturation and fuction(20–22). Drugs like Geldanamycin and Radicicol competitively bind to the ATP binding pocket of Hsp90 and hence prevent the binding of ATP; effectively preventing the ATPase activity of Hsp90 (23). Since the Hsp90 chaperone cycle is ATP driven, these drugs essentially block the functioning of Hsp90 in the cell (23).

1.2.2 Charged Linker Region (CL)

The charged linker region is a variable, unstructured region consisting of highly charged amino acids such as arginine and lysine which links the NTD and the MD of Hsp90. In the prokaryotic counterpart, HtPG, the CL is very short as compared to eukaryotic Hsp90 (24). Nevertheless, the charged linker region provides flexibility to the molecular chaperone in both eukaryotes as well as prokaryotes to effectively undergo the chaperone cycle for the maturation of client proteins (24). In eukaryotes, the CL also facilitates the binding of Hsp90 co-chaperone proteins, which are absent in prokaryotes, to Hsp90. This linker region is also known to enable the different conformations attained by Hsp90 during its chaperonic cycle including the closing of the NTD lid after binding ATP helping in effective ATPase activity of Hsp90 (25, 26).

1.2.3 Middle Domain (MD)

The MD has binding sites for clients and co-chaperones. The MD also contains interaction sites for the binding of the γ phosphate of ATP and hence, assists in the binding of ATP to the NTD and its subsequent hydrolysis (27). The MD helps in stabilizing the closed, ATP bound complex of Hsp90 as it facilitates the docking of the lid domain present in the NTD which contains the ATP binding pocket (27). The MD also contains hydrophobic patches which provide sites for the binding of Hsp90 clients (27).

1.2.4 C-Terminal Domain (CTD)

The CTD is predominantly known as the homodimerization domain of the Hsp90 dimer (28). Another characteristic feature of the CTD is the presence of a highly conserved unstructured MEEVD motif which is important for the binding of co-chaperones, such as HOP, having a TPR domain (29, 30). A nucleotide binding site is present in the CTD which acts as an allosteric regulatory site for the ATPase activity of Hsp90 (31).

1.2.5 Hsp90 isoforms

Hsp90 is evolutionary conserved across species with 60% identity between human and yeast Hsp90 homologs and 40% identity between human and bacterial Hsp90 homologs (32). In mammalian cells, Hsp90 exists in a variety of isoforms which are localized to different organelles, for example, GRP94 is present in the endoplasmic reticulum; Hsp90α and Hsp90β remain in the cytosol; and TRAP1 resides in the mitochondria (33). Although all these organelle isoforms have similar protein structure consisting of the N-terminal domain, the middle domain

and the C-terminal domain, they differ in their conformational changes during the chaperone cycle and also differ in client binding and specificity (17).

The cytoplasmic Hsp90 α and Hsp90 β comprise 1-2% of the whole cellular protein and serve as the main functional Hsp90s in the cell having a wide variety of clients. Hsp90 β remains constitutively expressed in the cell whereas Hsp90 α is the inducible isoform which gets upregulated in the presence of stress such as heat shock and starvation conditions.

In lower eukaryotes such as *Saccharomyces cerevisiae*, only the homologs of the cytoplasmic Hsp90s are present, namely; Hsc82 which is the homolog of Hsp90 β ; and Hsp82 which is the homolog of the Hsp90 α (34). In prokaryotes like *Escherichia coli*, only a single form of Hsp90 is present known as HtpG, which is homologous to Hsp90 α (34). Although the prokaryotic Hsp90 is dispensable, the yeast Hsp90s are indispensable and the deletion of both Hsc82 and Hsp82 renders the cell unviable (32, 35).

1.3 Hsp90 Chaperone cycle

Numerous proteins which participate in various essential cellular pathways governed by signal transduction are kept stabilized in the cell and are quickly activated at the correct moment to carry out their function by the help of the Hsp90 cycle. The Hsp90 cycle functions downstream of Hsp70 for the maturation of client proteins. Hsp90 keeps these client proteins in a stable, non functional form and when a signal is provided to the cell, Hsp90 releases the mature proteins using its dynamic chaperonic cycle (13).

During the chaperone cycle, the Hsp90 dimer undergoes a wide variety of conformational shifts (Figure 2) essential for the binding and maturation of the client proteins. When not bound with

any client proteins, Hsp90 exists in the 'open' conformation in the cell wherein the two monomers are bound together by the CTD but the two NTDs remain separate and unbound with ATP or ADP. Binding with ATP molecules to both the NTDs shifts the Hsp90 conformation to the 'closed 1' conformation wherein the ATP bound NTDs come close together and dock onto the MDs (36, 37). The client protein also binds when Hsp90 is in the intermediate stage between open to closed conformations (38). This is followed by a conformational switch to the 'closed 2' conformation which is more tightly closed than the closed 1 conformation and facilitates an enhancement of the Hsp90 ATPase activity (38). The shift from closed 1 to closed 2 complex requires the hydrolysis of one ATP molecule and the subsequent activation of the client protein requires the hydrolysis of the second ATP molecule. Once both ATPs are hydrolysed to ADP, the mature client is released from Hsp90 which subsequently shifts back to its open conformation (38–41).

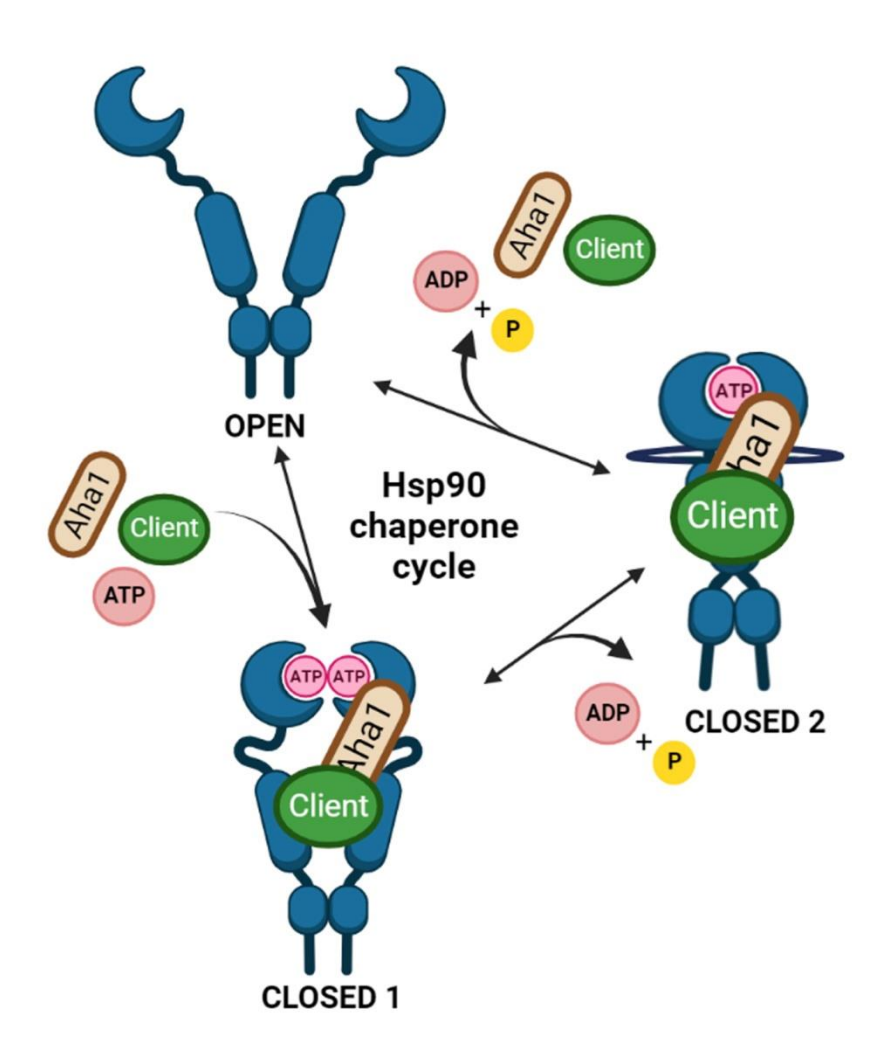


Fig. 2. Schematic diagram of the Hsp90 chaperone cycle showing its different conformational changes

1.4 Hsp90 Co-chaperones

In eukaryotic cells, Hsp90 is dynamically associated with a wide variety of co-chaperones which assist Hsp90 during its chaperonic cycle. Different co-chaperones specifically bind to different conformations of Hsp90 during its chaperonic cycle and hence regulate its function. These co-chaperones are largely conserved in eukaryotic cells; however, they are not present in prokaryotic cells. These Hsp90 co-chaperones help in the proper binding and dissociation of Hsp90 client proteins, ATP binding, the conformational changes that Hsp90 undergoes during the chaperone cycle, and ATP hydrolysis during the chaperone cycle progression, etc. (42–44).

According to their function, these chaperones are grouped into three different categories namely, remodelling co-chaperones; client recruiters and late acting co-chaperones.

1.4.1 Remodelling co-chaperones

Remodelling co-chaperones such as Aha1, peptidyl-prolyl isomerases and Ppt1 induce a conformational shift in Hsp90 during its chaperone cycle, hence helping in stabilizing the different conformations of Hsp90 ranging from 'open' to 'closed' so as to help maintain the dynamic chaperonic cycle of Hsp90. Aha1 is a unique co-chaperone which enhances the ATPase activity of Hsp90 (43).

1.4.2 Client recruiter co-chaperones

Since Hsp90 functions downstream of Hsp70, client recruiters like Cdc37, Sti1 and Sgt1 help in the movement of client proteins from Hsp70 to Hsp90. These co-chaperones inhibit the Hsp90 ATPase activity and hence stabilize the open conformation of Hsp90. Some of these client

recruiters are client specific, for example, Cdc37 aids in the transfering of kinase clients from Hsp70 to Hsp90 (44).

1.4.3 Late acting co-chaperones

Late acting co-chaperones such as Sba1 (yeast ortholog of mammalian p23) (45) stabilize the closed conformation of Hsp90 and also partially inhibit the ATPase activity of Hsp90, hence helping in the maturation of the client. Sba1 is a unique co-chaperone which possesses independent chaperone function and directly interacts with client proteins and support their maturation (42).

1.4.4 Co-chaperones with a TPR motif

Some of the co-chaperones contain the TPR motif such as Sti1, Ppt, Cpr6, Cpr7 etc. and specifically interact with the MEEVD domain present in the Hsp90 CTD. Some of these TPR domain containing co-chaperones also consist of a PPIase domain such as in Cpr6 and Cpr7 and can catalyse the cis-trans isomerization of peptide bonds (43, 44).

1.5 Hsp90 co-chaperones: functions other than the Hsp90 chaperone cycle

Apart from assisting Hsp90 during its chaperonic cycle, Hsp90 co-chaperones also have various other functions in the cell as well. Studies have revealed that Hop (mammalian ortholog of Sti1) is crucial in preserving the hormone binding ability of the progesterone receptor (46). Furthermore, in mammalian cells, the knockdown of Hop or Aha1 can prevent the degradation of misfolded mutant Δ F508CFTR protein which, if allowed to be expressed on the cell surface, has the ability to be functional (47, 48). Hence the knockdown of Hop/Aha1 allows Δ F508CFTR protein to reach the cell surface without being degraded, restoring its function (47, 48). Other

studies have proved that although Sti1 is a non-essential protein, the double knockout of Sti1 along with Ydj1 (yeast ortholog of Hsp40) or Sba1 leads to the loss of viability (49, 50). TPR containing co-chaperones such as FKBP38 in mammalian systems has been shown to affect neuronal apoptosis by preventing the anti-apoptotic activity of Bcl-2 (51). Furthermore, the knockdown of FKBP8, an isoform of FKBP38, in mammalian cells infected with Hepatitis C virus prevents its RNA replication (52). Previous literature indicates that few Hsp90 co-chaperones also have potential roles in the DNA repair pathway as well. In HeLa cell extracts, it was found that Aha1 could interact directly with the DNA repair proteins, Ku70, Ku80 and DNA-PKcs(53). Another study revealed that Sba1 deletion leads to sensitization of yeast cells towards different agents which cause genotoxic stress such as UV, bleomycin and MMS which could be reversed upon introduction of Sba1 in the \(\Delta sba1\) cells (54). Studies done with the essential Hsp90 co-chaperone, Cdc37 revealed that a loss of function mutation of Cdc37 leads to a synthetic growth defect which in turn led to a loss in genome integrity (55).

1.6 The cellular roles of Aha1, Sba1 and Cdc37

1.6.1 The unique relationship between Aha1 and Hsp90 conformational dynamics

As previously mentioned, the NTD and the MD of Hsp90 are linked by a highly charged, unstructured CL. The charged linker region is a 63 amino acids long sequence ranging from 211-272 amino acids in yeast Hsp82 and 224-285 in human Hsp90α. This linker region is primarily involved in providing flexibility to the Hsp90 structure, facilitating it to attain the many different conformations during its chaperonic cycle (56). The charged linker imparts a net negative charge to the Hsp90 molecule which varies between different species and post translational modifications that affect this net charge also affect the conformation of Hsp90 as well as its

binding with co-chaperones such as Aha1 (25, 57). In a study using the secreted form of Hsp90, Tsutsumi et. al discovered that a single mutation of I205A in yeast Hsp82 and the corresponding mutation of I218A in human Hsp90 present at the junction of the NTD and the CL led to an increase in the conformational flexibility in the Hsp90 structure which interestingly led to a negative effect in its chaperone function and also inhibited Aha1 mediated ATPase enhancement activity (58). This phenotype was found to be rescued by a CL deletion. In a study using successive CL deletion constructs of yeast Hsp82, it was observed that the deletion of the charged linker beyond 211-263 lead to a loss in the viability of cells while the shorter CL deletion mutants showed mild temperature sensitivity defects (59). It was further observed that although the co-chaperone Ahal could bind with all the CL deletion mutants, the successive deletions of the charged linker led to a successive decrease in the Aha1 mediated ATPase enhancement activity of Hsp82 with a complete inhibition of ATPase enhancement in the CL deletions beyond the 263rd amino acid (59). Studies have shown that post translational modifications of Hsp90 such as SUMOvlation(60), acetylation(61) and phosphorylation (62–64) regulates the recruitment and binding of Aha1 to the Hsp90 dimer. In a study by Mollapur et. al., it was shown that the SUMOylation of K191 lysine residue of human Hsp90α as well as the corresponding K178 of yeast Hsp90 lead to the recruitment of Aha1 to Hsp90 (60). Another study revealed that yeast Hsp90 is phosphorylated by SWE1WEE1 at Tyrosine24 which epigenetically modulates the interaction of Aha1 with Hsp90 (62). In a contrasting study, it was observed that the phosphorylation of Threonine 22 residue prevents the binding of Aha1 to Hsp90, hence affecting Hsp90 ATPase activity and chaperone function (63). Aha1 binds to Hsp90 in a sequential, asymmetric manner with the NTD of Aha1 binding to a highly conserved, phosphorylated tryrosine residue present at the 313 position of the MD of Hsp90 followed by the

binding of the CTD of Aha1 with the NTD of Hsp90 (64). This asymmetric binding of Aha1 then induces a unique conformational shift in Hsp90 from "closed 1" to "closed 2" which in turn enhances the ATP hydrolysis activity of the Hsp90 chaperone (64, 65).

Yeast cells contain another homolog of Aha1, known as Hch1, which is absent in mammalian cells. Hch1 was first identified as a high copy number suppressor of an Hsp90 temperature sensitive mutant, E381K (66). Hch1 shares 36.6% identity and 50.3% similarity to the N-terminal domain of Aha1 and also shares its ability to stimulate the Hsp90 ATP hydrolysis activity (67). In normal conditions, Hch1 and Aha1 are dispensable in yeast cells. However, during elevated temperature conditions and in the presence of Hsp90 inhibitors like NVP-AUY922, the presence of Aha1 and Hch1 is crucial for the normal functioning of Hsp90 required for the activation of client proteins (68, 69). In higher eukaryotes, Hsp90 has a lower rate of ATPase activity as compared to yeast; hence, the Aha1 mediated ATPase enhancement of Hsp90 is important in higher eukaryotes for the regulation of Hsp90 function and the activation of its client proteins (69).

1.6.2 Cdc37: linkng Hsp90 with signal transduction

The Hsp90 co-chaperone, Cdc37 was first discovered during a cell cycle screening (70) although it does not have any role in cell cycle checkpoints. However, it has been found that, Cdc37 is involved in the proper folding, maturation and activation of upto 300 protein kinases till date. Most of these protein kinases are important for various signal transduction pathways, including EGFR, CDKs, LCK, SRC, etc. making it an essential protein in the cell (55, 71). Studies have shown that the binding of the kinase family of clients to Hsp90 requires the assistance of Cdc37 which binds to the kinase client as well as to the Hsp90 dimer, forming a tripartite complex (72,

73). The amino acids 1-126 comprise the kinase binding domain of human Cdc37 where the kinase clients bind followed by phosphorylation of a serine 13 (S13) residue by casein kinase II which stabilises the binding of the kinase client to Cdc37 (74, 75). The amino acids 127-282 of Cdc37 comprise the Hsp90 binding domain and this region binds to Hsp90 NTD and hence, links the interaction between kinase clients and Hsp90. Apart from facilitating the binding of kinase clients to Hsp90, Cdc37 also regulates the chaperone activity of Hsp90 by inhibiting the ATPase hydrolysis activity of Hsp90, prolonging the interaction of Hsp90 with the kinase clients and hence promoting their proper folding. The dephosphorylation of the S13 residue of Cdc37 by protein phosphatase 5 (PP5) promotes the release of the mature kinase (76). Cdc37 is an oncogene and increasing levels of this Hsp90 co-chaperone promotes tumorigenesis (72). Studies have shown that when Cdc37 was overexpressed along with c-Myc, the proto-oncogene, it lead to the development of prostate cancer in mice (77). Since Cdc37 is crucial for the activation of CDKs which are essential for cell cycle progression and cell proliferation, it is not surprising that cancer cells have elevated levels of Cdc37, making it an attractive target for cancer therapy.

1.6.3 Sba1: expanding the Hsp90 chaperone network

Sba1 was first described in mammalian systems as p23 (78). Sba1/p23 was found to associate preferentially with the ATP-bound, NTD dimerized, closed complex of Hsp90 during the late stage of the Hsp90 chaperone cycle (79, 80). Sba1/p23 increases the efficiency of the Hsp90 chaperone cycle by slowing down the ATP hydrolysis step and prolonging the client bound state, enabling Hsp90 to efficiently fold and subsequently activate the client (81, 82). Studies have shown that the binding of Sba1 is sequential with Sti1 first binding to the Hsp90 open conformation, followed by the binding of ATP which reduces the affinity of Hsp90 with Sti1. Sti1 is then competitively displaced by Cpr6, allowing the Hsp90 dimer to switch to the closed

conformation subsequently allowing Sba1 binding to the closed NTDs of Hsp90 (82, 83). A recent study by Echtenkamp et. al. revealed that Sba1 has a vast interactome of proteins out of which only 25% coincided with the Hsp90 interactome (54). This study suggested that Sba1 has the independent ability to chaperone proteins and intersect with Hsp90 at different points of biological processes such as cell motility, DNA repair, post translational modifications of proteins and protein translocation, forming a triaxial relationship between various cellular pathways and Hsp90 and hence expanding the reach of regulation of cellular processes by the Hsp90 chaperone system (54). Atomic resolution structures of glucocorticoid receptor-Hsp90-p23 maturation complex revealed that apart from stabilizing the closed conformation of Hsp90, p23 also directly interacts with the client and stabilizes it via a conserved helix identified as a FxxMMNxM motif present in the C terminal end of p23 (84).

1.7 Hsp90 in disease: a novel target

Hsp90 has been known to play roles in different diseases such as cancer, infectious diseases as well as neurodegenerative disorders. Hence, further studies on Hsp90 can illuminate it as a novel drug target in the treatment of various diseases.

1.7.1 Hsp90 in Cancer

Tumour cells have an extensive dependency on signaling pathways driving the cell cycle, most of which are governed by Hsp90 and its clients such as p53, Proto-oncogene SRC, UHRF1 and HIF1α. Since cancer cells survive in stressful, nutrient deficient environments, these stressful conditions release HSF1 which then induces the increased expression of Hsp90 (85, 86). Although elevated levels of Hsp90 in cancer cells help in their survival rate (87), increased Hsp90 levels in normal cells does not induce tumorigenesis in normal cells (88, 89). In lower

eukaryotes, the over-expression of Hsp90 was found to negatively affect the steady state levels of Rad53 (90). It was observed that even upon DNA damage, Rad53 levels could not reach the threshold required to elicit an efficient DNA damage response leading to increased DNA damage sensitivity in the yeast cells (90). Hsp90 also enhances motility in malignant tumour cells by secretion into the extracellular matrix (91). Studies show that this secreted Hsp90 further activates the matrix metalloproteinase-2 (MMP-2) which in turn cleaves the components of the extracellular matrix, facilitating the invasion of malignant cells into the bloodstream (91–93).

1.7.2 Hsp90 role in neurodegenerative disorders

Many neurodegenerative disorders such as Huntington disease, Alzheimer's disease, Parkinson's disease, etc. are associated with an increased aggregation of misfolded proteins. Since molecular chaperones like Hsp70, Hsp90 and their co-chaperones are involved in the proper folding and final maturation of proteins, they are increasingly coming into the spotlight as drug targets for these neurodegenerative diseases (94).

Recent studies have shown that the inhibition of Hsp90 plays a dual therapeutic role in neurodegenerative diseases (95).

It has been found that Hsp90 stabilizes the kinases responsible for hyperphosphorylation of tau proteins which further leads to their aggregation which contributes to neurodegenerative diseases and hence, the inhibition of Hsp90 helps in activation of the Hsp70 pathway which in turn helps in the proper folding of the misfolded proteins (96–98). Further studies have shown that the inhibition of Hsp90 co-chaperones such as Cdc37 and Aha1 contributes to a reduction in Aβ and tau aggregates, serving as therapeutic targets for the treatment of neurodegenerative diseases (99, 100). Recent reports have found that the inducible form of Hsp90, i.e. Hsp90α was in elevated

levels at sites of inflammation which is associated with various neurodegenerative diseases and the reduction of Hsp90 α helped in the reduction of inflammation (101–104).

However, in contrast, reports have also suggested that the expression of Hsp90 activates phagocytosis in microglia which in turn helps in clearing A β aggregates (105). Furthermore, it has been found that the Hsp90 co-chaperones, CHIP and Hop assist in the clearance of abnormal tau aggregates (106–108).

1.7.3 Hsp90 in infectious diseases

During a viral infection, as the virus undergoes multiple rounds of replication, it also has to undergo vast amounts of translation using the host machinery to produce complex, multifunctional proteins. Hence, these viruses heavily depend on the Hsp90 chaperone machinery of the host for the proper functioning of their proteins during viral replication (52, 109, 110). Furthermore, the proteins encompassing the structural components of the viral particle are prone to misfolding and subsequent aggregation especially during fever temperatures and hence, require increased amounts of Hsp90 in the host to promote the stability of these proteins and assemble into mature viral particles (111, 112). These characteristics make Hsp90 an appealing target for antiviral drugs (113, 114).

The importance of the Hsp90 chaperone system has also been implicated in the development and differentiation of parasites such as *Leishmania donovani*, *Plasmodium falciparum*, *Toxoplasma*, *Trypanosoma*, *Theileria*, *Eimeria* etc (115).

The parasite known to cause malaria, *Plasmodium falciparum*, has been extensively studied and it has been revealed that it can cleverly utilize its Hsp90 chaperone machinery during periodic

fluctuations of host temperature as the human host experiences periodic high fever in response to the parasitic infection (116, 117). When the human host experiences fever, *Pf*Hsp90 levels also are increased in the parasite and the parasite uses this temperature cycle to transition between different stages from early ring stage to trophozoite stage in the erythrocytes with the help of its Hsp90 machinery (118, 119). Studies have reported that the inhibition of *Pf*Hsp90 led to severe growth defects in the malaria parasite making it an attractive drug target (120).

Another well known parasite which causes leishmaniasis, *Leishmania donovani*, is also closely dependent on Hsp90 for the transition of the motile promastigote stage to the non motile amastigote stage inside the human host. This occurs during the down regulation of Hsp90 with the help of Hop during a sudden temperature rise in the human host (121). Hsp90 suppression has been linked to the transition of promastigote to amastigote stage in vitro conditions as well (122, 123).

1.7.4 Hsp90 in Cystic fibrosis

Cystic fibrosis is a result of mutations in a transmembrane chloride channel known as the cystic fibrosis transmembrane conductance regulator (CFTR). The most common mutation encountered in the CFTR channel is $\Delta F508$ which inactivates the protein, which further results in its degradation leading to the inhibition of its translocation to the plasma membrane. Studies have shown that the Hsp90 chaperone machinery is important for the final folding and subsequent translocation of CFTR to the plasma membrane. The $\Delta F508$ mutation in CFTR leads to a defect in its folding, leading to its degradation rather than its movement to the plasma membrane. A recent study has shown that the downregulation of Aha1 helps to prevent misfolding of $\Delta F508$ CFTR resulting in its increased transport to the plasma membrane (48).

1.8 Non canonical roles of Hsp90

Apart from its classical chaperone role, Hsp90 is being recognised to perform various non canonical roles in the cell such as transcription regulation, chromatin remodelling, assembly of multimeric complexes, vesicular protein transport and telomere maintenance (124, 125).

1.8.1 Hsp90 in Telomere maintenance

Recent studies revealed that not only does Hsp90 stabilize the telomerase reverse transcriptase protein (TERT) and helps assemble the telomerase enzyme (8); but Hsp90 also facilitates telomerase function by aiding in the DNA binding and DNA extension activities of the telomerase enzyme (126, 127). Studies in both human and yeast systems, revealed that Hsp90 and p23/Sba1 work cooperatively to aid telomerase function wherein p23/Sba1 functions to dissociate the telomerase enzyme from DNA while Hsp90 works to facilitate its DNA binding (8, 127, 128). Furthermore it was also revealed that Human Hsp90 remains associated with telomerase during DNA extension leading to the addition of multiple telomere repeats (128). However, in yeast the association between Hsp90 and telomerase has a short half life leading to constant dissociation of Hsp90 and telomerase during telomere extension leading to short, degenerate telomeric repeats (129).

1.8.2 Hsp90 in Transcription regulation

Among the vast clientele of Hsp90, various transcription factors such as NF-κB, Specificity protein 1 (SP1), p53, B-cell lymphoma 6 (Bcl-6) and STATs also serve as clients of Hsp90 and indirectly impart the ability to Hsp90 to regulate transcription (130). Apart from ensuring steady state levels of mature transcription factors, Hsp90 has also been found to be essential for the late

folding of transcription factors which activates their DNA binding domain and enables the DNA binding capacity of transcription factors (131). Although Hsp90 does not have an NLS or a DNA binding domain, however early reports suggested a functional role of Hsp90 in the nucleus with relation to transcriptional regulation (132, 133). Morcillo et. al. found that upon heat shock, Hsp90 formed loci at chromosomal puffs which indicated transcriptionally active sites. Furthermore, it was observed that the prevention of transcription whilst keeping protein synthesis processes intact, prevented Hsp90 loci formation at the chromosomal puffs (133). A recent study revealed that Hsp90 is recruited near the promoters of various genes and regulates the pausing of RNA polymerase II during transcription, leading to the regulation of global genetic expression (134). In yeast cells, it was found that the upregulation of Hsp90 during heat shock leads to a subsequent upregulation of CUP9 protein which binds to the activator region of SIR2 gene and transcrptionally represses the production of Sir2 histone deacetylase which maintains the heterochromatinized state of various chromosomal regions such as the ribosomal DNA, telomeres, and the silent mating type loci (135). Hence, the Hsp90 mediated transcriptional regulation of Sir2 rewires the genetic expression during heat shock conditions (135).

1.8.3 Hsp90 in Chromatin remodelling

Expanding its nuclear role beyond transcription regulation, Hsp90 has also been known to associate with chromatin modifiers and hence, plays a role in chromatin remodelling as well. A recent study has revealed that Hsp90 and its co-chaperone, p23/Sba1 work cooperatively to regulate the remodel the structure of chromatin (RSC) complex (136). In the cell, RSC is required to remodel a number of nucleosomes across the genome within mins with a high efficiency. However, in vitro studies with purified RSC complex demonstrated that the speed and efficiency of nucleosome remodelling with only RSC is very low (137, 138). Hence, RSC is

assisted by Hsp90, which helps in RSC dissociation from DNA with a higher kinetics, and p23, which enhances the efficiency of nucleosome remodelling, hence increasing the overall kinetics of RSC function within the cell (136). Another study demonstrated that Hsp90 enhances the histone H3-lysine 4 (H3K4) specific methyltransferase activity of SMYD3 in colorectal cancer cells (139). Studies in *Drosophila* revealed that Hsp90 facilitates the function of Trithorax (Trx) which is a transcription factor responsible for the epigenetic modulation of the Trithorax group of genes (TrxG) resulting in phenotypic variations in *Drosophila* (140). In yeast cells, it was found that the activation of GAL genes required the removal of nucleosomes at the promoter regions which was facilitated by the Hsp90-Sti1-Hsp70 complex and the deletion of any of these components lead to inefficient nucleosome removal (141).

1.8.4 Hsp90 in multimeric protein complex assembly

Since Hsp90 is important for the stability and maturation of a variety of proteins, recent studies have found that it also plays a central role in the assembly and stabilization of various multimeric complexes. A study by Zhao et. al. revealed that Hsp90 and its co-chaperones, Pih1 and Tah1 form a Hsp90–Tah1–Pih1 ternary complex which then interacts with the helicases, Rvb1 and Rvb2 resulting in the formation of a R2TP complex. R2TP and Hsp90 then cooperatively function to ensure that the box C/D snoRNPs are properly assembled (142). The R2TP complex along with Hsp90 has also been found to facilitate cytoplasmic RNA polymerase II assembly (143). Studies have shown that apart from providing stability to PIKKs in mammalian cells such as DNA PKcs, ATR and ATM (144); Hsp90, along with the Serine/threonine protein kinase Tel1, has also been found to mediate the assembly of the PIKKs, ATR and mammalian target of rapamycin (mTOR) (145, 146). It was found that the inhibition of Hsp90 or the deletion of its cochaperone, Tel2 lead to the impairment of mTOR binding with TORC1 and TORC2 (145).

Furthermore, the deletion of Tel2 or the inhibition of Hsp90 inhibited the association of ATR with ATR-interacting protein (ATRIP) (146). Kinetochore assembly has also been linked to Hsp90 function in the cell. The kinetochore is a multimeric complex composed of many small complexes which are sequentially assembled at the centromere to form the kinetochore complex. The assembly of the kinetochore is initiated first by the assembly of the CBF3 which is composed of the proteins, Ctf13, Cep3, Skp1, and Ndc10. Studies have shown that Hsp90 is important for the assembly of this CBF3 complex (147, 148). Furthermore, Hsp90 has also shown to be important for the assembly of the RISC complex which is crucial in the RNA silencing pathway. Studies have shown using purified RISC protein components that the Hsp90/Hsp70 chaperone system is required for the ATP-dependent loading of RISC with small RNA duplexes (149-151). It was also observed that the inhibition of Hsp90 using ATPase inhibitors such as geldenamycin significantly reduced the activity of RISC (150). Studies have shown that the inhibition of Hsp90 causes the 26S proteasome to disassemble into its individual components, the lid complex and 20S core particle which demonstrated that Hsp90 was crucial in preserving the structural integrity of the 26S proteasome (152, 153).

1.8.5 Hsp90 and Protein transport

Compartmentalization in eukaryotic cells requires a multi-faceted delivery mechanism for the transport of proteins between various organelles within the cell. Recent studies are illuminating Hsp90 as a mediator of protein transport between different cellular compartments. The yeast Hsp90 isoforms have been found to interact with 202 proteins which drive the intracellular protein transport and secretion (154). Hsp90, has been shown to assist the post-translational import of nuclear encoded chloroplast and mitochondrial proteins to their respective outer membrane translocases, TOC and TOM respectively (155–157). Hsp90 has also been well

documented in the regulation of endosomal vesicular transport mechanisms via regulation of Rab cycling. Studies have revealed that Hsp90 modulates the Rab recycling process by facilitating the binding of GDP-dissociation inhibitors (GDIs) to Rab-GDP, allowing Rab to be retrieved from membranes and enabling continuous vesicular transport (158). Along with endosomal vesicular transport, Hsp90 has also been implicated in exocytic vesicular transport pathways. Studies have shown that the inhibition of Hsp90 impairs the endoplasmic reticulum to Golgi vesicular transport as well as intra-Golgi vesicular transport (11, 159). Furthermore, Hsp90 along with its co-chaperone, HOP, has been found to influence the membrane conformation and allows the secretion of proteins via exocytic vesicles (160).

1.8.6 Hsp90 in DNA repair

Recent studies have shown that Hsp90 has various clients which are involved in chromatin remodeling pathways and DNA repair pathways as well such as BRCA1, BRCA2, FANCA, ATM, DNA PKcs, CHK1, Rad51, components of the MRN complex and cohesion proteins(161). Previous studies revealed that the inhibition of Hsp90 leads to inefficient chromosome segregation, leading to chromosome loss (162). The inhibition of Hsp90 has been linked to decreased cell survivability in the presence of genotoxic stresses. Studies have shown that Hsp90 regulates ATM/ATR signaling complex as well as the MRN complex which are important for DNA damage response pathways (163). Another study revealed that Hsp90 inhibition leads to reduced levels of Rad51 foci formation which is a hallmark for homologous recombination mediated DNA repair pathway, the major pathway for DNA repair in lower eukaryotes like yeast (164).

1.9 Post translational modifications of Hsp90

Since Hsp90 has been implicated in a vast variety of canonical and non canonical functions and hence plays a regulatory role in a wide number of cellular processes, Hsp90 itself is required to be regulated in diverse ways. Hence, not only is Hsp90 function and conformation regulated by its co-chaperones, but also by various post translational modifications such as SUMOylation, phosphorylation, acetylation, deacetylation, methylation etc. (165) (Table 1).

Table 1. Hsp90 post-translational modifications and their effects

Post translational	Residue		Enzyme	Regulatory effect	References
modification					
	Hsp90α	Hsp90β			
Tyrosine	Y38	Y33	Swe1	Hsp90 chaperone	(62, 166)
phosphorylation				cycle	
	Y313	Y305		Hsp90 chaperone	(65, 167,
				cycle	168)
	Y197	Y192	v-Src, Yes	Hsp90 co-	(168–172)
				chaperone	
				binding	
	Y627	Y619		Hsp90 co-	(167, 168,
				chaperone	173)
				binding	
	Y309	Y301	c-Src	VEGF signalling	(174, 175)
Serine/threonine	S68	S63	CK2		(176)

phosphorylation	T5	NA	ATM, DNA-PK	DNA damage	(177–181)
				response/DNA	
				repair	
	S63	S58	CK2		(167, 176)
	S72	S67	CK2		(176)
	T88	T83	PKA		(167, 182,
					183)
					,
	T7	NA	ATM, DNA-PK	DNA damage	(177–181,
				· ·	
				response/DNA	184, 185)
				repair	
	T65	T60	CK2		(176, 186)
	T36	T31	CK2	Hsp90 chaperone	(63, 187,
				cycle	188)
					,
	T90	T85	PKA	Hsp90 chaperone	(167, 182,
				cycle	189–191)
	S164	S159	Cdo7 Dbf4	Compon	(162, 102)
	S104	3139	Cdc7-Dbf4	Cancer	(163, 192)
				regulation;	
				ATM/ATR	
				signalling	
	C211	5206	PKA/PKG	Carran	(102, 104)
	S211	S206	rka/rku	Cancer	(193, 194)
				regulation	
	S113	S108	HopBF1		(195)

T115	T110	Mps1, Cdc14,	Hsp90 chaperone	(196, 197)
		РКСγ	cycle	
N373	S365	CK2	Hsp90 chaperone	(198)
			cycle	
S399	S391		ATP binding to	(199–201)
			Hsp90	
G221	5336	CV2 DD5	1100	(202, 208)
S231	S226	CK2, PP5	Hsp90 co-	(202–208)
			chaperone	
			binding	
S263	S255	CK2, B-Raf, PP5	Hem00	(202–208)
3203	3233	CK2, B-Kai, FF3	Hsp90 co-	(202–208)
			chaperone	
			binding	
S460	S452	PKA		(194)
5400	5432	T KA		(1)4)
T425	S417	ΡΚСγ	Kinase client	(196)
			regulation	
S505	S497		ATP binding to	(201)
			Hsp90	
T603	T595	ΡΚСγ	Kinase client	(196)
			regulation	
S595	S587	Mitagan activated	Cancer	(166, 209,
3373	3301	Mitogen-activated		
		protein kinase 12	therapeutics	210)
		(p38γ)		

	M625	M617		Hsp90 chaperone	(201)
				cycle	
	T725	A717	CK2, CK1, GSK3β	Maintenance of	(211, 212)
				proteostasis	
	S623	S615		ATP binding to	(201, 213)
				Hsp90	
	T624	T616		EGFR regulation	(214, 215)
	S726	S718	CK2, CK1, GSK3β	Maintenance of	(211, 212)
				proteostasis	
	77.14	1706			(215, 210)
Acetylation	K41	K36		Drug resistance	(216–218)
	K74	K69		Hsp90 chaperone	(166, 210)
					(,)
				cycle	
	K69	K64	HAT p300	Hsp90 chaperone	(219–222)
			_	cycle	
				cycle	
	K292	K284	HAT p300	Hsp90 co-	(219, 221)
				chaperone	
				binding	
				omanig	
	K294	K286	HDAC6	Hsp90 co-	(61, 188, 216,
				chaperone	217, 223,
				binding	224)
	K100	K95	HAT p300	Hsp90 chaperone	(221)
				cycle	

	K407	K399		ATP binding to	(219, 225)
				Hsp90	
	K419	K411		ATP binding to	(225, 226)
				Hsp90	
	K327	K319	HAT p300	Hsp90 chaperone	(166, 221)
				cycle	
	K546	K538	HAT p300	Hsp90 chaperone	(221, 226)
	K340	K336	11A1 p300		(221, 220)
				cycle	
	K478	S470	HAT p300	Hsp90 chaperone	(221)
				cycle	
				Cycle	
	K558	K550	HAT p300	Hsp90 chaperone	(221)
				cycle	
Thiocarbamylation	C597	C589	STCA	Client	(227)
				degradation	
	G520	9521	C LYTTE A FE		(220)
	C529	C521	6-HITC-ME		(228)
Monomethylation	K209	K204	SMYD2	Myofilament	(188, 229)
-				organisation	
				organisanzon	
	K582	K574	SMYD2	Cancer cell	(230)
				proliferation	
	K539	K531	SMYD2	Cancer cell	(230)
				proliferation	
	17.64.7	17.005	CMANDO	11.00	(100 222
	K615	K607	SMYD2	Hsp90 co-	(188, 229,

				chaperone	231–233)
				binding;	
				Myofilament	
				organisation	
S-Nitrosylation	C597	C589	Nitric oxide	Hsp90 chaperone	(234, 235)
5 Titlosylation	(3)1	(230)	Titule Oxide		(234, 233)
				cycle	
SUMOylation	K191	K186	SUMO-1	Hsp90 co-	(60)
				chaperone	
				binding	
	K559	K551	SUMO peptidase		(236)
			sentrin/SUMO-		
			specific protease 2		
			(SENP2)		
Ubiquitination	K224	K219	CHIP		(237–239)
Colquitilation	K224	K219	Cim		(231-237)
	K112	K107	CHIP	DNA damage	(237, 238,
				bypass	240)
					ŕ
	K283	K275	CHIP		(237–239)
	K209	K204	CHIP		(237–239)
	K292	K284	CHIP		(237–239)
					/
	K407	K399	CHIP		(237–239)
	R355	K347	CHIP		(237)
	K485	K477	CHIP		(237, 238)
	12703	137//			(231, 230)

	K546	K538	CHIP	DNA damage	(237, 238,
				bypass	240)
	K558	K550	CHIP		(237, 238)
	K631	K623	СНІР		(237, 238,
					241)
	K489	K481	CHIP		(237–239)
	K615	K607	CHIP		(237, 238,
					242)
O-GlcNAcylation	S442	S434			(243)
	S460	S452			(243)
Nitration	Y38	Y33		Apoptosis;	(244, 245)
				Mitochondrial	
				metabolism	
	Y61	Y56		Apoptosis	(244)

1.10 DNA repair by Homologous recombination

Eukaryotic cells employ various mechanisms for the repair of breaks in the DNA such as BER, HR, NHEJ, and NER. In mammalian cells, the most common mechanism employed to repair DSBs is NHEJ. However, unlike mammalian cells, lower eukaryotes such as yeast employ HR as the preferred means to repair double strand DNA breaks as the three major proteins involved in NHEJ, namely DNA-PKcs, Artemis and BRCA1 are missing in yeast. The formation of a double

strand DNA break in yeast leads to the recruitment of sensor proteins such as Rad17, Rad24, Ddc1 and Mec3 along with signal transducers such as Rad53, Mec1/Ddc2 and Dun1. This is followed by the formation of a PCNA-like complex known as the 9-1-1 complex which includes Rad17/Mec3/Ddc1 and form a clamp-like structure at the DNA break site (246). This leads to the activation of Tell which is the yeast ortholog of the human ATM and Mec1 which is the yeast ortholog of the human ATR. the checkpoint kinases CHK11 and CHK2 are hyperphosphorylated by Tell and Mec1. Since CHK1 and CHK2 regulate the DNA damage checkpoint, they arrest the progression of the cell cycle until the DNA damage is repaired (247). The recruitment of the MRX complex (MRN in humans) to the DSB site initiates the recruitment of the 5' exonuclease, Sae2 (CtIP in humans) which leads to the initial resectioning of the 5' ends which is then completed by Exo1 to produce 3' single strand DNA overhangs (248-250). These single strand DNA overhangs are recognized and bound by the single strand DNA binding protein known as replication protein A (RPA). Rad51 replaces RPA with the help of Rad51 epistatic group of proteins such as Rad52 (BRCA2 in humans) which physically interacts with Rad51, RPA and ssDNA and facilitate the exchange of RPA with Rad51 at the resectioned ssDNA overhangs. Another group of mediator proteins include the Rad51 paralogs, Rad54 and Rad57 (Rad51B, Rad51C, Rad51D, XRCC2 and XRCC3 in humans) which form a heterodimer that can interact and stabilize the Rad51 nucleofilament and further helps in the Rad51 mediated strand exchange (248, 251, 252). Once the Rad51 nucleofilament is formed and stabilized, the next step in the HR mediated DNA repair pathway is homology search and strand invasion (251, 252). Rad54 is the motor protein that facilitates strand invasion by the Rad51 nucleo-filament in an ATP dependent manner to form the intermediate D-loop structure followed by the formation of the double Holliday junction (251–253). The double Holliday junction is then resolved into crossover/non

crossover products by the Sgs1-Top3-Rmi1 dissolvasome complex which consists of a RecQ helicase, Sgs1 (BLM in humans), type IA topoisomerase Top3 (TopoIIIα in humans) and the topoisomerase accessory factor Rmi1 (254). The recombination process is negatively regulated by Srs2, which is an anti recombinosome and prevents Rad51 nucleofilament formation (255). This process of DNA repair by HR is majorly conserved across species and is important for maintaining genomic integrity (256).

1.11 Hsp90 in homologous recombination mediated DNA repair

In our lab, studies have revealed that Hsp90 inhibition using inhibitors like 17AAG or by using the mutant Hsp90^{iG170D} leads to a reduction in the protein levels of Chl1, Rad51 and Rad52 (162, 164). These proteins were found to be dependent on Hsp90 for their stability and activation and under Hsp90 limiting conditions; these proteins underwent proteasomal degradation and hence were established as Hsp90 clients (162, 164). Furthermore, during DNA damaging conditions it was observed that Hsp90 displayed a dynamic interaction with Rad51 and perturbation of this dynamic interaction lead to severe DNA damage sensitivity in the cells (257).

Since many of Hsp90 clients belong to the DNA repair family, there was an indication of a potential function of Hsp90 in DNA repair. Studies have been done with mammalian cells which suggest the direct involvement of Hsp90 in DNA repair. In a study it was observed that when a DNA damage response was triggered using short double strand DNA molecules called Dbait 32 Hc(258), mammalian Hsp90 α was phosphorylated at the Thr7 residue by phosphatidylinositol-3-kinases such as DNA-PKcs which is also responsible for the phosphorylation of γ H2AX histone during the DNA damage response pathway (185). These two phosphorylation events were found

to have similar kinetics and the phosphorylated form of Hsp90 α was found to be recruited at the DNA break sites along with γ H2AX histone (185). Another study done using mouse embryonic fibroblasts (MEF) showed that mammalian Hsp90 α gets phosphorylated at the Thr5 and Thr7 residues in response to ionizing radiation. This phosphorylation event is primarily governed by ATM immediately after the cells are exposed to IR (181). It was also observed that only the nuclear localized Hsp90 α and not the cytoplasmic pool is phosphorylated by ATM in response to IR (181). It was furthermore shown that the deletion of Hsp90 α sensitized the MEF cells to IR (181).

However, in lower eukaryotes like *Saccharomyces cerevisiae*, the first 14 amino acids which are present in mammalian Hsp90α are absent in yeast Hsp82, thus the Thr5 and Thr7 residues are absent. Furthermore, yeast does not contain DNA-PKcs which has been shown in mammalian system to have a function of phosphorylating Hsp90α. In addition, Tel1, which is the yeast ortholog of ATM, does not have any reported function of Hsp82 phosphorylation. Since DNA repair mechanisms as well as Hsp90 structure and function are conserved from lower to higher eukaryotes, it is important to determine whether there is any conserved function of Hsp90 in DNA repair even in lower eukaryotes such as yeast.

1.12 Objectives of the study

Previous study from our lab demonstrated that Hsp90 provides clientship to Rad51, Rad52 and Chl1, the critical proteins which are crucial for the HR mediated DNA repair. However, whether Hsp90 directly regulates the nuclear function of Rad51 remains elusive. Our lab identified a separation of function mutant of Hsp90 which had no effect on Rad51 stability but it substantially reduces the formation of Rad51 foci in the nucleus in response to MMS treatment, which is a hallmark of HR mediated DNA repair. We hypothesize that Hsp90 acts as a positive regulator of HR mediated DNA repair pathway.

The main objective of my research is to decipher how Hsp90 controls the HR mediated DNA repair pathway. Using *Saccharomyces cerevisiae* as a model organism, we have addressed three important questions which has helped to decipher the potential function of Hsp90 in HR mediated DNA repair pathway. My study establishes that the dynamic interaction between Rad51 and Hsp90 is important for the nuclear function of Rad51 in the presence of genotoxic stress. Further, we have shown that Hsp90 is redistributed to the nucleus in the presence of DNA damage and is also associated to the damaged chromatin. We have identified that the nuclear import of Hsp90 is dependent on one of its co-chaperones Aha1.

SPECIFIC AIMS

1.13 Specific Aims

In our study, we have asked the following three main questions:

Q1. Whether yHsp90α regulates the nuclear function of Rad51 during DNA repair?

We will determine whether the physical association between Hsp90 and Rad51 play any regulatory role in the DNA damage induced Rad51 function. Using the wild-type Rad51 and a HR deficient Rad51 mutant Rad51^{E108L}, we have established that DNA damage induced dissociation between Rad51 and Hsp90 is one of the prerequisites for nuclear function of Rad51.

Q2. Whether $yHsp90\alpha$ is imported to the nucleus during genotoxic stress and recruited to the damaged chromatin?

To identify whether Hsp90 plays a direct role in HR mediated DNA repair, the chaperone should be present in the nucleus under such condition and physically be associated with the damaged chromatin. Using various DNA damaging agents we have established that Hsp90 is translocated to the nucleus during genotoxic stress and also recruited to the damaged chromatin in response to double strand break created in the chromosome.

Q3. What is the mechanism of the nuclear import of yHsp90α during DNA repair?

Using various N-terminal as well as CL deletion mutants we have established that Aha1 dependant conformational flexibility of Hsp90 is essential for its nuclear import during the condition of genotoxic stress.

Materials and Methods

2.1 Molecular Biology Techniques

2.1.1 Bacterial competent cell preparation

A single bacterial colony was inoculated in LB media and incubated at 37°C, overnight in a shaker incubator. Next day, 500 μl of primary culture was inoculated in 25 ml of LB media and the secondary culture was incubated at 37°C till the OD₆₀₀ reached 0.5. Cells were then harvested by centrifuging the culture at 8,000 rpm, 4°C, for 8 mins. The supernatant was discarded and the pellet was very gently re-suspended in 12.5 ml of sterile, ice-cold 0.1M CaCl₂ solution. The suspension was centrifuged at 8,000 rpm, 4°C for 8 mins and the supernatant was discarded. The pellet was again re-suspended in 12.5 ml of ice-cold 0.1M CaCl₂ and incubated on ice for 4-8 hrs to make cells competent. The cells were harvested by centrifuging the culture at 8,000 rpm, 4°C, for 8 mins. The pellet was re-suspended in 1.070 ml of ice-cold 0.1M CaCl₂ and 170 μl of sterile glycerol. The cell suspension was then divided into 100 μl aliquots in pre-chilled microfuge tubes, frozen in liquid nitrogen and kept at -80°C.

2.1.2 Bacterial transformation

Approximately 100 ng of DNA was added on the top layer of competent cells and kept on ice for 30 mins. Cells were exposed to heat shock at 42°C for 60 s and immediately chilled on ice for 2-3 mins. 900µl of Luria Broth was added to the cells and kept at 37°C shaker incubator for 1 hr. The cells were then centrifuged at 10,000 rpm for 2 mins and most of the supernatant was discarded. The pellet was re-suspended in the remaining supernatant and spread on Luria agar plate containing appropriate antibiotic. Plates were incubated at 37°C for 12-16 hrs.

2.1.3 Bacterial plasmid DNA isolation by alkaline lysis method

Bacterial cells harbouring the required plasmid were inoculated in 10 ml of LB medium and incubated overnight at 37°C, 200 rpm. The cells were harvested the next day by centrifugation at 4,000 rpm for 15 mins. The cell pellet was re-suspended in 400 ul of solution I (Tris 25 mM pH 8, EDTA 10 mM) and was transferred to a 2 ml micro-centrifuge tube. 400 µl of solution II (0.2 N NaOH, 1% SDS) was added to the tube and mixed well by inverting 4-5 times and incubated for less than 5 mins at RT. Subsequently, 300 µl of ice cold solution III (3 M sodium acetate) was added to the tube and incubated on ice for 5 mins with intermittent mixing. It was then centrifuged at 12,000 rpm for 15 mins at RT and the supernatant was collected in a 1.5 ml tube. The supernatant was then mixed with 2.2 volume of absolute alcohol and kept at - 20°C for 45 mins for precipitation. After incubation at -20°C, the sample was centrifuged at 12,000 rpm at 4°C to precipitate the DNA. The pellet was washed with 70 % alcohol and resuspended in 50 μl of 1X Tris-EDTA buffer. For removing RNA from the sample, 2-3 µl of 100 mg/ml RNase was added to the sample and kept at 37°C for 20 mins. Then, equal volume of PCIA was added and mixed well by vortexing for 3 mins. Subsequently, centrifuged at 12,000 rpm for 15 mins at RT and the upper aqueous layer containing DNA was taken out in micro-centrifuge tube. DNA was then precipitated by adding 2.2 volumes of 100% ethanol and 1/10th volume of solution III and placed at -80°C for 2 hrs. Plasmid was precipitated by centrifuging sample at 12,000 rpm, 4°C. Plasmid DNA was then washed with 70% alcohol by centrifuging for 5 min at 12,000 rpm, 4°C. The pellet containing plasmid was air-dried and re-suspended in 30 µl 1X TE buffer.

2.1.4 Site-directed mutagenesis

The CL deletion mutants, $hsp82\Delta(211-242)$ and human $hsp90\alpha\Delta(224-279)$ -FLAG were created using splice overlap extension PCR. To generate the $hsp82\Delta(211-242)$ deletion mutant, yeast genomic DNA was used as a template, and the full-length gene was amplified in two fragments to delete the desired region. For amplifying the first and second fragments, primer sets OSB21/OSB537 and OSB538/OSB22 were used respectively. Finally, $hsp82\Delta(211-242)$ deletion was generated by annealing the first two PCR products followed by a third PCR using the primer set OSB21/OSB22. To generate the human $hsp90\alpha\Delta(224-279)$ deletion mutant, the full-length gene was amplified as two fragments one using primer set OSB531/OSB533 and the other using OSB534/OSB539 primer pair. The two PCR products were denatured, allowed to hybridize with each other and subsequently amplified using the primer pair OSB531/OSB539 to create human $hsp90\alpha\Delta(224-279)$ deletion. To create the human $T7Ahsp90\alpha$ mutant by site directed mutagenesis, pcDNA3.1+/C-(K)-DYK vector was used as a template along with the primer set OSB535/OSB539. The codon ACC was changed to GCT within the primer OSB535 to create the human $T7Ahsp90\alpha$ mutant. All the mutants were confirmed by sequencing.

2.1.5 Plasmid DNA subcloning

Full length HSP82, AHA1 and RAD51 were amplified using the primer pairs OSB21/OSB22, OSB215/OSB216 and OMKB90/OMKB88 respectively and individually cloned in the 2μ vector pTA between the BamH1 and the Sal1 restriction sites to create pTA-HSP82, pTA-AHA1 and pTA-RAD51 respectively. Full length HSP82 was also cloned in pHCA vector between the BamH1 and the Sal1 restriction sites to create pHCA-HSP82. We purchased the mammalian expression vector pcDNA3.1+/C-(K)-DYK from GenScript, USA, which harbors full length human $HsHSP90\alpha$ with C-terminal FLAG tag. We amplified $HsHSP90\alpha$ -FLAG using the primer pairs OSB531/OSB539 and subcloned in the centromeric pHCA vector (259)between the BamH1

and the SalI restriction sites. Two mutants of $HsHsp90\alpha$ namely $hsp90\alpha T7A$ and the CL deletion mutant $hsp90\alpha\Delta(224-279)$ were generated by splice overlap extension (SOE) and ultimately subcloned in pHCA with C-terminal FLAG tag. The CL deletion mutant $hsp82\Delta(211-259)$ was amplified using the genomic DNA isolated from HH1a-p2HG/hsp82\(\Delta(211-259)\) strain(164, 260) with the primer pairs OSB21/OSB22. It was subsequently subcloned into pTA orpHCA vector within the BamHI and SalI restriction sites. Hsp82 deletion mutant hsp82Δ(211-242) was generated by SOE and subsequently subcloned in pHCA within the BamHI and SalI restriction sites to create pHCA-hsp82(\(\Delta 211-242\)). In order to create GFP-Hsp82 fusion constructs, GFP was first amplified from the plasmid, p2U/S65T using the primer pair OSB517/OSB518 and subcloned within the BamH1 restriction site, which is present in the N-terminal end of HSP82, $hsp82\Delta(211-259)$ and $hsp82\Delta(211-242)$. The orientation of GFP was checked using PstI pHCA- $GFPhsp82\Delta(211$ -259), digestion pHCA-GFPHSP82, create pHCA-GFPhsp82∆(211-242) fusion constructs, where GFP is fused at the N-terminal end of Hsp82 in all the cases. DNA sequencing (Eurofins) was done to confirm the cloning.

2.2 Methods in yeast genetics

2.2.1 Yeast transformation

Yeast cells were grown overnight in 5 ml of respected media at 30°C shaker incubator for obtaining the primary culture. Next day, the primary culture was used to inoculate the secondary culture for a final absorbance of 0.6-0.8 in 40 ml medium. The culture was incubated at 30°C till the OD₆₀₀ reached 0.6-0.8. The culture was then harvested by centrifugation at 3500 rpm for 5 mins and the cell pellet was washed with 10 ml sterilized water. Washed cells were finally resuspended in 300 µl Lithium solution (1X TE, 1X Lithium Acetate) to make them competent.

(0.5-1) μg of DNA was mixed with 10 μg of carrier in a tube and 200 μl of competent yeast cells were added gently over the DNA mixture in each transformation tube. 10 μg of carrier DNA in a tube with 200 μl of competent cells was taken as negative control. Next, 1.2 ml of PEG solution [10X LiOAc (Sigma), 10X TE, 50% PEG 2000 (Sigma)] was added and it was incubated at 30 °C for 30 mins with shaking. After that cells were exposed to heat shock at 42°C, 15 mins followed by incubation on ice for 5 mins. The cells were then collected by centrifugation at 10,000 rpm for 10 s. The pellet was re-suspended in 200 μl 1X Tris-EDTA buffer and then spread on appropriate plates. The plates were incubated at 30°C till transformed colonies were observed.

2.2.2 Gene tagging and gene knockout

In *W303a* yeast background, *SBA1* and *CDC37* genes were *MYC* tagged by homologous recombination using *HIS* cassettes(261) flanked by 40 bp homologous sequencespresent upstream and downstream of the stop codons of the respective genes to create the *MYC* tagged *SBA1* and *CDC37* strains namely, *NFY14* and *NFY15* respectively. For creating *NFY14* strain, the homologous sequence was added in the primers (OSB389 and OSB390) used for amplifying the *HIS* cassette from *pFA6a-His-Myc* plasmid. This cassette was then transformed into *W303a* strain and the cells were grown in a histidine drop out medium. The *MYC* tagging of *SBA1* was confirmed by PCR using the primer pairs OSB391 and OSB390. For creating *NFY15* strain, the homologous sequence was added in the primers (OSB398 and OSB399) used for amplifying the *HIS* cassette from *pFA6a-His-Myc* plasmid. This cassette was then transformed into *W303a* strain and the cells were grown in a histidine drop out medium. The *MYC* tagging of *CDC37* was confirmed by PCR using the primer pairs OSB400 and OSB399. *P82a*harboring wild-type *HSP82* expressing vector (*TRP*) was transformed with centromeric *pHCA-hsp82*Δ(211-242)

plasmid and the transformed strain was grown in histidine drop out complete medium to generate *KRAY16* strain, where the *HSP82* was replaced by the mutant by plasmid shuffling. In *W303a* yeast background, *AHA1* gene was knocked out by homologous recombination using a *HIS* cassette (261) flanked by 40 bp homologous sequence of the upstream and downstream regions of the *AHA1* gene to create the strain *NFY24*. The homologous sequence was added in the primers (OSB273 and OSB274) used for amplifying the *HIS* cassette from *pFA6a-His* plasmid. This cassette was then transformed into *W303a* strain and the cells were grown in a histidine drop out medium. The knockout was confirmed by PCR using the primer pairs OSB275 and OSB274.

2.2.3 Real-time RT-PCR

W303α strain was grown at 30°C till the OD₆₀₀ reaches to 0.5. It was subsequently exposed to 0.15% MMS for 2 hrs. Total RNA was isolated from the untreated and MMS treated cells using the acid phenol method as described previously (164). Further cDNA was synthesized using the reverse transcriptase enzyme (Omni Script; Qiagen, Hilden, Germany) as described previously (164). The primer-pair, OSB 14 and OSB 16 was used to amplify 307 bp at the 3' end of ACT1. In order to amplify 326 bp at the 3' end of RAD51, the primer-pair OSB 44 and OSB 45 was used. Similarly, to amplify 291 bp at the 3' end of AHA1 transcript the primer-pair OSB 216 and OSB 394 was used. Finally, to amplify 276 bp at the 3' end of SBA1, the primer-pair OSB 391 and OSB 445 was used. For RT-PCR, cDNA was diluted (1:50) and used for PCR using a Takara TB Green RT-PCR kit as described earlier (164). GraphPad Prism 6 software was used to plot the mean values (±SD) from independent experiment sets.

2.3 Yeast Cell biology methods

2.3.1 Fluorescence imaging

GFP fluorescence imaging was done using the strains NFY31, NFY32, NFY33, and NFY35as described earlier (262). Typically, the cells were grown till 0.5 OD₆₀₀ in selective media. Half batch of cells were treated with 0.15% of MMS and grown for 2 h along with the untreated batch of cells. NFY31 was additionally treated with 15 µg/ml of Nocodazole (Cell Signalling Technology) for 2 hrs. Nocodazole-induced cell cycle arrest at G2/M was confirmed by visualization of large number of dumbbell-shaped budding cells under the microscope. Subsequently, the cells were harvested and washed with Milli-O water. The cells were then treated with 70% ethanol for 1 min at 30°C with shaking and were again washed with water. The cells were resuspended in 100 µl of water and the nuclei of the live cells were stained using Hoechst 33342 (Thermo Fisher Scientific) stain at a concentration of 20 µg/ml for 10 min. The cells were mounted on glass slides using 25 % glycerol and were visualized under the 100X objective using a Nikon Eclipse (Ni-E AR) upright fluorescence microscope. The images were captured, using monochrome camera (Andor), which were subsequently processed and deconvoluted using NIS elements Advanced Research software (TOWA OPTICS PRIVATE LIMITED). Three independent sets of experiments were performed and more than 100 cells per condition were analysed. The results represent mean \pm SD.

2.3.2 Indirect immunofluorescence assay

W303a strain was grown in YPD media till 0.5 OD600 and half batch of cells were treated with 0.15% MMS and both the batches were grown for additional two hrs. The cells were washed and fixed using 4% formaldehyde for 2 hrs. 107 – 108 cells were taken and washed with 1XPBS (containing 1mM DTT and 0.5mM PMSF). The cells were resuspended in spheroplast buffer

(18.2% Sorbitol, 1% Glucose, 0.2% Yeast Nitrogen Base, 0.2% Casamino acids, 25 mM HEPES pH 7.4, 50 mM Tris, 1 mM DTT) containing YPDS (YPD, 1M sorbitol) and Lyticase. The cells were then incubated for 1.5 hrs at 30°C with gentle shaking for spheroplasts to form. The slides were meanwhile prepared by coating each well with 0.1% poly L lysine and incubated for more than 20 mins at RT. Extra liquid was removed by aspiration and the wells were dried completely. The fixed yeast spheroplasts were then loaded into each well and allowed to settle for 20 mins. Extra liquid was aspirated and the wells were washed with 1X PBS for 5 mins. Permeabilization of the cell membrane of the fixed yeast cells was done with a 1:3 mixture of acetone and methanol for 15 mins. After washing with 1X PBS, the wells were blocked using 3% BSA for 1.5 hrs. The liquid was aspirated and 1:50 dilution of rabbit anti-Aha1 primary antibody (Invitrogen) diluted in 3% BSA was added to each well and incubated at 37°C for 1 hr. After incubation, the extra liquid was aspirated and the wells were washed subsequently with 1X PBS, 1X PBST and 1X PBS for 15 mins each at 37°C. To each well, 1:250 dilution of the secondary antibody, Goat anti-Rabbit IgG (H+L) Cross-Adsorbed Secondary Antibody, Alexa Fluor™ 488 (Life Technologies) diluted in 3% BSA along with 10 µg/ml Hoechst 33342 vital stain (Thermo Fisher Scientific), was added and the slides were incubated at 37°C for 45 mins. All the liquid was then aspirated and the slides were allowed to dry completely after which the samples were mounted using gold antifade (Thermo Fisher Scientific) and the slides were visualized under the 100X objective using a Nikon Eclipse (Ni-E AR) upright fluorescence microscope. The images were captured using monochrome camera (Andor), which were subsequently processed and deconvoluted using the NIS elements Advanced Researchsoftware (TOWA OPTICS PRIVATE LIMITED). Three independent sets of experiments were performed and more than 100 cells per

condition were analysed. The results represent mean \pm SD. The two-tailed Student's t test was used to calculate P values.

2.4 Biochemical methods

2.4.1 Protein isolation

Yeast cells were inoculated in 5 ml of appropriate medium and grown overnight at 30°C at 200 rpm. Overnight grown culture was inoculated into fresh 20 ml of appropriate media and grown till the OD₆₀₀ reached 0.5. Cells were harvested by centrifuging the secondary culture at 3000 rpm for 5 mins. Pellet was washed in 500 μl of autoclaved water followed by a TCA wash. The supernatant was removed and the pellet resuspended in TCA. Glass beads were then added in the sample and vortexed thoroughly. Supernatant containing protein was taken in a new 1.5 ml microfuge tube. The mixture of cells and glass beads was washed with TCA by vortexing with intermittent cooling on ice and the supernatant was again collected into the same tube. Sample was centrifuged and the supernatant was discarded. The precipitated protein was dissolved in 60 μl 1X sample buffer (Tris-HCl, pH 6.8, 2% SDS and bromophenol blue). The sample was then boiled for 3-5 mins and centrifuged at top speed for 5 min and then subjected to western blot analysis.

2.4.2 Cellular Fractionation

The nuclear fractionation was done with wild-type, NA14(263), $\Delta sba1$ (SLY6), $\Delta aha1$ (NFY24) and tscdc37S14A strains (grown at restrictive temperature 37°C). Similar fractionations were also performed with the strains carrying wild type $HsHsp90\alpha$ -FLAG (KRAY15) and that carrying the human $hsp90\alpha T7A$ -FLAG (KRAY17) and human $hsp90\alpha \Delta(224-279)$ -FLAG (KRAY18). To

measure whether the nuclear level of yHSP90α depends on Aha1, we did nuclear fractionation of $\Delta ahal$ strain carrying empty plasmid (NFY26) and that carrying AHAl over-expression plasmid (NFY27). Finally, various mutants of hsp82 namely; $HH1a-p2HG/hsp82\Delta(211-259)$, T101Ihsp82, $hsp82\Delta(211-242)$ (KRAY16) and the isogenic control strain P82a were also subjected to nuclear fractionation. Typically, cells were grown till 0.5 OD₆₀₀ in selective media. Half batch of cells were treated with 0.15% of MMS and continuously grown at 30°C for 2 hrs along with the untreated batch of cells. In NA14 strain, DNA damage was induced as a specific double strand DNA break at an HO restriction site by inducing HO endonuclease within the cell using 3% Galactose (263). After DNA damage 100 OD₆₀₀ cells were harvested and washed with PBS containing DTT and PMSF. In each case, cells were then incubated with spheroplast buffer (18.2% Sorbitol, 1% Glucose, 0.2% Yeast Nitrogen Base, 0.2% Casamino acids, 25 mM HEPES pH 7.4, 50 mM Tris, 1 mM DTT) for 15 mins at 30°C with gentle shaking. After incubation, cells were re-suspended in spheroplast buffer containing YPDS (YPD, 1M Sorbitol) and lyticase enzyme. It was then allowed to grow at 30°C with gentle shaking for 1.5 hrs. Again, YPDS was added into spheroplast and spun at 4000 rpm for 10 mins. Washing of the spheroplast was performed with ice cold YPDS followed by spinning at 4000 rpm for 5 mins. Spheroplast was resuspended in ice-cold sorbitol and spun at 4000 rpm for 5 mins. Ultimately the spheroplast was re-suspended in 5 ml of Buffer N (25 mM K₂SO₄, 30 mM HEPES pH 7.6, 5 mM MgSO₄, 1 mM EDTA, 10% Glycerol, 0.5% NP40, 3 mM DTT, 1% protease inhibitor cocktail) and homogenized by giving 20 strokes under chilled condition. Homogenized spheroplast was spun at 2000 rpm at 4°C for 15-20 mins to pellet down the cell debris. The nuclei were pelleted down at 6000 rpm for 25 mins at 4°C. This nuclear fraction sample was then re-suspended in 50 µl of buffer N. The sample was then boiled for 10 mins and used for the western blotting analysis.

2.4.3 Coimmunoprecipitation

Wild-type and E108Lrad51 cells harboring yHsp90 over expression plasmid (under GPD promoter, 2µ vector) were grown to an OD₆₀₀ of 0.5. 10 ml of each culture was harvested, resuspended in 1 ml spheroplast buffer (50 mM Tris-HCl [pH 8], 25 mM HEPES [pH 7.4], 0.2% Casamino Acids, 0.2% yeast nitrogen base [YNB], 1% glucose, 18.2% sorbitol) containing dithiothreitol (DTT) and Lyticase, and incubated at 30°C for 90 min. Subsequently, glass beads were added and the cells were intermittently vortexed and incubated on ice six times for a period of 30 s each. An anti-Rad51 antibody was added to the supernatant for overnight incubation at 4°C. Protein A Agarose (25%; Calbiochem) was added, and the mixture was incubated for 2 hr at RT. The beads were then spun down for 15 s at 1,000 rpm, and the pellet was washed 3 times with NETNS buffer (20 mM Tris-HCl [pH 8], 1 mM EDTA, 1M NaCl, 0.5% [vol/vol] NP-40 with protease inhibitor) and twice with NETN buffer (20 mM Tris-HCl [pH 8], 1 mM EDTA, 100 mM NaCl, 0.5% [vol/vol] NP-40 with protease inhibitor). The bound protein was eluted with 4X Laemmli buffer by boiling for 10 mins which was further spun down and the supernatant was collected and used for Western blotting. The proteins in the supernatant were precipitated using 20% Trichloroacetic acid and were eluted using 4X SDS loading dye containing dithiothreitol (DTT) and Tris (pH 8.8) and boiled for 10 mins. The sample was spun down and the proteins in the supernatant were used for Western blot analysis. After the coimmunoprecipitation we calculated the relative association of Hsp90 with Rad51 for each experiment using the formula given below:

Relative association of Hsp90 with Rad51 = (Hsp90 in the pellet/Hsp90 in the input) \div (Rad51 in the pellet/Rad51 in the input)

2.4.4 Western blotting

Protein samples obtained via protein extraction or coimmunoprecipitation or cellular fractionation studies were loaded on SDS polyacrylamide gel. Polyvinylidene difluoride (PVDF) membrane was used for the western which was pre-treated with methanol for 20 s followed by water wash then transfer buffer (Tris buffer, glycine, SDS and methanol) for 5 mins. Protein from gel was then transferred to pre-treated PVDF membrane. Subsequently, the blot was incubated with the blocking buffer (5 % nonfat milk powder dissolved in 1X TBS-T) for 2 hrs at RT. The blot was then incubated with the required primary antibodies for overnight at 4°C. Next day, the blot was washed with 1X TBS-T buffer (0.2 M Tris base, 9 % NaCl, pH 7.6, 0.1 % Tween-20). After washing, the, blot was incubated with appropriate secondary antibody for 2 hrs at RT followed by washing with TBS-T buffer.

2.4.5 MMS sensitivity assays

W303a, KRAY16, and HH1a- $p2HG/hsp82\Delta(211$ -259) strains were grown in YPD medium for overnight at 30°C. Next day, secondary culture was grown till 0.5 OD₆₀₀ at 30°C. After OD₆₀₀ reached to 0.5, the culture was divided into two sets. One set of cells was treated with 0.03 % (vol/vol) of MMS (Sigma Aldrich) and grown at 30°C for 2 hrs and another set was continuously grown at 30°C for 2 hrs without MMS. After that the cells were washed twice, serially diluted and 1000 cells of each culture were spread on YPD plates. The plates were incubated at 30°C for 40 hrs and the colonies obtained were counted in both treated and untreated conditions. Subsequently, the % survivability was calculated using the following formulae:

% survivability = [(Number of cells grown on MMS plate) / (Number of cells grown on untreated plate)] *100

2.4.6 Repair Kinetics of a single double strand DNA break

NA14 cells (263) were grown in YPD media in the presence of 3% glycerol till 0.3 at OD₆₀₀. 60 OD of cells were harvested (untreated or 0 h) and the remaining cells were treated with 3% galactose for different time points (1 h, 2 h, 3 h and 4 h). At each time point, 5 OD₆₀₀ of cells were harvested. The yeast cells were disrupted using 0.3 g glass beads and 200 μl breaking buffer [2% Triton X 100, 1% SDS, 10 mM NaCl, 10 mM Tris (pH 8), 1 mM EDTA (pH 8). The genomic DNA was subsequently extracted from the yeast cells using PCIA. The extracted genomic DNA was treated with RNase and resuspended in 30 μl 1X Tris-EDTA solution. The kinetics of a single double stranded break repair at the *HO* restriction site was monitored by PCR using the primers OSB289 and KanB1 which are specific to the upstream and downstream regions of the *HO* restriction site.

2.4.7 Chromatin immunoprecipitation

The strains, *NFY21*, *NFY22*, *NFY23*, *NFY25* and *KRAY19* were grown in the selective media without tryptophan till 0.3 at OD₆₀₀ in presence of 3% glycerol. 60 OD₆₀₀ of cell was taken out and treated with 1% formaldehyde for 15 mins (untreated or 0 h) and the remaining cells were treated with 3% galactose for different time points (1 h, 2 h, 3 h and 4 h). At each time point, 60 OD₆₀₀ of cells were taken out and treated with 1% formaldehyde for 15 mins each. Formaldehyde mediated protein crosslinking was stopped using 2.5 M glycine. After formaldehyde treatment, each set of cells were harvested and washed with 1 X PBS. ChIP assay was performed for each set of cells as described earlier (135). Pull down was done with each set using 10 μg anti-Hsp90 antibody (Calbiochem), 10 μg anti-Rad51 antibody (Abcam), 10 μg anti-Aha1 antibody (Abcam) and 10 μg anti-GFP antibody (Abcam) to precipitate HSP90α, Rad51,

Aha1 and GFP bound DNA fragments respectively at each time point. Recruitment of HSP90α, Rad51 and Aha1 were then monitored at the *HO* cleavage proximal site and up to -5 kb distal position by PCR using the immune precipitate and input DNA samples for each time point. Recruitment near the broken region was studied by subjecting the samples to PCR using the primers OSB519 and OSB520 while recruitment to the 1 kb, 2 kb, 3 kb, 4 kb and 5 kb away from the *HO* cleavage side towards the left direction were measured using the primers OSB567/OSB568, OSB569/OSB570, OSB571/OSB572, OSB573/OSB574 and OSB575/OSB576, respectively. Samples were subjected to electrophoresis on 2 % agarose. For a negative control, ChIP was performed with IgG antibody. We amplified 300 bp at the 3' end of *ACT1* using OSB14 and OSB16 (259), which was used as a normalization control.

Table 2. Yeast strains used in this study

Strain	Genotype	Source
W303a	MATa 15 ade2-1 ura3-1,112 his3-11 trp1 leu2-3	This study
NFY14	MATa 15ade2-1 ura3-1,112 his3-11 trp1 leu2-3, SBA1- 13MYC-HIS3MX6	This study
NFY15	MATa 15ade2-1 ura3-1,112 his3-11 trp1 leu2-3, CDC37- 13MYC-HIS3MX6	This study
NA14	MATa -inc ura3-HOcs lys2::ura3-HOcs-i nc ade3:: GALHO ade2-1 leu2-3112 his3-11,15 trp1-1 can1-100	(263)
KRAY19	MATa -inc ura3-HOcs lys2::ura3-HOcs-i nc ade3:: GALHO ade2-1 leu2-3112 his3-11,15 trp1-1 can1-100, AHA1-2μ-TRP [pTA/AHA1]	This study

NFY21	MATa -inc ura3-HOcs lys2::ura3-HOcs-i nc ade3:: GALHO ade2-1 leu2-3112 his3-11,15 trp1-1 can1-100 HSP82-2μ- TRP [pTA/HSP82]	This study
NFY22	MATa -inc ura3-HOcs lys2::ura3-HOcs-i nc ade3:: GALHO ade2-1 leu2-3112 his3-11,15 trp1-1 can1-100, RAD51-2μ- TRP [pTA/RAD51]	This study
NFY23	MATa -inc ura3-HOcs lys2::ura3-HOcs-i nc ade3:: GALHO ade2-1 leu2-3112 his3-11,15 trp1-1 can1-100, GFP-HSP82- 2μ-TRP [pTA/GFP-HSP82]	This study
NFY25	MATa -inc ura3-HOcs lys2::ura3-HOcs-i nc ade3:: GALHO ade2-1 leu2-3112 his3-11,15 trp1-1 can1-100, GFP- hsp82Δ(211-259) -2μ-TRP [pTA/GFP- hsp82Δ(211-259)]	This study
NFY24	MATa 15ade2-1 ura3-1,112 his3-11 trp1 leu2-3 AHA1::HIS	This study
NFY 26	MATa 15ade2-1 ura3-1,112 his3-11 trp1 leu2-3 AHA1::HIS, 2μ-TRP[pTA]	This study
NFY27	MATa 15ade2-1 ura3-1,112 his3-11 trp1 leu2-3 AHA1::HIS, AHA1-2μ-TRP[pTA/AHA1]	This study
NFY31	MATa 15 ade2-1 ura3-1,112 his3-11 trp1 leu2-3, GFP- HSP82-CEN-HIS [pHCA/GFP-yHSP90α]	This study
NFY32	MATa his3Δ1 leu2Δ0 met15Δ0 ura3Δ0 aha1::kanMX4, GFP- HSP82-CEN-HIS [pHCA/GFP-HSP82]	This study
NFY33	MATa 15 ade2-1 ura3-1,112 his3-11 trp1 leu2-3, GFP-	This study

	hsp82Δ(211-259) -CEN-HIS [pHCA/GFP-hsp82Δ(211-259)]	
NFY35	MATa can1-100 ade2-1 his3-11,15 leu2-3,112 trp1 ura3-1 hsp82::LEU2 hsc82::LEU2, GFP-hsp82Δ(211-242)-CEN- HIS [pHCA/GFP hsp82Δ(211-242)]	This study
SLY6	MATa 15ade2-1, ura3-1, 112 his 3-11, trp1, leu2-3, VII::ADE2 SBA1::KAN ^r	(259)
KRAY15	MATa 15ade2-1 ura3-1,112 his3-11 trp1 leu2-3, hHSP90α- FLAG-CEN-HIS [pHCA/hHSP90α-FLAG]	This study
KRAY16	MATa can1-100 ade2-1 his3-11,15 leu2-3,112 trp1 ura3-1 hsp82::LEU2 hsc82::LEU2, hsp82Δ(211-242)-CEN-HIS [pHCA/ hsp82Δ(211-242)]	This study
KRAY17	MATa 15ade2-1 ura3-1,112 his3-11 trp1 leu2-3, hT7Ahsp90α-FLAG-CEN-HIS [pHCA/hT7Ahsp90α-FLAG]	This study
KRAY18	MATa 15ade2-1 ura3-1,112 his3-11 trp1 leu2-3, Hshsp90αΔ(224-279)-FLAG-CEN-HIS [pHCA/hsp90αΔ(224-279)-FLAG]	This study
KRAY29	MATa can1-100 ade2-1 his3-11,15 leu2-3,112 trp1 ura3-1 hsp82::LEU2 hsc82::LEU2, HSP82-CEN-HIS [pHCA/HSP82], AHA1-FLAG-2μ-TRP [pTA/AHA1-FLAG]	This study
HH1a- p2HG/hsp82Δ(211- 259)	MATa hsp82::LEU2 hsc82::LEU2 ade2 his3 leu2 trp1 ura3, hsp82Δ(211-259)-2μ-HIS [p2HG/hsp82Δ(211-259)]	(260)
T101I	MATa can1-100 ade2-1 his3-11,15 leu2-3,112 trp1 ura3-1 hsp82::LEU2 hsc82::LEU2 CEN pTGPD/T3-138	(264)

P82a	MATa can1-100 ade2-1 his3-11,15 leu2-3,112 trp1 ura3-1 hsp82::LEU2 hsc82::LEU2 CEN pTGPD/P82	(264)
BY4741	MATa his3∆1 leu2∆0 met15∆0 ura3∆0 aha1::kanMX4	Open Biosystems

Table 3. Primers used in this study

Primer	g	n.
Name	Sequence	Purpose
OSB389	5'AGAAGATGAAGAAGAGGAAATAGAGCCGGAAGTGAAA	FP to MYC tag SBA1
	GCTCGGATCCCCGGGTTAATTAA 3'	
0.77.00		
OSB390	5'GTTACTCATTCTAGCACTCCAGGTTGATTTGCTCCT	RP to MYC tag SBA1
	CCTTGAATTCGAGCTCGTTTAAAC 3'	
OSB391	5' GATGAAGATGAACAAGACGAAG 3'	FP to confirm MYC
		tagged SBA1
OSB445	5' GACGTCGACTTAAGCTTTCACTTCCGGCTC 3'	RP to amplify 3' end
		of SBA1
OSB398	5'TAACCATGAAGAGGTCA ACATACTGCCGACAC	FP to MYC tag
	TGTTGACCGGATCCCCGGGTTAATTAA 3'	CDC37
	TOTTOACCOORTCCCCOOOTTAATTAAS	CDC37
OSB399	5'GTAGATGCACGCTGCACCAGTAAAATAGCTACA	RP to MYC tag
	TAAATTTGAATTCGAGCTCGTTTAAAC 3'	CDC37
OSB400	5' AAAAATGCAAGAAGCCATAATGAC 3'	FP to confirm MYC
		tagged CDC37

OSB273	5'TCTTATTCTTAATCGTTTATAGTAGCAACAATATATCAA TCGGATCCCCGGGTTAATTAA 3'	FP to knockout AHA1
OSB274	5'ATTTACGCATACTTTTATTGAAACATGAGAACAATATAT CGAATTCGAGCTCGTTTAAAC 3'	RP to knockout AHA1
OSB275	5' GTGTTACCCAGTTCACAATGG 3'	FP to confirm ∆aha1
OSB21	5'GACGGATCCATGGCTAGTGAAACTTTTGAATTTC 3'	FP to amplify full length HSP82
OSB22	5' CGGGTCGACCTAATCTACCTCTTCCATTTCGG 3'	RP to amplify full length HSP82
OSB215	5'ATCGGATCCATGGTCGTGAAAACCCAAATAAC 3'	FP to amplify full length AHA1
OSB216	5' GTCGTCGACTTATAATACGGCACCAAAGCCG 3'	RP to amplify full length AHA1
OSB394	5'CTG GAG ACC AAA GAA AAA TTC G	FP to amplify ~300bp of 3' end of AHA1
OMKB90	5'GGATCCTGTCTCAAGTTCAAGAAC 3'	FP to amplify full length RAD51
OMKB88	5' CTG CAG CTA CTC GTC TTC TC 3'	RP to amplify full length RAD51
OSB531	5' GACGGATCCATGCCTGAGGAAACCCAGAC 3'	FP to amplify full length $hHSP90\alpha$ - $FLAG$

OSB539	5'GACGTCGACTTATCACTTATCGTCGTCATCC3'	RP to amplify full
		length hHSP90α-
		FLAG
OSB535	5'GACGGATCCATGCCTGAGGAAACCCAGGCTCAAGAC 3'	FP to create
OSDSSS	5 GACGGATCCATGCCTGAGGAAACCCAGGCTCAAGAC 5	
		hT7Ahsp90α
		mutation
OSB517	5' GCAGGATCCATGAGTAAAGGAGAAGAAC 3'	FP to amplify full
		length GFP
OSB518	5'GCAGGATCCCTGCAGCTTGTATAGTTCATCCTAG 3'	RP to amplify full
		length GFP
		lengar of r
OSB537	5'TCGACTTCTTCCAATTTGGTGACGACTAATTGGATTGGGT	RP to create
	AGG3'	han 924/211 242)
	AGUS	hsp82∆(211-242)
		mutation
0.000.000		
OSB538	5'CCAATTAGTCGTCACCAAATTGGAAGAAGTCGATGA	FP to create
	AGAAG 3'	hsp82∆(211-242)
		mutation
OSB533	5'ATGTACTTTTCCTTAATCTCCACAAAAAGAGTAATGGGAT	RP to create human
	ATC 3'	hsp90α∆(224-279)
		,
		mutation
OSB534	5'TACTCTTTTTGTGGAGATTAAGGAAAAGTACATCGATCAA	FP to create human
030334		
	G3'	hsp90α∆(224-279)
		mutation
OSB289	5' GTTAGTTGAAGCATTAGGTCC 3'	FP to study repair
		kinetics of a single

		DSB at HO site
KanB1	5' TGTACGGGCGACAGTCACAT 3'	RP to study repair kinetics of a single DSB at HO site
OSB519	5' ATGTCGAAAGCTACATATAAG 3'	FP used to study recruitment at the HO cleavage site
OSB520	5' AATGCTTCAACTAACTCCAG 3'	RP used to study recruitment at the HO cleavage site
OSB14	5' TTAGAAACACTTGTGGTGAACG 3'	RP to amplify ACT1
OSB16	5' TGACCAAACTACTTACAACTCC 3'	FP to amplify 307 base pair of 3' end of ACT1
OSB567	5' GGAGAATCCATACAAGAAATCG 3'	FP to amplify -1 kb upstream of HO site
OSB568	5' CATCTCATTAGTTGGAATTTCG 3'	RP to amplify -1 kb upstream of HO site
OSB569	5' TTTGGTAGATCATTTAAGGGTC 3'	FP to amplify -2 kb upstream of HO site
OSB570	5' CAGGAGATGGCTTAGGCAAG 3'	RP to amplify -2 kb upstream of <i>HO</i> site

MATERIALS AND METHODS

OSB571	5' TTTCATTGCTTCCGACTCCG 3'	FP to amplify -3 kb
		upstream of HO site
OSB572	5' TACGCAGACGAGAAGGCTTC 3'	RP to amplify -3 kb
		upstream of HO site
OSB573	5' ATTGAAGGCCGATACAATTGG 3'	FP to amplify -4 kb
		upstream of HO site
OSB574	5' GGATCCTGGAATTTGATCTTG 3'	RP to amplify -4 kb
		upstream of HO site
OSB575	5' ATATTGGCATAAGAGGTAAACC 3'	FP to amplify -5 kb
		upstream of HO site
OSB576	5' TTTATTGTCTATGGTTTACAAGC 3'	RP to amplify -5 kb
		upstream of HO site
OSB44	5' GTGGTGAACTAAGCGCAAG 3'	FPto amplify 326 bp
		of the 3' end of
		RAD51
OSB45	5' CTACTCGTCTTCTCTGG 3'	RPto amplify 326 bp
		of the 3' end of
		RAD51

Specific Aim 1: To study whether yHsp90α regulates the nuclear function of Rad51 during DNA repair

3.1 Introduction

Previous studies in our lab have found Rad51 to be a direct client of γHsp90α since it depends on yHsp90α for its stability and undergoes proteasomal degradation upon the inhibition of yHsp90α (164). Studies in our lab have also characterised a separation of function mutant of yHsp90a wherein the CL is deleted, giving rise to yHsp $90\alpha^{\Delta 211-259}$ mutant. This CL mutant was found to retain its chaperone function and hence the stability of Rad51 was not found to be affected. However, the nuclear function of Rad51 during DNA repair was severely reduced leading to a reduction in the Rad51 mediated gene targeting function as well as the formation of Rad51 foci which is the hallmark of HR mediated DNA repair (164). Furthermore, yeast cells harbouring the $vHsp90\alpha^{\Delta 211-259}$ mutant were severely sensitive to agents which cause DNA damage such as MMS, showing a phenotype similar to that of \(\Delta rad 51 \) strain (164). Since the charged linker region is responsible for providing structural flexibility between amino and carboxyl terminal domain of yHsp90α (265), an optimum interaction between Rad51 and yHsp90α may be compromised in the mutant. Hence, we hypothesized that effective Hsp90 and Rad51 interaction may be crucial for nuclear function of Rad51. To that end, we have determined the physical association between Rad51 and yHsp90a in presence and absence of MMS treatment. We observed that there exists a dynamic equilibrium between Rad51WT association with yHsp90α. In response to MMS treatment, Rad51 dissociates from yHsp90awhich is one of the regulatory events for Rad51 nuclear function. We utilized a point mutant Rad51 E108L, which has been characterised in our lab and has been found to show a stronger affinity towards yHsp90α (257).

In case of Rad 51^{E108L} , due to tighter association, the interaction between yHsp 90α and mutant Rad51 becomes irreversible, and hence even under DNA damaging conditions, the mutant Rad 51^{E108L} protein could not proficiently dissociate from yHsp 90α rendering the cells HR deficient.

3.2 Results

3.2.1 yHsp90 α exists in a dynamic physical association with Rad51 WT

In order to investigate the interaction between Rad51^{WT} and yHsp90 α , we performed coimmunoprecipitation experiments under normal as well as MMS treated conditions. In order to capture detectable association between yHsp90 α and Rad51^{WT} we over-expressed both yHSP90 α and RAD51 from two 2 μ vectors, each having GPD promoter. The yHsp90 α -Rad51^{WT} complex was co-immunoprecipitated from the whole cell extract with α -Rad51 antibody, followed by detection on Western blot using α -Hsp82 antibody (Fig.3). We find that under normal conditions, a small fraction of yHsp90 α is associated with Rad51^{WT} which is further reduced upon the addition of 0.15% MMS. Thus, from this experiment, we concluded that there exists a dynamic equilibrium between Rad51^{WT}-yHsp90 α complexes: in the presence of DNA damage, the

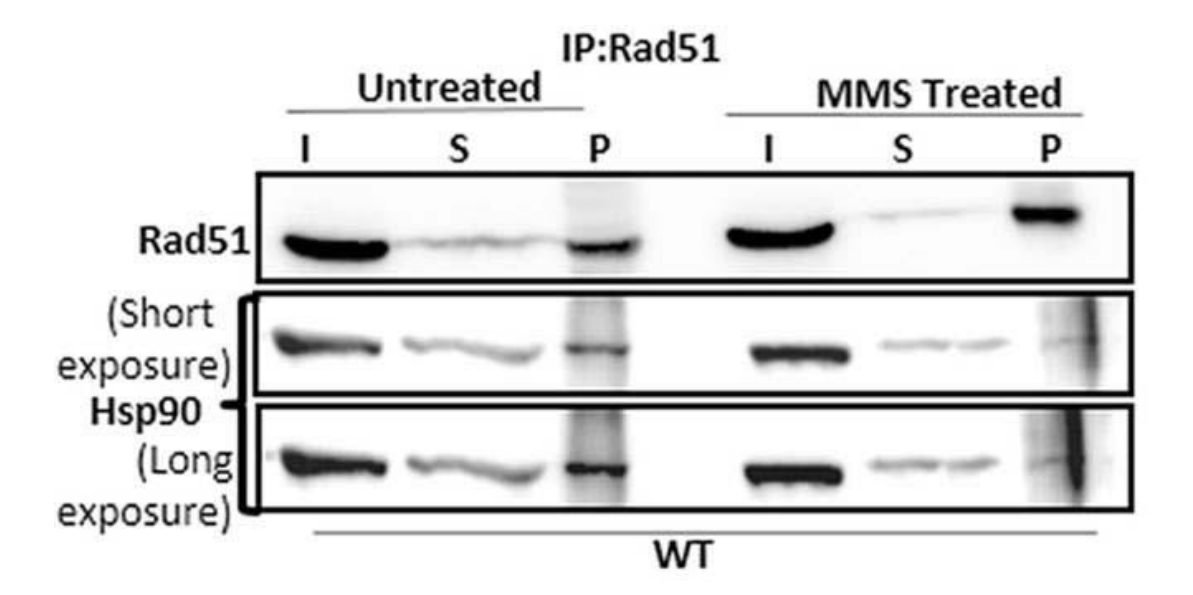


Fig. 3. Western blot showing coimmunoprecipitation of Rad51 WT with yHsp90 α from whole cell extracts of wild-type strain in conditions of cells untreated and treated with 0.15% MMS for 2 hrs. Immunoprecipitation (IP) was performed using an anti-Rad51 antibody. An anti-Hsp90 antibody was used for Western blotting. I: input; S: supernatant P: pellet.

3.2.2 The dynamic physical association of yHsp90 α with Rad51 WT is lost in the case of the mutant Rad51 E108L

Studies in our lab identified the Rad 51^{E108L} mutant as an HR dead mutant. Rad 51^{E108L} exhibits a defective nuclear function during HR mediated DNA repair and hence, is defective in Rad51 mediated gene conversion activity and cannot recruit to the broken DNA site as efficiently as Rad $51^{WT}(257)$. Cells harbouring Rad 51^{E108L} were found to be highly sensitive to DNA damage, a phenotype similar to $\Delta rad51$ strain (257).

In order to investigate the interaction between Rad51^{E108L} and yHsp90 α , we performed co-immunoprecipitation experiments under normal as well as MMS treated conditions. In order to capture detectable association between yHsp90 α and Rad51^{E108L} we over-expressed both *yHSP90\alpha* and *E108Lrad51* from two 2 μ vectors, each having GPD promoter. The yHsp90 α -Rad51^{E108L} complex was co-immunoprecipitated from the whole cell extract with α -Rad51 antibody, followed by detection on Western blot using α -Hsp82 antibody (Fig.4). We found that under normal conditions, in case of the mutant strain, a significantly large fraction of yHsp90 α is associated with Rad51^{E108L} as compared to the wild type strain. In the *E108Lrad51* strain, even in the presence of 0.15% MMS, there was no detectable reduction in the association between yHsp90 α and Rad51^{E108L}. Thus, from this experiment, we conclude that the dynamic equilibrium observed between the Rad51^{WT}-yHsp90 α complex is lost in case of *E108Lrad51* and the Rad51^{E108L}-yHsp90 α complex remains in the associated form even in DNA damage conditions created by the addition of 0.15% MMS.

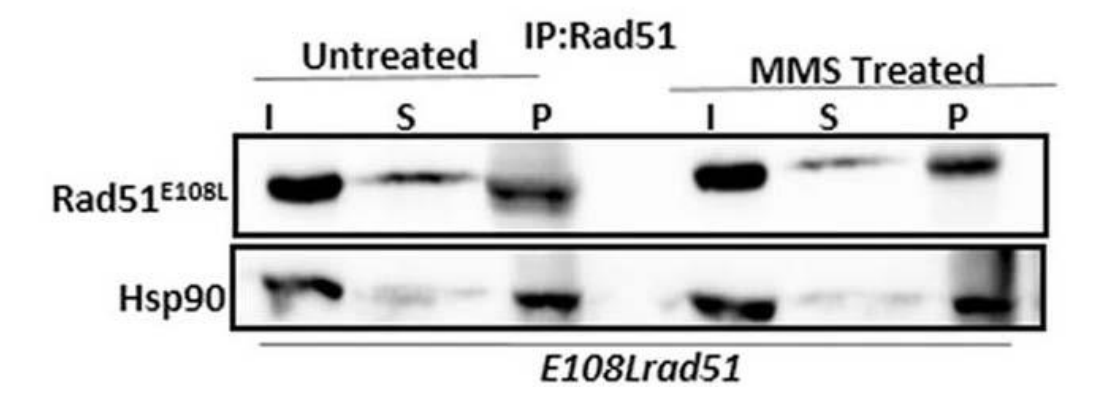


Fig. 4. Western blot showing coimmunoprecipitation of Rad51^{E108L} with yHsp90 α from whole cell extracts of *E108Lrad51* mutant strain in conditions of cells untreated and treated with 0.15% MMS for 2 hrs. Immunoprecipitation (IP) was performed using an anti-Rad51 antibody. An anti-Hsp90 antibody was used for Western blotting. I, Input; S, supernatant; P, pellet

3.2.3 Quantitative analysis shows stronger association of yHsp90 α with Rad51 E108L as compared to Rad51 WT

Quantification of the several coimmunoprecipitation repeats shows that the relative association between yHsp90 α and Rad51^{E108L} is almost double than the association found between yHsp90 α and Rad51^{WT}. This signifies stronger association of yHsp90 α with Rad51^{E108L} compared to Rad51^{WT}. In the presence of 0.15% MMS, yHsp90 α and Rad51^{WT} association was found to be reduced by approximately 50% in the wild type strain. On the other hand, in *E108Lrad51* strain, even in the presence of 0.15% MMS, there was no detectable reduction in the strong association between yHsp90 α and Rad51^{E108L} (Fig.5). Hence, it was concluded that apart from imparting stability to Rad51, yHsp90 α also regulates the nuclear function of Rad51 during genotoxic stress conditions.

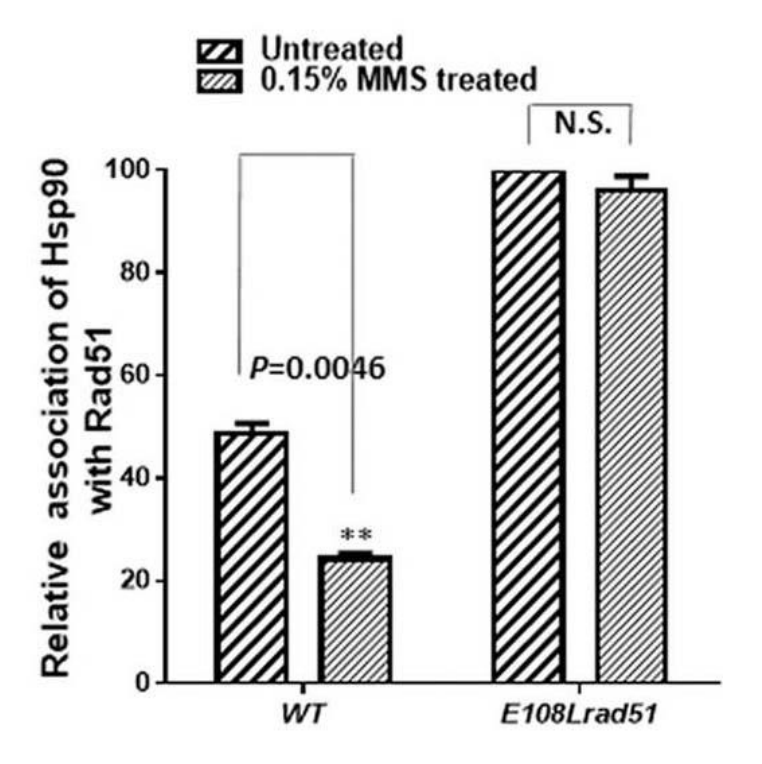


Fig. 5. Relative association of yHsp90 α with Rad51 is calculated from at least three independent coimmunoprecipitation experiments and standard deviations are plotted for both wild type *RAD51* and mutant *E108Lrad51* strain. *P* values were calculated using the two-tailed Student's *t* test, **: P = 0.0046; ***: P = 0.0008

Specific Aim 2: To study whether yHsp90 α is imported to the nucleus during genotoxic stress and recruited to the damaged chromatin

4.1 Introduction

It was reported earlier that upon DNA damage, human HSP90α is phosphorylated by DNAdependent protein kinase (DNA-PKcs) at threonine 5/7 residues and the phosphorylated HsHsp90α forms foci at the site of DNA damage (181, 266). Although DNA-PK_{cs} can phosphorylate both the cytoplasmic and nuclear pool of HsHsp90α upon DNA damage, it was never addressed whether there is a DNA damage induced upsurge of Hsp90α in the nucleus and whether this import is dependent on the threonine 5/7 phosphorylation. In lower eukaryotes such as in budding yeast, neither does yHsp90a possess the first 14 stretch of amino acids, including the Thr5 and Thr7 residues, nor does it harbour DNA-PK. Furthermore, although the orthologs of ATM i.e., Tell/Mec1 are present in yeast, there is no report showing their physical association with yHsp90α. This raises the question of whether DNA damage induced chromatin recruitment of Hsp90α occurs in these organisms. We investigated whether the nuclear translocation of yHsp90α occurs in aforementioned phosphorylation independent manner in S. cerevisiae, in which the first 14 amino-acids are absent (Fig.6, red circle). We observed significant import of yHsp90α into the nucleus in response to genotoxic stress conditions imparted by the addition of MMS. To delineate whether the nuclear import of Hsp90a is due to the DNA damage or due to the cell cycle arrest, we used agents that cause S-phase arrest (hydroxyurea) or G2/M arrest (nocodazole) and monitored the nuclear import of Hsp90α. We observed that there was no detectable nuclear import ofHsp90a in presence of HU/Nocodazole, thus confirming that the nuclear import of Hsp90α is induced by DNA damage. We further investigated whether the

nuclear pool of yHsp90 α is recruited to the damaged chromatin in response to a single specific double strand break created in the chromosome. To that end, we used *NA14* strain (263), where a site specific DSB was created within the mutant ura3 locus by expressing a galactose-inducible HO endonuclease.In NA14 yeast cells, the DSB created at the ura3 locus can be repaired by homologous recombination using a donor template (URA3) that is located 3 kb apart.We performed ChIP analysis immediately after HO induction and at every 1-hr interval, up to 4 hrsand observed that yHsp90 α is recruited to the damaged chromatin with maximum recruitment observed at 2hrs post HO induction when the DNA breakage appeared to be maximum. We further monitored the extent of occupancy of yHsp90 α upto -5kb of the DNA break site and found thatyHsp90 α binds to the flanking region of the DNA break site with kinetics comparable to that of Rad51, a known protein involved in the HR pathway.

HS90A_HUMAN	1 MPEETQTQDQPMEE EVETFAFQAEIAQLMSLIINTFYSNKEIFLRELIS	50
HSP82	1 MASETFEFQAEITQLMSLIINTVYSNKEIFLRELIS	36
HS90A_HUMAN	51 NSSDALDKIRYESLTDPSKLDSGKELHINLIPNKQDRTLTIVDTGIGMTK	100
HSP82	37 NASDALDKIRYKSLSDPKQLETEPDLFIRITPKPEQKVLEIRDSGIGMTK	86
HS90A_HUMAN	101 ADLINNLGTIAKSGTKAFMEALQAGADISMIGQFGVGFYSAYLVAEKVTV	150
HSP82	87 AELINNLGTIAKSGTKAFMEALSAGADVSMIGQFGVGFYSLFLVADRVQV	136
HS90A_HUMAN	151 ITKHNDDEQYAWESSAGGSFTVRTD-TGEPMGRGTKVILHLKEDQTEYLE	199
HSP82	137 ISKSNDDEQYIWESNAGGSFTVTLDEVNERIGRGTILRLFLKDDQLEYLE	186
HS90A_HUMAN	200 ERRIKEIVKKHSQFIGYPITLFVEKERDKEVSDDEAEEKEDKEEEKEKEE	249
HSP82	: :: : : : 187 EKRIKEVIKRHSEFVAYPIQLVVTKEVEKEVPIPEEEKKDEEKKDEE	233
HS90A_HUMAN	250 KESEDKPEIEDVGSDEEEEKKDGDKKKKKKIKEKYIDQEELNKTKPIW	297
HSP82	:. :: : . : ::. : 234 KKDEDDKKPKLEEVDEEEEKKPKTKKUKEEVQEIEELNKTKPLW	277
HS90A_HUMAN	298 TRNPDDITNEEYGEFYKSLTNDWEDHLAVKHFSVEGQLEFRALLFVPRRA	347
HSP82	. . . :: . .	327
HS90A_HUMAN	348 PFDLFENRKKKNNIKLYVRRVFIMDNCEELIPEYLNFIRGVVDSEDLPLN	397
HSP82	::	377
HS90A_HUMAN	398 ISREMLQQSKILKVIRKNLVKKCLELFTELAEDKENYKKFYEQFSKNIKL : : : : :	447
HSP82	378 LSREMLQQNKIMKVIRKNIVKKLIEAFNEIAEDSEQFEKFYSAFSKNIKL	427
HS90A_HUMAN	448 GIHEDSQNRKKLSELLRYYTSASGDEMVSLKDYCTRMKENQKHIYYITGE	497
HSP82	428 GVHEDTQNRAALAKLLRYNSTKSVDELTSLTDYVTRMPEHQKNIYYITGE	477
HS90A_HUMAN	498 TKDQVANSAFVERLRKHGLEVIYMIEPIDEYCVQQLKEFEGKTLVSVTKE	547
HSP82	: ::: ::::: :: : 478 SLKAVEKSPFLDALKAKNFEVLFLTDPIDEYAFTQLKEFEGKTLVDITKD	527
HS90A_HUMAN	548 GLELPEDEEEKKKQEEKKTKFENLCKIMKDILEKKVEKVVVSNRLVTSPC	597
HSP82	. . .: .:: :: . : : : : . 528 -FELEETDEEKAEREKEIKEYEPLTKALKEILGDQVEKVWSYKLLDAPA	576
HS90A_HUMAN	598 CIVTSTYGWTANMERIMKAQALRDNSTMGYMAAKKHLEINPDHSIIETLR	647
HSP82	. . .: : : :: : :: : 577 AIRTGQFGWSANMERIMKAQALRDSSMSSYMSSKKTFEISPKSPIIKELK	626
HS90A_HUMAN	648 QKA-EADKNDKSVKDLVILLYETALLSSGFSLEDPQTHANRIYRMIKLGL	696
HSP82	::. : .	676
HS90A_HUMAN	697 GIDEDDPTADDTSAAVTEEMPPLEGDDDTSRMEEVD- 732	
HSP82	. :. .:.: : . . 677 NIDEDEETETAPEASTAAPVEEVPADT-EMEEVD* 710	

Fig. 6. The pairwise sequence alignment between human Hsp90 α and yeast Hsp82 shows that the first 14 amino acids are absent in Hsp82 as indicated by the red circle. Green parenthesis show the charged linker region of human Hsp90 α and yeast Hsp82.

4.2 Results

4.2.1 Nuclear accumulation of yHSP90α during DNA damage

We examined the level of yHsp90 α in whole-cell extract and in nuclear fraction of W303a strain upon exposure to MMS treatment (0.15%). We found that there was no difference in the expression of yHsp90α in response to DNA damage (Fig.7A, left panel), however, it was redistributed to the nucleus (Fig.7A, right panel). The experiment was repeated multiple times and one set of the representative western blot images is presented. Rad51 level was monitored as a positive control which showed more than 2-fold and 3-fold of induction in the whole-cell extract and in the nuclear fraction respectively (Fig.7B). The nuclear fractionation data showed that upon MMS treatment, there was a 2.5-fold nuclear enrichment of yHSP90a (Fig. 7B). Nsp1, the nuclear marker protein was used as a loading control. The nuclear accumulation of yHsp90a was further supported by the live cell imaging of the strain NFY31, that harbors a single-copy GFP fused vHSP90 α plasmid. We observed that in untreated condition, GFP-vHsp90 α was uniformly distributed throughout the cell (Fig.7C). However, when treated with 0.15% MMS, GFP-vHsp90α moved to the nucleus and coincided with Hoechst 33342 (Fig.7D). As MMS delays S-phase progression, we wanted to distinguish whether the nuclear translocation of yHsp90α occurs due to cell cycle arrest or as a consequence of DNA damage. For that, we used hydroxyurea induced S-phase arrested cells and the nocodazole-induced G2/M arrested cells and looked for the distribution of GFP-yHsp90a. We found that GFP fluorescence was distributed majorly in the cytoplasm and to a little extent in the nucleus of the hydroxyurea-arrested cells (Fig.7E). We also found that GFP-vHsp90α was evenly distributed throughout the cytoplasm in the nocodazole-arrested cells (Fig.7F) and didn't coincide with the blue fluorescence of Hoechst.

Thus, our study concludes that nuclear redistribution of yHsp90 α is associated with MMS induced DNA damage.

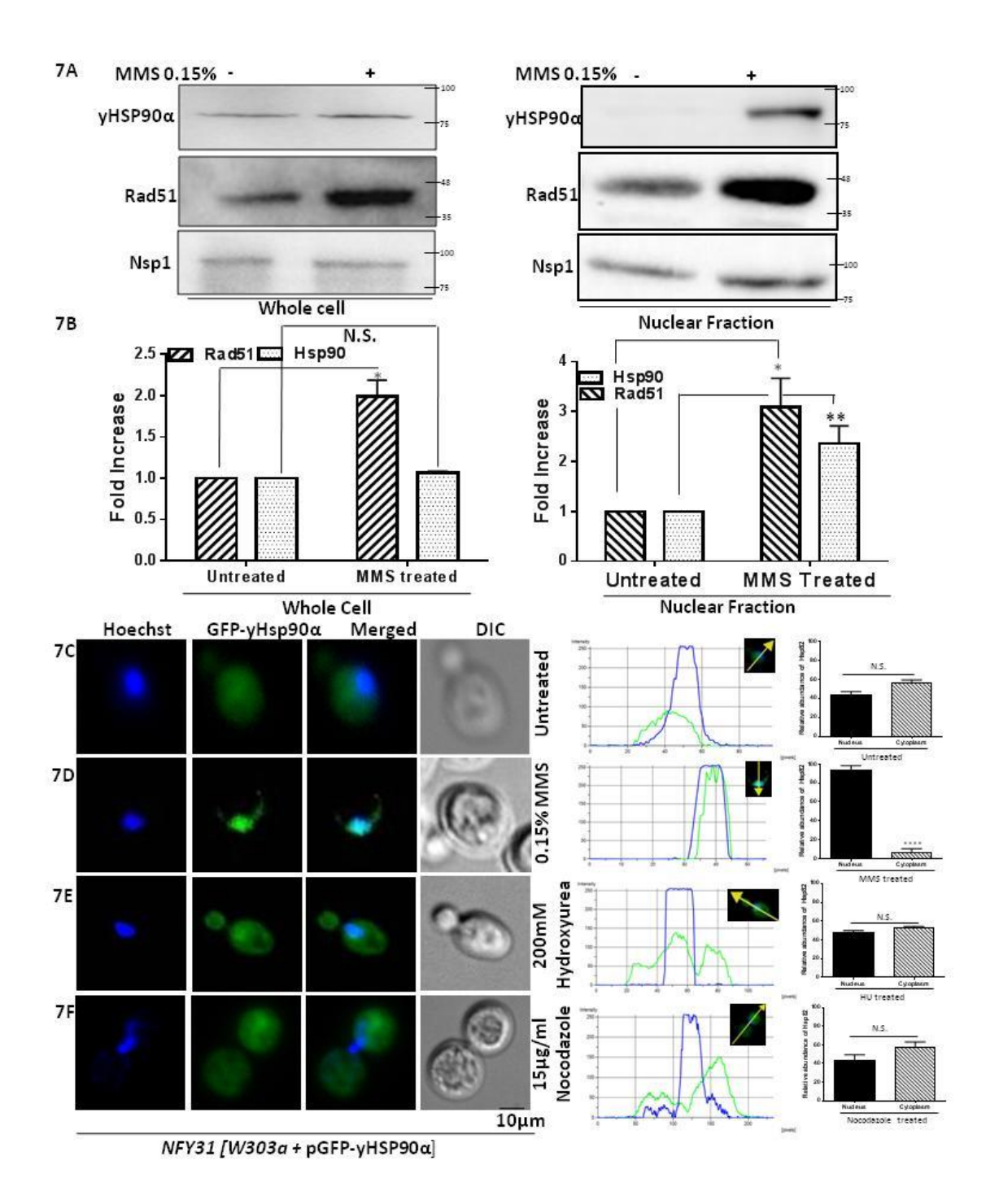


Fig. 7. Accumulation of yHsp90 α in the nucleus in response to MMS induced DNA damage: (A) Western blots showing no difference in the steady state expression of yHsp90 α in the whole cell with (+) and without (-) MMS treatment (left panel). yHsp90 α was accumulated in the nuclear fraction upon MMS treatment (right panel); Rad51 acted as a positive control for MMS treatment; Nsp1 acted as a nuclear marker. (B) The above experiment was repeated three times, and the mean values (\pm SD) were plotted. (C) Live-cell imaging shows the distribution of GFP-

yHsp90 α (green) in the whole cell in untreated condition (D) Fluorescence imaging of 0.15% MMS treated cells show the localization of GFP-yHsp90 α (green) inside the nucleus (blue) (E) Fluorescence images showing no nuclear accumulation of GFP-yHsp90 α (green) in 200mM hydroxyurea-arrested early S phase cells (F) Fluorescence images showing no nuclear accumulation of GFP-yHsp90 α (green) in 15 μ g/ml nocodazole-arrested G2/M cells. Nucleus was stained using Hoechst 33342. Intensity profiles were derived for all fluorescence experiments using NIS elements AR software; the relative fluorescence intensities of GFP-yHsp90 α in the nucleus and cytoplasm were quantified and the mean values (\pm SD) were plotted using GraphPad Prism 6. P values were calculated using the two-tailed Student's t test (****, P< 0.0001; N.S., Not significant).

4.2.2 The nuclear import of $HsHsp90\alpha$ during genotoxic stress is independent of Thr7 phosphorylation

We further examined whether human HsHsp90 α shows similar localization dynamics in response to MMS treatment. We used the strain harbouring a plasmid that expresses human $HSP90\alpha$ fused with FLAG. The nuclear fractionations showed increased level of HsHsp90 α in MMS treated sample compared to the untreated sample (Fig.8A). Quantification of gel images from independent set of experiments showed about 4-fold increase in the HsHsp90 α level within the nucleus (Fig.8B). We sought to determine whether this import is dependent on the presence of Thr 7 residue of HsHsp90 α . Using a mutant protein HsHsp90 α ^{T7A}, where threonine is mutated to alanine, we observed that its nuclear import remained unperturbed (Fig.8C). Estimation of multiple WBs showed about 5-fold increase in the nuclear fraction with respect to the untreated cell (Fig.8D). Thus, our study shows that DNA damage induces an increased import of HSP90 α in the nucleus from the cytoplasm which is independent of phosphorylation of the threonine 7 residue.

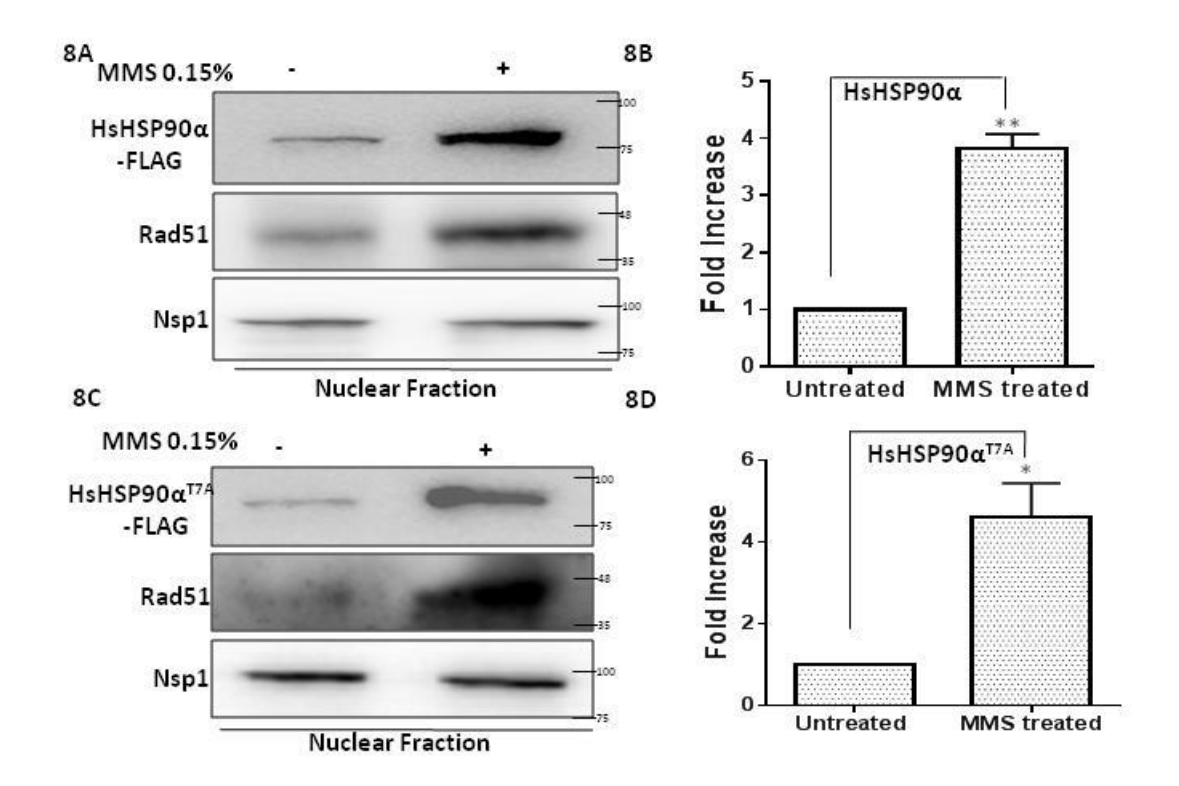


Fig. 8. Accumulation of HsHsp90 α in the nucleus in response to MMS induced DNA damage: (A) Western blot showing the nuclear fractionation of FLAG tagged $HsHSP90\alpha$ strain with and without MMS treatment conditions. (B) The experiment was repeated with fresh batch of cells and estimation of band intensities showed 4-fold increase in the nuclear accumulation of HsHsp90 α in presence of MMS. (C) Western blot showing the results of nuclear fractionation of FLAG tagged $Hshsp90\alpha T7A$ strain with and without MMS treatment conditions. (D) Quantification of band intensities of independent experiments showed 5-fold increase in the nuclear distribution of the mutant protein (**, P< 0.01; *, P< 0.05).

4.2.3 Nuclear accumulation of yHSP90α upon induction of a single double strand break

MMS alkylates DNA bases and thereby causes DNA-base mispairing (267). To understand whether the increased nuclear vHSP90a reflects a true response to DNA damage, we induced a single double strand break in DNA and determined the cellular redistribution of vHSP90a. To that end, we used NA14 strain (263), where a site specific DSB was created within the mutant ura3 locus by expressing a galactose-inducible HO endonuclease (Fig.9A). By designing the primers complementary to the region adjacent of the *HOcs* (OSB 289), and the regions within the KANMX cassette (kanB1), we measured the extent of DNA cleavage by the HO endonuclease. We have repeated the repair kinetics upon HO induction with 3 independent batch of cells and one of the representative images is provided (Fig.9B). We found that the HO endonuclease resulted in 75% cleavage at the *ura3* locus within the 1st hr of induction and 100% by the end of the 2nd hr (Fig.9C). The DSBs are repaired by HR using a donor *URA3* sequence, that is placed 3 kb apart. We observed that 50% repair was achieved at the end of the 3rd hr and the damage was completely healed by the end of the 4th hr (Fig.9B and 9C). As, in our experimental set-up, we always observed maximum damage at the 2nd hr of galactose induction (Fig.9C), we harvested the cells before and at the 2nd hr after the galactose treatment, and performed the nuclear fractionation. We observed that there was no difference in the expression of yHSP90α in the whole cell and at the 2nd hr post induction, the protein showed significant nuclear enrichment upon formation of a single DSB in chromosome (Fig.9D). Quantification of the independent WB image showed about 4-fold increase in the nuclear level of yHSP90α at 2 h post HO induction (Fig.9E). Hence, we observe that even a single DSB in chromosome causes an increased nuclear accumulation of yHSP90α.

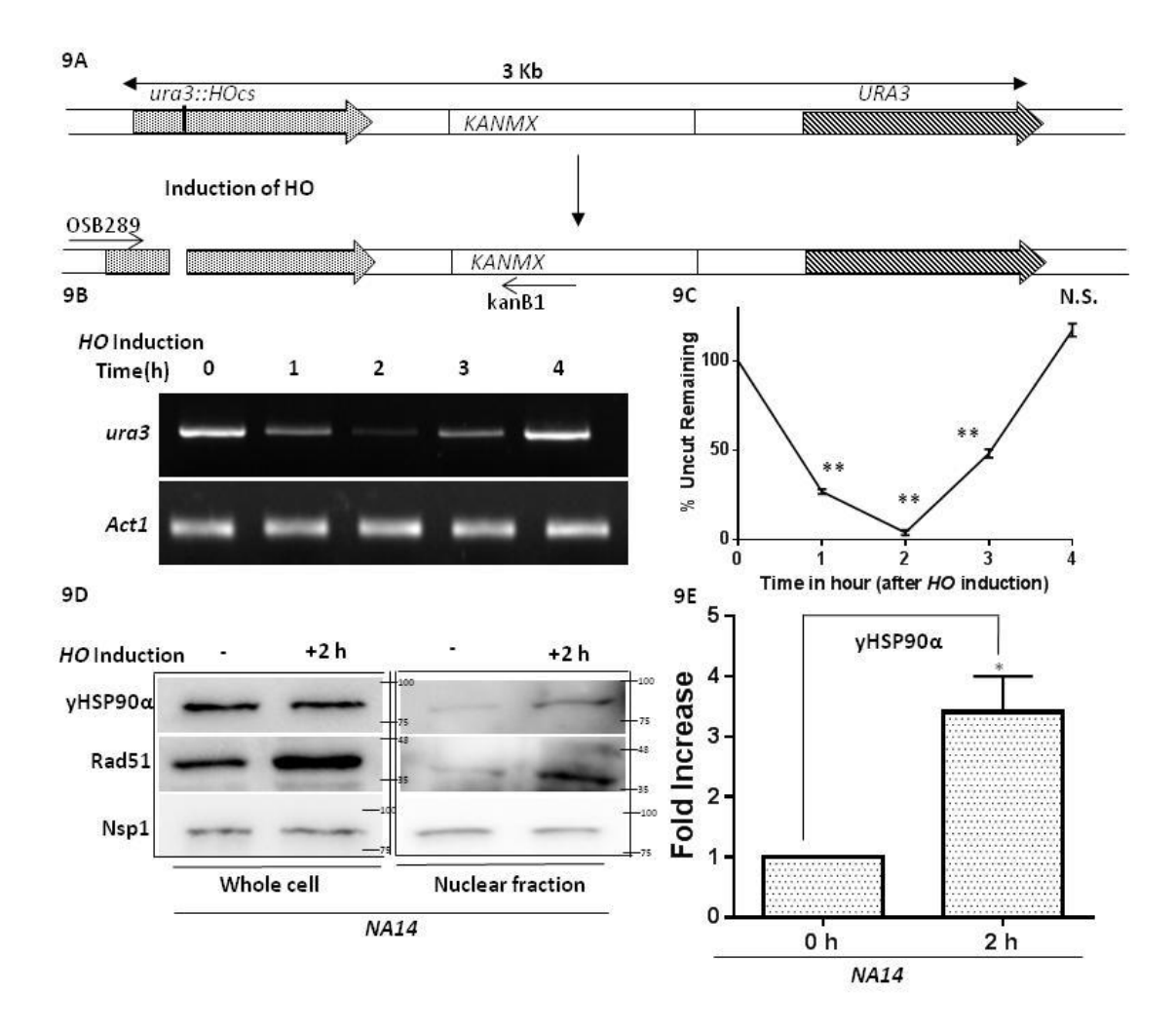


Fig. 9. Nuclear accumulation of yHSP90 α upon induction of a single double strand break: (A) Schematic representation of the cassette incorporated in the *NA14* strain in which two homologous *URA3* sequences are separated by 3 kb intervals on chromosome V with the sequence of *KANMX* integrated in between. One of the *URA3* sequences has *HO* endonuclease recognition site (*HOcs*) incorporated in it. The relative positions of the primer pairs OSB289 and KanB1 were shown, which were used to detect the DNA damage upon *HO* induction. (B) *NA14* cells were grown and *HO* induction was done by growing cells in galactose medium. Genomic DNA was extracted at different time intervals (0 to 4 h) and subsequently amplified using the primer pairs OSB289 and KanB1, where the absence of band indicated DNA damage. DNA levels were normalised with respect to *ACT1*. (C) Three independent experiments were done and the mean values (\pm SD) were plotted. The repair kinetics showed maximum damage at 2^{nd} h of *HO* induction and complete repair was seen at 4^{th} h of induction. The mean values (\pm SD) were plotted; the significance was calculated with respect to the untreated sample (0 h); *P* values were calculated using the two-tailed

Student's t test (***, P< 0.01, NS, not significant). (D) The steady state levels of yHsp90 α in NA14 strain were presented at 2 h before (-) and after (+) HO induction (left panel). In the same conditions nuclear fractionations were done which showed increased nuclear accumulation of yHsp90 α at the 2nd h of induction (right panel). Rad51 upregulation served as a control for DSB; protein levels were normalized with respect to Nsp1. (E) Quantification of yHsp90 α levels as obtained from independent set of experiment showed 4-fold increase, at 2 h post HO induction. The mean values (\pm SD) were plotted.

4.2.4 Extent and kinetics of occupancy of yHSP90α at DSB ends

In mammalian cells it was demonstrated that DNA-damage induced T7-phosphorylated form of $HsHsp90\alpha$ is recruited to the damaged chromatin. However, whether this phosphorylation is a criterion for its chromatin recruitment was not addressed. In Saccharomyces cerevisiae yHsp90a lacks the stretch of 14 residues, including T7 of HsHsp90a. We wanted to check whether the nuclear pool of yHsp90α was associated with the damaged chromatin. We utilized the chromatin immunoprecipitation technique to visualize the extent and kinetics of yHsp90α binding following DSB induction and during its repair by homologous recombination. In NA14 yeast cells, the DSB created at the *ura3* locus can be repaired by homologous recombination using a donor template (URA3) that is located 3 kb apart (Fig. 10A). We monitored the binding of vHSP90a to DSB ends, using ChIP analysis which we performed immediately after HO induction and at every 1-hr interval, up to 4 hrs (the time required for its complete repair). We found significant binding of vHsp 90α to sequences close to the HO cleavage site at the 2^{nd} and 3^{rd} hrs, using a pair of primers (shown in red colour), OSB 519 and OSB 520, that amplify sequences 55 bp to 205 bp proximal to the HO cut site (Fig.10B). There was no association of yHsp90α to other locus (ACTI). The maximum recruitment of yHsp90α to DSB was observed at the 2nd hr. It is noteworthy that the maximum break was generated during the 2nd hr post HO treatment and by the third hr 50% break was repaired (Fig.9C). Thus, the entry and exit of Hsp90 correlated well with the presence of maximum break as seen in Fig.9B and it remained associated up to the 3rd hr until 50% of the DSB remained unrepaired (Fig.9C). At a later time-point (4th hr), the recruitment was substantially reduced. As a reference, we monitored the recruitment of Rad51 under similar condition and observed a slightly different pattern (Fig. 10C). We calculated the fraction of recruitment of yHsp90α and Rad51 and plotted against different time intervals. We found that

yHsp90 α recruitment was highest at the time of maximum damage (2nd hr) and it was dislodged from the chromatin at the 4th hr of HO induction, once repair was complete (Fig.10D). Rad51 recruitment had been initiated at the 2nd hr, which remained maximum at the 3rd hr and significant amount of Rad51 remained associated even at the 4th hr (Fig.10D). We also measured the association of yHsp90 α and Rad51, at the leftward direction (up to 5 kb) from the cleavage sites. We found a similar pattern, *i.e.*, significant recruitment of yHsp90 α and Rad51 was observed throughout - 4 kb regions during 2nd and 3rd hr post HO induction (Fig.10E). Thus, our study has established that DNA damage induced increase in association of yHSP90 α to the chromatin is independent of the N-terminal 14 residues present in HsHsp90 α .

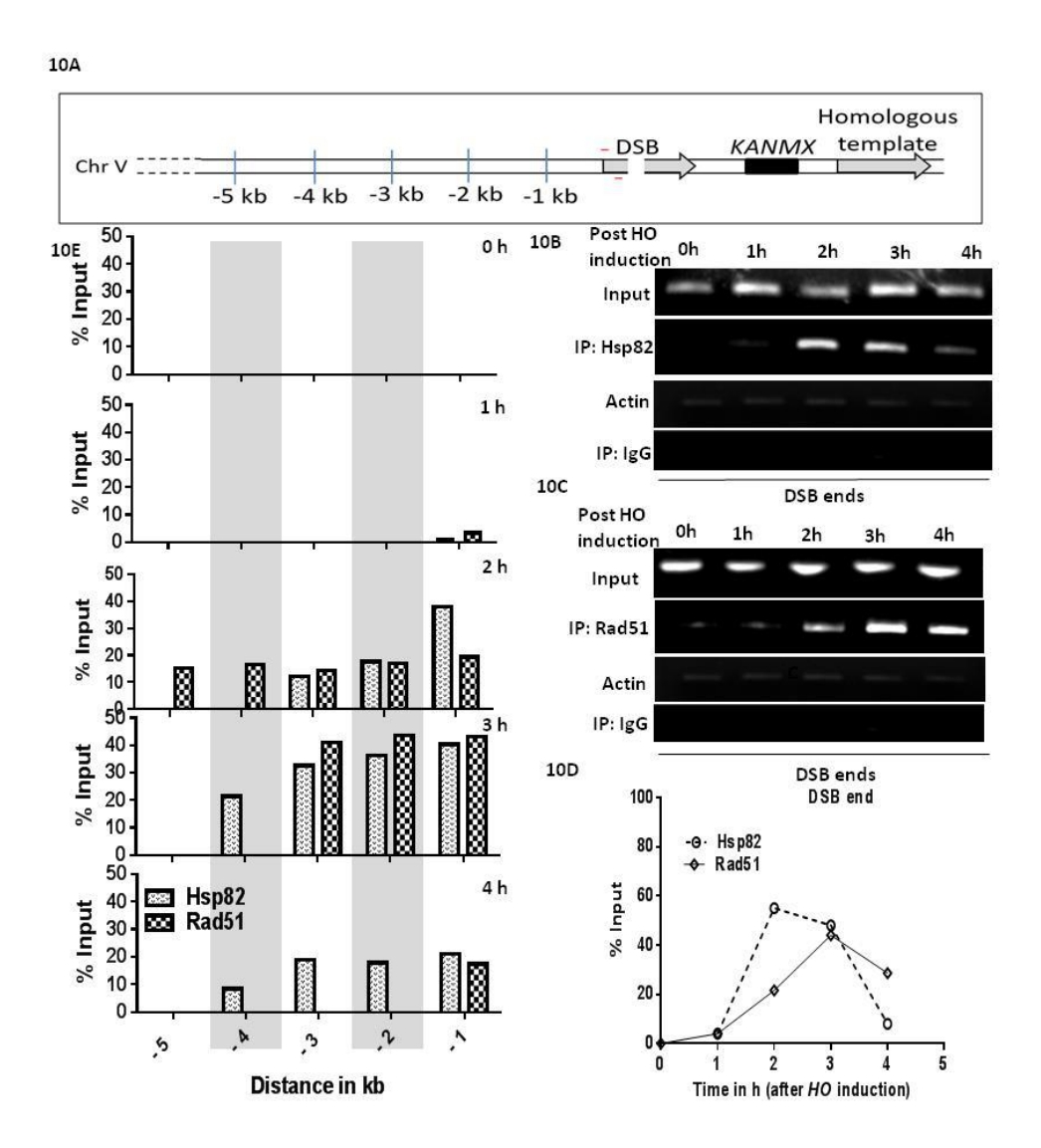


Fig. 10. Extent and kinetics of occupancy of yHSP90α at DSB ends: (A) Schematic representation of the position of DSB, at the *ura3* locus and the presence of a homologous template (*URA3*). The position of the primers (as indicated in red colour) near the DSB were presented, which were used to detect the recruitment of yHsp90α and Rad51 near the *HO* cleavage site. The map of the sites (up to - 5 kb) distal to the DSB were shown. (B) yHsp90α bound chromatin was amplified to detect the kinetics of its recruitment to the *HO* cleavage site and at the *ACT1* locus. (C) ChIP analysis showing the kinetics of Rad51 recruitment to the DSB ends as well as at the *ACT1* locus following *HO* induction. (D) Quantification of the independent ChIP experiments (n=3, in each case), was plotted. Error bars indicated standard deviation. (E) The association of yHsp90α and Rad51 were measured at increasing distances up to 5 kb upstream of the *HO* cleavage site at different time points post *HO* induction. Quantification of

two independent ChIP experiments were plotted to compare the extent of recruitment between yHsp90 α and Rad51.

Error bars indicated standard deviation. ChIP assay done with IgG antibody as a negative control.

Specific aim 3: To study the mechanism of yHsp90α nuclear import during DNA repair

4.3 Introduction

Hsp 90α is associated with a wide variety of co-chaperones that are essential for its reaction cycle and also assists the conformational changes that Hsp90α undergoes during its chaperone cycle. Although the contribution of co-chaperones towards the conformational cycle of HSP90α is well understood, however, their physiological significance remains obscure. Previous studies have identified three co-chaperones, Sba1, Cdc37 and Aha1 to have potential roles in the DNA repair pathway. In HeLa cell extracts, Aha1 was found to interact with the proteins Ku70, Ku80 and DNA-PKcs which are involved in DNA repair (53). The Sba1 network was found to have a significant nuclear component that includes DNA repair activities (54). A previous study showed that $\Delta sbal$ strain shows susceptibility towards various DNA damaging agents like MMS, bleomycin and ultraviolet light, which could be reversed by the complementation of Sba1 in the null Δsba1 cell. Loss of function of Cdc37 causes synthetic growth defect with several genes involved in genome integrity (55). Although previous studies indicate that these co-chaperones may play a role in DNA repair, their exact function during the HR pathway have never been addressed. In our present study, we have addressed the potential involvement of the above cochaperones in the nuclear import of yHsp90\alpha during the condition of genotoxic stress. To this end, we used cell fractionation studies as well as fluorescence studies which establish that Aha1 plays an important role in the DNA damage mediated nuclear import of yHsp90α. We found that Aha1 shows an increased nuclear accumulation in response to DNA damage conditions created with the addition of 0.15% MMS. We further observed that $\Delta ahal$ cells show a defect in Hsp90

nuclear import upon DNA damage, rendering the cells sensitive to DNA damaging agents and this phenotype is reversed upon the re-introduction of Aha1 to these cells.

During the chaperone cycle, Hsp90α faces large-scale conformational rearrangements from an open inactive conformation to a closed active conformation, (268) which in turn modulates its catalytic activity. The NTD and the MD are separated by a disordered CL, which provides flexibility for the domain rearrangement during Hsp90α chaperone cycle (25). This linker region is evolutionarily conserved among all eukaryotic orthologs of Hsp90α studied till date, although its physiological significance is poorly understood. To address the importance of CL domain in the mechanism of the in-vitro function of Hsp90α, a series of successively shortened CL mutants of yHSP90α were generated (269). It was observed that successive deletion of CL gradually reduces the capability of Aha1 to stimulate the ATP turnover in the mutants, without altering its binding affinity to those mutants (269). It was reported that Aha1 mediated ATPase activity of vHsp $90\alpha^{\Delta(211-259)}$ was reduced by 2.5-fold, although that of vHSP $90\alpha^{\Delta(211-242)}$ showed a similar fold stimulation similar to $yHSP90\alpha^{WT}$. One of the CL mutants was characterized in detail for its role in DNA repair pathway. It was reported that although Rad51 levels remain stable in the $hsp82(\Delta 211-259)$ mutant, the strain displays a severe reduction in the gene targeting efficiency (164). Moreover, the MMS induced Rad51 foci formation, which is the hallmark of HR mediated DNA repair, was significantly reduced in this mutant background. However, the mechanism behind such phenotype is not understood well. In our current study, we have determined the structural determinant that is crucial for the DNA damage induced import of yHsp90a. To this end, we investigated the MMS induced nuclear import of the two mutant proteins yHSP90 $\alpha^{\Delta(211-)}$ ²⁵⁹⁾ andyHSP90 $\alpha^{\Delta(211-242)}$. We observed that the yHSP90 $\alpha^{\Delta(211-259)}$ mutant showed a complete abrogation in its nuclear import in response to DNA damage. However, the phenotype was

reversed in the case of the shorter CL deletion mutant, yHSP90 $\alpha^{\Delta(211-242)}$. Furthermore the cells harbouring yHSP90 $\alpha^{\Delta(211-259)}$ mutant showed high DNA damage sensitivity which was reversed in cells harbouring the yHSP90 $\alpha^{\Delta(211-242)}$ mutant similar to wild type condition. Hence, our study establishes that the nuclear function of yHSP90 α is essential for effective DNA repair in yeast. If the nuclear import of yHsp90 α during genotoxic stress is hampered; the cells are rendered sensitive to the DNA damaging agents.

4.4 Results

4.4.1 Increased nuclear localization of Aha1 in response to DNA damage

We further investigated DNA damage induced nuclear accumulation of Hsp90 co-chaperone Aha1. We employed indirect immunofluorescence to monitor the cellular localization of Aha1 in W303a strain. We observed that Aha1 was equally distributed in the nucleus and in the cytoplasm before (Fig.11A) and after MMS treatment (Fig.11B). However, there was an overall increase in the Aha1 fluorescence intensity in the cell in response to MMS (Fig.11B). Such induction corroborated well with our western data with the whole cell, where we found that endogenous level of Aha1 was significantly induced upon MMS treatment (Fig.11C, left panel). We also observed a concomitant increase in Aha1 level in the nucleus (Fig.11C, right panel) upon MMS treatment. We wanted to determine whether induction of single ds break in the chromosome could also induce the import of Aha1 to the nucleus. For that, we used the NA14 strain. Our results showed that in this strain, the Aha1 protein level in the nucleus was significantly increased, about 1.5-fold, at the 2nd hr of HO induction (Fig.11D and 11E), whereas yHsp90α level was increased about 3-fold. Next, to investigate whether other cochaperones such as Sba1 and Cdc37 are imported to the nucleus upon DNA damage, we used carboxy-terminal MYC tagged SBA1 and CDC37 strains for our analysis. We found that there

was no such increase in the levels for Cdc37 in the whole cell as well as in the nucleus upon DNA damage (Fig.11F). In case of Sba1, we found that its endogenous level was significantly induced upon MMS treatment similar to that of Aha1 (Fig.11G, left panel). However, unlike Aha1, there was no such increase in Sba1 level in the nucleus (Fig.11G, right panel). We have repeated these experiments 3-times and the nuclear distribution of each of the co-chaperones were plotted in presence and absence of MMS. It was found that in the whole cell extract, the abundance of Aha1 and Sba1 were 3-fold and 4-fold respectively (Fig.11H), however only Aha1 showed about 2-fold increased accumulation in nucleus upon MMS treatment, while Sba1 and Cdc37 showed no significant increase (Fig.111). In order to address whether MMS induced upregulation of Aha1 and Sba1 occurs at the transcription level, we compared the relative expression of the above-mentioned co-chaperones in absence and presence of 0.15% MMS (Fig. 12A). Quantitative RT-PCR shows 1.5-fold increase in expression of AHA1 and no significant increase in expression of SBA1 upon MMS treatment (Fig.12B). Increase in RAD51 transcript was used as a positive control in our study. We speculate that the higher abundance of SBA1 may result due to increased protein stability during genotoxic stress

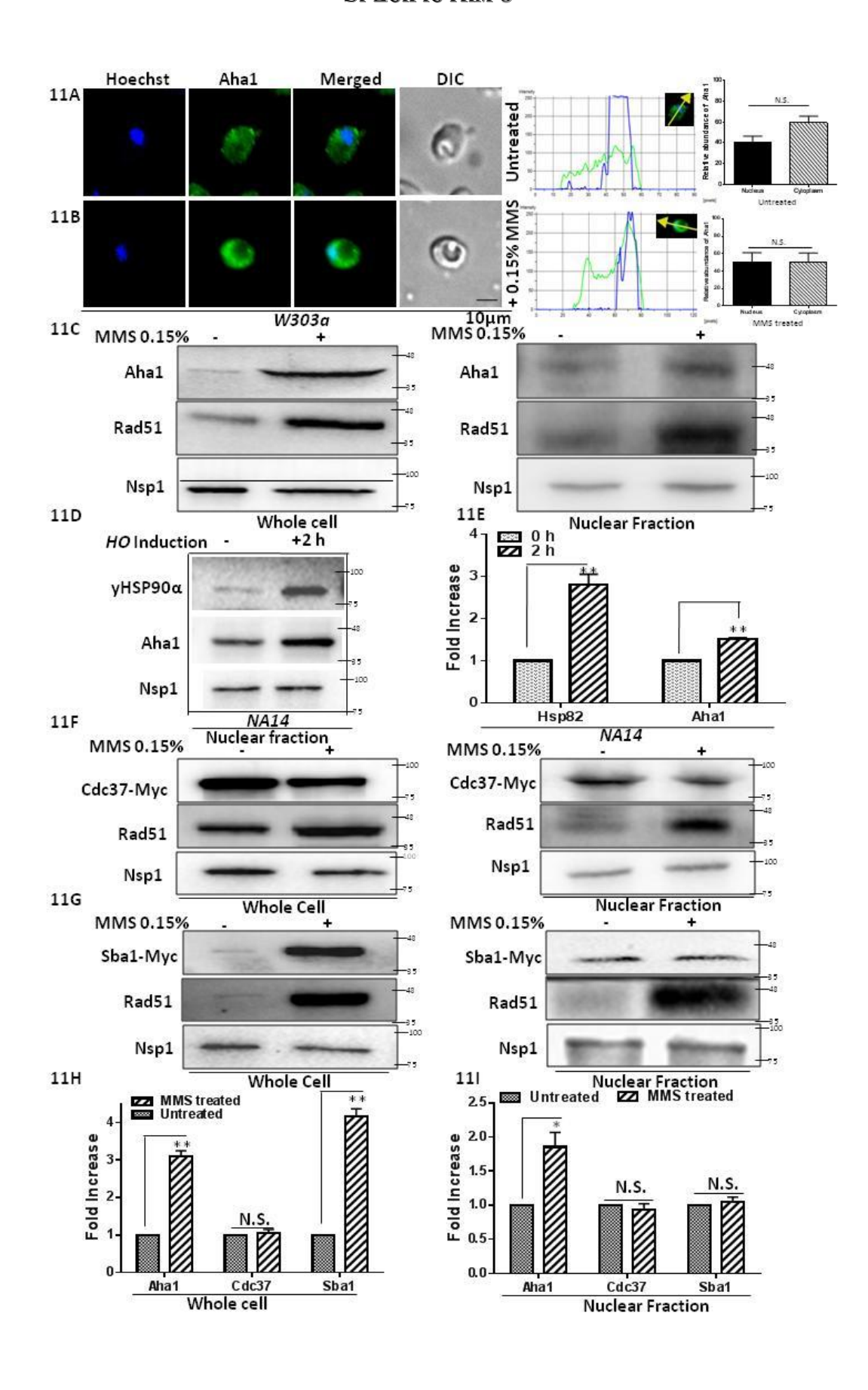


Fig. 11. Increased nuclear presence of Aha1 during the conditions of DNA damage: (A) Indirect immunofluorescence shows the distribution of Aha1 (green) in the whole cell of W303a. (B) A part of Aha1 fluorescence (green) merges with the Hoechst fluorescence (blue) in the MMS treated condition, although at is distributed in the cytoplasm as well. Nuclear staining was done using Hoechst dye and Aha1 was detected using Alexa fluor 488 conjugated secondary antibodies. Intensity profiles were derived for all fluorescence experiments using NIS elements AR software; relative fluorescence intensities of Aha1 in the nucleus and cytoplasm were quantified and the mean values (±SD) were plotted using GraphPad Prism. P values were calculated using the twotailed Student's t test (N.S., Not significant).(C) Aha1 is induced in the whole cell (left panel) in presence of MMS and its level in the nucleus in increased (right panel) in response to 0.15% MMS treatment. (D) NA14 strain was subjected to HO induction in the same manner as discussed in Fig.9.A representative Western blot was presented out of the multiple independent repeats of the experiment. (E) Quantification of the levels of γHsp90α and Aha1 showed 3-fold and 1.5-fold increased nuclear accumulation respectively at 2 h post HO induction. The mean values (±SD) were plotted. P values were calculated using the two-tailed Student's t test (**, P < 0.01). (F) Cdc37 level is not altered significantly upon 0.15% MMS treatment in the whole cell (left panel) as well as in the nucleus (right panel). (G) Sba1 is induced in the whole cell (left panel) in response to 0.15% MMS, however nuclear fractionation shows no change in nuclear level of Sba1 in presence and absence of MMS (right panel). (H) and (I) The experiments C), F) and G) were repeated with independent batch of cells and the quantification of the data was done using Image J and mean values (±SD) were plotted. Left panel shows the levels of individual co-chaperones in the whole cell and right panel shows the levels of the same in the nuclear fraction.

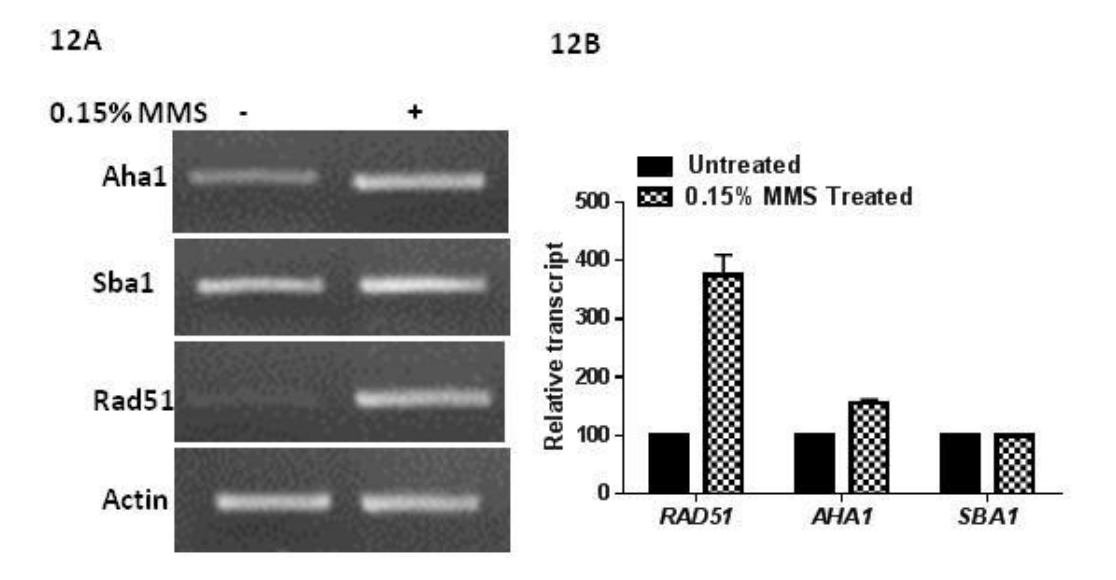


Fig. 12. Expression of *AHA1* **and** *SBA1* **in response to MMS:** (A) Semi-quantitative RT-PCR showed relative expression of *AHA1* and *SBA1* upon exposure to 0.15% MMS for 2 hrs. *RAD51* acts as a positive control. (B) Quantitative RT-PCR analysis showed a 1.5-fold increase in expression of *AHA1* and no significant increase in expression of *SBA1* upon MMS treatment.

4.4.2 yHsp90α transport to the nucleus upon DNA damage is independent of Cdc37 and Sba1

Next, we wanted to address whether DNA damage dependent increased nuclear accumulation of yHsp90 α is dependent on Cdc37 and Sba1. A temperature sensitive cdc37S14A mutant strain was used, which shows normal phenotype at 25°C but displays complete loss of function when grown at restrictive temperature, 37°C. Our study showed no difference in the endogenous level of yHsp90 α in cdc37S14Amutant strain, when grown at 37°C in presence or absence of MMS (Fig.13A). The nuclear fractionation under similar conditions showed 4-fold increase in the accumulation of yHsp90 α upon DNA damage (Fig.13B and 13C), as was also observed in the wild-type strain. In order to address the dependency on Sba1, we generated $\Delta sba1$ strain in isogenic W303a background. We found that in $\Delta sba1$ strain, yHsp90 α level was induced by 3.6-fold in the whole-cell in response to MMS treatment (Fig.13D and 13F). In addition, DNA damage dependent nuclear import was observed to be identical to the phenotype of wild-type cells (Fig.13E and 13F). Together, this study concludes that MMS induced nuclear import of yHsp90 α is independent of Cdc37 and Sba1

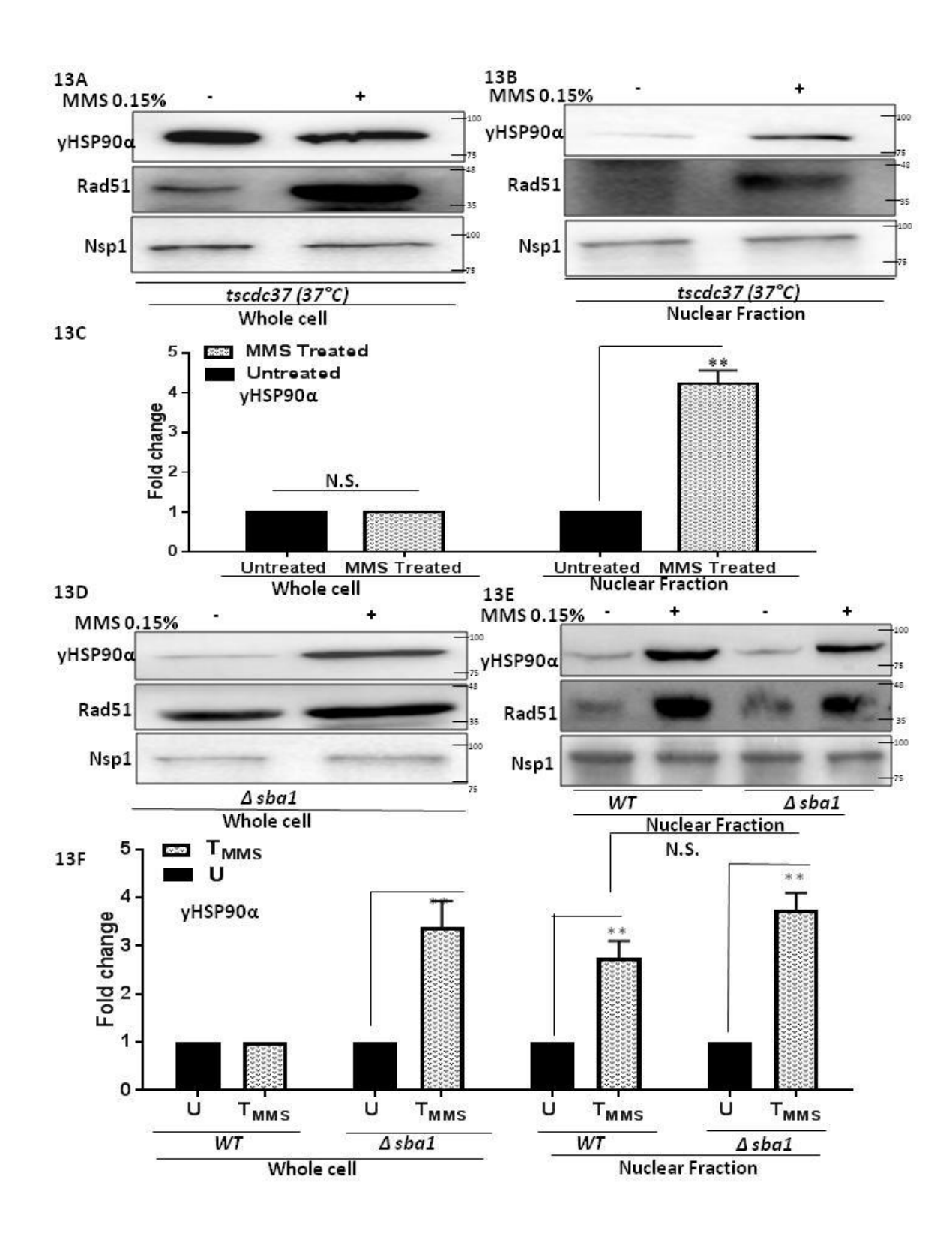


Fig. 13. yHsp90α transport to the nucleus upon DNA damage is independent of Cdc37 and Sba1: (A) Western blot showing no change in the endogenous level of yHsp90αupon MMS treatment in the temperature sensitive

tscdc37514A strain at non-permissive temperature (37°C). (B) Western blot shows that cdc37 loss of function mutation does not alter increased nuclear accumulation of yHsp90 α upon MMS treatment. (C) The above experiments (A and B) were repeated with three independent batch of cells and the densitometric image analysis of yHsp90 α was presented, P values were calculated using the two-tailed Student's t test (**, P< 0.01; NS, not significant). (D) In $\Delta sba1$ strain endogenous level of yHsp90 α are induced upon MMS treatment (E) Nuclear fractionation of untreated and MMS treated wild-type and $\Delta sba1$ strain shows accumulation of yHsp90 α in the wild-type W303aas well as isogenic $\Delta sba1$ strains. (F) The experiments (6D and 6E) were repeated three times and the mean values (\pm SD) were plotted, P values were calculated using the two-tailed Student's t test (**, P< 0.01, NS: not significant).

4.4.3 yHsp90α transport to the nucleus upon DNA damage is dependent on Aha1

To decipher whether Aha1 plays any role during MMS induced nuclear import of vHsp90α, we generated \(\Delta aha 1 \) strain. We transformed empty plasmid and \(AHA 1 \) over-expression plasmid to ∆aha1 strain to generate two isogenic strains. AHA1 expression was detected specifically in △aha1 strain harbouring the AHA1 over-expression plasmid (Fig.14A, third lane). Interestingly, we found that Aha1 deletion was positively correlated with MMS induced upregulation of endogenous yHsp90α (Fig.14A), and the phenotype is reversed with ectopic expression of AHA1 as presented in Fig.14A (first lane). Further, we observed that although Aha1 deletion resulted in 3.5-fold increase in the endogenous level of γHsp90α upon MMS treatment (Fig.14B), it couldn't be translocated to the nucleus (Fig.14C, first lane). However, ectopic expression of AHA1 resulted in the increased nuclear import of both yHsp90α (approximately 3-fold) and Aha1 upon DNA damage (Fig.14C and 14D). We used live-cell fluorescence to visualize the localization of yHsp90 α in the $\triangle aha1$ strain NFY32, that harbours a centromeric GFP-yHSP90 α plasmid. We didn't find any nuclear localization of yHsp90a under MMS treated (Fig.14F) or untreated (Fig.14E) condition. This experiment was performed along with its isogenic control strain (Fig.7C and 7D).

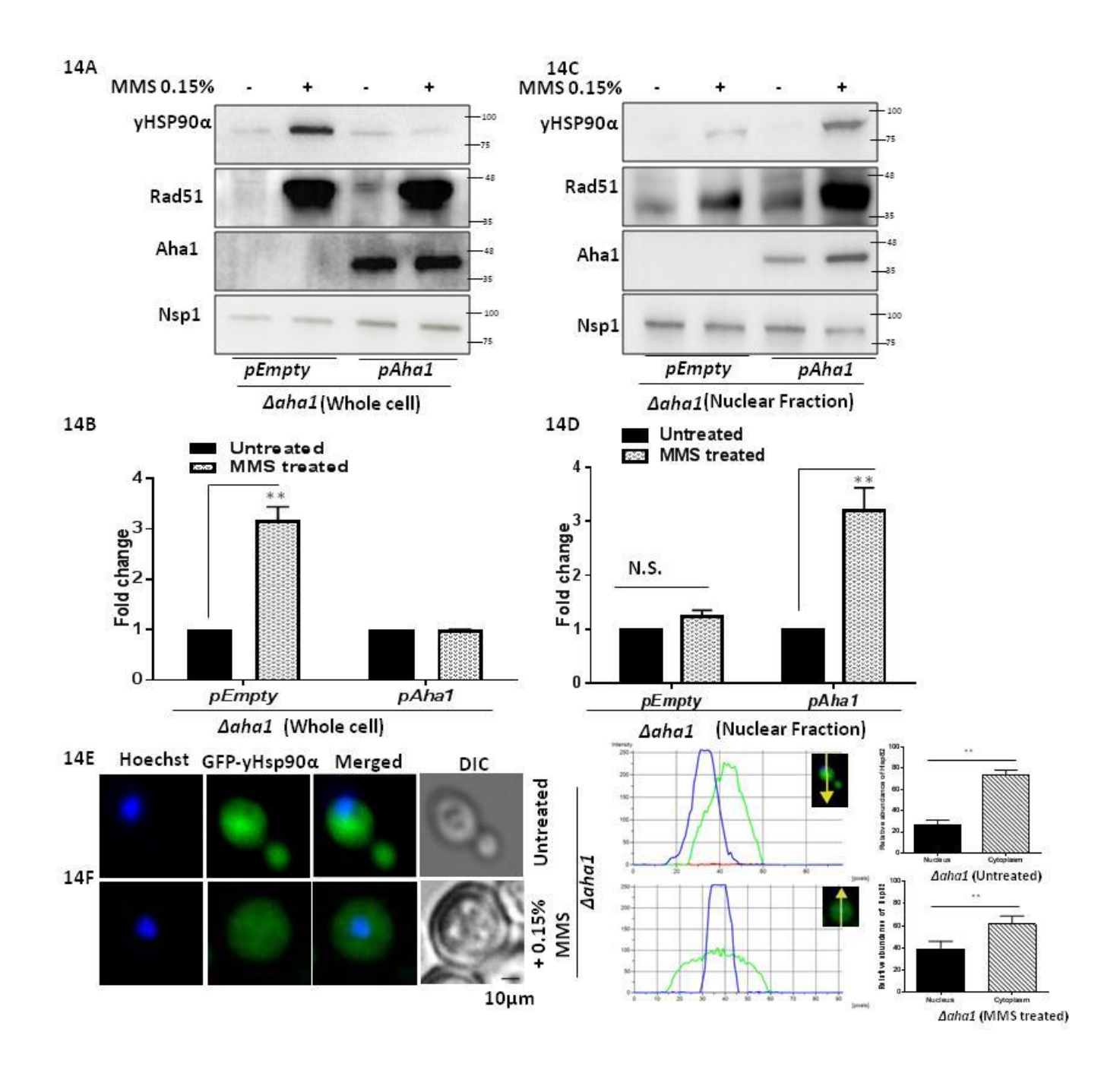


Fig. 14. yHsp90 α transport to the nucleus upon DNA damage is dependent on Aha1: (A) The endogenous level of yHsp90 α is induced in $\Delta aha1$ cells upon 0.15% MMS treatment. There is no difference in its expression between untreated and treated condition upon ectopic expression of AHA1. (B) yHsp90 α level was estimated from multiple independent experiments and plotted, Pvalues were calculated using the two-tailed Student's t test (**, P< 0.01, NS:

not significant). (C) Negligible accumulation of yHsp90 α occurs in the nucleus of $\Delta aha1$ cells upon 0.15% MMS treatment, whereas a marked increase was observed upon ectopic expression of AHA1 in $\Delta aha1$ cells under similar condition. (D) The nuclear level of yHsp90 α was estimated from multiple independent experiments and presented, P values were calculated using the two-tailed Student's t test (**, P< 0.01, NS: not significant). (E) Fluorescence images showing the distribution of GFP-yHsp90 α (green) in the whole cell of $\Delta aha1$ untreated cells. (F) Fluorescence images showing the distribution of GFP-yHsp90 α (green) in the whole cell of $\Delta aha1$ cells treated with 0.15% MMS. Nucleus (blue) was stained with Hoechst dye. Intensity profiles were derived for all fluorescence experiments using NIS elements AR software. Isogenic WT control are presented in Fig.7C, 7D. Relative fluorescence intensities of GFP-yHsp90 α in the nucleus and cytoplasm were quantified and the mean values (\pm SD) were plotted using GraphPad Prism.

4.4.4 The Aha1 dependent nuclear import of yHsp90 α is independent of genotypic background

To understand whether the Aha1 dependent nuclear import of yHsp90 α is a generalized phenomenon in budding yeasts, we used another $\Delta aha1$ strain in BY4741 background and wanted to test the same in this strain background. In BY4741 whole cell extract, where Aha1 protein was completely absent (Fig.15A, left panel), we found similar upregulation of yHsp90 α in response to MMS. However, we find complete abrogation of the nuclear accumulation of yHsp90 α (Fig.15A, right panel). We loaded higher amount of protein in MMS treated condition compared to the other lanes, as seen by the amount of Nsp1 (Fig.15A right panel, last lane), however there was no signal of yHsp90 α in the nuclear fraction. We overexpressed AHA1 in $BY4741\Delta aha1$ strain and performed the nuclear fractionation in presence and absence of MMS. The western blot of the whole cell extract showed no change in the endogenous level of yHsp90 α in presence and absence of MMS (Fig.15B, left panel). However, the presence of Aha1 promoted the nuclear import of yHsp90 α in MMS dependent manner (Fig.15B, right panel). Together, our data establish that presence of the Aha1 is essential for the nuclear localization of yHsp90 α

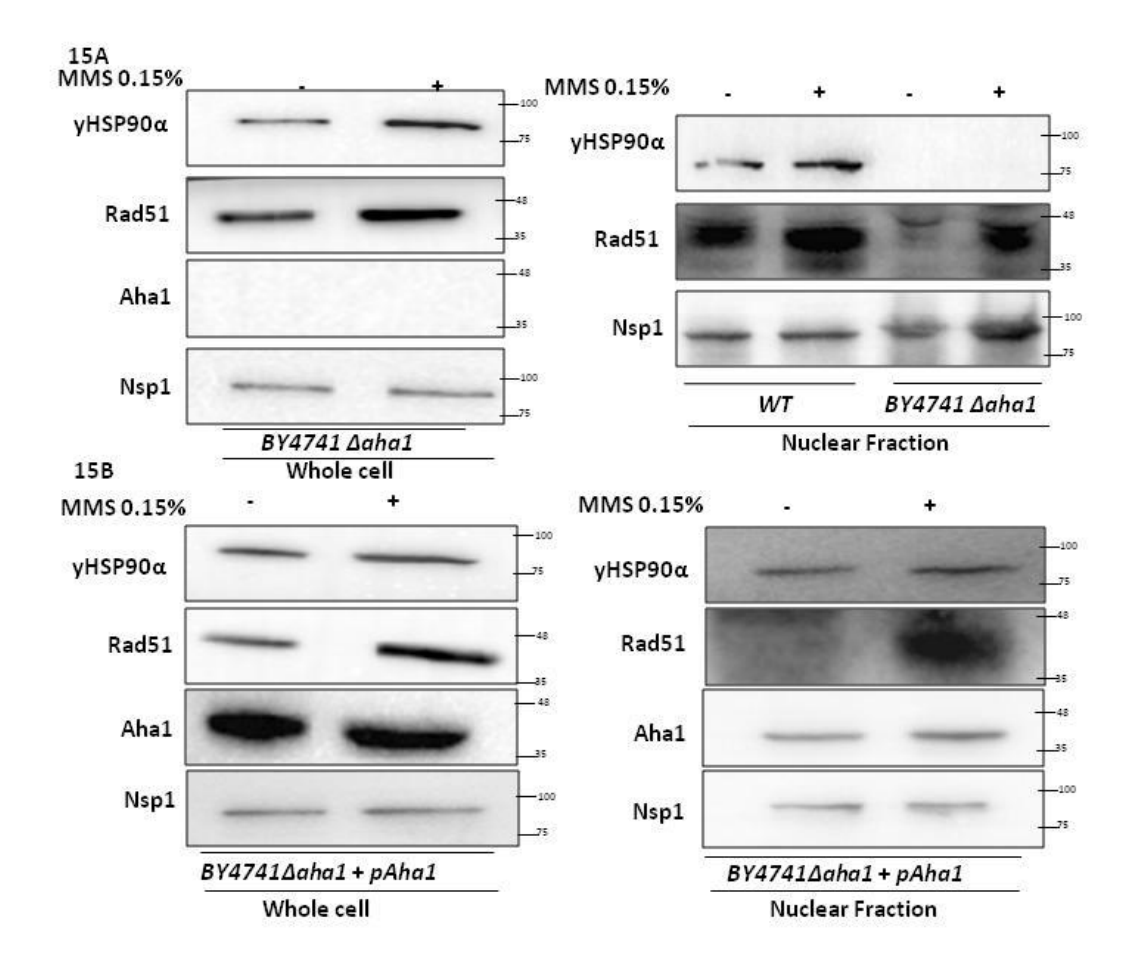


Fig. 15. yHsp90 α transport to the nucleus upon DNA damage is dependent on Aha1 in BY4741 strain: (A) Western blot analysis shows significant induction of endogenous levels of yHsp90 α upon 0.15% MMS treatment in BY4741 Δ aha1 strain (left panel). The increased nuclear accumulation of yHsp90 α was observed in WT strain but no signal of yHsp90 α was traced in the BY4741 Δ aha1 strain upon 0.15% MMS treatment (right panel). (B) The left panel represents the expression of respective proteins in the whole cell extract of BY4741 Δ aha1 strain harbouring AHA1 expression plasmid. The right panel displays that ectopic expression of AHA1 rescued the defect in nuclear accumulation of yHsp90 α in BY4741 Δ aha1 strain. In all the experiments Rad51 served as a control for DNA damage and Nsp1 acted as a loading control.

4.4.5 The charged linker domain of yHsp90 α is essential for its nuclear translocation upon DNA damage

It was earlier established that the conformational flexibility between the NTD andMD of vHsp90α is mediated by a flexible CL spanning 211-259 residues, as presented in the schematic diagram (Fig. 16A). The deletion of these highly charged amino acid stretches (211-259), leads to significant reduction in Aha1-stimulated ATP hydrolysis of yHsp90α(269). However, deletion of a shorter stretch (211-242) does not alter the conformational flexibility of the mutant protein and it shows comparable Aha1 mediated ATPase activation of vHsp90α as that of the wild-type protein(269). We wanted to determine whether this domain known for providing conformational flexibility between the NTD and the MD is important for its nuclear import. We investigated the MMS induced nuclear import of the two mutant proteins yHsp $90\alpha^{\Delta(211-259)}$ andyHsp $90\alpha^{\Delta(211-242)}$ using live-cell fluorescence imaging. For that, we generated NFY33 and NFY35 strains that harbor a centromeric plasmid expressing GFP-yHsp $90\alpha^{\Delta(211-259)}$ and GFP-yHsp $90\alpha^{\Delta(211-242)}$ respectively. We observe that in the GFP-yHsp $90\alpha^{\Delta(211-259)}$ harboring strain, GFP fluorescence does not merge with Hoechst fluorescence in the presence (Fig.16C) as well as absence of MMS (Fig.16B). However, there is a distinct nuclear accumulation in case of the shorter deletion mutant GFP-yHsp $90\alpha^{\Delta(211-242)}$ upon MMS treatment (Fig.16D and 16E). A representative image from each sample is presented. In order to confirm the result by an alternate method, we isolated the nuclear fraction from the previously characterized CL deletion strain(260) which was shown to be severely defective in HR activity(164).

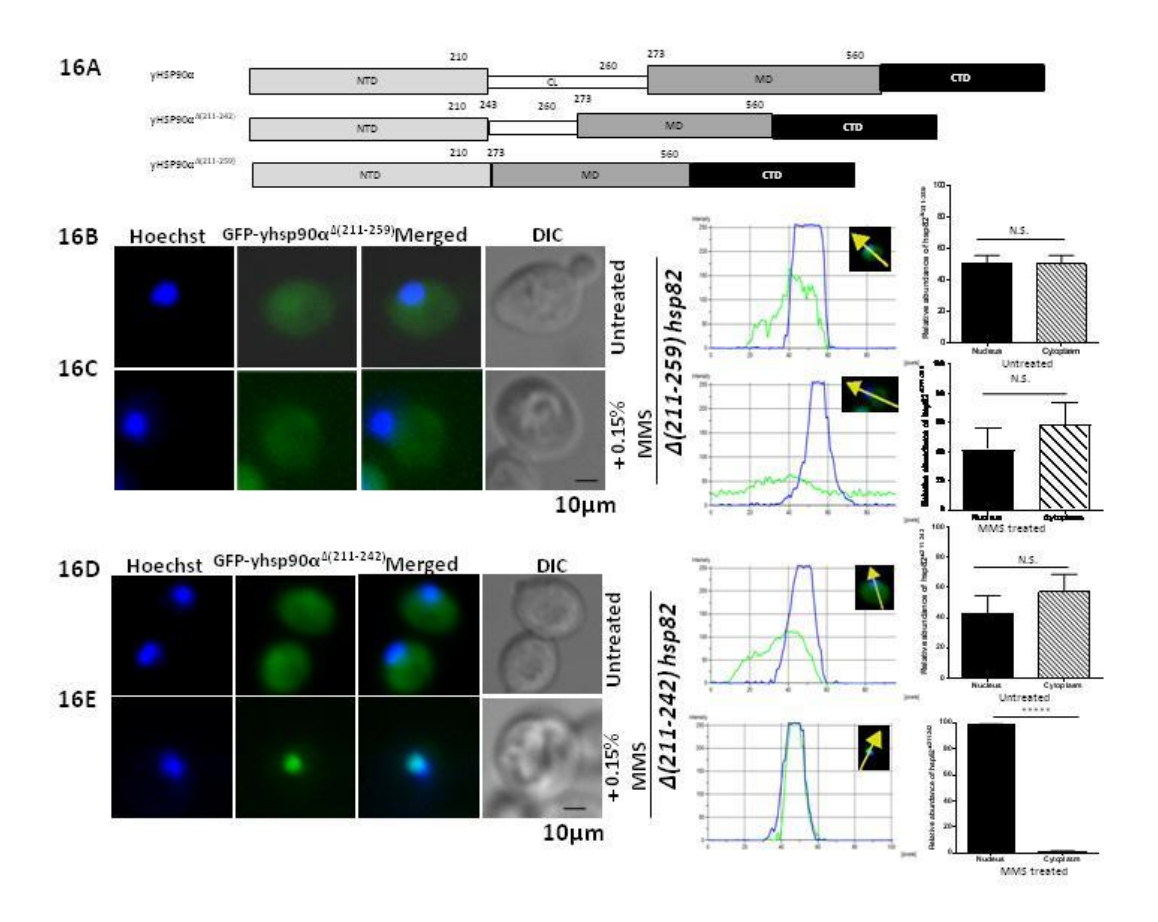


Fig. 16. The domain responsible for the conformational flexibility between the NTD and the MD of yHsp90 α is essential for its nuclear translocation upon DNA damage: (A) Schematic representation of wild-type and two CL deletion mutants of yHsp90 α . (B) Fluorescence images showing the distribution of GFP-yHsp90 $\alpha^{\Delta(211-259)}$ (green) in the whole cell both in the untreated and (C) in 0.15% MMS treated condition. (D) Fluorescence images showing the distribution of GFP-yHsp90 $\alpha^{\Delta(211-242)}$ (green) in the whole cell in untreated condition but (E) nuclear localization in 0.15% MMS treated condition. Intensity profiles were derived for all fluorescence experiments using NIS elements AR software; relative fluorescence intensities of GFP-yHsp90 α mutants in the nucleus and cytoplasm were quantified and the mean values (±SD) were plotted using GraphPad Prism. P values were calculated using the two-tailed Student's t test (*****, P< 0.00001; N.S., Not significant).

We observed complete absence of the mutant protein vHsp90 $\alpha^{\Delta(211-259)}$ in the nucleus of the MMS treated cell (Fig.17A, right panel). We loaded higher amount of the mutant protein compared to the wild-type as seen by the level of Nsp1 (last lane, Fig.17A, right panel), but could not detect the protein in the nucleus. The western blot analysis of the whole-cell extracts with the mutant strain confirmed the expression of the mutant protein (Fig.17A, left panel). To test whether Aha1 over-expression can promote the MMS induced nuclear import of the longer CL deletion mutant, we transformed AHA1 over-expression plasmid in the $hsp82\Delta(211-259)$ strain. We found that AHA1 over-expression did not impact the movement of the mutant protein to the nucleus (Fig.17B, right panel). It was previously shown that the charged linker region of human Hsp90a provides flexibility for domain rearrangements and acts as a modulator of chaperone activity(25). We wanted to determine whether the deletion of identical stretch of charged residues from human Hsp90a causes a similar defect. To that end, we have generated a strain harbouring human $HsHsp90\alpha^{\Delta(224-279)}$, still expressing endogenous yHsp90 α (Fig.6). We found that the mutant human protein did not show (Fig.17C) any increased nuclear accumulation upon DNA damage. The level of γHsp90α was increased in the nucleus under such conditions (third panel, Fig.17C). Next, we performed the nuclear fractionation to detect the level of the shorter CL deletion mutant yHsp $90\alpha^{\Delta(211-242)}$ upon MMS treatment. For that, we created a strain KRAY16, in which the endogenous Hsp82 and Hsc82 are knocked out and the strain expresses yHsp90^{Δ(211-242)} from a single copy plasmid. We observed that the mutant protein is accumulated to the nucleus in response to MMS treatment, correlating our live-cell imaging data (Fig.17D). The experiment was repeated 3-times and we estimated that the band intensities showed about 4fold increase in the nuclear level of the mutant yHsp $90\alpha^{\Delta(211-242)}$ in this strain background (Fig. 17E). Taken together, we conclude that the CL domain of Hsp90α is essential for its import

to the nucleus. To support our conclusion further, we measured the single DSB induced chromatin recruitment of the mutant yHsp $90\alpha^{\Delta(211-259)}$. For that, we created a modified NA14 strain harboring a plasmid that expressed the mutant yHsp $90\alpha^{\Delta(211-259)}$ fused with GFP at its amino terminal end. We studied the recruitment of wild-type (GFP-yHsp90a) and mutant GFP $yHsp90\alpha^{\Delta(211-259)}$ on the broken DNA at $2^{nd}hr$ post DNA damage induction, as there was maximum damage at the 2ndhr time point. We found no detectable recruitment of GFPyHsp $90\alpha^{\Delta(211-259)}$; whereas wild-type GFP-yHsp 90α was detected at the HO cleavage site, 2-hr post HO induction and IgG precipitation acted as a negative control (Fig.17F). Using western blot analysis, we determined the levels of the wild-type and the mutant protein in the immunoprecipitated samples of the 2-hr post HO induction, and didn't observe any noticeable difference (Fig.17F, lower panel). We repeated the chromatin immunoprecipitation assay thrice with these two strains and quantified the occupancy of the wild type and the CL deleted protein at the HO cleavage site. We found that the mutant protein was severely defective in its recruitment compared to the WT protein (Fig.17G). In order to determine the specificity of the CL domain for the nuclear import we have investigated the effect of an ATPase dead mutant, hsp82T101I(264), that also affects the amino-terminal association of yHsp90 $\alpha(270)$. We exposed the mutant strain and the isogenic wild-type strain to MMS and observed that the nuclear import of the mutant protein showed a similar trend as that of the wild-type yHsp90α (Fig.17H). We have estimated the levels of yHsp90α and Rad51 from the P82a and mutant strain and presented graphically (Fig.17I). We observed that both yHsp90α and yHsp90α^{T101I} showed nearly 2-fold increased level in the nucleus. However, as expected and reported earlier(164), the level of Rad51 was highly reduced in the mutant strain, although showed similar fold upregulation in the nucleus upon MMS treatment. Thus, using two separation of function mutants of yHsp90α our

study reveals that the CL domain of yHSP90, which is responsible for the Aha1 mediated conformational rearrangement, but not the ATPase domain, is required for the nuclear import of yHsp90 α .

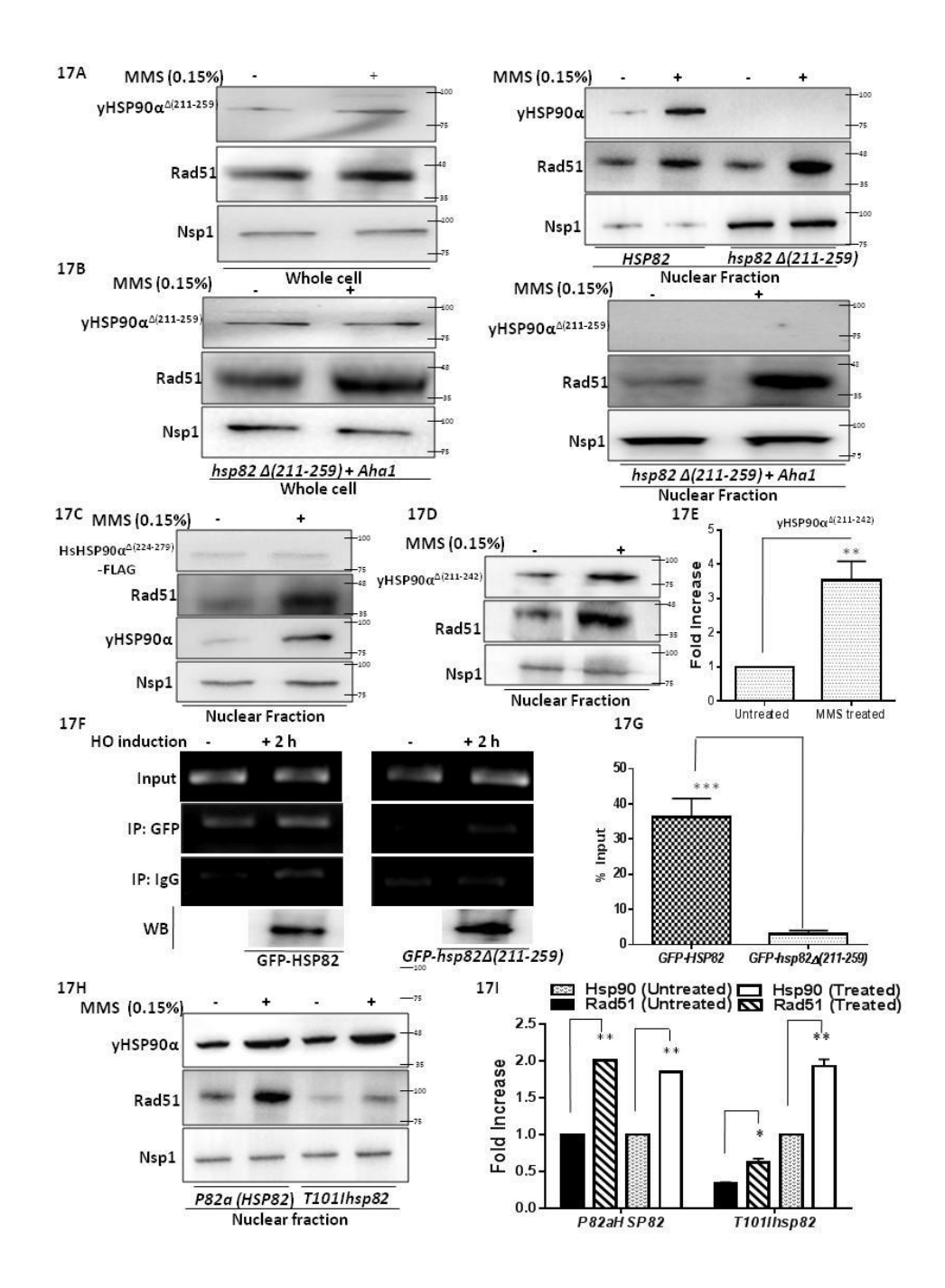


Fig. 17. The subcellular fractionation of various mutants of yHSP90 α in response to DNA damage: (A) Western blots showing the endogenous levels of yHsp90 $\alpha^{\Delta(211-259)}$ in whole cell extract in presence and absence of MMS treatment (Left panel). Increased nuclear accumulation of yHsp90 α^{WT} but no nuclear accumulation of yHsp90 $\alpha^{\Delta(211-259)}$ upon 0.15% MMS treatment was observed (Right panel). (B) Endogenous levels of yHsp90 $\alpha^{\Delta(211-259)}$ in whole cell extract (left panel) and in nucleus (right panel) shows that no nuclear accumulation of

yHsp $90\alpha^{\Delta(211-259)}$ upon 0.15% MMS treatment even if AHA1 was over-expressed in the cells. (C)Western blot showing no nuclear accumulation of FLAG tagged HsHsp $90\alpha^{\Delta(224-279)}$ upon 0.15% MMS treatment. (D) Western blot showing increased nuclear accumulation of vHsp $90\alpha^{\Delta(211-242)}$ upon 0.15% MMS treatment. (E) The experiment was repeated and the quantification of the western blots showed 4-fold increase in the nuclear level of the mutant yHsp $90\alpha^{\Delta(211-242)}$ upon MMS treatment. (F) Chromatin immunoprecipitation (ChIP) assay were done using NA14 strain harboring either GFP tagged yHSP90 α vector or GFP tagged CL deleted mutant yhsp90 α vector. Anti GFP antibody was used to pull down WT and CL deleted mutant γHsp90α from uninduced and 2 h HO induced samples. The pellet fraction was PCR amplified; the recruitment of GFP tagged yHsp90aWT was detected at 2h of HO induction while the recruitment of the mutant protein was not detected. The samples were normalized with respect to input. The lower panel shows the western blotting of the IP sample, which detects the presence of comparable amount of the wild-type and the mutant protein in the +2 h galactose treated samples. (G) The ChIP assay was repeated twice (n=2) and the occupancy of the GFP-Hsp82WT and the GFP-Hsp82^{\(\Delta\)} at the HO cleavage site were plotted. (H) Western blot showing increased nuclear accumulation of vHsp90 α in P82a strain as well as in an isogenic hsp82T1011 strain upon 0.15% MMS treatment. Rad51 levels were very less in the hsp82T1011 strain as expected, nonetheless it shows significant upregulation upon MMS treatment. (I) Quantification of the western blots from multiple experiments shows significant increase in the nuclear level of both yHsp90α and Rad51 in the WT and the mutant strain.

4.4.6 Loss of nuclear translocation of yHsp90 α is correlated with increased sensitivity to MMS

Earlier study in our laboratory demonstrated that the mutant yHsp90 $\alpha^{\Delta(211-259)}$ displays extreme MMS sensitivity and drastic reduction in Rad51-mediated gene targeting efficiency in yeast(164). Our present study shows that this mutant is defective in nuclear import associated with the induction of DNA damage. To study whether the nuclear import of yHsp90 α during genotoxic stress condition is directly linked to the protection against MMS induced cell death, we measured the MMS sensitivity of the mutant yHsp90 $\alpha^{\Delta(211-242)}$ and compared with the isogenic wild-type and yHsp90 $\alpha^{\Delta(211-259)}$ strains. We observed that yHsp90 $\alpha^{\Delta(211-242)}$ strain showed similar viability as that of the wild-type strain in presence of 0.03% MMS (Fig.18) whereas the larger CL deleted mutant yHsp90 $\alpha^{\Delta(211-259)}$ showed significant reduction in cell survivability. Hence, our study establishes that DNA damage induced enhanced nuclear accumulation of yHsp90 α is a major determinant for providing protective activity against genotoxic stress.

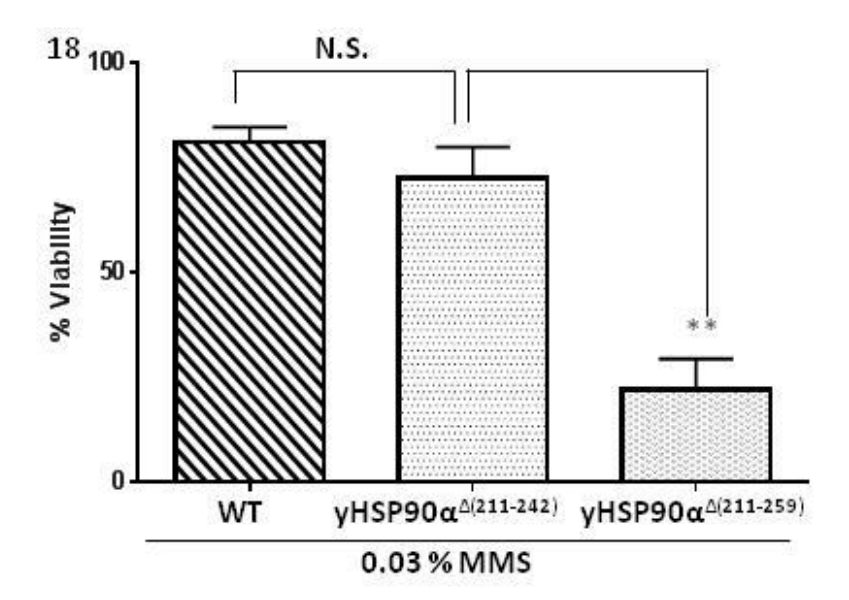


Fig. 18. Loss of nuclear translocation of yHSP90 α is correlated with increased sensitivity to MMS: Percent survivability of yHsp90 $\alpha^{\Delta(211-259)}$, yHsp90 $\alpha^{\Delta(211-242)}$ and isogenic wild-type strains were determined after exposure to 0.03% MMS for 2 hrs.

Discussion

Rad51 protein, which facilitates the homologous strand exchange, is the central player for HR in mammalian cells. The Rad51 foci formation in response to DNA damage is one of the regulatory events in HR. Previous studies in our lab have established that, besides providing the stability to Rad51 protein, yHsp90α also controls its nuclear function (164). We found that yeast cells harbouring a CL deletion mutant of yHsp90α, yHsp90α^{Δ211-259}(59), show reduced Rad51 mediated DNA damage induced foci formation (164). In our present study, we have deciphered that the dynamic interaction between yHsp90a and Rad51 can influence the nuclear function of Rad51. We have found that DNA damage triggers the dissociation between Rad51 and yHsp90a which could be a prerequisite for the nuclear function of Rad51. Studies in our lab have characterised an HR dead mutant of Rad51, i.e, Rad51E108L which shows severe reduction in Rad51 mediated gene conversion and cells harbouring this mutant are highly sensitive to DNA damage agents (257). In Rad51^{E108L}, we observed that Rad51^{E108L} remains locked along with yHsp90α even when treated with 0.15% MMS and hence the dynamic association observed with Rad51^{WT} is lost. We have thus found that there exists a positive correlation between the extent of yHsp90α-Rad51 dissociation post DNA damage and Rad51 nuclear activity during DNA repair. We have, for the first time, demonstrated that apart from regulating Rad51 function, yHSP90a displays a non-canonical nuclear function during DNA repair in yeast. We observed that cytoplasmic yHSP90a is redistributed to the nucleus in response to DNA damage and this phenomenon is crucial for maintaining genome stability. We analysed two well-characterized CL deletion mutants of yHSP90a that are different by the presence of 17 amino-acid stretches in the linker region (59). The mutant vHSP90 $\alpha^{\Delta(211-242)}$ shows wild-type like survivability upon MMS

treatment and displays increase in cytoplasm to nuclear accumulation under similar treatment. However, the mutant yHSP90 $\alpha^{\Delta(211-259)}$ fails to get accumulated in the nucleus and displays 4-fold reduction in cell survivability compared to the mutant yHSP90 $\alpha^{\Delta(211-242)}$. This suggests essential nuclear function of yHSP90 α during DNA damage.

Comparing the kinetics of the DSB repair and extent of its recruitment we conclude that yHSP90α may not be involved in maintenance of protein complexes that are recruited immediately after generation of DSB. In our assay, yHSP90α didn't show its immediate association at the 1st hr, even when majority of the DNA was broken. Rather its binding during 2nd and 3rd hr indicates its probable function during DNA repair. Furthermore, at those time points, γHSP90α shows significant association up to 4 kb distal position from the cleavage site, in a similar pattern to the known HR protein, Rad51. Hence, in this study we propose that the nuclear import and subsequent recruitment of yHSP90α to the DNA repair site is a pre-requisite for effective DNA repair. To establish that further, we studied the extent of chromatinassociation of the mutant GFP-yHSP90 $\alpha^{\Delta(211-259)}$ which has been previously found to be HR deficient (164). We found that this mutant is completely defective in its recruitment to the DSB ends. Hence, we concluded that nuclear import of yHSP90α, followed by its recruitment to the broken ends of DNA is a pre-requisite for effective DNA repair via HR mediated DNA repair pathway failure of which can significantly reduce Rad51 nucleoprotein filament formation. It is noteworthy that yHSP90α does not have any DNA binding domain, so it probably associates with chromatin via some unidentified proteins.

In this study we have also identified the structural determinant of yHSP90 α that enables its nuclear translocation. yHSP90 α adopts multiple conformational changes in its chaperone cycle, one of them being mediated by the ATPase stimulator Aha1, that regulates yHSP90 α 's allosteric

timing. However, how these conformational changes alter its physiological function remains obscure. An earlier biochemical study showed that the conformational flexibility within the NTD and MD of yHSP90 α is crucial for Aha1 mediated acceleration of ATP hydrolysis of yHSP90 α (59). We speculated that the initial step of Aha1-mediated partially closed conformational rearrangement of yHSP90 α could be essential for its nuclear import(271). Firstly, the absence of *AHA1* completely abrogates the nuclear import of yHSP90 α in two different strain backgrounds which are completely reversed on ectopic expression of *AHA1*. Secondly the conformationally-rigid CL deletion mutant yHSP90 α ^{A(211-259)}, which has a 2.5-fold reduction in Aha1-dependent ATPase activity, is fully defective in its nuclear accumulation, although the smaller CL deletion mutant that has wild-type like Aha1-dependent ATPase activity is fully competent in nuclear import. Lastly, the yHSP90 α ^{T1011} mutant which is an ATPase-dead mutant with reduced aminoterminal association shows no defect in nuclear translocation.

Earlier studies in our lab (164) demonstrated that the cytoplasmic function of yHSP90α is essential for DNA repair. However, our present study illustrates that the nuclear function of yHSP90α is also an important determinant for effective DNA repair. It is noteworthy that although the nuclear import of yHSP90α does not depend on its canonical ATPase activity, as seen in case of *T101Ihsp82*, however, being an ATPase dead mutant, Rad51 stability is greatly reduced in this mutant background. In our earlier study we reported that this mutant shows severe sensitivity to DNA damaging agents (164). Thus, using two separation of function mutants, namely *T101Ihsp82* and CL deletion mutant, we demonstrate that the N-terminal domain and the CL domain have distinct functions in DNA repair: while the NTD is required for the functional stability of the client proteins belonging to the HR pathway, the CL is important

for the nuclear import of yHsp90, which is a pre-requisite for its nuclear role at the time of DSB repair.

It was earlier reported by two independent studies that DNA-PK (266) and ATM (181), are responsible for the Thr-5/7 phosphorylation of human HSP90α in response to DNA damage. Both the enzymes are the members of PIKK family that are the sensors of DNA damage. However, an ortholog of DNA-PK is absent in yeast. Besides, the first 14 amino-acids are also absent from yHSP90α. It was never addressed whether there is an induction in the nuclear level of *Hs*Hsp90α in response to genotoxic stress or whether T7/5 phosphorylation is essential for its nuclear import as well as chromatin-recruitment. Using human HSP90α and its mutant (T7-A) we have shown that in yeast the nuclear translocation of *Hs*Hsp90α is independent of T7 phosphorylation. Further, the ChIP analysis confirms that the association of yHSP90α to the damaged chromatin is independent of the presence of first 14 amino-acid residues (including T-7). This kind of stress induced nuclear translocation of yHSP90α was also reported earlier in budding yeast, under the condition of glucose starvation (262).

We have established for the first time that Aha1 is an important regulator for DNA repair pathway. We observed AHA1 was transcriptionally up-regulated in response to DNA damage and showed about 3-fold upregulation in protein level. Using two different strain background of $\Delta aha1$, we showed that Aha1 regulates nuclear import of yHSP90 α . The absence of nuclear accumulation of yHSP90 α in $\Delta aha1$ strain was fully restored with ectopic expression of AHA1. Although enhanced accumulation of Aha1 was observed into the nucleus under MMS treatment as well as upon induction of single DSB in the genome, its nuclear function during DNA repair has not been addressed in this study.

In this study we observed that yHSP90 α and two of its co-chaperones Sba1 and Aha1 behaved differently upon MMS treatment. yHSP90 α is not induced but it is redistributed to the nucleus during genotoxic stress. Although both Aha1 and Sba1 are induced during genotoxic stress, in the case of Aha1, a concomitant increase in its nuclear level was observed, whereas there was no such increase in nuclear level of Sba1 was found. It could be possible that Aha1 has both nuclear and cytoplasmic roles whereas Sba1 has a cytoplasmic role during DNA repair. However, further studies are required to illuminate the significance of this finding.

To summarise, we have proposed a model (Fig.19) for this study where we claim that yHsp90 α not only regulates Rad51 function during the HR mediated DNA repair pathway but itself displays a nuclear function important for the maintenance of genomic stability during genotoxic stress. Furthermore, if the Aha1 mediated nuclear import of yHsp90 α is hampered by the deletion of *AHA1* or the deletion of the charged linker region which prevents the Aha1 mediated conformational switch, the cells are rendered HR deficient.

We speculate that in mammalian system also such Aha1 assisted nuclear import of Hsp90 α might exist, which need to be explored in future. Our finding is very significant as it may open new avenues of research to target Aha1 for arresting HR mediated DSB repair in cancer cells. Besides, it has been reported earlier in Drosophila and mammals that HSP90 α occupies the promoter regions of several coding and non-coding genes and regulates the gene expression in response to external stimuli (130, 134). If further studies confirm that even in higher eukaryotes the nuclear import of HSP90 α is dependent on Aha1, then the inhibition of Aha1 can be used as a tool to decipher the nuclear function of HSP90 α .

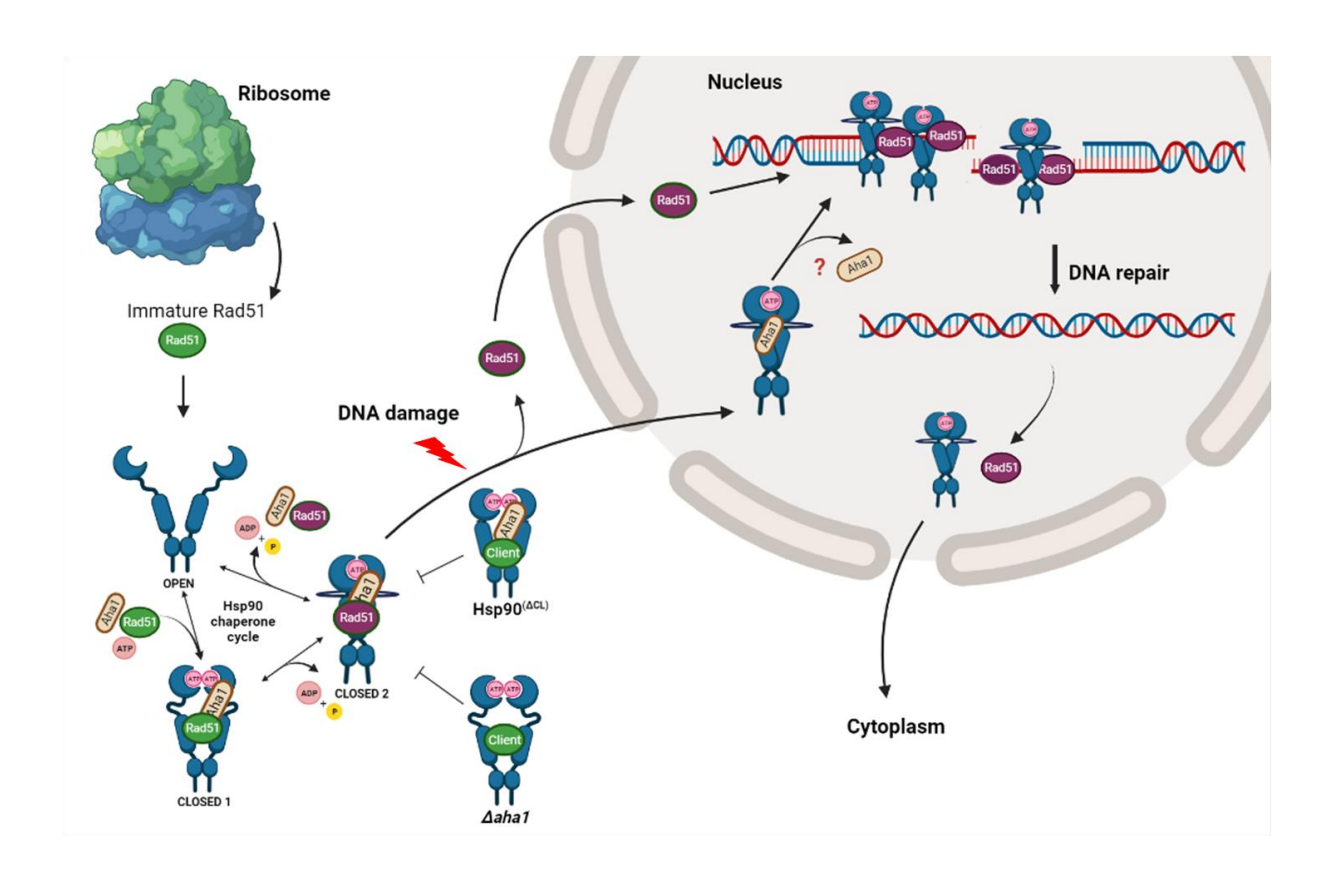


Fig. 19. Schematic diagram showing a representative model of the study

References

- 1. Craig, E. A., Gambill, B. D., and Nelson, R. J. (1993) Heat shock proteins: molecular chaperones of protein biogenesis. *Microbiol. Rev.* **57**, 402–414
- Kim, Y. E., Hipp, M. S., Bracher, A., Hayer-Hartl, M., and Ulrich Hartl, F. (2013)
 Molecular Chaperone Functions in Protein Folding and Proteostasis. *Annu. Rev. Biochem.* 82, 323–355
- 3. Buchner, J. (2019) Molecular chaperones and protein quality control: An introduction to the JBC Reviews thematic series. *J. Biol. Chem.* **294**, 2074–2075
- 4. Hartl, F. U., Bracher, A., and Hayer-Hartl, M. (2011) Molecular chaperones in protein folding and proteostasis. *Nature*. **475**, 324–332
- Schuh, S., Yonemoto, W., Brugge, J., Bauer, V. J., Riehl, R. M., Sullivan, W. P., and Toft,
 D. O. (1985) A 90,000-dalton binding protein common to both steroid receptors and the
 Rous sarcoma virus transforming protein, pp60v-src. J. Biol. Chem. 260, 14292–14296
- 6. Sanchez, E. R., Toft, D. O., Schlesinger, M. J., and Pratt, W. B. (1985) Evidence that the 90-kDa phosphoprotein associated with the untransformed L-cell glucocorticoid receptor is a murine heat shock protein. *J. Biol. Chem.* **260**, 12398–12401
- 7. García-Cardeña, G., Fan, R., Shah, V., Sorrentino, R., Cirino, G., Papapetropoulos, A., and Sessa, W. C. (1998) Dynamic activation of endothelial nitric oxide synthase by Hsp90. *Nature*. **392**, 821–824

- 8. Holt, S. E., Aisner, D. L., Baur, J., Tesmer, V. M., Dy, M., Ouellette, M., Trager, J. B., Morin, G. B., Toft, D. O., Shay, J. W., Wright, W. E., and White, M. A. (1999) Functional requirement of p23 and Hsp90 in telomerase complexes. *Genes Dev.* 13, 817–826
- 9. Minet, E., Mottet, D., Michel, G., Roland, I., Raes, M., Remacle, J., and Michiels, C. (1999) Hypoxia-induced activation of HIF-1: role of HIF-1alpha-Hsp90 interaction. *FEBS Lett.* **460**, 251–256
- 10. Sato, N., Yamamoto, T., Sekine, Y., Yumioka, T., Junicho, A., Fuse, H., and Matsuda, T. (2003) Involvement of heat-shock protein 90 in the interleukin-6-mediated signaling pathway through STAT3. *Biochem. Biophys. Res. Commun.* **300**, 847–852
- 11. Lotz, G. P., Brychzy, A., Heinz, S., and Obermann, W. M. J. (2008) A novel HSP90 chaperone complex regulates intracellular vesicle transport. *J. Cell Sci.* **121**, 717–723
- Lin, J. J., and Hemenway, C. S. (2010) Hsp90 Directly Modulates the Spatial Distribution of AF9/MLLT3 and Affects Target Gene Expression. *J. Biol. Chem.* 285, 11966
- 13. Taipale, M., Jarosz, D. F., and Lindquist, S. (2010) HSP90 at the hub of protein homeostasis: Emerging mechanistic insights. *Nat. Rev. Mol. Cell Biol.* **11**, 515–528
- 14. Johnson, J. L. (2012) Evolution and function of diverse Hsp90 homologs and cochaperone proteins. *Biochim. Biophys. Acta Mol. Cell Res.* **1823**, 607–613
- 15. Johnson, J. L., and Brown, C. (2009) Plasticity of the Hsp90 chaperone machine in divergent eukaryotic organisms. *Cell Stress Chaperones*. **14**, 83
- 16. Jackson, S. E. (2013) Hsp90: structure and function. *Top. Curr. Chem.* **328**, 155–240

- 17. Hoter, A., El-Sabban, M., and Naim, H. (2018) The HSP90 Family: Structure, Regulation, Function, and Implications in Health and Disease. *Int. J. Mol. Sci.* **19**, 2560
- 18. Dutta, R., and Inouye, M. (2000) GHKL, an emergent ATPase/kinase superfamily. *Trends Biochem. Sci.* **25**, 24–28
- Guarnieri, M. T., Zhang, L., Shen, J., and Zhao, R. (2008) The Hsp90 Inhibitor Radicicol Interacts with the ATP-Binding Pocket of Bacterial Sensor Kinase PhoQ. *J. Mol. Biol.* 379, 82–93
- 20. Panaretou, B., Prodromou, C., Roe, S. M., O'brien, R., Ladbury, J. E., Piper, P. W., and Pearl, L. H. (1998) ATP binding and hydrolysis are essential to the function of the Hsp90 molecular chaperone in vivo. *EMBO J.* **17**, 4829–4836
- 21. Prodromou, C., Roe, S. M., O'Brien, R., Ladbury, J. E., Piper, P. W., and Pearl, L. H. (1997) Identification and structural characterization of the ATP/ADP-binding site in the Hsp90 molecular chaperone. *Cell.* **90**, 65–75
- Prodromou, C., Roe, S. M., Piper, P. W., and Pearl, L. H. (1997) A molecular clamp in the crystal structure of the N-terminal domain of the yeast Hsp90 chaperone. *Nat. Struct. Biol.* 4, 477–482
- 23. Roe, S. M., Prodromou, C., O'Brien, R., Ladbury, J. E., Piper, P. W., and Pearl, L. H. (1999) Structural basis for inhibition of the Hsp90 molecular chaperone by the antitumor antibiotics radicicol and geldanamycin. *J. Med. Chem.* **42**, 260–266
- 24. Shiau, A. K., Harris, S. F., Southworth, D. R., and Agard, D. A. (2006) Structural

- Analysis of E. coli hsp90 Reveals Dramatic Nucleotide-Dependent Conformational Rearrangements. *Cell.* **127**, 329–340
- 25. Tsutsumi, S., Mollapour, M., Prodromou, C., Lee, C. T., Panaretou, B., Yoshida, S., Mayer, M. P., and Neckers, L. M. (2012) Charged linker sequence modulates eukaryotic heat shock protein 90 (Hsp90) chaperone activity. *Proc. Natl. Acad. Sci. U. S. A.* 109, 2937–2942
- 26. Jahn, M., Rehn, A., Pelz, B., Hellenkamp, B., Richter, K., Riefa, M., Buchner, J., and Hugel, T. (2014) The charged linker of the molecular chaperone Hsp90 modulates domain contacts and biological function. *Proc. Natl. Acad. Sci. U. S. A.* **111**, 17881–17886
- 27. Meyer, P., Prodromou, C., Hu, B., Vaughan, C., Roe, S. M., Panaretou, B., Piper, P. W., and Pearl, L. H. (2003) Structural and functional analysis of the middle segment of hsp90: implications for ATP hydrolysis and client protein and cochaperone interactions. *Mol. Cell.* 11, 647–658
- 28. Meng, X., Devin, J., Sullivan, W. P., Toft, D., Baulieu, E. E., and Catelli, M. G. (1996) Mutational analysis of Hsp90 alpha dimerization and subcellular localization: dimer disruption does not impede "in vivo" interaction with estrogen receptor." J. Cell Sci. 109, 1677–1687
- 29. Scheufler, C., Brinker, A., Bourenkov, G., Pegoraro, S., Moroder, L., Bartunik, H., Hartl, F. U., and Moarefi, I. (2000) Structure of TPR domain-peptide complexes: Critical elements in the assembly of the Hsp70-Hsp90 multichaperone machine. *Cell.* 101, 199–210

- 30. Prodromou, C., Siligardi, G., O'Brien, R., Woolfson, D. N., Regan, L., Panaretou, B., Ladbury, J. E., Piper, P. W., and Pearl, L. H. (1999) Regulation of Hsp90 ATPase activity by tetratricopeptide repeat (TPR)-domain co-chaperones. *EMBO J.* **18**, 754
- 31. Soti, C., Vermes, A., Haystead, T. A. J., and Csermely, P. (2003) Comparative analysis of the ATP-binding sites of Hsp90 by nucleotide affinity cleavage: a distinct nucleotide specificity of the C-terminal ATP-binding site. *Eur. J. Biochem.* **270**, 2421–2428
- 32. Graf, C., Lee, C.-T., Eva Meier-Andrejszki, L., Nguyen, M. T. N., and Mayer, M. P. (2014) Differences in conformational dynamics within the Hsp90 chaperone family reveal mechanistic insights. *Front. Mol. Biosci.* **1**, 4
- 33. Felts, S. J., Owen, B. A. L., Nguyen, P. M., Trepel, J., Donner, D. B., and Toft, D. O. (2000) The hsp90-related protein TRAP1 is a mitochondrial protein with distinct functional properties. *J. Biol. Chem.* **275**, 3305–3312
- 34. Chen, B., Zhong, D., and Monteiro, A. (2006) Comparative genomics and evolution of the HSP90 family of genes across all kingdoms of organisms. *BMC Genomics*. **7**, 1–19
- Jahn, M., Tych, K., Girstmair, H., Steinmaßl, M., Hugel, T., Buchner, J., and Rief, M.
 (2018) Folding and Domain Interactions of Three Orthologs of Hsp90 Studied by Single-Molecule Force Spectroscopy. *Structure*. 26, 96-105.e4
- 36. Csermely, P., Kajtár, J., Hollósi, M., Jalsovszky, G., Holly, S., Kahn, C. R., Gergely, P., Söti, C., Mihály, K., and Somogyi, J. (1993) ATP induces a conformational change of the 90-kDa heat shock protein (hsp90). *J. Biol. Chem.* **268**, 1901–1907

- Grenert, J. P., Sullivan, W. P., Fadden, P., Haystead, T. A. J., Clark, J., Mimnaugh, E., Krutzsch, H., Ochel, H. J., Schulte, T. W., Sausville, E., Neckers, L. M., and Toft, D. O. (1997) The amino-terminal domain of heat shock protein 90 (hsp90) that binds geldanamycin is an ATP/ADP switch domain that regulates hsp90 conformation. *J. Biol. Chem.* 272, 23843–23850
- 38. Schopf, F. H., Biebl, M. M., and Buchner, J. (2017) The HSP90 chaperone machinery.

 Nat. Rev. Mol. Cell Biol. 18, 345–360
- 39. Sullivan, W., Stensgard, B., Caucutt, G., Bartha, B., McMahon, N., Alnemri, E. S., Litwack, G., and Toft, D. (1997) Nucleotides and two functional states of hsp90. *J. Biol. Chem.* 272, 8007–8012
- 40. Southworth, D. R., and Agard, D. A. (2008) Species-dependent ensembles of conserved conformational states define the Hsp90 chaperone ATPase cycle. *Mol. Cell.* **32**, 631–640
- 41. Hessling, M., Richter, K., and Buchner, J. (2009) Dissection of the ATP-induced conformational cycle of the molecular chaperone Hsp90. *Nat. Struct. Mol. Biol.* **16**, 287–293
- 42. Bose, S., Weikl, T., Bügl, H., and Buchner, J. (1996) Chaperone function of Hsp90-associated proteins. *Science*. **274**, 1715–1717
- 43. Li, J., Soroka, J., and Buchner, J. (2012) The Hsp90 chaperone machinery: Conformational dynamics and regulation by co-chaperones. *Biochim. Biophys. Acta Mol. Cell Res.* **1823**, 624–635

- 44. Sahasrabudhe, P., Rohrberg, J., Biebl, M. M., Rutz, D. A., and Buchner, J. (2017) The Plasticity of the Hsp90 Co-chaperone System. *Mol. Cell.* **67**, 947-961.e5
- 45. Fang, Y., Fliss, A. E., Rao, J., and Caplan, A. J. (1998) SBA1 encodes a yeast hsp90 cochaperone that is homologous to vertebrate p23 proteins. *Mol. Cell. Biol.* **18**, 3727–34
- 46. Kosano, H., Stensgard, B., Charlesworth, M. C., McMahon, N., and Toft, D. (1998) The assembly of progesterone receptor-hsp90 complexes using purified proteins. *J. Biol. Chem.* **273**, 32973–32979
- Marozkina, N. V., Yemen, S., Borowitz, M., Liu, L., Plapp, M., Sun, F., Islam, R., Erdmann-Gilmore, P., Townsend, R. R., Lichti, C. F., Mantri, S., Clapp, P. W., Randell, S. H., Gaston, B., and Zaman, K. (2010) Hsp 70/Hsp 90 organizing protein as a nitrosylation target in cystic fibrosis therapy. *Proc. Natl. Acad. Sci.* 107, 11393–11398
- Wang, X., Venable, J., LaPointe, P., Hutt, D. M., Koulov, A. V., Coppinger, J., Gurkan,
 C., Kellner, W., Matteson, J., Plutner, H., Riordan, J. R., Kelly, J. W., Yates, J. R., and
 Balch, W. E. (2006) Hsp90 Cochaperone Aha1 Downregulation Rescues Misfolding of
 CFTR in Cystic Fibrosis. Cell. 127, 803–815
- 49. Flom, G., Weekes, J., Williams, J. J., and Johnson, J. L. (2006) Effect of mutation of the tetratricopeptide repeat and asparatate-proline 2 domains of Sti1 on Hsp90 signaling and interaction in Saccharomyces cerevisiae. *Genetics*. **172**, 41–51
- Flom, G., Weekes, J., and Johnson, J. L. (2005) Novel interaction of the Hsp90 chaperone machine with Ssl2, an essential DNA helicase in Saccharomyces cerevisiae. *Curr. Genet.* 47, 368–380

- 51. Edlich, F., Erdmann, F., Jarczowski, F., Moutty, M. C., Weiwad, M., and Fischer, G. (2007) The Bcl-2 Regulator FKBP38-Calmodulin-Ca2+ Is Inhibited by Hsp90. *J. Biol. Chem.* **282**, 15341–15348
- 52. Okamoto, T., Nishimura, Y., Ichimura, T., Suzuki, K., Miyamura, T., Suzuki, T., Moriishi, K., and Matsuura, Y. (2006) Hepatitis C virus RNA replication is regulated by FKBP8 and Hsp90. *EMBO J.* **25**, 5015
- 53. Sun, L., Prince, T., Manjarrez, J. R., Scroggins, B. T., and Matts, R. L. (2012) Characterization of the interaction of Aha1 with components of the Hsp90 chaperone machine and client proteins. *Biochim. Biophys. Acta Mol. Cell Res.* **1823**, 1092–1101
- 54. Echtenkamp, F. J., Zelin, E., Oxelmark, E., Woo, J. I., Andrews, B. J., Garabedian, M., and Freeman, B. C. (2011) Global Functional Map of the p23 Molecular Chaperone Reveals an Extensive Cellular Network. *Mol. Cell.* **43**, 229–241
- 55. Caplan, A. J., Ma'Ayan, A., and Willis, I. M. (2007) Multiple Kinases and System Robustness: A Link Between Cdc37 and Genome Integrity. *Cell Cycle*. **6**, 3145
- 56. Graf, C., Stankiewicz, M., Kramer, G., and Mayer, M. P. (2009) Spatially and kinetically resolved changes in the conformational dynamics of the Hsp90 chaperone machine. *EMBO J.* **28**, 602
- 57. Wayne, N., and Bolon, D. N. (2010) Charge-rich regions modulate the anti-aggregation activity of Hsp90. *J. Mol. Biol.* **401**, 931
- 58. Tsutsumi, S., Mollapour, M., Graf, C., Lee, C. T., Scroggins, B. T., Xu, W., Haslerova, L.,

- Hessling, M., Konstantinova, A. A., Trepel, J. B., Panaretou, B., Buchner, J., Mayer, M. P., Prodromou, C., and Neckers, L. (2009) Hsp90 charged-linker truncation reverses the functional consequences of weakened hydrophobic contacts in the N domain. *Nat. Struct. Mol. Biol.* **16**, 1141–1147
- 59. Hainzl, O., Lapina, M. C., Buchner, J., and Richter, K. (2009) The charged linker region is an important regulator of Hsp90 function. *J. Biol. Chem.* **284**, 22559–22567
- Mollapour, M., Bourboulia, D., Beebe, K., Woodford, M. R., Polier, S., Hoang, A., Chelluri, R., Li, Y., Guo, A., Lee, M. J., Fotooh-Abadi, E., Khan, S., Prince, T., Miyajima, N., Yoshida, S., Tsutsumi, S., Xu, W., Panaretou, B., Stetler-Stevenson, W. G., Bratslavsky, G., Trepel, J. B., Prodromou, C., and Neckers, L. (2014) Asymmetric Hsp90 N-domain SUMOylation recruits Aha1 and ATP-competitive inhibitors. *Mol. Cell.* 53, 317
- Scroggins, B. T., Robzyk, K., Wang, D., Marcu, M. G., Tsutsumi, S., Beebe, K., Cotter,
 R. J., Felts, S., Toft, D., Karnitz, L., Rosen, N., and Neckers, L. (2007) An Acetylation
 Site in the Middle Domain of Hsp90 Regulates Chaperone Function. *Mol. Cell.* 25, 151–159
- 62. Mollapour, M., Tsutsumi, S., Donnelly, A. C., Beebe, K., Tokita, M. J., Lee, M. J., Lee, S., Morra, G., Bourboulia, D., Scroggins, B. T., Colombo, G., Blagg, B. S., Panaretou, B., Stetler-Stevenson, W. G., Trepel, J. B., Piper, P. W., Prodromou, C., Pearl, L. H., and Neckers, L. (2010) Swe1Wee1-Dependent Tyrosine Phosphorylation of Hsp90 Regulates Distinct Facets of Chaperone Function. *Mol. Cell.* 37, 333–343

- 63. Mollapour, M., Tsutsumi, S., Truman, A. W., Xu, W., Vaughan, C. K., Beebe, K., Konstantinova, A., Vourganti, S., Panaretou, B., Piper, P. W., Trepel, J. B., Prodromou, C., Pearl, L. H., and Neckers, L. (2011) Threonine 22 Phosphorylation Attenuates Hsp90 Interaction with Cochaperones and Affects Its Chaperone Activity. *Mol. Cell.* 41, 672–681
- 64. Retzlaff, M., Hagn, F., Mitschke, L., Hessling, M., Gugel, F., Kessler, H., Richter, K., and Buchner, J. (2010) Asymmetric Activation of the Hsp90 Dimer by Its Cochaperone Aha1. *Mol. Cell.* **37**, 344–354
- 65. Xu, W., Beebe, K., Chavez, J. D., Boysen, M., Lu, Y., Zuehlke, A. D., Keramisanou, D., Trepel, J. B., Prodromou, C., Mayer, M. P., Bruce, J. E., Gelis, I., and Neckers, L. (2019) Hsp90 middle domain phosphorylation initiates a complex conformational program to recruit the ATPase-stimulating cochaperone Aha1. *Nat. Commun.* 10, 2574
- 66. Nathan, D. F., Vos, M. H., and Lindquist, S. (1999) Identification of SSF1, CNS1, and HCH1 as multicopy suppressors of a Saccharomyces cerevisiae Hsp90 loss-of-function mutation. *Proc. Natl. Acad. Sci. U. S. A.* **96**, 1409–14
- 67. Meyer, P., Prodromou, C., Liao, C., Hu, B., Roe, S. M., Vaughan, C. K., Vlasic, I., Panaretou, B., Piper, P. W., and Pear, L. H. (2004) Structural basis for recruitment of the ATPase activator Aha1 to the Hsp90 chaperone machinery. *EMBO J.* **23**, 511–519
- 68. Armstrong, H., Wolmarans, A., Mercier, R., Mai, B., and LaPointe, P. (2012) The Co-Chaperone Hch1 Regulates Hsp90 Function Differently than Its Homologue Aha1 and Confers Sensitivity to Yeast to the Hsp90 Inhibitor NVP-AUY922. *PLoS One.* **7**, e49322
- 69. Lotz, G. P., Lin, H., Harst, A., and Obermann, W. M. J. (2003) Aha1 binds to the middle

- domain of Hsp90, contributes to client protein activation, and stimulates the ATPase activity of the molecular chaperone. *J. Biol. Chem.* **278**, 17228–17235
- 70. Reed, S. I. (1980) The selection of amber mutations in genes required for completion of start, the controlling event of the cell division cycle of S. cerevisiae. *Genetics*. **95**, 579–588
- 71. Caplan, A. J., Mandal, A. K., and Theodoraki, M. A. (2007) Molecular chaperones and protein kinase quality control. *Trends Cell Biol.* **17**, 87–92
- 72. Gray, P. J., Prince, T., Cheng, J., Stevenson, M. A., and Calderwood, S. K. (2008)

 Targeting the oncogene and kinome chaperone CDC37. *Nat. Rev. Cancer.* **8**, 491–495
- Vaughan, C. K., Gohlke, U., Sobott, F., Good, V. M., Ali, M. M. U., Prodromou, C.,
 Robinson, C. V., Saibil, H. R., and Pearl, L. H. (2006) Structure of an Hsp90-Cdc37-Cdk4
 Complex. Mol. Cell. 23, 697–707
- 74. Miyata, Y., and Nishida, E. (2005) CK2 binds, phosphorylates, and regulates its pivotal substrate Cdc37, an Hsp90-cochaperone. *Mol. Cell. Biochem.* 2005 2741. 274, 171–179
- 75. Shao, J., Prince, T., Hartson, S. D., and Matts, R. L. (2003) Phosphorylation of serine 13 is required for the proper function of the Hsp90 co-chaperone, Cdc37. *J. Biol. Chem.* **278**, 38117–38120
- Oberoi, J., Dunn, D. M., Woodford, M. R., Mariotti, L., Schulman, J., Bourboulia, D.,
 Mollapour, M., and Vaughan, C. K. (2016) Structural and functional basis of protein
 phosphatase 5 substrate specificity. *Proc. Natl. Acad. Sci.* 113, 9009–9014

- 77. Stepanova, L., Yang, G., DeMayo, F., Wheeler, T. M., Finegold, M., Thompson, T. C., and Harper, J. W. (2000) Induction of human Cdc37 in prostate cancer correlates with the ability of targeted Cdc37 expression to promote prostatic hyperplasia. *Oncogene*. **19**, 2186–2193
- 78. Smith, D. F., Faber, L. E., and Toft, D. O. (1990) Purification of unactivated progesterone receptor and identification of novel receptor-associated proteins. *J. Biol. Chem.* **265**, 3996–4003
- 79. Johnson, J. L., and Toft, D. O. (1995) Binding of p23 and hsp90 during assembly with the progesterone receptor. *Mol. Endocrinol.* **9**, 670–678
- 80. Fang, Y., Fliss, A. E., Rao, J., and Caplan, A. J. (1998) SBA1 Encodes a Yeast Hsp90 Cochaperone That Is Homologous to Vertebrate p23 Proteins . *Mol. Cell. Biol.* **18**, 3727–3734
- 81. Young, J. C., and Hartl, F. U. (2000) Polypeptide release by Hsp90 involves ATP hydrolysis and is enhanced by the co-chaperone p23. *EMBO J.* **19**, 5930–40
- 82. Richter, K., Walter, S., and Buchner, J. (2004) The Co-chaperone Sba1 Connects the ATPase Reaction of Hsp90 to the Progression of the Chaperone Cycle. *J. Mol. Biol.* **342**, 1403–1413
- 83. Ali, M. M. U., Mark Roe, S., Vaughan, C. K., Meyer, P., Panaretou, B., Piper, P. W., Prodromou, C., and Pearl, L. H. (2006) Crystal structure of an Hsp90-nucleotide-p23/Sba1 closed chaperone complex. *Nature*. **440**, 1013

- 84. Noddings, C. M., Wang, R. Y.-R., Johnson, J. L., and Agard, D. A. (2022) Structure of Hsp90–p23–GR reveals the Hsp90 client-remodelling mechanism. *Nature*. **601**, 465–469
- 85. Barrott, J. J., and Haystead, T. A. J. (2013) Hsp90, an unlikely ally in the war on cancer. *FEBS J.* **280**, 1381–96
- 86. Zagouri, F., Sergentanis, T. N., Nonni, A., Papadimitriou, C. A., Michalopoulos, N. V., Domeyer, P., Theodoropoulos, G., Lazaris, A., Patsouris, E., Zogafos, E., Pazaiti, A., and Zografos, G. C. (2010) Hsp90 in the continuum of breast ductal carcinogenesis: Evaluation in precursors, preinvasive and ductal carcinoma lesions. *BMC Cancer.* 10, 353
- 87. Birbo, B., Madu, E. E., Madu, C. O., Jain, A., Lu, Y., Birbo, B.;, Madu, E. E.;, Madu, C.
 O.;, Jain, A.;, and Lu, Y. (2021) Role of HSP90 in Cancer. *Int. J. Mol. Sci.* 22, 10317
- 88. Li, W., Sahu, D., and Tsen, F. (2012) Secreted Heat Shock Protein-90 (Hsp90) in Wound Healing and Cancer. *Biochim. Biophys. Acta.* **1823**, 730
- 89. Sahu, D., Zhao, Z., Tsen, F., Cheng, C. F., Park, R., Situ, A. J., Dai, J., Eginli, A., Shams, S., Chen, M., Ulmer, T. S., Conti, P., Woodley, D. T., and Li, W. (2012) A potentially common peptide target in secreted heat shock protein-90α for hypoxia-inducible factor-1α–positive tumors. *Mol. Biol. Cell.* **23**, 602
- 90. Khurana, N., Laskar, S., Bhattacharyya, M. K., and Bhattacharyya, S. (2016) Hsp90 induces increased genomic instability toward DNA-damaging agents by tuning down RAD53 transcription. *Mol. Biol. Cell.* 27, 2463–2478
- 91. McCready, J., Sims, J. D., Chan, D., and Jay, D. G. (2010) Secretion of extracellular

- hsp 90α via exosomes increases cancer cell motility: a role for plasminogen activation. BMC Cancer. 10, 294
- 92. Haas, T. L. (2005) Endothelial cell regulation of matrix metalloproteinases. *Can. J. Physiol. Pharmacol.* **83**, 1–7
- 93. Ray, J. M., and Stetler-Stevenson, W. G. (1995) Gelatinase A activity directly modulates melanoma cell adhesion and spreading. *EMBO J.* **14**, 908
- 94. Bohush, A., Bieganowski, P., and Filipek, A. (2019) Hsp90 and Its Co-Chaperones in Neurodegenerative Diseases. *Int. J. Mol. Sci.* **20**, 4976
- 95. Luo, W., Sun, W., Taldone, T., Rodina, A., and Chiosis, G. (2010) Heat shock protein 90 in neurodegenerative diseases. *Mol. Neurodegener.* **5**, 24
- 96. Miyata, Y., Nakamoto, H., and Neckers, L. (2013) The Therapeutic Target Hsp90 and Cancer Hallmarks. *Curr. Pharm. Des.* **19**, 347
- 97. Salminen, A., Ojala, J., Kaarniranta, K., Hiltunen, M., and Soininen, H. (2011) Hsp90 regulates tau pathology through co-chaperone complexes in Alzheimer's disease. *Prog. Neurobiol.* **93**, 99–110
- 98. Luo, W., Dou, F., Rodina, A., Chip, S., Kim, J., Zhao, Q., Moulick, K., Aguirre, J., Wu, N., Greengard, P., and Chiosis, G. (2007) Roles of heat-shock protein 90 in maintaining and facilitating the neurodegenerative phenotype in tauopathies. *Proc. Natl. Acad. Sci.* **104**, 9511–9516
- 99. Jinwal, U. K., Trotter, J. H., Abisambra, J. F., Koren, J., Lawson, L. Y., Vestal, G. D.,

- O'Leary, J. C., Johnson, A. G., Jin, Y., Jones, J. R., Li, Q., Weeber, E. J., and Dickey, C. A. (2011) The Hsp90 Kinase Co-chaperone Cdc37 Regulates Tau Stability and Phosphorylation Dynamics. *J. Biol. Chem.* **286**, 16976
- 100. Shelton, L. B., Koren, J., and Blair, L. J. (2017) Imbalances in the Hsp90 Chaperone Machinery: Implications for Tauopathies. *Front. Neurosci.* 11, 724
- 101. Kakeda, M., Arock, M., Schlapbach, C., and Yawalkar, N. (2014) Increased expression of heat shock protein 90 in keratinocytes and mast cells in patients with psoriasis. *J. Am. Acad. Dermatol.* 70, 683-690.e1
- 102. Mu, H., Wang, L., and Zhao, L. (2017) HSP90 inhibition suppresses inflammatory response and reduces carotid atherosclerotic plaque formation in ApoE mice. *Cardiovasc*. *Ther.* **35**, e12243
- 103. Li, F., Song, X., Su, G., Wang, Y., Wang, Z., Qing, S., Jia, J., Wang, Y., Huang, L., Zheng, K., and Wang, Y. (2019) AT-533, a Hsp90 inhibitor, attenuates HSV-1-induced inflammation. *Biochem. Pharmacol.* **166**, 82–92
- 104. Metz, K., Ezernieks, J., Sebald, W., and Duschl, A. (1996) Interleukin-4 upregulates the heat shock protein Hsp90alpha and enhances transcription of a reporter gene coupled to a single heat shock element. *FEBS Lett.* **385**, 25–28
- 105. Kakimura, J.-I., Kitamura, Y., Takata, K., Umeki, M., Suzuki, S., Shibagaki, K., Taniguchi, T., Nomura, Y., Gebicke-Haerter, P. J., Smith, M. A., Perry, G., and Shimohama, S. (2002) Microglial activation and amyloid-beta clearance induced by exogenous heat-shock proteins. *FASEB J.* **16**, 601–603

- 106. Dickey, C. A., Koren, J., Zhang, Y.-J., Xu, Y., Jinwal, U. K., Birnbaum, M. J., Monks, B., Sun, M., Cheng, J. Q., Patterson, C., Bailey, R. M., Dunmore, J., Soresh, S., Leon, C., Morgan, D., and Petrucelli, L. (2008) Akt and CHIP coregulate tau degradation through coordinated interactions. *Proc. Natl. Acad. Sci.* 105, 3622–3627
- 107. Dickey, C. A., Kamal, A., Lundgren, K., Klosak, N., Bailey, R. M., Dunmore, J., Ash, P., Shoraka, S., Zlatkovic, J., Eckman, C. B., Patterson, C., Dickson, D. W., Nahman, N. S., Hutton, M., Burrows, F., and Petrucelli, L. (2007) The high-affinity HSP90-CHIP complex recognizes and selectively degrades phosphorylated tau client proteins. *J. Clin. Invest.* 117, 648
- 108. Ambegaokar, S. S., and Jackson, G. R. (2011) Functional genomic screen and network analysis reveal novel modifiers of tauopathy dissociated from tau phosphorylation. *Hum. Mol. Genet.* **20**, 4947
- 109. Nagy, P. D., Wang, R. Y., Pogany, J., Hafren, A., and Makinen, K. (2011) Emerging picture of host chaperone and cyclophilin roles in RNA virus replication. *Virology*. **411**, 374–382
- 110. Geller, R., Taguwa, S., and Frydman, J. (2012) Broad action of Hsp90 as a host chaperone required for viral replication. *Biochim. Biophys. Acta.* **1823**, 698
- 111. Hung, J.-J., Chung, C.-S., and Chang, W. (2002) Molecular Chaperone Hsp90 Is Important for Vaccinia Virus Growth in Cells. *J. Virol.* **76**, 1379
- 112. Mah, D. C. W., Leone, G., Jankowski, J. M., and Lee, P. W. K. (1990) The N-terminal quarter of reovirus cell attachment protein sigma 1 possesses intrinsic virion-anchoring

- function. *Virology*. **179**, 95–103
- 113. Geller, R., Vignuzzi, M., Andino, R., and Frydman, J. (2007) Evolutionary constraints on chaperone-mediated folding provide an antiviral approach refractory to development of drug resistance. *Genes Dev.* **21**, 195
- Nakagawa, S. ichiro, Umehara, T., Matsuda, C., Kuge, S., Sudoh, M., and Kohara, M.
 (2007) Hsp90 inhibitors suppress HCV replication in replicon cells and humanized liver mice. *Biochem. Biophys. Res. Commun.* 353, 882–888
- 115. Roy, N., Nageshan, R. K., Ranade, S., and Tatu, U. (2012) Heat shock protein 90 from neglected protozoan parasites. *Biochim. Biophys. Acta Mol. Cell Res.* **1823**, 707–711
- 116. Banumathy, G., Singh, V., Pavithra, S. R., and Tatu, U. (2003) Heat Shock Protein 90 Function Is Essential for Plasmodium falciparum Growth in Human Erythrocytes. *J. Biol. Chem.* 278, 18336–18345
- 117. Shahinas, D., and Pillai, D. R. (2021) Role of Hsp90 in Plasmodium falciparum Malaria. in *Advances in experimental medicine and biology*, pp. 125–139, Springer Netherlands, Dordrecht, **1340**, 125–139
- 118. Pavithra, S. R., Banumathy, G., Joy, O., Singh, V., and Tatu, U. (2004) Recurrent Fever Promotes Plasmodium falciparum Development in Human Erythrocytes. *J. Biol. Chem.* **279**, 46692–46699
- 119. Kwiatkowski, D. (1989) Febrile temperatures can synchronize the growth of Plasmodium falciparum in vitro. *J. Exp. Med.* **169**, 357

- 120. Pallavi, R., Roy, N., Nageshan, R. K., Talukdar, P., Pavithra, S. R., Reddy, R., Venketesh, S., Kumar, R., Gupta, A. K., Singh, R. K., Yadav, S. C., and Tatu, U. (2010) Heat shock protein 90 as a drug target against protozoan infections: biochemical characterization of HSP90 from Plasmodium falciparum and Trypanosoma evansi and evaluation of its inhibitor as a candidate drug. *J. Biol. Chem.* 285, 37964–75
- Morales, M. A., Watanabe, R., Dacher, M., Chafey, P., Osorio y Fortéa, J., Scott, D. A., Beverley, S. M., Ommen, G., Clos, J., Hem, S., Lenormand, P., Rousselle, J.-C., Namane, A., and Späth, G. F. (2010) Phosphoproteome dynamics reveal heat-shock protein complexes specific to the Leishmania donovani infectious stage. *Proc. Natl. Acad. Sci.* 107, 8381–8386
- 122. Wiesgigl, M., and Clos, J. (2001) Heat shock protein 90 homeostasis controls stage differentiation in Leishmania donovani. *Mol. Biol. Cell.* **12**, 3307–3316
- 123. Zilberstein, D., and Shapira, M. (1994) The role of pH and temperature in the development of Leishmania parasites. *Annu. Rev. Microbiol.* **48**, 449–70
- 124. Zhao, R., Davey, M., Hsu, Y. C., Kaplanek, P., Tong, A., Parsons, A. B., Krogan, N., Cagney, G., Mai, D., Greenblatt, J., Boone, C., Emili, A., and Houry, W. A. (2005)
 Navigating the Chaperone Network: An Integrative Map of Physical and Genetic
 Interactions Mediated by the Hsp90 Chaperone. Cell. 120, 715–727
- 125. McClellan, A. J., Xia, Y., Deutschbauer, A. M., Davis, R. W., Gerstein, M., and Frydman, J. (2007) Diverse cellular functions of the Hsp90 molecular chaperone uncovered using systems approaches. *Cell.* 131, 121–135

- 126. Toogun, O. A., DeZwaan, D. C., and Freeman, B. C. (2008) The Hsp90 Molecular Chaperone Modulates Multiple Telomerase Activities. *Mol. Cell. Biol.* **28**, 457–467
- 127. Keppler, B. R., Grady, A. T., and Jarstfer, M. B. (2006) The biochemical role of the heat shock protein 90 chaperone complex in establishing human telomerase activity. *J. Biol. Chem.* **281**, 19840–19848
- 128. Forsythe, H. L., Jarvis, J. L., Turner, J. W., Elmore, L. W., and Holt, S. E. (2001) Stable Association of hsp90 and p23, but Not hsp70, with Active Human Telomerase. *J. Biol. Chem.* **276**, 15571–15574
- 129. Forstemann, K., Hoss, M., and Lingner, J. (2000) Telomerase-dependent repeat divergence at the 3' ends of yeast telomeres. *Nucleic Acids Res.* **28**, 2690–2694
- 130. Khurana, N., and Bhattacharyya, S. (2015) Hsp90, the concertmaster: tuning transcription. *Front. Oncol.* **5**, 100
- 131. Gvozdenov, Z., Bendix, L. D., Kolhe, J., and Freeman, B. C. (2019) The Hsp90 Molecular Chaperone Regulates the Transcription Factor Network Controlling Chromatin Accessibility. *J. Mol. Biol.* **431**, 4993–5003
- 132. Yost, H. J., and Lindquist, S. (1986) RNA splicing is interrupted by heat shock and is rescued by heat shock protein synthesis. *Cell.* **45**, 185–193
- 133. Morcillo, G., Diez, J. L., Carbajal, M. E., and Tanguay, R. M. (1993) HSP90 associates with specific heat shock puffs (hsr omega) in polytene chromosomes of Drosophila and Chironomus. *Chromosoma*. **102**, 648–659

- 134. Sawarkar, R., Sievers, C., and Paro, R. (2012) Hsp90 Globally Targets Paused RNA Polymerase to Regulate Gene Expression in Response to Environmental Stimuli. *Cell*. 149, 807–818
- Laskar, S., K, S., Bhattacharyya, M. K., Nair, A. S., Dhar, P., and Bhattacharyya, S.
 (2015) Heat Stress-Induced Cup9-Dependent Transcriptional Regulation of SIR2. *Mol. Cell. Biol.* 35, 437–450
- Echtenkamp, F. J., Gvozdenov, Z., Adkins, N. L., Zhang, Y., Lynch-Day, M., Watanabe,
 S., Peterson, C. L., and Freeman, B. C. (2016) Hsp90 and p23 Molecular Chaperones
 Control Chromatin Architecture by Maintaining the Functional Pool of the RSC
 Chromatin Remodeler. *Mol. Cell.* 64, 888–899
- 137. Logie, C., Tse, C., Hansen, J. C., and Peterson, C. L. (1999) The core histone N-terminal domains are required for multiple rounds of catalytic chromatin remodeling by the SWI/SNF and RSC complexes. *Biochemistry*. **38**, 2514–2522
- 138. Lorch, Y., Zhang, M., and Kornberg, R. D. (2001) RSC Unravels the Nucleosome. *Mol. Cell.* **7**, 89–95
- 139. Hamamoto, R., Furukawa, Y., Morita, M., Iimura, Y., Silva, F. P., Li, M., Yagyu, R., and Nakamura, Y. (2004) SMYD3 encodes a histone methyltransferase involved in the proliferation of cancer cells. *Nat. Cell Biol.* 2004 68. **6**, 731–740
- 140. Tariq, M., Nussbaumer, U., Chen, Y., Beisel, C., and Paro, R. (2009) Trithorax requires

 Hsp90 for maintenance of active chromatin at sites of gene expression. *Proc. Natl. Acad.*Sci. **106**, 1157–1162

- 141. Floer, M., Bryant, G. O., and Ptashne, M. (2008) HSP90/70 chaperones are required for rapid nucleosome removal upon induction of the GAL genes of yeast. *Proc. Natl. Acad.* Sci. 105, 2975–2980
- 142. Zhao, R., Kakihara, Y., Gribun, A., Huen, J., Yang, G., Khanna, M., Costanzo, M., Brost, R. L., Boone, C., Hughes, T. R., Yip, C. M., and Houry, W. A. (2008) Molecular chaperone Hsp90 stabilizes Pih1/Nop17 to maintain R2TP complex activity that regulates snoRNA accumulation. *J. Cell Biol.* 180, 563–578
- 143. Boulon, S., Pradet-Balade, B., Verheggen, C., Molle, D., Boireau, S., Georgieva, M., Azzag, K., Robert, M. C., Ahmad, Y., Neel, H., Lamond, A. I., and Bertrand, E. (2010) HSP90 and its R2TP/Prefoldin-like cochaperone are involved in the cytoplasmic assembly of RNA polymerase II. *Mol. Cell.* 39, 912–924
- 144. Horejsí, Z., Takai, H., Adelman, C. A., Collis, S. J., Flynn, H., Maslen, S., Skehel, J. M., de Lange, T., and Boulton, S. J. (2010) CK2 phospho-dependent binding of R2TP complex to TEL2 is essential for mTOR and SMG1 stability. *Mol. Cell.* **39**, 839–50
- 145. Takai, H., Xie, Y., De Lange, T., and Pavletich, N. P. (2010) Tel2 structure and function in the Hsp90-dependent maturation of mTOR and ATR complexes. *Genes Dev.* **24**, 2019–2030
- 146. Zou, L., and Elledge, S. J. (2003) Sensing DNA Damage Through ATRIP Recognition of RPA-ssDNA Complexes. *Science* (80-.). **300**, 1542–1548
- 147. Rodrigo-Brenni, M. C., Thomas, S., Bouck, D. C., and Kaplan, K. B. (2004) Sgt1p and Skp1p Modulate the Assembly and Turnover of CBF3 Complexes Required for Proper

- Kinetochore Function. Mol. Biol. Cell. 15, 3366–3378
- 148. Lingelbach, L. B., and Kaplan, K. B. (2004) The Interaction between Sgt1p and Skp1p Is Regulated by HSP90 Chaperones and Is Required for Proper CBF3 Assembly. *Mol. Cell. Biol.* 24, 8938–8950
- 149. Makhnevych, T., and Houry, W. A. (2012) The role of Hsp90 in protein complex assembly. *Biochim. Biophys. Acta Mol. Cell Res.* **1823**, 674–682
- 150. Miyoshi, T., Takeuchi, A., Siomi, H., and Siomi, M. C. (2010) A direct role for Hsp90 in pre-RISC formation in Drosophila. *Nat. Struct. Mol. Biol.* **17**, 1024–1026
- 151. Iwasaki, S., Kobayashi, M., Yoda, M., Sakaguchi, Y., Katsuma, S., Suzuki, T., and Tomari, Y. (2010) Hsc70/Hsp90 Chaperone Machinery Mediates ATP-Dependent RISC Loading of Small RNA Duplexes. *Mol. Cell.* 39, 292–299
- 152. Imai, J., Maruya, M., Yashiroda, H., Yahara, I., and Tanaka, K. (2003) The molecular chaperone Hsp90 plays a role in the assembly and maintenance of the 26S proteasome. *EMBO J.* **22**, 3557–3567
- 153. Yamano, T., Mizukami, S., Murata, S., Chiba, T., Tanaka, K., and Udono, H. (2008)
 Hsp90-mediated Assembly of the 26 S Proteasome Is Involved in Major
 Histocompatibility Complex Class I Antigen Processing. *J. Biol. Chem.* **283**, 28060–28065
- 154. Mankovich, A. G., and Freeman, B. C. (2022) Regulation of Protein Transport Pathways by the Cytosolic Hsp90s. *Biomolecules*. **12**, 1077

- 155. Fan, A. C. Y., Bhangoo, M. K., and Young, J. C. (2006) Hsp90 functions in the targeting and outer membrane translocation steps of Tom70-mediated mitochondrial import. *J. Biol. Chem.* **281**, 33313–33324
- 156. Young, J. C., Hoogenraad, N. J., and Hartl, F. U. (2003) Molecular chaperones Hsp90 and Hsp70 deliver preproteins to the mitochondrial import receptor Tom70. *Cell.* **112**, 41–50
- 157. Qbadou, S., Becker, T., Mirus, O., Tews, I., Soll, J., and Schleiff, E. (2006) The molecular chaperone Hsp90 delivers precursor proteins to the chloroplast import receptor Toc64. *EMBO J.* **25**, 1836–1847
- 158. Chen, C. Y., and Balch, W. E. (2006) The Hsp90 Chaperone Complex Regulates GDI-dependent Rab Recycling. *Mol. Biol. Cell.* **17**, 3494
- 159. Wu, Y., Ding, Y., Zheng, X., and Liao, K. (2020) The molecular chaperone Hsp90 maintains Golgi organization and vesicular trafficking by regulating microtubule stability. *J. Mol. Cell Biol.* **12**, 448–461
- 160. Lauwers, E., Wang, Y. C., Gallardo, R., Van der Kant, R., Michiels, E., Swerts, J., Baatsen, P., Zaiter, S. S., McAlpine, S. R., Gounko, N. V., Rousseau, F., Schymkowitz, J., and Verstreken, P. (2018) Hsp90 Mediates Membrane Deformation and Exosome Release.
 Mol. Cell. 71, 689-702.e9
- 161. Dubrez, L., Causse, S., Borges Bonan, N., Dumétier, B., and Garrido, C. (2020) Heat-shock proteins: chaperoning DNA repair. *Oncogene*. **39**, 516–529
- 162. Khurana, N., Bakshi, S., Tabassum, W., Bhattacharyya, M. K., and Bhattacharyya, S.

- (2018) Hsp90 Is Essential for Chl1-Mediated Chromosome Segregation and Sister Chromatid Cohesion. *mSphere*. 10.1128/mSphere.00225-18
- 163. Cheng, A. N., Fan, C.-C., Lo, Y.-K., Kuo, C.-L., Wang, H.-C., Lien, I.-H., Lin, S.-Y., Chen, C.-H., Jiang, S. S., Chang, I.-S., Juan, H.-F., Lyu, P.-C., and Lee, A. Y.-L. (2017) Cdc7-Dbf4-mediated phosphorylation of HSP90-S164 stabilizes HSP90-HCLK2-MRN complex to enhance ATR/ATM signaling that overcomes replication stress in cancer. *Sci. Rep.* **7**, 17024
- 164. Suhane, T., Laskar, S., Advani, S., Roy, N., Varunan, S., Bhattacharyya, D., Bhattacharyya, S., and Bhattacharyya, M. K. (2015) Both the charged linker region and ATPase domain of Hsp90 are essential for Rad51-dependent DNA repair. *Eukaryot. Cell.* 14, 64–77
- 165. Backe, S. J., Sager, R. A., Woodford, M. R., Makedon, A. M., and Mollapour, M. (2020)

 Post-translational modifications of Hsp90 and translating the chaperone code. *J. Biol. Chem.* **295**, 11099–11117
- Hornbeck, P. V., Zhang, B., Murray, B., Kornhauser, J. M., Latham, V., and Skrzypek, E.
 (2015) PhosphoSitePlus, 2014: Mutations, PTMs and recalibrations. *Nucleic Acids Res.*43, D512–D520
- 167. Kettenbach, A. N., Schweppe, D. K., Faherty, B. K., Pechenick, D., Pletnev, A. A., and Gerber, S. A. (2011) Quantitative phosphoproteomics identifies substrates and functional modules of Aurora and Polo-like kinase activities in mitotic cells. *Sci. Signal.* **4**, rs5
- 168. Xu, W., Mollapour, M., Prodromou, C., Wang, S., Scroggins, B. T., Palchick, Z., Beebe,

- K., Siderius, M., Lee, M. J., Couvillon, A., Trepel, J. B., Miyata, Y., Matts, R., and Neckers, L. (2012) Dynamic Tyrosine Phosphorylation Modulates Cycling of the HSP90-P50 CDC37-AHA1 Chaperone Machine. *Mol. Cell.* **47**, 434–443
- 169. Bachman, A. B., Keramisanou, Di., Xu, W., Beebe, K., Moses, M. A., Vasantha Kumar, M. V., Gray, G., Noor, R. E., van der Vaart, A., Neckers, L., and Gelis, I. (2018) Phosphorylation induced cochaperone unfolding promotes kinase recruitment and client class-specific Hsp90 phosphorylation. *Nat. Commun.* 9, 265
- 170. Rikova, K., Guo, A., Zeng, Q., Possemato, A., Yu, J., Haack, H., Nardone, J., Lee, K., Reeves, C., Li, Y., Hu, Y., Tan, Z., Stokes, M., Sullivan, L., Mitchell, J., Wetzel, R., MacNeill, J., Ren, J. M., Yuan, J., Bakalarski, C. E., Villen, J., Kornhauser, J. M., Smith, B., Li, D., Zhou, X., Gygi, S. P., Gu, T. L., Polakiewicz, R. D., Rush, J., and Comb, M. J. (2007) Global Survey of Phosphotyrosine Signaling Identifies Oncogenic Kinases in Lung Cancer. *Cell.* 131, 1190–1203
- Walter, R., Pan, K. T., Doebele, C., Comoglio, F., Tomska, K., Bohnenberger, H., Young,
 R. M., Jacobs, L., Keller, U., Bönig, H., Engelke, M., Rosenwald, A., Urlaub, H., Staudt,
 L. M., Serve, H., Zenz, T., and Oellerich, T. (2017) HSP90 promotes Burkitt lymphoma
 cell survival by maintaining tonic B-cell receptor signaling. *Blood.* 129, 598–608
- 172. Gu, T. L., Goss, V. L., Reeves, C., Popova, L., Nardone, J., MacNeill, J., Walters, D. K., Wang, Y., Rush, J., Comb, M. J., Druker, B. J., and Polakiewicz, R. D. (2006) Phosphotyrosine profiling identifies the KG-1 cell line as a model for the study of FGFR1 fusions in acute myeloid leukemia. *Blood*. 108, 4202–4204

- 173. Zuehlke, A. D., Reidy, M., Lin, C., LaPointe, P., Alsomairy, S., Lee, D. J., Rivera-Marquez, G. M., Beebe, K., Prince, T., Lee, S., Trepel, J. B., Xu, W., Johnson, J., Masison, D., and Neckers, L. (2017) An Hsp90 co-chaperone protein in yeast is functionally replaced by site-specific posttranslational modification in humans. *Nat. Commun.* 8, 15328
- 174. Duval, M., Le Bœuf, F., Huot, J., and Gratton, J. P. (2007) Src-mediated phosphorylation of Hsp90 in response to vascular endothelial growth factor (VEGF) is required for VEGF receptor-2 signaling to endothelial NO synthase. *Mol. Biol. Cell.* **18**, 4659–4668
- 175. Desjardins, F., Delisle, C., and Gratton, J.-P. (2012) Modulation of the Cochaperone AHA1 Regulates Heat-Shock Protein 90 and Endothelial NO Synthase Activation by Vascular Endothelial Growth Factor. *Arterioscler. Thromb. Vasc. Biol.* **32**, 2484–2492
- 176. Rose, D. W., Kramer, G., Hardesty, B., Wettenhall, R. E. H., and Kudlicki, W. (1987) The 90-Kilodalton Peptide of the Heme-Regulated eIF-2α Kinase Has Sequence Similarity with the 90-Kilodalton Heat Shock Protein. *Biochemistry*. **26**, 6583–6587
- 177. Solier, S., Kohn, K. W., Scroggins, B., Xu, W., Trepel, J., Neckers, L., and Pommier, Y. (2012) Heat shock protein 90α (HSP90α), a substrate and chaperone of DNA-PK necessary for the apoptotic response. *Proc. Natl. Acad. Sci.* **109**, 12866–12872
- 178. Park, S. J., Gavrilova, O., Brown, A. L., Soto, J. E., Bremner, S., Kim, J., Xu, X., Yang, S., Um, J. H., Koch, L. G., Britton, S. L., Lieber, R. L., Philp, A., Baar, K., Kohama, S. G., Abel, E. D., Kim, M. K., and Chung, J. H. (2017) DNA-PK Promotes the Mitochondrial, Metabolic, and Physical Decline that Occurs During Aging. *Cell Metab*.

- **25**, 1135-1146.e7
- 179. Pennisi, R., Antoccia, A., Leone, S., Ascenzi, P., and di Masi, A. (2017) Hsp90α regulates ATM and NBN functions in sensing and repair of DNA double-strand breaks. *FEBS J.* **284**, 2378–2395
- 180. Lees-Miller, S. P., and Anderson, C. W. (1989) The human double-stranded DNA-activated protein kinase phosphorylates the 90-kDa heat-shock protein, hsp90 alpha at two NH2-terminal threonine residues. *J. Biol. Chem.* **264**, 17275–80
- 181. Elaimy, A. L., Ahsan, A., Marsh, K., Pratt, W. B., Ray, D., Lawrence, T. S., and Nyati, M. K. (2016) ATM is the primary kinase responsible for phosphorylation of Hsp90α after ionizing radiation. *Oncotarget*. 7, 82450–82457
- 182. Molina, H., Horn, D. M., Tang, N., Mathivanan, S., and Pandey, A. (2007) Global proteomic profiling of phosphopeptides using electron transfer dissociation tandem mass spectrometry. *Proc. Natl. Acad. Sci.* **104**, 2199–2204
- 183. Lei, H., Venkatakrishnan, A., Yu, S., and Kazlauskas, A. (2007) Protein kinase Adependent translocation of Hsp90α impairs endothelial nitric-oxide synthase activity in high glucose and diabetes. *J. Biol. Chem.* **282**, 9364–9371
- 184. Hasan, M., Hama, S., and Kogure, K. (2019) Low Electric Treatment activates Rho GTPase via Heat Shock Protein 90 and Protein Kinase C for Intracellular Delivery of siRNA. *Sci. Rep.* **9**, 4114
- 185. Quanz, M., Herbette, A., Sayarath, M., De Koning, L., Dubois, T., Sun, J. S., and Dutreix,

- M. (2012) Heat shock protein 90α (Hsp90α) is phosphorylated in response to DNA damage and accumulates in repair foci. *J. Biol. Chem.* **287**, 8803–8815
- 186. Sharma, K., D'Souza, R. C. J., Tyanova, S., Schaab, C., Wiśniewski, J. R., Cox, J., and Mann, M. (2014) Ultradeep Human Phosphoproteome Reveals a Distinct Regulatory Nature of Tyr and Ser/Thr-Based Signaling. *Cell Rep.* **8**, 1583–1594
- 187. Mollapour, M., Tsutsumi, S., Kim, Y. S., Trepel, J., and Neckers, L. (2011) Casein kinase 2 phosphorylation of Hsp90 threonine 22 modulates chaperone function and drug sensitivity. *Oncotarget*. **2**, 407
- 188. He, Q., Liu, K., Tian, Z., and Du, S. J. (2015) The Effects of Hsp90α1 Mutations on Myosin Thick Filament Organization. *PLoS One*. **10**, e0142573
- 189. Dagar, M., Singh, J. P., Dagar, G., Tyagi, R. K., and Bagchi, G. (2019) Phosphorylation of HSP90 by protein kinase A is essential for the nuclear translocation of androgen receptor. *J. Biol. Chem.* 294, 8699–8710
- 190. Wang, X., Lu, X. A., Song, X., Zhuo, W., Jia, L., Jiang, Y., and Luo, Y. (2012) Thr 90 phosphorylation of Hsp90α by protein kinase A regulates its chaperone machinery. *Biochem. J.* **441**, 387–397
- 191. Xiaofeng, W., Xiaomin, S., Wei, Z., Yan, F., Hubing, S., Yun, L., Maomeng, T., Guodong, C., and Yongzhang, L. (2009) The regulatory mechanism of Hsp90α secretion and its function in tumor malignancy. *Proc. Natl. Acad. Sci. U. S. A.* **106**, 21288–21293
- 192. Tsai, C.-F., Wang, Y.-T., Yen, H.-Y., Tsou, C.-C., Ku, W.-C., Lin, P.-Y., Chen, H.-Y.,

- Nesvizhskii, A. I., Ishihama, Y., and Chen, Y.-J. (2015) Large-scale determination of absolute phosphorylation stoichiometries in human cells by motif-targeting quantitative proteomics. *Nat. Commun.* **6**, 6622
- Klammer, M., Kaminski, M., Zedler, A., Oppermann, F., Blencke, S., Marx, S., Müller,
 S., Tebbe, A., Godl, K., and Schaab, C. (2012) Phosphosignature predicts dasatinib
 response in non-small cell lung cancer. *Mol. Cell. Proteomics.* 11, 651–668
- 194. Huang, S. Y., Tsai, M. L., Chen, G. Y., Wu, C. J., and Chen, S. H. (2007) A systematic MS-based approach for identifying in vitro substrates of PKA and PKG in rat uteri. *J. Proteome Res.* **6**, 2674–2684
- 195. Lopez, V. A., Park, B. C., Nowak, D., Sreelatha, A., Zembek, P., Fernandez, J., Servage, K. A., Gradowski, M., Hennig, J., Tomchick, D. R., Pawłowski, K., Krzymowska, M., and Tagliabracci, V. S. (2019) A Bacterial Effector Mimics a Host HSP90 Client to Undermine Immunity. Cell. 179, 205-218.e21
- 196. Lu, X. A., Wang, X., Zhuo, W., Jia, L., Jiang, Y., Fu, Y., and Luo, Y. (2014) The regulatory mechanism of a client kinase controlling its own release from Hsp90 chaperone machinery through phosphorylation. *Biochem. J.* **457**, 171–183
- 197. Woodford, M. R., Truman, A. W., Dunn, D. M., Jensen, S. M., Cotran, R., Bullard, R., Abouelleil, M., Beebe, K., Wolfgeher, D., Wierzbicki, S., Post, D. E., Caza, T., Tsutsumi, S., Panaretou, B., Kron, S. J., Trepel, J. B., Landas, S., Prodromou, C., Shapiro, O., Stetler-Stevenson, W. G., Bourboulia, D., Neckers, L., Bratslavsky, G., and Mollapour, M. (2016) Mps1 Mediated Phosphorylation of Hsp90 Confers Renal Cell Carcinoma

- Sensitivity and Selectivity to Hsp90 Inhibitors. Cell Rep. 14, 872–884
- 198. Nguyen, M. T. N., Knieß, R. A., Daturpalli, S., Le Breton, L., Ke, X., Chen, X., and Mayer, M. P. (2017) Isoform-Specific Phosphorylation in Human Hsp90β Affects Interaction with Clients and the Cochaperone Cdc37. *J. Mol. Biol.* **429**, 732–752
- 199. Mayya, V., Lundgren, D. H., Hwang, S.-I., Rezaul, K., Wu, L., Eng, J. K., Rodionov, V., and Han, D. K. (2009) Quantitative phosphoproteomic analysis of T cell receptor signaling reveals system-wide modulation of protein-protein interactions. *Sci. Signal.* 2, ra46
- 200. Wiśniewski, J. R., Nagaraj, N., Zougman, A., Gnad, F., and Mann, M. (2010) Brain phosphoproteome obtained by a fasp-based method reveals plasma membrane protein topology. *J. Proteome Res.* **9**, 3280–3289
- 201. Soroka, J., Wandinger, S. K., Mäusbacher, N., Schreiber, T., Richter, K., Daub, H., and Buchner, J. (2012) Conformational Switching of the Molecular Chaperone Hsp90 via Regulated Phosphorylation. *Mol. Cell.* 45, 517–528
- 202. Lees-Miller, S. P., and Anderson, C. W. (1989) Two human 90-kDa heat shock proteins are phosphorylated in vivo at conserved serines that are phosphorylated in vitro by casein kinase II. *J. Biol. Chem.* **264**, 2431–2437
- 203. Kim, S. W., Hasanuzzaman, M., Cho, M., Heo, Y. R., Ryu, M. J., Ha, N. Y., Park, H. J., Park, H. Y., and Shin, J. G. (2015) Casein kinase 2 (CK2)-mediated phosphorylation of Hsp90β as a novel mechanism of rifampin-induced MDR1 expression. *J. Biol. Chem.* **290**, 17029–17040

- 204. Olesen, S. H., Ingles, D. J., Zhu, J. Y., Martin, M. P., Betzi, S., Georg, G. I., Tash, J. S., and Schönbrunn, E. (2015) Stability of the human Hsp90-p50Cdc37 chaperone complex against nucleotides and Hsp90 inhibitors, and the influence of phosphorylation by casein kinase 2. *Molecules*. **20**, 1643–1660
- 205. Kurokawa, M., Zhao, C., Reya, T., and Kornbluth, S. (2008) Inhibition of Apoptosome Formation by Suppression of Hsp90β Phosphorylation in Tyrosine Kinase-Induced Leukemias. *Mol. Cell. Biol.* **28**, 5494–5506
- 206. Woo, S. H., An, S., Lee, H. C., Jin, H. O., Seo, S. K., Yoo, D. H., Lee, K. H., Rhee, C. H., Choi, E. J., Hong, S. II, and Park, I. C. (2009) A truncated form of p23 down-regulates telomerase activity via disruption of Hsp90 function. *J. Biol. Chem.* **284**, 30871–30880
- 207. Wang, Z., Gucek, M., and Hart, G. W. (2008) Cross-talk between GlcNAcylation and phosphorylation: Site-specific phosphorylation dynamics in response to globally elevated O-GlcNAc. *Proc. Natl. Acad. Sci. U. S. A.* 105, 13793–13798
- 208. Ogiso, H., Kagi, N., Matsumoto, E., Nishimoto, M., Arai, R., Shirouzu, M., Mimura, J., Fujii-Kuriyama, Y., and Yokoyama, S. (2004) Phosphorylation analysis of 90 kDa heat shock protein within the cytosolic arylhydrocarbon receptor complex. *Biochemistry*. 43, 15510–15519
- 209. Qi, X., Xie, C., Hou, S., Li, G., Yin, N., Dong, L., Lepp, A., Chesnik, M. A., Mirza, S. P., Szabo, A., Tsai, S., Basir, Z., Wu, S., and Chen, G. (2014) Identification of a ternary protein-complex as a therapeutic target for K-Ras-dependent colon cancer. *Oncotarget*. 5, 4269–4282

- Mertins, P., Qiao, J. W., Patel, J., Udeshi, N. D., Clauser, K. R., Mani, D. R., Burgess, M. W., Gillette, M. A., Jaffe, J. D., and Carr, S. A. (2013) Integrated proteomic analysis of post-translational modifications by serial enrichment. *Nat. Methods.* 10, 634–637
- 211. Dephoure, N., Zhou, C., Villén, J., Beausoleil, S. A., Bakalarski, C. E., Elledge, S. J., and Gygi, S. P. (2008) A quantitative atlas of mitotic phosphorylation. *Proc. Natl. Acad. Sci.* 105, 10762–10767
- 212. Muller, P., Ruckova, E., Halada, P., Coates, P. J., Hrstka, R., Lane, D. P., and Vojtesek, B. (2013) C-terminal phosphorylation of Hsp70 and Hsp90 regulates alternate binding to co-chaperones CHIP and HOP to determine cellular protein folding/degradation balances. *Oncogene*. 32, 3101–3110
- 213. Zhou, H., Di Palma, S., Preisinger, C., Peng, M., Polat, A. N., Heck, A. J. R., and Mohammed, S. (2013) Toward a comprehensive characterization of a human cancer cell phosphoproteome. *J. Proteome Res.* **12**, 260–271
- Deb, T. B., Zuo, A. H., Wang, Y., Barndt, R. J., Cheema, A. K., Sengupta, S., Coticchia,
 C. M., and Johnson, M. D. (2011) Pnck induces ligand-independent EGFR degradation by
 probable perturbation of the Hsp90 chaperone complex. *Am. J. Physiol. Physiol.* 300,
 C1139–C1154
- 215. Shiromizu, T., Adachi, J., Watanabe, S., Murakami, T., Kuga, T., Muraoka, S., and Tomonaga, T. (2013) Identification of missing proteins in the neXtProt database and unregistered phosphopeptides in the PhosphoSitePlus database as part of the Chromosome-centric. *ACS Publ.* **12**, 2414–2421

- 216. Li, X., Robbins, N., O'Meara, T. R., and Cowen, L. E. (2017) Extensive functional redundancy in the regulation of Candida albicans drug resistance and morphogenesis by lysine deacetylases Hos2, Hda1, Rpd3 and Rpd31. *Mol. Microbiol.* 103, 635–656
- 217. Lamoth, F., Juvvadi, P. R., Soderblom, E. J., Moseley, M. A., Asfaw, Y. G., and Steinbacha, W. J. (2014) Identification of a key lysine residue in heat shock protein 90 required for azole and echinocandin resistance in Aspergillus fumigatus. *Antimicrob. Agents Chemother.* 58, 1889–1896
- 218. Wu, D., Gu, Q., Zhao, N., Xia, F., and Li, Z. (2015) Structure-based rational design of peptide hydroxamic acid inhibitors to target tumor necrosis factor- α converting enzyme as potential therapeutics for hepatitis. *J. Drug Target.* **23**, 936–942
- Choudhary, C., Kumar, C., Gnad, F., Nielsen, M. L., Rehman, M., Walther, T. C., Olsen,
 J. V., and Mann, M. (2009) Lysine Acetylation Targets Protein Complexes and Co-Regulates Major Cellular Functions. *Science* (80-.). 325, 834–840
- 220. Fiskus, W., Rao, R., Fernandez, P., Herger, B., Yang, Y., Chen, J., Kolhe, R., Mandawat, A., Wang, Y., Joshi, R., Eaton, K., Lee, P., Atadja, P., Peiper, S., and Bhalla, K. (2008) Molecular and biologic characterization and drug sensitivity of pan-histone deacetylase inhibitor resistant acute myeloid leukemia cells. *Blood*. 112, 2896–2905
- Yang, Y., Rao, R., Shen, J., Tang, Y., Fiskus, W., Nechtman, J., Atadja, P., and Bhalla, K.
 (2008) Role of acetylation and extracellular location of heat shock protein 90α in tumor cell invasion. *Cancer Res.* 68, 4833–4842
- 222. Wang, Y., Fiskus, W., Chong, D. G., Buckley, K. M., Natarajan, K., Rao, R., Joshi, A.,

- Balusu, R., Koul, S., Chen, J., Savoie, A., Ustun, C., Jillella, A. P., Atadja, P., Levine, R. L., and Bhalla, K. N. (2009) Cotreatment with panobinostat and JAK2 inhibitor TG101209 attenuates JAK2V617F levels and signaling and exerts synergistic cytotoxic effects against human myeloproliferative neoplastic cells. *Blood.* **114**, 5024–5033
- 223. Yang, C., Rahimpour, S., Lu, J., Pacak, K., Ikejiri, B., Brady, R. O., and Zhuang, Z. (2013) Histone deacetylase inhibitors increase glucocerebrosidase activity in Gaucher disease by modulation of molecular chaperones. *Proc. Natl. Acad. Sci. U. S. A.* 110, 966–971
- 224. Jochems, J., Teegarden, S. L., Chen, Y., Boulden, J., Challis, C., Ben-Dor, G. A., Kim, S. F., and Berton, O. (2015) Enhancement of stress resilience through histone deacetylase 6-mediated regulation of glucocorticoid receptor chaperone dynamics. *Biol. Psychiatry.* 77, 345–355
- 225. Woodford, M. R., Hughes, M., Sager, R. A., Backe, S. J., Baker-Williams, A. J., Bratslavsky, M. S., Jacob, J. M., Shapiro, O., Wong, M., Bratslavsky, G., Bourboulia, D., and Mollapour, M. (2019) Mutation of the co-chaperone tsc1 in bladder cancer diminishes HSP90 acetylation and reduces drug sensitivity and selectivity. *Oncotarget*. 10, 5824–5834
- 226. Weinert, B. T., Schölz, C., Wagner, S. A., Iesmantavicius, V., Su, D., Daniel, J. A., and Choudhary, C. (2013) Lysine succinylation is a frequently occurring modification in prokaryotes and eukaryotes and extensively overlaps with acetylation. *Cell Rep.* **4**, 842–851

- 227. Zhang, Y., Dayalan Naidu, S., Samarasinghe, K., Van Hecke, G. C., Pheely, A., Boronina, T. N., Cole, R. N., Benjamin, I. J., Cole, P. A., Ahn, Y. H., and Dinkova-Kostova, A. T. (2014) Sulphoxythiocarbamates modify cysteine residues in HSP90 causing degradation of client proteins and inhibition of cancer cell proliferation. *Br. J. Cancer.* 110, 71–82
- 228. Shibata, T., Kimura, Y., Mukai, A., Mori, H., Ito, S., Asaka, Y., Oe, S., Tanaka, H., Takahashi, T., and Uchida, K. (2011) Transthiocarbamoylation of proteins by thiolated isothiocyanates. *J. Biol. Chem.* **286**, 42150–42161
- 229. Abu-Farha, M., Lanouette, S., Elisma, F., Tremblay, V., Butson, J., Figeys, D., and Couture, J. F. (2011) Proteomic analyses of the SMYD family interactomes identify HSP90 as a novel target for SMYD2. *J. Mol. Cell Biol.* **3**, 301–308
- 230. Hamamoto, R., Toyokawa, G., Nakakido, M., Ueda, K., and Nakamura, Y. (2014) SMYD2-dependent HSP90 methylation promotes cancer cell proliferation by regulating the chaperone complex formation. *Cancer Lett.* **351**, 126–133
- 231. Rehn, A., Lawatscheck, J., Jokisch, M.-L., Mader, S. L., Luo, Q., Tippel, F., Blank, B., Richter, K., Lang, K., Kaila, V. R. I., and Buchner, J. (2020) A methylated lysine is a switch point for conformational communication in the chaperone Hsp90. *Nat. Commun.* 11, 1219
- 232. Olsen, J. B., Cao, X. J., Han, B., Chen, L. H., Horvath, A., Richardson, T. I., Campbell, R. M., Garcia, B. A., and Nguyen, H. (2016) Quantitative profiling of the activity of protein lysine methyltransferase SMYD2 using silac-based proteomics. *Mol. Cell. Proteomics.* 15, 892–905

- 233. Donlin, L. T., Andresen, C., Just, S., Rudensky, E., Pappas, C. T., Kruger, M., Jacobs, E. Y., Unger, A., Zieseniss, A., Dobenecker, M. W., Voelkel, T., Chait, B. T., Gregorio, C. C., Rottbauer, W., Tarakhovsky, A., and Linke, W. A. (2012) Smyd2 controls cytoplasmic lysine methylation of Hsp90 and myofilament organization. *Genes Dev.* 26, 114–119
- 234. Retzlaff, M., Stahl, M., Eberl, H. C., Lagleder, S., Beck, J., Kessler, H., and Buchner, J. (2009) Hsp90 is regulated by a switch point in the C-terminal domain. *EMBO Rep.* **10**, 1147–1153
- 235. Martínez-Ruiz, A., Villanueva, L., De Orduña, C. G., López-Ferrer, D., Ángeles Higueras, M., Tarín, C., Rodríguez-Crespo, I., Vázquez, J., and Lamas, S. (2005) S-nitrosylation of Hsp90 promotes the inhibition of its ATPase and endothelial nitric oxide synthase regulatory activities. *Proc. Natl. Acad. Sci. U. S. A.* 102, 8525–8530
- 236. Preuss, K. D., Pfreundschuh, M., Fadle, N., Regitz, E., and Kubuschok, B. (2015) Sumoylated HSP90 is a dominantly inherited plasma cell dyscrasias risk factor. *J. Clin. Invest.* **125**, 316–323
- 237. Kundrat, L., and Regan, L. (2010) Identification of Residues on Hsp70 and Hsp90 Ubiquitinated by the Cochaperone CHIP. *J. Mol. Biol.* **395**, 587–594
- 238. Akimov, V., Barrio-Hernandez, I., Hansen, S. V. F., Hallenborg, P., Pedersen, A. K., Bekker-Jensen, D. B., Puglia, M., Christensen, S. D. K., Vanselow, J. T., Nielsen, M. M., Kratchmarova, I., Kelstrup, C. D., Olsen, J. V., and Blagoev, B. (2018) Ubisite approach for comprehensive mapping of lysine and n-terminal ubiquitination sites. *Nat. Struct. Mol. Biol.* 25, 631–640

- 239. Wagner, S. A., Beli, P., Weinert, B. T., Nielsen, M. L., Cox, J., Mann, M., and Choudhary, C. (2011) A proteome-wide, quantitative survey of in vivo ubiquitylation sites reveals widespread regulatory roles. *Mol. Cell. Proteomics.* **10**, M111.013284
- 240. Povlsen, L. K., Beli, P., Wagner, S. A., Poulsen, S. L., Sylvestersen, K. B., Poulsen, J. W., Nielsen, M. L., Bekker-Jensen, S., Mailand, N., and Choudhary, C. (2012) Systems-wide analysis of ubiquitylation dynamics reveals a key role for PAF15 ubiquitylation in DNA-damage bypass. *Nat. Cell Biol.* 14, 1089–1098
- Udeshi, N. D., Svinkina, T., Mertins, P., Kuhn, E., Mani, D. R., Qiao, J. W., and Carr, S. A. (2013) Refined preparation and use of anti-diglycine remnant (k-ε-gg) antibody enables routine quantification of 10,000s of ubiquitination sites in single proteomics experiments.
 Mol. Cell. Proteomics. 12, 825–831
- 242. Danielsen, J. M. R., Sylvestersen, K. B., Bekker-Jensen, S., Szklarczyk, D., Poulsen, J. W., Horn, H., Jensen, L. J., Mailand, N., and Nielsen, M. L. (2011) Mass spectrometric analysis of lysine ubiquitylation reveals promiscuity at site level. *Mol. Cell. Proteomics*. 10, M110.003590
- 243. Overath, T., Kuckelkorn, U., Henklein, P., Strehl, B., Bonar, D., Kloss, A., Siele, D., Kloetzel, P. M., and Janek, K. (2012) Mapping of O-GlcNAc sites of 20 S proteasome subunits and Hsp90 by a novel biotin-cystamine tag. *Mol. Cell. Proteomics.* 11, 467–477
- 244. Franco, M. C., Ye, Y., Refakis, C. A., Feldman, J. L., Stokes, A. L., Basso, M., Melero Fernández de Mera, R. M., Sparrow, N. A., Calingasan, N. Y., Kiaei, M., Rhoads, T. W., Ma, T. C., Grumet, M., Barnes, S., Beal, M. F., Beckman, J. S., Mehl, R., and Estévez, A.

- G. (2013) Nitration of Hsp90 induces cell death. Proc. Natl. Acad. Sci. 110, E1102-11
- 245. Franco, M. C., Ricart, K. C., Gonzalez, A. S., Dennys, C. N., Nelson, P. A., Janes, M. S., Mehl, R. A., Landar, A., and Estévez, A. G. (2015) Nitration of Hsp90 on Tyrosine 33 regulates mitochondrial metabolism. *J. Biol. Chem.* 290, 19055–19066
- 246. Parrilla-Castellar, E. R., Arlander, S. J. H., and Karnitz, L. (2004) Dial 9-1-1 for DNA damage: The Rad9-Hus1-Rad1 (9-1-1) clamp complex. *DNA Repair (Amst)*. 3, 1009–1014
- 247. Waterman, D. P., Haber, J. E., and Smolka, M. B. (2020) Checkpoint Responses to DNA Double-Strand Breaks. *Annu. Rev. Biochem.* **89**, 103–133
- 248. Aylon, Y., and Kupiec, M. (2004) DSB repair: The yeast paradigm. *DNA Repair (Amst)*.

 3, 797–815
- 249. Bernstein, K. A., and Rothstein, R. (2009) At Loose Ends: Resecting a Double-Strand Break. *Cell.* **137**, 807–810
- 250. Sartori, A. A., Lukas, C., Coates, J., Mistrik, M., Fu, S., Bartek, J., Baer, R., Lukas, J., and Jackson, S. P. (2007) Human CtIP promotes DNA end resection. *Nature*. **450**, 509–514
- 251. Sullivan, M. R., and Bernstein, K. A. (2018) RAD-ical New Insights into RAD51 Regulation. *Genes (Basel)*. **9**, 629
- 252. Andriuskevicius, T., Kotenko, O., and Makovets, S. (2018) Putting together and taking apart: Assembly and disassembly of the Rad51 nucleoprotein filament in DNA repair and genome stability. *Cell Stress.* **2**, 96–112
- 253. Shibata, A., and Jeggo, P. A. (2014) DNA double-strand break repair in a cellular context.

- Clin. Oncol. (R. Coll. Radiol). 26, 243-249
- 254. Bizard, A. H., and Hickson, I. D. (2014) The dissolution of double Holliday junctions. *Cold Spring Harb. Perspect. Biol.* **6**, a016477
- 255. Godin, S. K., Sullivan, M. R., and Bernstein, K. A. (2016) Novel insights into RAD51 activity and regulation during homologous recombination and DNA replication. *Biochem. Cell Biol.* **94**, 407–418
- 256. Li, X., and Heyer, W. D. (2008) Homologous recombination in DNA repair and DNA damage tolerance. *Cell Res.* **18**, 99–113
- 257. Suhane, T., Bindumadhavan, V., Fangaria, N., Nair, A. S., Tabassum, W., Muley, P., Bhattacharyya, M. K., and Bhattacharyya, S. (2019) Glu-108 in Saccharomyces cerevisiae Rad51 Is Critical for DNA Damage-Induced Nuclear Function. *mSphere*. 10.1128/mSphere.00082-19
- 258. Quanz, M., Berthault, N., Roulin, C., Roy, M., Herbette, A., Agrario, C., Alberti, C., Josserand, V., Coll, J. L., Sastre-Garau, X., Cosset, J. M., Larue, L., Sun, J. S., and Dutreix, M. (2009) Small-molecule drugs mimicking DNA damage: A new strategy for sensitizing tumors to radiotherapy. *Clin. Cancer Res.* 15, 1308–1316
- 259. Laskar, S., Bhattacharyya, M. K., Shankar, R., and Bhattacharyya, S. (2011) HSP90 controls SIR2 mediated gene silencing. *PLoS One*. **6**, e23406
- 260. Louvion, J.-F., Warth, R., and Picard, D. (1996) Two eukaryote-specific regions of Hsp82 are dispensable for its viability and signal transduction functions in yeast. *Proc. Natl.*

- Acad. Sci. 93, 13937–13942
- 261. Longtine, M. S., McKenzie, A., Demarini, D. J., Shah, N. G., Wach, A., Brachat, A., Philippsen, P., and Pringle, J. R. (1998) Additional modules for versatile and economical PCR-based gene deletion and modification in Saccharomyces cerevisiae. *Yeast.* 14, 953–61
- 262. Tapia, H., and Morano, K. A. (2010) Hsp90 Nuclear Accumulation in Quiescence Is Linked to Chaperone Function and Spore Development in Yeast. *Mol. Biol. Cell.* **21**, 63–72
- 263. Agmon, N., Pur, S., Liefshitz, B., and Kupiec, M. (2009) Analysis of repair mechanism choice during homologous recombination. *Nucleic Acids Res.* **37**, 5081–5092
- 264. Nathan, D. F., and Lindquist, S. (1995) Mutational analysis of Hsp90 function: interactions with a steroid receptor and a protein kinase. *Mol. Cell. Biol.* **15**, 3917–3925
- 265. Jahn, M., Rehn, A., Pelz, B., Hellenkamp, B., Richter, K., Riefa, M., Buchner, J., and Hugel, T. (2014) The charged linker of the molecular chaperone Hsp90 modulates domain contacts and biological function. *Proc. Natl. Acad. Sci. U. S. A.* **111**, 17881–17886
- Quanz, M., Herbette, A., Sayarath, M., De Koning, L., Dubois, T., Sun, J. S., and Dutreix,
 M. (2012) Heat shock protein 90α (Hsp90α) is phosphorylated in response to DNA damage and accumulates in repair foci. *J. Biol. Chem.* 287, 8803–8815
- 267. Lundin, C., North, M., Erixon, K., Walters, K., Jenssen, D., Goldman, A. S. H., and Helleday, T. (2005) Methyl methanesulfonate (MMS) produces heat-labile DNA damage

- but no detectable in vivo DNA double-strand breaks. Nucleic Acids Res. 33, 3799–3811
- 268. Mader, S. L., Lopez, A., Lawatscheck, J., Luo, Q., Rutz, D. A., Gamiz-Hernandez, A. P., Sattler, M., Buchner, J., and Kaila, V. R. I. (2020) Conformational dynamics modulate the catalytic activity of the molecular chaperone Hsp90. *Nat. Commun.* **11**, 1410
- 269. Hainzl, O., Lapina, M. C., Buchner, J., and Richter, K. (2009) The charged linker region is an important regulator of Hsp90 function. *J. Biol. Chem.* **284**, 22559–22567
- 270. Prodromou, C., Panaretou, B., Chohan, S., Siligardi, G., O'Brien, R., Ladbury, J. E., Roe,
 S. M., Piper, P. W., and Pearl, L. H. (2000) The ATPase cycle of Hsp90 drives a molecular 'clamp' via transient dimerization of the N-terminal domains. *EMBO J.* 19, 4383
- 271. Wolmarans, A., Lee, B., Spyracopoulos, L., and LaPointe, P. (2016) The Mechanism of Hsp90 ATPase Stimulation by Aha1. *Sci. Rep.* **6**, 33179

Appendix-I

6.1 Subcloning of yHsp90 α , yHsp90 $\alpha^{\Delta 211-259}$ and yHsp90 $\alpha^{\Delta 211-259}$ in *pHCA* vector and their subsequent GFP tagging

Full length HSP82, was amplified from yeast genomic DNA using the primer pairs OSB21/OSB22 and cloned in pHCA vector between the BamH1 and the Sal1 restriction sites to create pHCA-HSP82. The CL deletion mutant hsp82\(\Delta(211-259)\) was amplified using the genomic DNA isolated from HH1a-p2HG/hsp82\(\Delta(211-259)\) strain(164, 260) with the primer pairs OSB21/OSB22. It was subsequently subcloned into pHCA vector within the BamHI and SalI restriction sites to create pHCA-hsp82 Δ (211-259). Hsp82 deletion mutant hsp82 Δ (211-242) was generated by SOE and subsequently subcloned in pHCA within the BamHI and SalI restriction sites to create pHCA-hsp82(Δ211-242). Confirmation of the pHCA-HSP82, pHCA $hsp82\Delta(211-259)$, and pHCA-hsp82($\Delta(211-242)$) was done by the release of the insert of size 2130bp, 1983bp, 2034bp respectively upon digestion of the plasmid with BamH1 and Sal1 restriction enzymes (Fig.20). In order to create GFP-Hsp82 fusion constructs, GFP was first amplified from the plasmid, p2U/S65T using the primer pair OSB517/OSB518 and subcloned within the BamH1 restriction site, which is present in the N-terminal end of HSP82, hsp82Δ(211-259) and hsp82\(\Delta(211-242)\). The orientation of GFP was checked using PstI digestion. Upon PstI digestion, a vector specific band of size 940bp was observed in all the plasmids. Along with this, if the GFP insert was incorporated in the correct orientation, an additional band of 1368bp was observed; whereas, if GFP insert was incorporated in the wrong orientation, an additional band of 668bp was observed. Hence, the fusion constructs pHCA-GFPHSP82, pHCA-

 $GFPhsp82\Delta(211-259)$, and pHCA- $GFPhsp82\Delta(211-242)$ where GFP is fused at the N-terminal end of Hsp82 in all the cases were created (Fig.21).

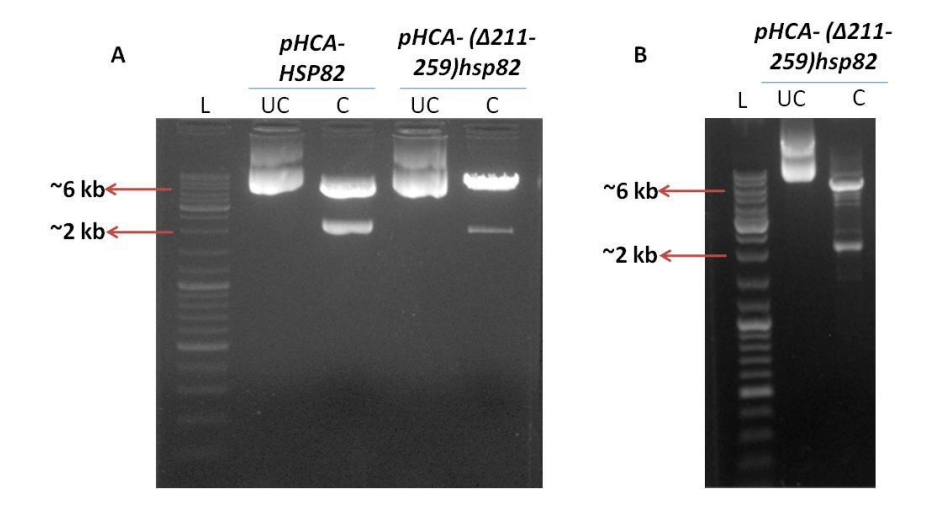


Fig. 20. Cloning of HSP82, $hsp82\Delta(211-259)$ and $hsp82\Delta(211-242)$ into pHCA-vector: (A) Clone confirmation of pHCA-Hsp82 (left panel) and pHCA- $hsp82\Delta(211-259)$ (right panel) was done by the release of insert of size 2130bp and 1983bp respectively upon digestion of the plasmid using BamH1 and Sal1 enzymes (B) Clone confirmation of pHCA- $hsp82\Delta(211-242)$ was done by the release of 2034bp band upon digestion of the plasmid using BamH1 and Sal1 enzymes. L: Ladder, UC: Uncut plasmid, C: Plasmid digested with BamH1 and Sal1 restriction enzymes.

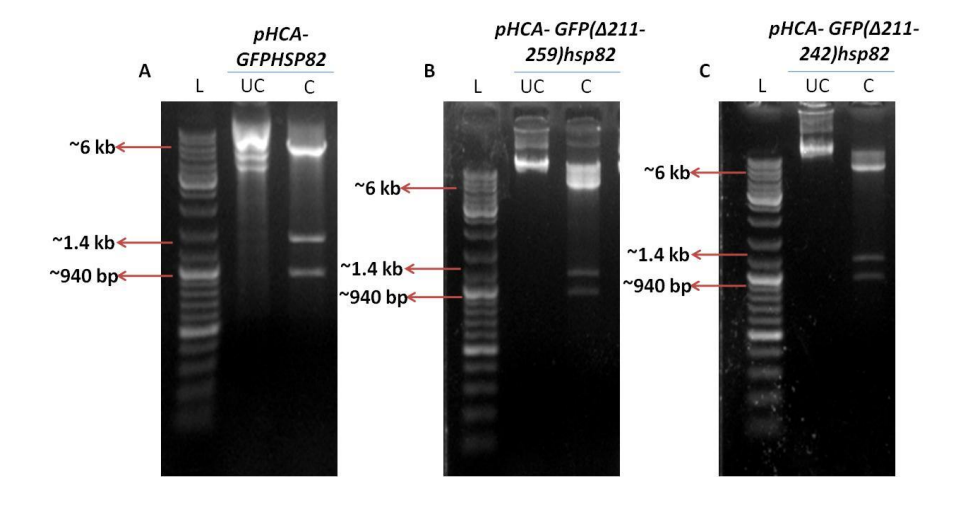


Fig. 21. GFP tagging of pHCA-HSP82, pHCA-hsp82 Δ (211-259) and pHCA-hsp82 Δ (211-242): (A) Clone confirmation of pHCA-GFPHSP82, (B) Clone confirmation of pHCA-GFPhsp82 Δ (211-259), (C) Clone

confirmation of pHCA- $GFPhsp82\Delta(211-242)$. The correct orientation of GFP insert incorporation at the N-terminal of all the fusion constructs was determined by the release of an additional band of size 1368bp along with the vector specific band of size 940bp when the plasmid was digested with Pst1. L: Ladder, UC: Uncut plasmid, C: Plasmid digested with Pst1 restriction enzyme.

6.2 Cloning of FLAG tagged HsHSP90 α , Hshsp90 α T7A and Hshsp90 α Δ (224-279) into pHCA vector

We purchased the mammalian expression vector pcDNA3.1+/C-(K)-DYK from GenScript, USA, which harbors full length human $HsHSP90\alpha$ with C-terminal FLAG tag. We amplified $HsHSP90\alpha$ -FLAG using the primer pairs OSB531/OSB539 and subcloned in the centromeric pHCA vector (259) between the BamHI and the SalI restriction sites to create $pHCA-HsHSP90\alpha$ -FLAG. Clone confirmation was done by digesting the plasmid with the restriction enzymes BamHI and SalI and observing the release of the insert of size 2218bp (Fig.22). Two mutants of $HsHsp90\alpha$ namely $hsp90\alpha T7A$ and the CL deletion mutant $hsp90\alpha\Delta(224-279)$ were generated by splice overlap extension (SOE) and ultimately subcloned in pHCA with C-terminal FLAG tag to create $pHCA-Hshsp90\alpha T7A-FLAG$ and $pHCA-Hshsp90\alpha\Delta(224-279)-FLAG$ respectively. Clone confirmation was done by digesting each of the plasmids with the restriction enzymes BamHI and SalI and observing the release of the inserts with size 2218bp and 2050bp respectively (Fig.22).

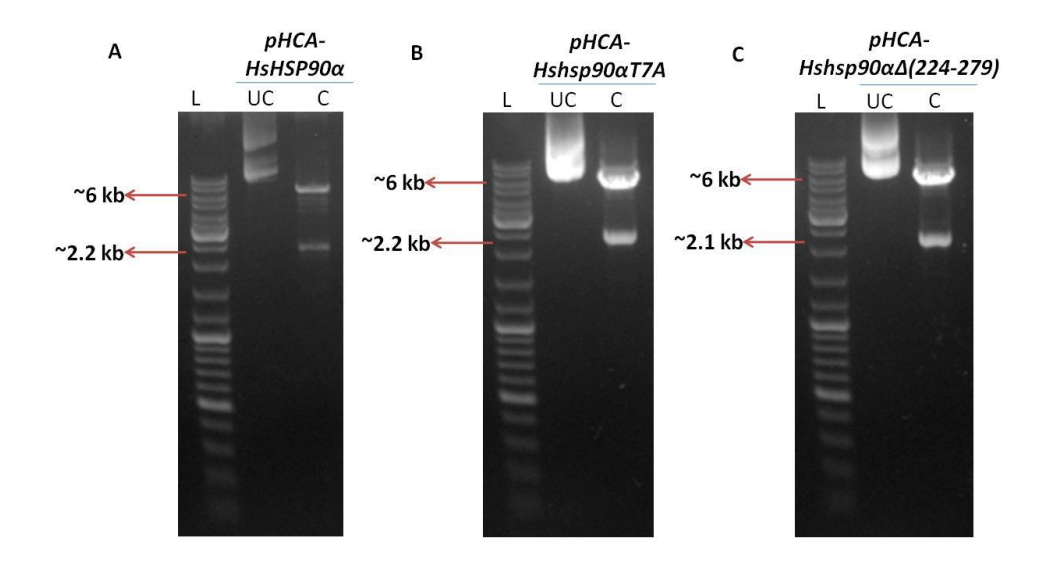


Fig. 22. Cloning of FLAG tagged $HsHSP90\alpha$, $Hshsp90\alpha T7A$ and $Hshsp90\alpha \Delta(224-279)$ into pHCA vector: (A) Clone confirmation of pHCA- $HsHSP90\alpha$ -FLAG(B) Clone confirmation of pHCA- $Hshsp90\alpha T7A$ -FLAG (C) Clone confirmation of $Hshsp90\alpha \Delta(224-279)$ -FLAG. L: Ladder, UC: Uncut plasmid, C: Plasmid digested with BamH1 and Sal1 restriction enzymes.

6.3 Subcloning AHA1 into pBEVYT vector

Full length AHA1 of size 1053bp was amplified using the primer pair OSB215/OSB216 and cloned in the 2μ vector pTA between the BamH1 and the Sal1 restriction sites to create pTA-AHA1. Clone confirmation was done by the release of insert of size 1053bp upon digestion of the plasmid with BamH1 and Sal1 restriction enzymes (Fig.23).

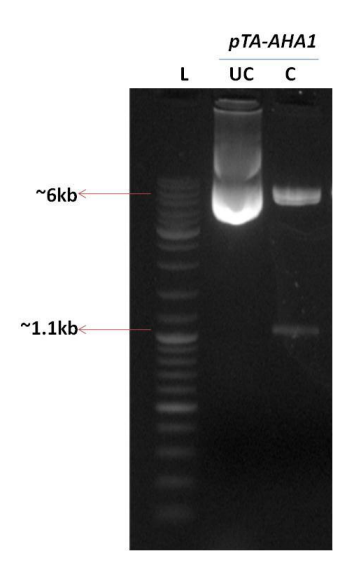


Fig. 23. Cloning of *AHA1* **into** *pTA* **vector:** Clone confirmation of *pTA-AHA1* was done by the release of the insert of size 1053bp upon digestion of the plasmid using *BamH1* and *Sal1* restriction enzymes. L: Ladder, UC: Uncut plasmid, C: Plasmid digested with *BamH1* and *Sal1* restriction enzymes.

Appendix-II

7.1 Synopsis

Maintaining the genome integrity is vital for all cells. Eukaryotic cells, however, face various DNA aberrations such as damages on the DNA bases, double and single strand DNA breaks which challenge the stability of their genome (248). Hence, eukaryotic cells need to employ various methods such as NER, BER, HR and NHEJ to repair such DNA damages. Higher eukaryotes prefer the pathway of NHEJ for the repair of double strand DNA breaks while lower eukaryotes such as yeast employ HR mediated DNA repair for the same (248). The formation of a double strand DNA break in yeast leads to the recruitment of a cohort of proteins which sense the double strand break, activate the DNA damage checkpoint and stall the cell cycle until the damage is repaired (246, 247). The 5' ends are resectioned to produce 3' single strand DNA overhangs at the DSB site by the cooperative function of the MRX complex, followed by the 5' exonucleases, Sae2 and Exo1 (248-250). These 3' single stranded DNA overhangs are recognized and bound by the single strand DNA binding protein, RPA which is replaced by Rad51 with the help of Rad51 epistatic group of proteins to form a stable Rad51 nucleoprotein filament (248, 251, 252). This is followed by homology search and strand invasion by the Rad51resulting in the formation of the double Holliday junction which is resolved into crossover/non crossover products (251-254). This process of DNA repair by HR is majorly conserved across species and is important for maintaining genomic integrity (256).

Hsp90 is a molecular chaperone which cannot fold nascent proteins, but is involved in the final protein folding of partially folded proteins to give rise to stable, mature proteins. Hsp90 interacts

with a select subset of proteins known as its clients, a vast majority of which are involved in signal transduction pathways. Apart from providing stability to its clients, Hsp90 also helps in the activation of these client proteins in accordance with cellular signals. Apart from kinases and transcription factors, many of the Hsp90 clients belong to the DNA repair family, giving an indication that Hsp90 may have a potential role in DNA repair pathways. Studies done with mammalian cells suggest that Hsp90 is directly involved in the DNA repair pathway. In a study it was observed that when a DNA damage response was triggered using short double strand DNA molecules called Dbait 32 Hc(258), the nuclear pool of mammalian Hsp90α was phosphorylated at the Thr7 residue by DNA-PKcs which is also responsible for the phosphorylation of vH2AX histone during the DNA damage response pathway (185). Furthermore, the phosphorylated form of Hsp90a present in the nucleus was found to be recruited at the DNA break sites along with yH2AX histone (185). However, in lower eukaryotes like Saccharomyces cerevisiae, Hsp82 which is the ortholog of mammalian Hsp90a predominantly remains in the cytoplasm. Furthermore, the first 14 amino acids which are present in mammalian Hsp90α are absent in yeast Hsp82, thus the Thr7 residue is absent. Furthermore, yeast does not contain DNA-PKcs which has been shown in mammalian system to be responsible of phosphorylating Hsp90α at the Thr7 residue. Since DNA repair mechanisms as well as Hsp90 structure and function are conserved from lower to higher eukaryotes, it is important to determine whether there is any conserved function of Hsp90 in DNA repair even in lower eukaryotes such as yeast.

Previous studies in our lab have revealed that Hsp90 inhibition using inhibitors like 17AAG or by using loss of function mutants likeHsp90^{T101I} or Hsp90^{iG170D} leads to a reduction in the protein levels of Rad51 rendering the cells HR deficient (162, 164). Rad51, which is the central

player of the HR mediated DNA repair pathway was found to be a direct client of Hsp90 and hence, is dependent on Hsp90 for its stability and activation (162, 164). Furthermore, our lab identified a separation of function mutant of Hsp90, *i.e.* Hsp82^{Δ211-259}, which retained its chaperone function and hence had no effect on Rad51 stability. However, the cells harboring this separation of function mutant of Hsp90 showed substantial reduction in Rad51 function including Rad51 mediated gene targeting activity as well as DNA damage induced Rad51 nuclear foci formation, which is a hallmark of HR mediated DNA repair. However, whether Hsp90 directly regulates the nuclear function of Rad51 remained elusive.

In our present study, we hypothesized that Hsp90 acts as a positive regulator of the HR mediated DNA repair pathway. To address this, we framed the following three questions which outlined the basis of the study:

- Q1. Does yHsp90α regulate the nuclear function of Rad51 during DNA repair?
- Q2. Does yHsp 90α have any nuclear function during DNA damage apart from regulation of Rad51 function?
- Q3. What is the mechanism of the nuclear import of yHsp90 α during DNA repair?

We first studied whether yHsp90 α regulates the nuclear function of Rad51 during DNA repair. For this purpose, we used a mutant of Rad51 i.e, Rad51^{E108L} which has been reported in our lab to be completely defective in gene targeting activity and the cells harboring Rad51^{E108L} behave like $\Delta rad51$ cells with regard to DNA damage sensitivity (257). Coimmunoprecipitation studies using wild type Rad51 or Rad51^{E108L} was used to study whether the physical association between Hsp90 and Rad51 plays any regulatory role in the DNA damage induced Rad51 function. It was

revealed that yHsp90 α shows a dynamic interaction with wild type Rad51 during DNA damage conditions. However, this dynamic relationship is completely abrogated in the case of the Rad51^{E108L} mutant which binds strongly to yHsp90 α even in the presence of DNA damage conditions.

To identify whether Hsp90 plays a direct role in HR mediated DNA repair, the chaperone should be present in the nucleus under such condition and physically be associated with the damaged chromatin. To this end, we used cell fractionation and fluorescence microscopy studies to study whether vHsp90α is imported to the nucleus upon DNA damage and recruited to the damaged chromatin. We used methyl methanesulfonate (MMS) as a DNA damaging agent which is reported to cause S-phase arrest. To delineate whether the nuclear import ofHsp90α is due to the DNA damage or due to the cell cycle arrest, we used agents that cause S-phase arrest (hydroxyurea) or G2/M arrest (nocodazole) and monitored the nuclear import of Hsp90α. We observed that there was no detectable nuclear import ofHsp90α in presence of HU/Nocodazole, thus confirming that the nuclear import of Hsp90a is induced by DNA damage. We further investigated whether the nuclear pool of yHsp90a is recruited to the damaged chromatin in response to a single specific double strand break created in the chromosome. To that end, we used NA14 strain (263), where a site specific DSB was created within the mutant ura3 locus by expressing a galactose-inducible HO endonuclease. In NA14 yeast cells, the DSB created at the ura3 locus can be repaired by homologous recombination using a donor template (URA3) that is located 3 kb apart. We performed ChIP analysis immediately after HO induction and at every 1hrintervals, up to 4 hrsand observed that yHsp90α is recruited to the damaged chromatin with maximum recruitment observed at 2hrs post HO induction when the DNA breakage appeared to be maximum. We further monitored the extent of occupancy of yHsp90α upto -5kb of the DNA

break site and found thatyHsp90α binds to the flanking region of the DNA break site with kinetics comparable to that of Rad51, a known protein involved in the HR pathway.

Hsp90 is associated with a number of proteins that assist with its chaperone cycle, known as Hsp90 cochaperones. These cochaperones are largely conserved in eukaryotic cells; however, they are not present in prokaryotic cells. These Hsp90 cochaperones help in the proper binding and dissociation of Hsp90 client proteins, ATP binding, the conformational changes that Hsp90 undergoes during the chaperone cycle, and ATP hydrolysis during the chaperone cycle progression, etc. (42-44). Apart from assisting with the Hsp90 chaperone cycle, the cochaperones also perform various other functions in the cell. Studies have revealed that Hop/Sti1 is important for the hormone binding ability of the progesterone receptor (46). In mammalian cells, it was observed that the knockdown of Hop or Ahal can prevent the degradation of misfolded mutant cystic fibrosis transmembrane conductance regulator $(\Delta F508CFTR)$ protein which, if allowed to be expressed on the cell surface, has the ability to be functional (47, 48). Hence the knockdown of Hop/Aha1 allows ΔF508CFTR protein to reach the cell surface without being degraded, restoring its function (47, 48). Other studies have proved that although Sti1 is a non-essential protein, the double knockout of Sti1 along with Ydj1/Hsp40 or Sba1 leads to the loss of viability (49, 50). Previous literature also indicates that some Hsp90 cochaperones have potential roles in the DNA repair pathway as well. In HeLa cell extracts, it was found that Aha1 could interact directly with the DNA repair proteins, Ku70, Ku80 and DNA-PKcs(53). Another study revealed that Sba1 deletion leads to sensitization of yeast cells towards different DNA damaging agents such as ultraviolet radiation (UV), bleomycin and MMS which could be reversed upon introduction of Sba1 in the \(\Delta sba1 \) cells (54). Studies done with the

essential Hsp90 cochaperone, Cdc37 revealed that a loss of function mutation of Cdc37 leads to a synthetic growth defect which in turn led to a loss in genome integrity (55).

Hence, we wanted to study whether the three Hsp90 cochaperones, Aha1, Cdc37 and Sba1 play any role in assisting the nuclear import of γHsp90α during DNA repair. To this end we used cell fractionation studies as well as fluorescence studies which establish that Aha1 plays an important role in the DNA damage mediated nuclear import of yHsp90α. We found that Aha1 shows an increased nuclear accumulation in response to DNA damage conditions created with the addition of 0.15% MMS. We further observed that ∆aha1 cells show a defect in Hsp90 nuclear import upon DNA damage, rendering the cells sensitive to DNA damaging agents and this phenotype is reversed upon the re-introduction of Aha1 to these cells. We have also identified the structural determinant of Hsp90, which is essential for its import into the nucleus during DNA damage. It was earlier established that the conformational flexibility between the amino terminal domain and the middle domain of yHSP90a is mediated by a flexible charged linker domain spanning 211-259 residues. The deletion of these highly charged amino acid stretches (211-259), leads to significant reduction in Aha1-stimulated ATP hydrolysis of yHSP90α (257). However, deletion of a shorter stretch (211-242) does not alter the conformational flexibility of the mutant protein and it shows comparable Aha1 mediated ATPase activation of yHSP90α as that of the wild-type protein (257). We wanted to determine whether this domain known for providing conformational flexibility between the amino-terminal and the middle-domain is important for its nuclear import. To this end, we performed cell fractionation and fluorescence microscopy studies to investigate the MMS induced nuclear import of the two mutant proteins yHSP90 $\alpha^{\Delta(211-259)}$ andyHSP90 $\alpha^{\Delta(211-259)}$ ²⁴²⁾. We observed that the yHSP90 $\alpha^{\Delta(211-259)}$ mutant showed a complete abrogation in its nuclear import in response to DNA damage. However, the phenotype was reversed in the case of the

shorter CL deletion mutant, yHSP90 $\alpha^{\Delta(211-242)}$. Furthermore the cells harbouring yHSP90 $\alpha^{\Delta(211-259)}$ mutant showed high DNA damage sensitivity which was reversed in cells harbouring the yHSP90 $\alpha^{\Delta(211-242)}$ mutant similar to wild type condition. Hence, it was established that if the nuclear import of yHsp90 α during genotoxic stress is hampered; the cells are rendered sensitive to the DNA damaging agents.

The importance of this study lies in the fact that Hsp90 has been increasingly found to play various roles in different diseases such as cancer, infectious diseases as well as neurodegenerative disorders. Hence, further studies on Hsp90 and its cochaperones can illuminate Hsp90 or its cochaperones as novel drug targets in the treatment of various diseases.

DNA damage-induced nuclear import of HSP90 α is promoted by Aha1

Nupur Fangaria^a, Khushboo Rani^a, Priyanka Singh^a, Sandeep Dey^b, Kota Arun Kumar^b, and Sunanda Bhattacharyya^{a,*}

^aDepartment of Biotechnology and Bioinformatics, School of Life Sciences, University of Hyderabad, Hyderabad 500046, Telangana, India; ^bDepartment of Animal Biology, School of Life Sciences, University of Hyderabad, Hyderabad 500046, Telangana, India

ABSTRACT The interplay between yHSP90α (Hsp82) and Rad51 has been implicated in the DNA double-strand break repair (DSB) pathway in yeast. Here we report that nuclear translocation of yHSP90 α and its recruitment to the DSB end are essential for homologous recombination (HR)-mediated DNA repair in yeast. The HsHSP90α possesses an amino-terminal extension which is phosphorylated upon DNA damage. We find that the absence of the amino-terminal extension in yHSP90 α does not compromise its nuclear import, and the nonphosphorylatable-mutant HsHSP90α^{T7A} could be imported to the yeast nucleus upon DNA damage. Interestingly, the flexible charged-linker (CL) domains of both yHSP90α and HsHSP90α play a critical role during their nuclear translocation. The conformational restricted CL mutant yHSP90 $\alpha^{\Delta(211-259)}$, but not a shorter deletion version yHSP90 $\alpha^{\Delta(211-242)}$, fails to reach the nucleus. As the CL domain of yHSP90 α is critical for its interaction with Aha1, we investigated whether Aha1 promotes the nuclear import of yHSP90a. We found that the nuclear import of yHSP90 α is severely affected in $\Delta aha1$ strain. Moreover, Aha1 is accumulated in the nucleus during DNA damage. Hence Aha1 may serve as a potential target for inhibiting nuclear function of yHSP90 α . The increased sensitivity of $\Delta aha1$ strain to genotoxic agents strengthens this notion.

Monitoring Editor Karsten Weis ETH Zurich

Received: Nov 5, 2021 Revised: Sep 29, 2022 Accepted: Oct 11, 2022

INTRODUCTION

Eukaryotic cells are susceptible to a wide variety of genotoxic stresses which cause several types of DNA lesions including DNA

This article was published online ahead of print in MBoC in Press (http://www.molbiolcell.org/cgi/doi/10.1091/mbc.E21-11-0554) on October 19, 2022.

Conflict of interest: The authors declare no conflicts of interest.

Author contributions: S.B. conceived the idea, designed the experiments, guided, and wrote the paper; N.F. conducted experiments and wrote the paper; K.R. and P.S. conducted experiments; N.F., S.D., and K.A.K. conducted the fluorescence microscopic studies.

Funding: The work was supported by the Department of Science and Engineering Research Board (DST-SERB), India [EMR/2017/001173] to S.B.

All supporting data in relation to the studies reported here are provided in this manuscript.

*Address correspondence to: Sunanda Bhattacharyya (sdeb70@gmail.com; sbtsl@uohyd.ac.in).

Abbreviations used: Aha1, activator of hsp90 ATPase; Cdc37, cell division cycle 37; HOcs, homothallic endonuclease cut site; Hsp90, heat shock protein 90; Sba1, sensitivity to benzoquinone ansamycins.

© 2022 Fangaria et al. This article is distributed by The American Society for Cell Biology under license from the author(s). Two months after publication it is available to the public under an Attribution–Noncommercial-Share Alike 4.0 International Creative Commons License (http://creativecommons.org/licenses/by-nc-sa/4.0).

"ASCB®," "The American Society for Cell Biology®," and "Molecular Biology of the Cell®" are registered trademarks of The American Society for Cell Biology.

double-strand breaks (DSBs). If DSBs remain unrepaired in the cell, they can cause genomic instability (Aylon and Kupiec, 2004). One of the commonly employed mechanisms to repair DSB is by homologous recombination (HR). Unlike the mammalian system, this mode of DNA repair is preferred in budding yeast over the error-prone nonhomologous end joining pathway. In HR-mediated DNA repair, Rad52 and Rad51 are assembled at the 3' ssDNA tail in an organized manner (Li and Heyer, 2008). These proteins are recruited during the end resection of DNA DSB and catalyze the formation of DNA (Andriuskevicius et al., 2018). Studies in the model eukaryote, Saccharomyces cerevisiae, have shown that yHSP90 α , the budding yeast ortholog of human HSP90 α (HsHSP90 α), provides stability to Rad51 protein and plays a regulatory role in the effective recruitment of Rad51 to the broken DNA (Suhane et al., 2014, 2019).

HSP90 α is associated with a wide variety of cochaperones that are essential for its reaction cycle. Sba1 binds to HSP90 α in the presence of ATP and stabilizes the ATP bound conformation which is required for the client protein activation (Ali et al., 2006). Cdc37 aids in folding and activation of specific client protein kinases. It suppresses the ATP turnover by HSP90 α and thereby helps in client protein loading (Kimura et al., 1997; Siligardi et al., 2002). Aha1

accelerates the ATPase activity of HSP90 α and plays an important role in regulating the timing of $HSP90\alpha$ chaperone cycle (Kimura et al., 1997). Upon binding to the middle domain (MD) of $HSP90\alpha$, Aha1 causes a large conformational change to the amino terminal domain (NTD) of $HSP90\alpha$ and acts as an allosteric activator of HSP90α ATPase. Subsequently, monomeric Aha1 binds asymmetrically to the NTD of one of the protomers of HSP90 α and accelerates the dimerization of $\mbox{HSP90}\alpha$ by forming a bridge between the two protomers (Li et al., 2012). Although the contribution of cochaperones toward the conformational cycle of $HSP90\alpha$ is well understood, their physiological significance remains obscure. Previous studies have indicated the involvement of the above-mentioned cochaperones in the DNA repair pathways in general (Caplan et al., 2007; Echtenkamp et al., 2011; Sun et al., 2012). In HeLa cell extracts, Aha1 was found to interact with the proteins Ku70 and Ku80 and DNA-dependent protein kinase (DNA-PK)cs which are involved in DNA repair (Sun et al., 2012). The Sba1 network was found to have a significant nuclear component that includes DNA repair activities (Echtenkamp et al., 2011). A previous study showed that $\Delta sba1$ strain shows susceptibility toward various DNA-damaging agents like MMS, bleomycin, and ultraviolet light, which could be reversed by the complementation of Sba1 in the null \(\Delta sba1 \) cell. Loss of function of Cdc37 causes synthetic growth defect with several genes involved in genome integrity (Caplan et al., 2007). Although previous studies indicate that these cochaperones may play a role in DNA repair, their exact function during the HR pathway has never been addressed.

During its chaperone cycle, HSP90α undergoes large-scale conformational rearrangements from an open inactive state to a closed active state (Mader et al., 2020) which in turn modulates its catalytic activity. The NTD and the MD are separated by a disordered region termed the charged linker (CL), which provides flexibility for the domain rearrangement during the $HSP90\alpha$ chaperone cycle (Tsutsumi et al., 2012). This linker region is evolutionarily conserved among all eukaryotic orthologs of HSP90 α studied to date, although its physiological significance is poorly understood. To address the importance of CL domain in the mechanism of the in vitro function of HSP90 α , a series of successively shortened CL mutants of yHSP90 α were generated (Hainzl et al., 2009). It was observed that successive deletion of CL gradually reduces the ability of Aha1 to stimulate the ATP turnover in the mutants without altering its binding affinity to those mutants (Hainzl et al., 2009). It was reported that Aha1-mediated ATPase activity of yHSP90 $\alpha^{\Delta(211-259)}$ was reduced by 2.5-fold, although that of yHSP90 $\alpha^{\Delta(211-242)}$ showed a similar fold stimulation as that of the wild-type yHSP90 α . One of the CL mutants was characterized in detail for its role in DNA repair pathway. It was reported that although the stability of Rad51 remains unaffected in the $hsp82(\Delta 211-259)$ mutant, the strain displays a severe reduction in the gene targeting efficiency (Suhane et al., 2014). Moreover, the MMS-induced Rad51 foci formation, which is the hallmark of HRmediated DNA repair, was significantly reduced in this mutant background. However, the mechanism behind such phenotype is not understood well.

A recent study in mammalian systems shows that DNA-PK-mediated Thr7 phosphorylation of HsHSP90 α in response to DNA damage causes its recruitment to the DSBs (Quanz et al., 2012). In a separate study it has been demonstrated that exposure to ionizing radiation causes the phosphorylation of Thr5/Thr7 residues of the nuclear pool of Hsp90 by ataxia telangiectasia mutated (ATM) kinase and this is vital for the maintenance of γ H2AX levels (Elaimy et al., 2016). In lower eukaryotes such as in budding yeast, yHSP90 α neither possesses the first 14 stretch of amino acids, including the

Thr5 and Thr7 residues, nor harbors DNA-PK. Furthermore, although the orthologs of ATM, i.e., Tel1/Mec1 are present in yeast, there is no report showing their physical association with yHSP90 α . This raises the question of whether DNA damage-induced chromatin recruitment of HSP90 α occurs in these organisms. Furthermore, it was never addressed whether cellular redistribution of yHSP90 α occurs in response to DNA damage and whether phosphorylation of Thr5/Thr7 of HsHSP90 α is a prerequisite for the nuclear import. Also, it remains unanswered whether the nuclear function of HSP90 α is essential for HR-mediated DSB repair pathway.

In our present study, we have addressed all the above-mentioned questions and identified a novel pathway for DNA damageinduced nuclear translocation of yHSP90 α . We have discovered that Aha1 regulates the nuclear import of yHSP90α. To better understand the function of yHSP90 α in HR-mediated DNA repair pathway, we have used chromatin immune precipitation assay to investigate the association of yHSP90 α and Rad51 with damaged DNA after we artificially induce the DSB. Concurrently, the repair kinetics of the damaged DNA were analyzed. The combined results of these two approaches enabled us to compare the extent of occupancy of yHSP90 α and Rad51 with the DSB ends and its flanking regions. In a HR-defective CL-deleted yHSP90lpha mutant strain (Suhane et al., 2014), we observed a defect in the nuclear import and chromatin association of the Hsp90^{Δ(211-259)} protein. Collectively, Aha1 appears to play a critical role in the nuclear import of yHSP90 α , which in turn is vital for HR-mediated DNA repair pathway. This is supported by the sensitivity of $\Delta aha1$ strain toward different genotoxic agents.

RESULTS

Accumulation of yHSP90 α in the nucleus in response to MMS-induced DNA damage

It was reported earlier that upon DNA damage, human $HSP90\alpha$ is phosphorylated by DNA-PK at threonine 5/7 residues and that the phosphorylated form of HsHSP90 α is accumulated at the site of DNA damage (Quanz et al., 2012; Elaimy et al., 2016). Although DNA-PK can phosphorylate both the cytoplasmic and the nuclear pool of HsHSP90 α upon DNA damage, it was never addressed whether there is a DNA damage-induced upsurge of HSP90 α in the nucleus and whether this import is dependent on the threonine 5/7 phosphorylation. We investigated whether the nuclear translocation of yHSP90 α occurs in an aforementioned phosphorylation-independent manner in S. cerevisiae, in which the first 14 amino acids are absent (Supplemental Figure S1, red circle). Earlier we observed that the association between Rad51 and yHSP90lpha was reduced in the presence of MMS (0.15%); hence we used the same dose of MMS for our present study (Suhane et al., 2019). We examined the level of yHSP90 α in whole-cell extract and in nuclear fraction of W303a strain upon exposure to MMS treatment (0.15%). We found that there was no difference in the expression of yHSP90 α in response to DNA damage (Figure 1A, left panel); however, it was redistributed to the nucleus (Figure 1A, right panel). The experiment was repeated more than three times and one set of the representative Western blot images is presented. Rad51 level was monitored as a positive control which showed more than two- and threefold of induction in the whole-cell extract and in the nuclear fraction, respectively (Figure 1B). The nuclear fractionation data showed that upon MMS treatment, there was a 2.5-fold nuclear enrichment of yHSP90 α (Figure 1B). Nsp1, the nuclear marker protein, was used as a loading control. The nuclear accumulation of yHSP90 α was further supported by the live-cell imaging of the strain NFY31 that harbors a single-copy GFP fused yHSP90 α plasmid. We observed that in the untreated condition, GFP-yHSP90α was uniformly distributed throughout the

2 N. Fangaria et al. Molecular Biology of the Cell

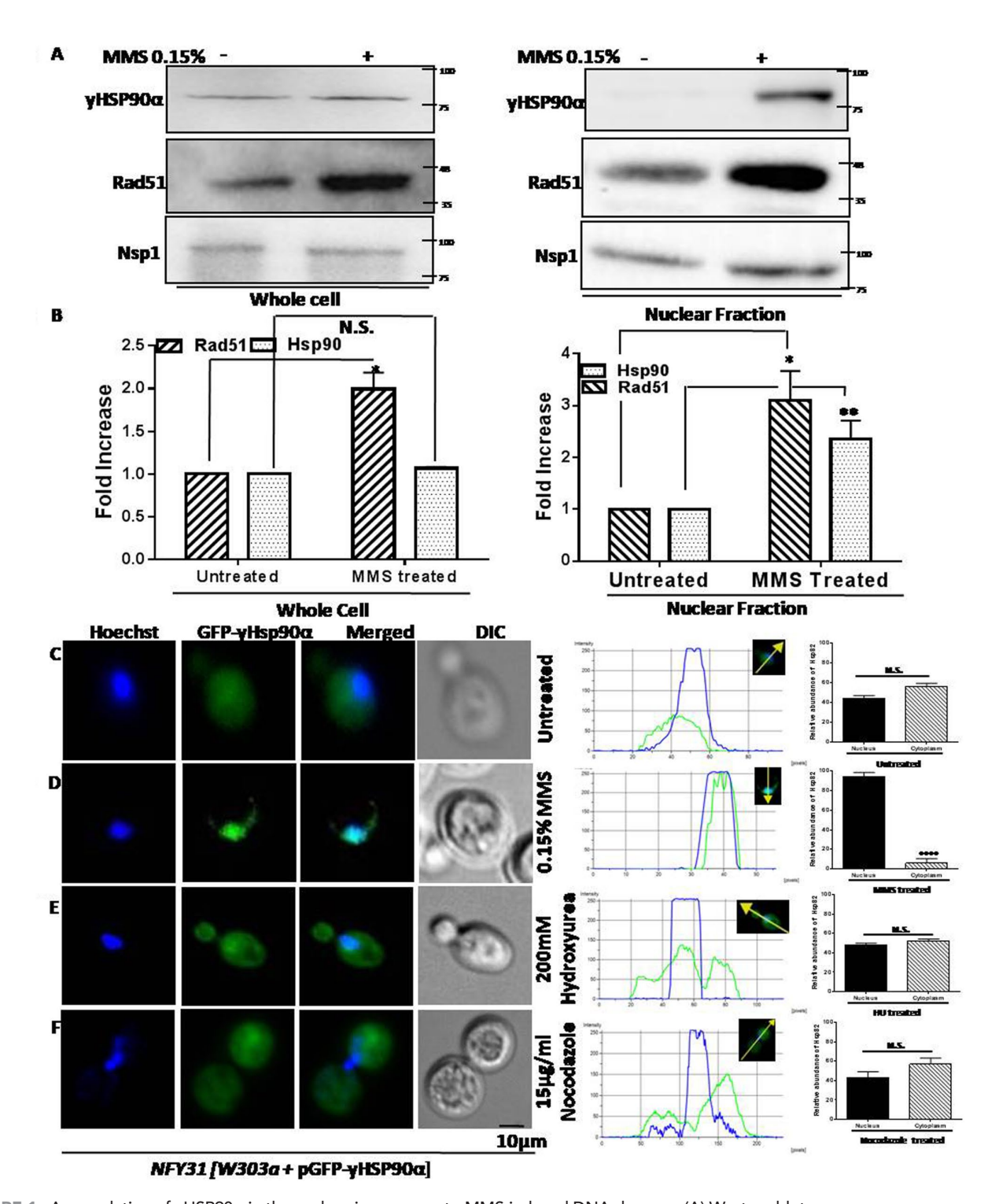


FIGURE 1: Accumulation of $yHSP90\alpha$ in the nucleus in response to MMS-induced DNA damage. (A) Western blots showing no difference in the steady state expression of $yHSP90\alpha$ in the whole cell with (+) and without (-) MMS treatment (left panel). yHSP90 α was accumulated in the nuclear fraction upon MMS treatment (right panel); Rad51 acted as a positive control for MMS treatment; Nsp1 acted as a nuclear marker. (B) The above experiment was repeated three times, and the mean values (\pm SD) were plotted. P values were calculated using the two-tailed Student's t test (**P< 0.01; *P < 0.05). (C) Live-cell imaging shows the distribution of GFP-yHsp90 α (green) in the whole cell in the untreated condition. (D) Fluorescence imaging of 0.15% MMS-treated cells shows the localization of GFP-yHsp90 α (green) inside the nucleus (blue). (E) Fluorescence images showing no nuclear accumulation of GFP-yHsp90 α (green) in 200 mM hydroxyurea-arrested early S phase cells (F) Fluorescence images showing no nuclear accumulation of GFP-yHsp90 α (green) in 15 µg/ml nocodazole-arrested G2/M cells. Nucleus was stained using Hoechst 33342. Intensity profiles were derived for all fluorescence experiments using NIS elements AR software; the relative fluorescence intensities of GFP-yHsp90 α in the nucleus and cytoplasm were quantified and the mean values (\pm SD) were plotted using GraphPad Prism 6. P values were calculated using the two-tailed Student's t test (****P< 0.0001; N.S., not significant).

cell (Figure 1C). However, when treated with 0.15% MMS, GFPvHSP90 α moved to the nucleus and coincided with Hoechst 33342 (Figure 1D). As MMS delays S-phase progression, we wanted to distinguish whether the nuclear translocation of yHSP90 α occurs as a consequence of cell cycle arrest or as a consequence of DNA damage. For that, we used hydroxyurea-induced S-phase-arrested cells and the nocodazole-induced G2/M-arrested cells and looked for the distribution of GFP-yHsp90 α . We found that GFP fluorescence was distributed majorly in the cytoplasm and to a little extent in the nucleus of the hydroxyurea-arrested cells (Figure 1E). We also found that GFP-yHsp90 α was evenly distributed throughout the cytoplasm in the nocodazole-arrested cells (Figure 1F) and didn't coincide with the blue fluorescence of Hoechst. Thus our study concludes that nuclear redistribution of yHsp 90α is associated with MMS-induced DNA damage. We further examined whether human $HsHSP90\alpha$ shows similar localization dynamics in response to MMS treatment. We used the strain harboring a plasmid that expresses human $\mathsf{HSP90}\alpha$ fused with FLAG. We verified that FLAG antibody does not show any cross-reactivity with other yeast proteins (Supplemental Figure S2A). The nuclear fractionations showed increased levels of $\mbox{HsHSP90}\alpha$ in the MMS-treated sample compared with the untreated sample (Figure 2A). Quantification of gel images from an independent set of experiments showed about a fourfold increase in the $HsHSP90\alpha$ level within the nucleus (Figure 2B). We sought to determine whether this import is dependent on the presence of Thr 7 residue of HsHSP90 α . Using a mutant protein HsHSP90 α^{T7A} where threonine is mutated to alanine, we observed that its nuclear import remained unperturbed (Figure 2C). Estimation of multiple WBs showed about a fivefold increase in the nuclear fraction with respect to the untreated cell (Figure 2D). Thus our study shows that DNA damage induces an increased import of $\mbox{HSP90}\alpha$ in the nucleus from the cytoplasm which is independent of phosphorylation of the threonine 7 residues.

Nuclear accumulation of yHSP90 α upon induction of a single double-strand break

MMS alkylates DNA bases and thereby causes DNA-base mispairing (Lundin et al., 2005). To understand whether the increased nuclear yHSP90 α reflects a true response to DNA damage, we induced a single double-strand break in DNA and determined the cellular redistribution of yHSP90 α . To that end, we used the NA14 strain (Agmon et al., 2009), where a site-specific DSB was created within the mutant ura3 locus by expressing a galactose-inducible HO endonuclease (Figure 3A). By designing the primers complementary to the region adjacent of the HOcs (OSB 289) and the regions within the KANMX cassette (kanB1), we measured the extent of DNA cleavage by the HO endonuclease. We have repeated the repair kinetics upon HO induction with three independent batch of cells and one of the representative images is provided (Figure 3B). We found that the HO endonuclease resulted in 75% cleavage at the ura3 locus within the first hour of induction and 100% by the end of the second hour (Figure 3C). The DSBs are repaired by HR using a donor URA3 sequence that is placed 3 kb apart. We observed that 50% repair was achieved at the end of the third hour and the damage was completely healed by the end of the fourth hour (Figure 3, B and C). As in our experimental setup, we always observed maximum damage at the second hour of galactose induction (Figure 3C), we harvested the cells before and at the second hour after the galactose treatment, and performed the nuclear fractionation. We observed that there was no difference in the expression of yHSP90 α in the whole cell and at the second hour postinduction, the protein showed significant nuclear enrichment upon formation of a single

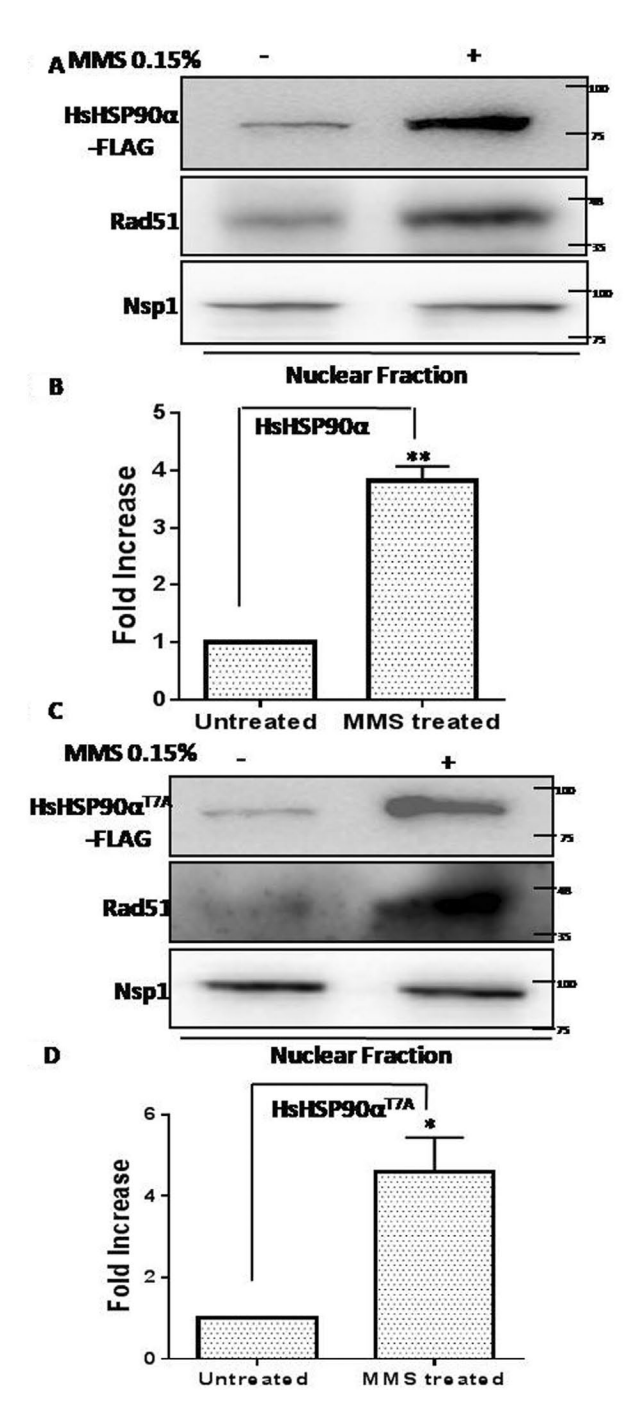


FIGURE 2: Accumulation of HsHSP90α in the nucleus in response to MMS-induced DNA damage. (A) Western blot showing the nuclear fractionation of *FLAG* tagged *HsHSP90*α strain in the presence and absence of MMS treatment. (B) The experiment was repeated with a fresh batch of cells and estimation of band intensities showed a fourfold increase in the nuclear accumulation of HsHSP90α in the presence of MMS. (C) Western blot showing the results of nuclear fractionation of *FLAG* tagged *Hshsp90*α. T7A strain in the presence and absence of MMS treatment. (D) Quantification of band intensities of independent experiments showed a fivefold increase in the nuclear distribution of the mutant protein; *P* values were calculated using the two-tailed Student's *t* test (**P < 0.01; *P < 0.05).

DSB in chromosome (Figure 3D). Quantification of the independent WB image showed about a fourfold increase in the nuclear level of yHSP90 α at 2 h post-HO induction (Figure 3E). Hence we observe

4 | N. Fangaria et al. Molecular Biology of the Cell

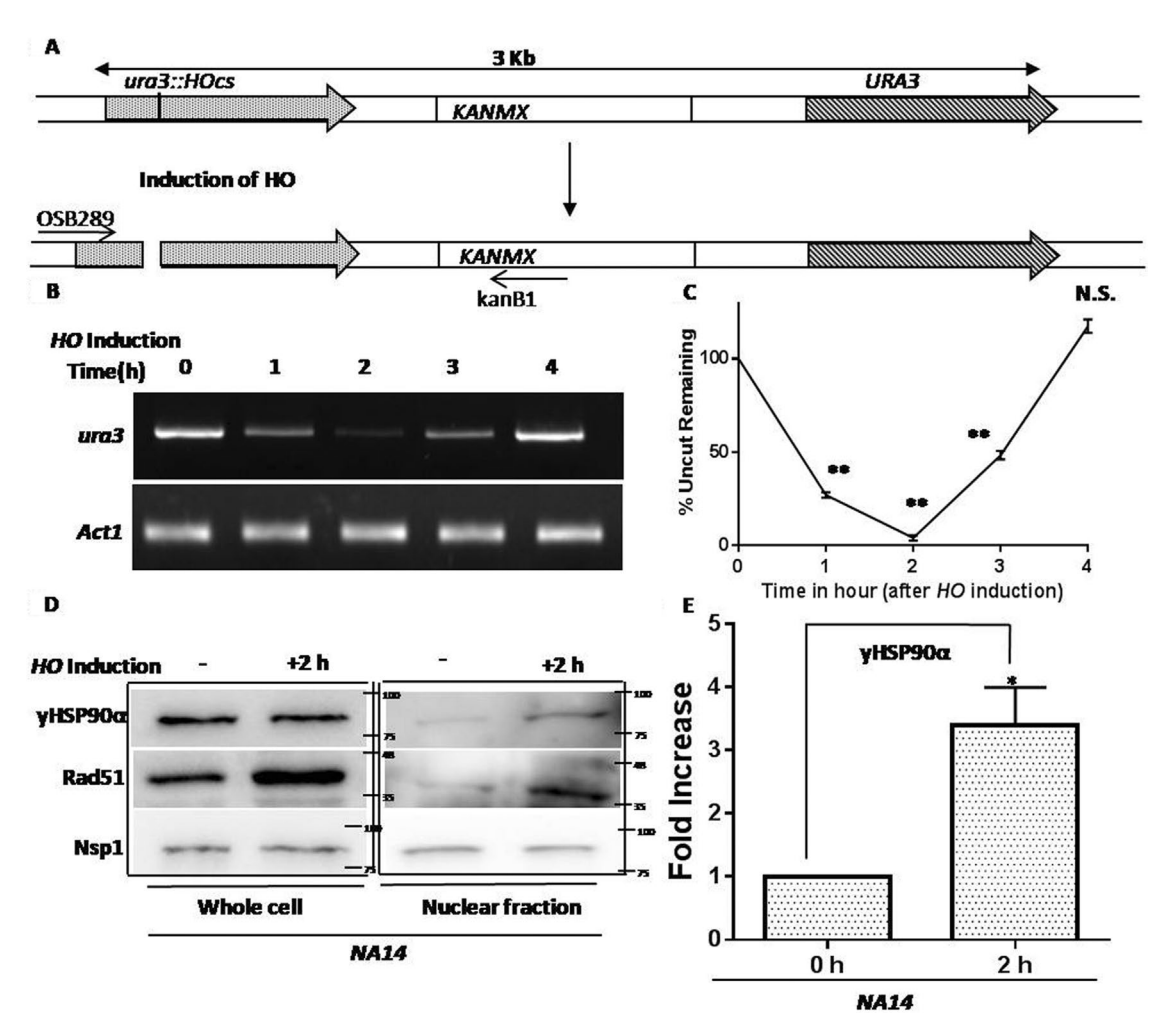


FIGURE 3: Nuclear accumulation of yHSP90 α upon induction of a single double-strand break. (A) Schematic representation of the cassette incorporated in the NA14 strain in which two homologous URA3 sequences are separated by 3-kb intervals on chromosome V with the sequence of KANMX integrated in between. One of the URA3 sequences has HO endonuclease recognition site (HOcs) incorporated in it. The relative positions of the primer pairs OSB289 and KanB1 were shown, which were used to detect the DNA damage upon HO induction. (B) NA14 cells were grown and HO induction was done by growing cells in galactose medium. Genomic DNA was extracted at different time intervals (0 to 4 h) and subsequently amplified using the primer pairs OSB289 and KanB1, where the absence of band indicated DNA damage. DNA levels were normalized with respect to ACT1. (C) The above experiment was repeated with three independent batches of cells and the mean values (±SD) were plotted. The repair kinetics showed maximum damage at the second hour of HO induction and complete repair was seen at the fourth hour of induction. The mean values (±SD) were plotted; the significance was calculated with respect to the untreated sample (0 h); P values were calculated using the two-tailed Student's t test (**P < 0.01, NS, not significant). (D) The steady state levels of yHSP90 α in NA14 strain were presented at 2 h before (-) and after (+) HO induction (left panel). In the same conditions, nuclear fractionations were done which showed increased nuclear accumulation of yHSP90 α at the second hour of induction (right panel). Rad51 up-regulation served as a control for DSB; protein levels were normalized with respect to Nsp1. (E) Quantification of yHSP90 α levels as obtained from independent set of experiment showed fourfold increase at 2 h post-HO induction. The mean values (±SD) were plotted, P values were calculated using the two-tailed Student's t test (*P < 0.05).

that even a single DSB in chromosome causes an increased nuclear accumulation of yHSP90 α .

Kinetics and extent of occupancy of yHSP90α at DSB ends

In mammalian cells it was demonstrated that DNA damage-induced T7-phosphorylated form of HsHSP90 α is recruited to the damaged chromatin. However, whether this phosphorylation is a criterion for its chromatin recruitment was not addressed. In S. cerevisiae yHSP90 α lacks the stretch of 14 residues, including T7 of HsHSP90 α . We wanted to check whether the nuclear pool of yHSP90 α was associated with the damaged chromatin. We utilized the chromatin immunoprecipitation technique to visualize the kinetics and extent of yHSP90 α binding following DSB induction and during its repair by HR. In NA14 yeast cells, the DSB created at the ura3 locus can be repaired by HR using a donor template (URA3) that is located 3 kb apart (Figure 4A). To monitor yHSP90α binding to DSB ends, we performed ChIP analysis immediately after HO induction and at every 1-h interval up to 4 h (the time required for its complete repair). Significant yHSP90 α binding to sequences close to the HO cleavage site was observed at the second and third hours using a pair of primers (shown as horizontal bars), OSB 519 and OSB 520, that amplify sequences 55 to 205 bp proximal to the HO cut site (Figure 4B).

There was no association of yHSP90 α to other locus (ACT1). The maximum recruitment of yHSP90 α to DSB was observed at the second hour. It is noteworthy that the maximum break was generated during the second hour post-HO treatment and by the third hour 50% break was repaired (Figure 3C). Thus the entry and exit of Hsp90 correlated well with the presence of maximum break as seen in Figure 3B and it remained associated up to the third hour until 50% of the DSB remained unrepaired (Figure 3C). At a later time point (the fourth hour), the recruitment was substantially reduced. As a reference, we monitored the recruitment of Rad51 under similar conditions and observed a slightly different pattern (Figure 4C). We calculated the fraction of recruitment of yHSP90 α and Rad51 and plotted against different time intervals. We found that yHSP90 α recruitment was highest at the time of maximum damage (second hour) and it was dislodged from the chromatin at the fourth hour of HO induction once repair was complete (Figure 4D). Rad51 recruitment had been initiated at the second hour, which remained maximum at the third hour and a significant amount of Rad51 remained associated even at the fourth hour (Figure 4D). We also measured the association of yHSP90 α and Rad51, at the leftward direction (up to 5 kb) from the cleavage sites. We found a similar pattern, i.e., significant recruitment of yHSP90 α and Rad51 was observed throughout 4 kb regions during the second and third hours post-HO induction (Figure 4E). Thus our study has established that a DNA damage-induced increase in association of yHSP90 α to the chromatin is independent of the N-terminal 14-residues present in HsHSP90 α .

Increased nuclear localization of Aha1 in response to DNA damage

We further investigated DNA damage-induced nuclear accumulation of the Hsp90 cochaperone Aha1. We employed indirect immunofluorescence to monitor the cellular localization of Aha1 in W303a strain. We observed that Aha1 was equally distributed in the nucleus and in the cytoplasm before (Figure 5A) and after MMS treatment (Figure 5B). However, there was an overall increase in the Aha1 fluorescence intensity in the cell in response to MMS (Figure 5B). Such induction corroborated well with our Western data with the whole cell, where we found that endogenous level of Aha1 was significantly induced upon MMS treatment (Figure 5C, left panel). We also observe a concomitant increase in the Aha1 level in the nucleus (Figure 5C, right panel) upon MMS treatment. It is noteworthy that Aha1 antibody used in this study is highly specific and does not cross-react with any other proteins in WB and does not give any background in IFA (Supplemental Figure S2D). We wanted to determine whether induction of a single double-strand break in the chromosome could also induce the import of Aha1 to the nucleus. For that, we used the NA14 strain. Our results showed that in this strain, the Aha1 protein level in the nucleus was significantly increased, about 1.5-fold, at the second hour of HO induction (Figure 5, D and E), whereas the yHSP90 α level was increased about threefold. We also monitored whether Aha1 was also recruited to DSB ends like yHSP90 α . However, we could not detect Aha1 in the ChIP assay (data not shown). We speculate that Aha1 may be transiently associated to chromatin, which could not be detected in our assay. Next, to investigate whether other cochaperones such as Sba1 and Cdc37 are imported to the nucleus upon DNA damage, we used carboxy-terminal MYC tagged Sba1 and Cdc37 strains for our analysis. We found that there was no such increase in the levels for Cdc37 in the whole cell as well as in the nucleus upon DNA damage (Figure 5F). In the case of Sba1, we found that its endogenous level was significantly induced upon MMS treatment similar to that of Aha1 (Figure 5G, left panel). However, unlike Aha1, there was no such increase in Sba1 level in the

nucleus (Figure 5G, right panel). We have repeated these experiments three times and the nuclear distribution of each of the cochaperones was plotted in the presence and absence of MMS. It was found that in the whole-cell extract, the abundance of Aha1 and Sba1 was threefold and fourfold, respectively (Figure 5H); however, only Aha1 showed about a twofold increased accumulation in the nucleus upon MMS treatment, while Sba1 and Cdc37 showed no significant increase (Figure 5I). To address whether MMS-induced up-regulation of Aha1 and Sba1 occurs at the transcription level, we compared the relative expression of the above-mentioned cochaperones in the absence and presence of 0.15% MMS (Supplemental Figure S3A). Quantitative reverse transcription PCR (RT-PCR) shows a 1.5-fold increase in expression of AHA1 and no significant increase in expression of SBA1 upon MMS treatment (Supplemental Figure S3B). An increase in RAD51 transcript was used as a positive control in our study. We speculate that the higher abundance of SBA1 may result due to increased protein stability during genotoxic stress.

yHsp90 α transport to the nucleus upon DNA damage is independent of Cdc37 and Sba1

Next, we wanted to address whether DNA damage-dependent increased nuclear accumulation of yHSP90 α is dependent on Cdc37 and Sba1. We used the temperature-sensitive cdc37S14A mutant strain, which shows normal phenotype at 25°C but displays a complete loss of function when grown at a restrictive temperature 37°C. Our study showed no difference in the endogenous level of yHSP90 α in the cdc37S14A mutant strain when grown at 37°C in the presence or absence of MMS (Figure 6A). The nuclear fractionation under similar conditions showed a fourfold increase in the accumulation of yHSP90 α upon DNA damage (Figure 6, B and C), similar to that observed in the wild-type strain. To address the dependency on Sba1, we generated a Asba1 strain in an isogenic W303a background. We found that in the $\Delta sba1$ strain, the yHSP90 α level was induced by 3.6-fold in the whole cell in response to MMS treatment (Figure 6, D and F). In addition, DNA damage-dependent nuclear import was observed in a manner nearly indistinguishable from the wild-type cells (Figure 6, E and F). Together, this study concludes that MMS-induced nuclear import of yHSP90 α is independent of Cdc37 and Sba1.

yHSP90 α transport to the nucleus upon DNA damage is dependent on Aha1

To decipher whether Aha1 plays any role during MMS-induced nuclear import of yHSP90 α , we generated $\Delta aha1$ strain. We transformed empty plasmid and AHA1 overexpression plasmid to $\Delta aha1$ strain to generate two isogenic strains. AHA1 expression was detected specifically in Δaha1 strain harboring the AHA1 overexpression plasmid (Figure 7A, third lane). Interestingly, we found that Aha1 deletion was positively correlated with MMS-induced upregulation of endogenous yHSP90 α (Figure 7A), and the phenotype is reversed with ectopic expression of AHA1 as presented in Figure 7A (first lane). Further, we observed that although Aha1 deletion resulted in a 3.5-fold induction in the endogenous level of yHSP90α upon MMS treatment (Figure 7B), it couldn't be translocated to the nucleus (Figure 7C, first lane). However, ectopic expression of Aha1 resulted in the increased nuclear import of both yHSP90α (approximately threefold) and Aha1 upon DNA damage (Figure 7, C and D). We used live-cell fluorescence to visualize the localization of yHSP90 α in the $\Delta aha1$ strain NFY32 that harbors a centromeric GFP-yHSP90α plasmid. We didn't find any nuclear localization of yHSP90 α under the MMS-treated (Figure 7F) or untreated (Figure 7E) condition. This experiment was performed

6 N. Fangaria et al. Molecular Biology of the Cell

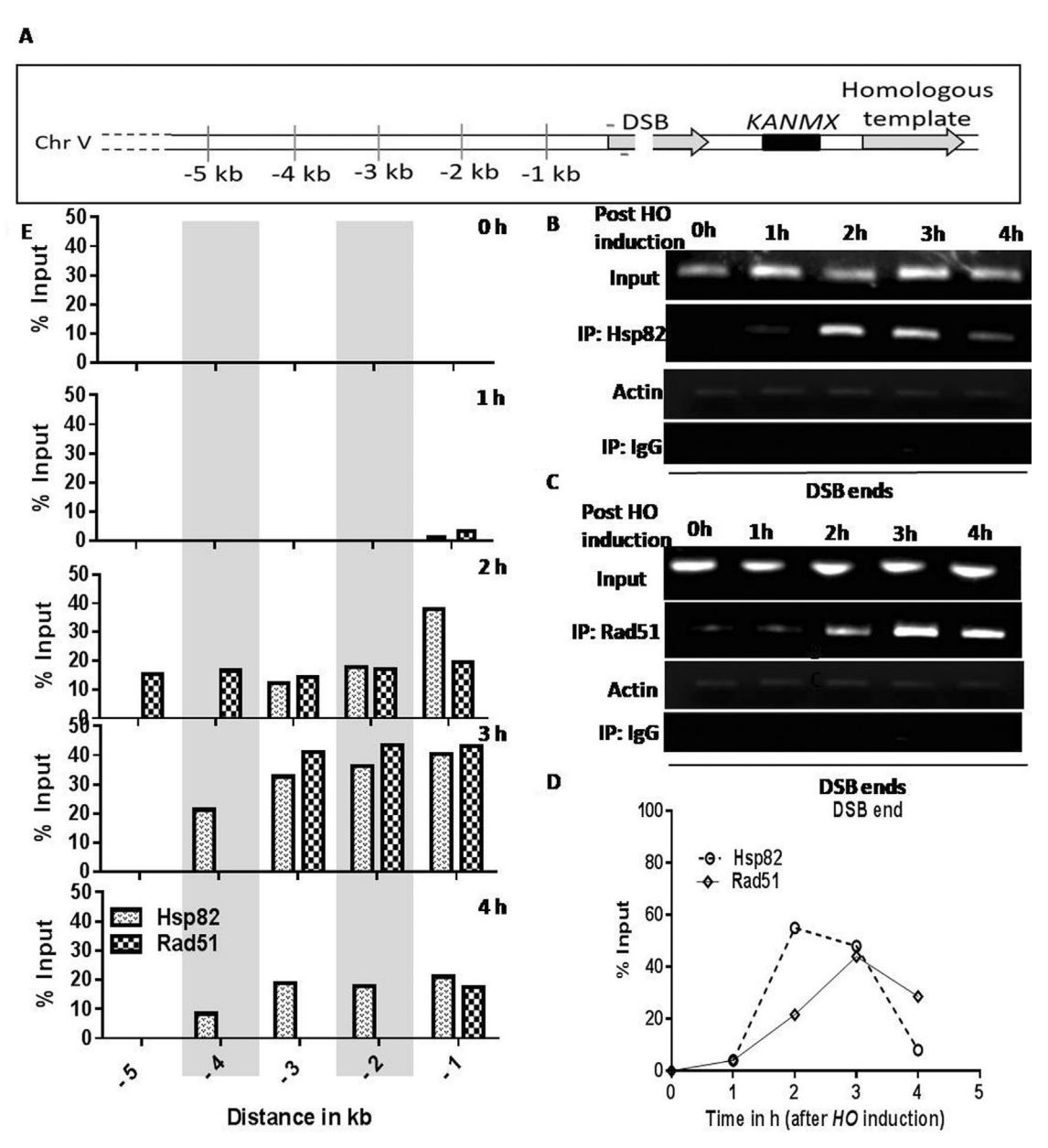
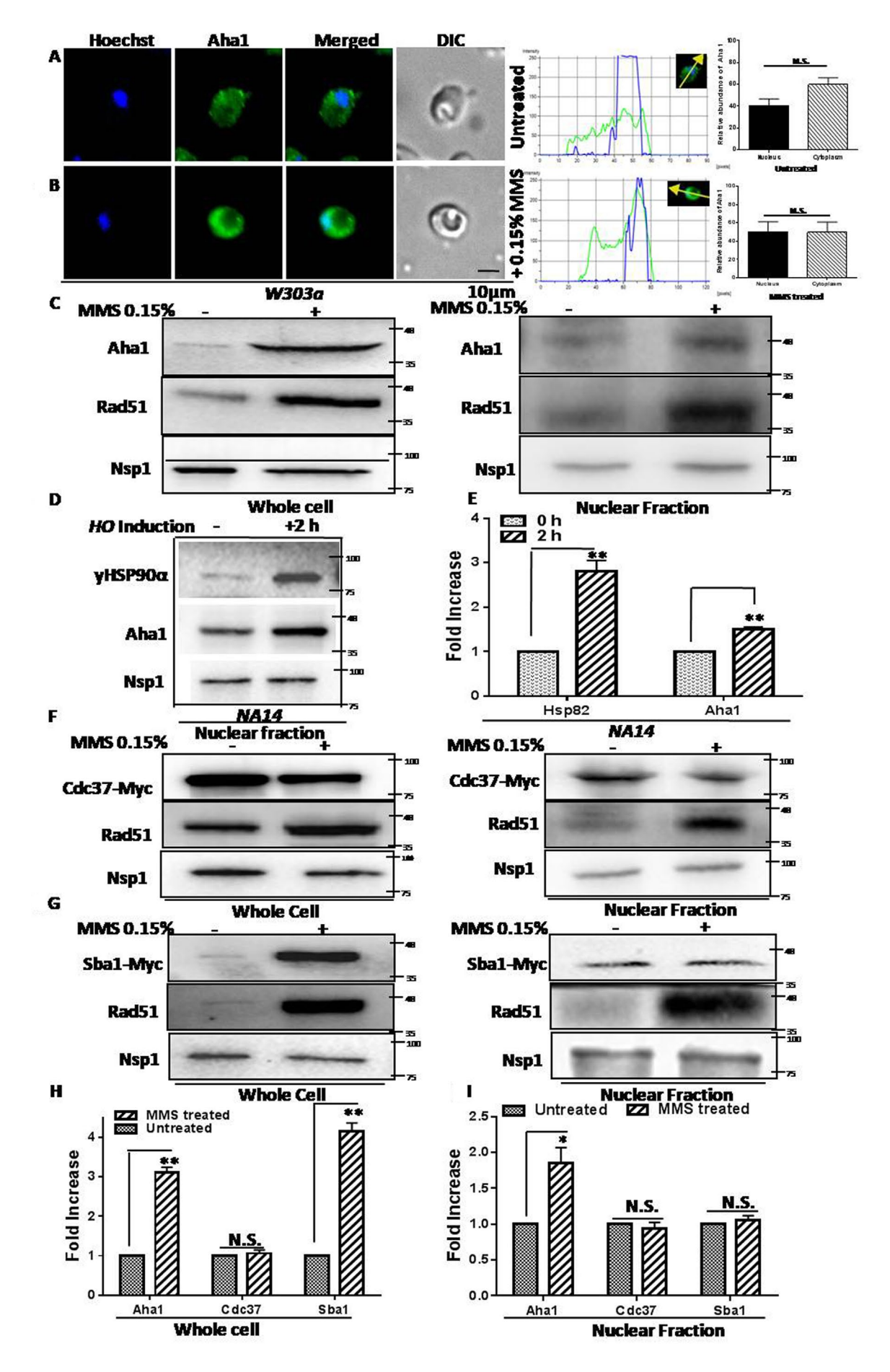


FIGURE 4: Kinetics and extent of occupancy of yHSP90 α at DSB ends. (A) Schematic representation of the position of DSB at the ura3 locus and the presence of a homologous template (URA3). The position of the primers (as indicated in horizontal bar) near the DSB was presented, which was used to detect the recruitment of yHSP90 α and Rad51 near the HO cleavage site. The map of the sites (up to - 5 kb) distal to the DSB was shown. (B) yHSP90lpha bound chromatin was amplified to detect the kinetics of its recruitment to the HO cleavage site and at the ACT1 locus. (C) ChIP analysis showing the kinetics of Rad51 recruitment to the DSB ends as well as at the ACT1 locus following HO induction. (D) Quantification of the independent ChIP experiments (n = 3, in each case) was plotted. Error bars indicated SD. (E) The association of yHSP90 α and Rad51 was measured at increasing distances up to 5 kb upstream of the HO cleavage site at different time points post-HO induction. Quantification of two independent ChIP experiments were plotted to compare the extent of recruitment between yHSP90 α and Rad51. Error bars indicated SD. ChIP assay was done with IgG antibody that was used as a negative control.

along with its isogenic control strain (Figure 1, C and D). To understand whether yHSP90 α and Aha1 remain associated under the MMS-treated condition, we performed coimmunoprecipitation study. We used a strain KRAY29, that harbors a plasmid with C-terminal FLAG tagged Aha1. Aha1 was pulled down with anti-FLAG antibody in MMS-treated and untreated conditions and we looked for the presence of yHSP90 α in the IP fraction. We found that Aha1 and yHSP90 α remained physically associated in both the conditions (Figure 7G).

To understand whether the Aha1-dependent nuclear import of yHSP90 α is a generalized phenomenon in budding yeasts, we used another Δaha1 strain in the BY4741 background and wanted to test the same in this strain background. In BY4741 whole-cell extract, where Aha1 protein was completely absent (Figure 8A, left panel), we found similar up-regulation of yHSP90 α in response to MMS. However, we find complete abrogation of the nuclear accumulation of yHSP90 α (Figure 8A, right panel). We loaded a higher amount of protein in the MMS-treated condition compared with the other



8 | N. Fangaria et al. Molecular Biology of the Cell

lanes as seen by the amount of Nsp1 (Figure 8A, right panel, last lane); however, there was no signal of yHSP90 α in the nuclear fraction. We overexpressed AHA1 in the BY4741∆aha1 strain and performed the nuclear fractionation in the presence and absence of MMS. The Western blot of the whole-cell extract showed no change in the endogenous level of yHSP90 α in the presence and absence of MMS (Figure 8B, left panel). However, the presence of Aha1 promoted the nuclear import of yHSP90 α in a MMS-dependent manner (Figure 8B, right panel). Together, our data establish that the presence of Aha1 is essential for the nuclear localization of yHSP90 α .

The domain responsible for the conformational flexibility between the amino terminal and the MD of yHSP90 α is essential for its nuclear translocation upon DNA damage

It was earlier established that the conformational flexibility between the amino terminal domain and the MD of yHSP90 α is mediated by a flexible CL domain spanning 211-259 residues, as presented in the schematic diagram (Figure 9A). The deletion of these highly charged amino acid stretches (211-259) leads to a significant reduction in Aha1-stimulated ATP hydrolysis of yHSP90 α (Hainzl et al., 2009). However, deletion of a shorter stretch (211-242) does not alter the conformational flexibility of the mutant protein and it shows comparable Aha1-mediated ATPase activation of yHSP90 α as that of the wild-type protein (Hainzl et al., 2009). We wanted to determine whether this domain known for providing conformational flexibility between the amino-terminal and the middle domain is important for its nuclear import. We investigated the MMS-induced nuclear import of the two mutant proteins yHSP90 $\!\alpha^{\!\Delta\!(211\text{-}259)}$ and yHSP90 $\alpha^{\Delta(211-242)}$ using live-cell fluorescence imaging. For that, we generated NFY33 and NFY35 strains that harbor a centromeric plasmid expressing GFP-yHSP90 $\alpha^{\Delta(211-259)}$ and GFP-yHSP90 $\alpha^{\Delta(211-242)}$, respectively. We observe that in the GFP-yHSP90 $\alpha^{\Delta(211-259)}$ harboring strain, GFP fluorescence does not merge with Hoechst fluorescence in the presence (Figure 9C) as well as the absence of MMS (Figure 9B). However, there is a distinct nuclear accumulation in the case of the shorter deletion mutant GFP-yHSP90 $\alpha^{\Delta(211\text{-}242)}$ upon MMS treatment (Figure 9, D and E). A representative image from each sample is presented. To confirm the result by an alternate method, we isolated the nuclear fraction from the previously characterized CL deletion strain (Louvion et al., 1996) which was shown to be severely defective in HR activity (Suhane et al., 2014). We observed a complete absence of the mutant protein yHSP90 $\alpha^{\Delta(211-259)}$ in the nucleus of the MMS-treated cell (Figure 10A, right panel). We loaded a higher amount of the mutant protein compared with the wild-type as seen by the level of Nsp1 (last lane, Figure 10A, right panel) but could not detect the protein in the nucleus. The Western blot analysis of the whole-cell extracts with the mutant strain confirmed the expression of the mutant protein (Figure 10A, left panel). To test whether Aha1 overexpression can promote the MMS-induced nuclear import of the longer CL deletion mutant, we transformed the AHA1 overexpression plasmid in the hsp82Δs211-259) strain. We found that AHA1 overexpression did not impact the translocation of the mutant protein to the nucleus (Figure 10B, right panel). It was previously shown that the CL region of human HSP90α provides flexibility for domain rearrangements and acts as a modulator of chaperone activity (Tsutsumi et al., 2012). We wanted to determine whether the deletion of identical stretch of charged residues from human $HSP90\alpha$ causes a similar defect. To that end, we have generated a strain harboring human HsHSP90 $\alpha^{\Delta(224-279)}$, still expressing endogenous yHSP90α (Supplemental Figure S1). The mutant protein showed expression as presented (Supplemental Figure S2B). We found that the mutant human protein did not show (Figure 10C) any increased nuclear accumulation upon DNA damage. The level of yHSP90 α was increased in the nucleus under such conditions (third panel, Figure 10C). It is noteworthy that the antibody recognizing HsHSP90 α (anti-FLAG) does not recognize yHSP90 α (Supplemental Figure S2B). Next, we performed the nuclear fractionation to detect the level of the shorter CL deletion mutant yHSP90 $lpha^{\Delta(211-242)}$ upon MMS treatment. For that, we created a strain KRAY16 in which the endogenous Hsp82 and Hsc82 are knocked out and the strain expresses yHSP90^{Δ(211-242)} from a single copy plasmid. We observed that the mutant protein is accumulated to the nucleus in response to MMS treatment, correlating our live-cell imaging data (Figure 10D). The experiment was repeated three times and the estimation of band intensities showed about a fourfold increase in the nuclear level of the mutant yHSP90 $\alpha^{\Delta(211-242)}$ in this strain background (Figure 10E). Taken together, we conclude that the CL domain of $HSP90\alpha$ is essential for its import to the nucleus. To support our conclusion further, we measured the single DSB-induced chromatin recruitment of the mutant yHSP90 $\alpha^{\Delta(211-259)}$. To that end, we generated a modified NA14 strain which harbors a plasmid that expressed the mutant yHSP90 $\alpha^{\Delta(211-259)}$ fused with GFP at its amino terminal end. The isogenic strain was generated which harbors wild-type GFPyHSP90 α - constructs, and both the fusion proteins were found to be

FIGURE 5: Increased nuclear localization of Aha1 in response to DNA damage. (A) Indirect immunofluorescence shows the distribution of Aha1 (green) in the whole cell of W303a (B) A part of Aha1 fluorescence (green) merges with the Hoechst fluorescence (blue) in the MMS-treated condition, although at is distributed in the cytoplasm as well. Nuclear staining was done using Hoechst dye and Aha1 was detected using Alexa Fluor 488-conjugated secondary antibodies. Intensity profiles were derived for all fluorescence experiments using NIS elements AR software; relative fluorescence intensities of Aha1 in the nucleus and cytoplasm were quantified and the mean values (±SD) were plotted using GraphPad Prism. P values were calculated using the two-tailed Student's t test (N.S., not significant). (C) Aha1 is induced in the whole cell (left panel) in the presence of MMS and its level in the nucleus in increased (right panel) in response to 0.15% MMS treatment. (D) NA14 strain was subjected to HO induction in the same manner as discussed in Figure 3. The experiment was repeated and one of the representative Western blots was presented. (E) Quantification of the levels of yHSP90 α and Aha1 showed threefold and 1.5-fold increased nuclear accumulation, respectively, at 2 h post-HO induction. The mean values (±SD) were plotted. P values were calculated using the two-tailed Student's t test (**P < 0.01). (F) Cdc37 level is not altered significantly upon 0.15% MMS treatment in the whole cell (left panel) as well as in the nucleus (right panel). (G) Sba1 is induced in the whole cell (left panel) in response to 0.15% MMS; however, nuclear fractionation shows no change in nuclear level of Sba1 in the presence and absence of MMS (right panel). (H) and (I) The experiments in C, F, and G were repeated with an independent batch of cells and the quantitation of the data was done using ImageJ and mean values (±SD) were plotted; P values were calculated using the two-tailed Student's t test (**P < 0.01; *P < 0.05; NS, not significant). The left panel shows the levels of individual cochaperones in the whole cell and the right panel shows the levels of the same in the nuclear fraction.

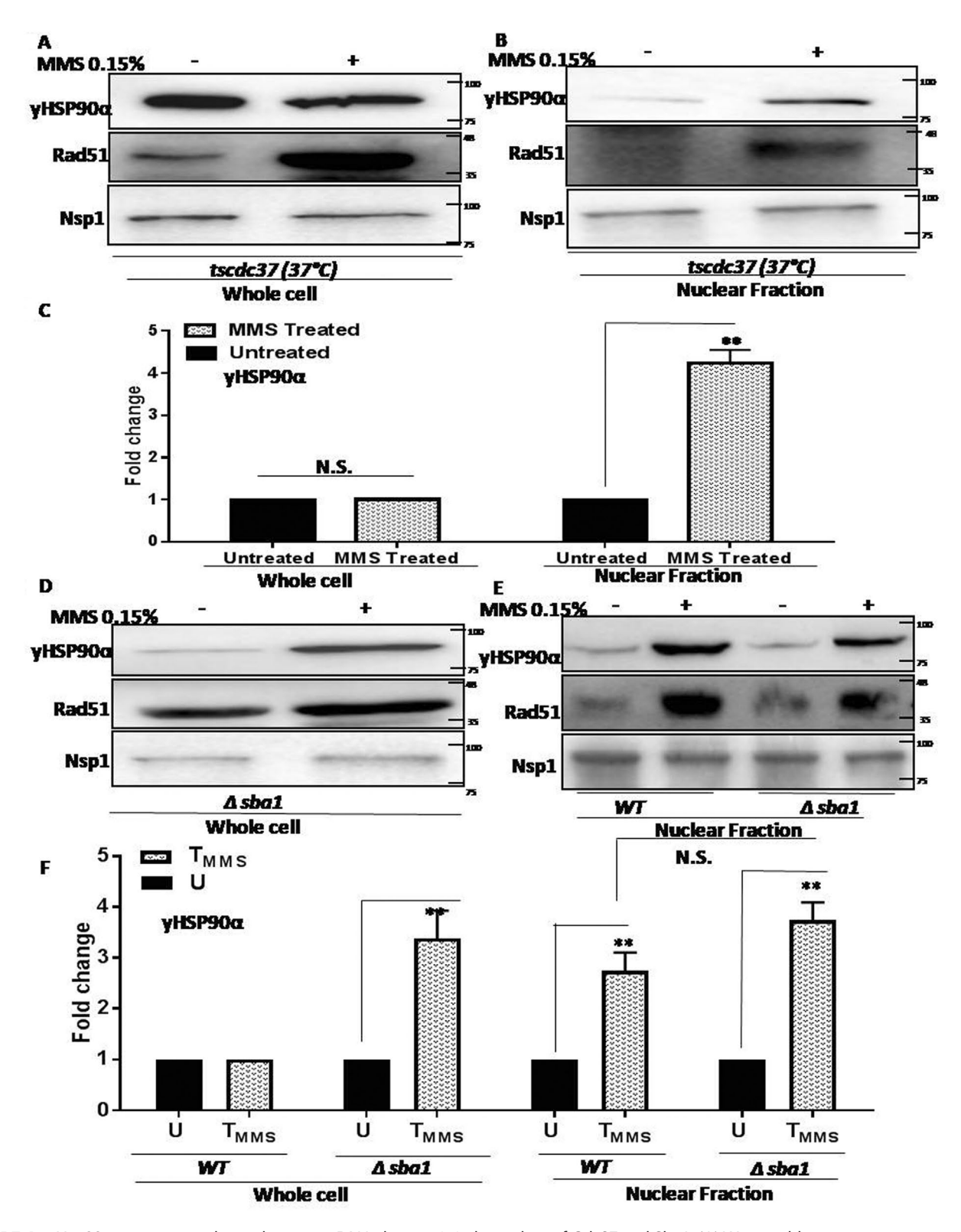


FIGURE 6: yHsp90 α transport to the nucleus upon DNA damage is independent of Cdc37 and Sba1. (A) Western blot showing no change in the endogenous level of yHSP90 α upon MMS treatment in the temperature-sensitive tscdc37S14A strain at nonpermissive temperature (37°C). (B) Western blot shows that cdc37 loss of function mutation does not alter increased nuclear accumulation of yHSP90 α upon MMS treatment. (C) The above experiments (A and B) were repeated with three independent batches of cells and the densitometric image analysis of yHSP90 α was presented, P values were calculated using the two-tailed Student's t test (**P < 0.01; NS, not significant). (D) In the $\Delta sba1$ strain endogenous levels of yHSP90 α are induced in response to MMS treatment (E) Nuclear fractionation of untreated and MMS-treated wild type and $\Delta sba1$ strain shows accumulation of yHSP90 α in both the wild-type W303a and isogenic $\Delta sba1$ strains. (F) The experiments (D and E) were repeated three times and the mean values (\pm SD) were plotted, P values were calculated using the two-tailed Student's t test (**P < 0.01; N.S., not significant).

10 | N. Fangaria et al. Molecular Biology of the Cell

expressed in a similar level (Supplemental Figure S2C). Owing to a large molecular weight, the small difference between the molecular weights of GFP-yHSP90 $\!\alpha$ and GFP-yHSP90 $\!\alpha^{(\!\Delta 211\text{-}259)}\!$ was not detectable in the Western blot (Supplemental Figure S2C). We studied the recruitment of wild-type (GFP-yHSP90α) and mutant GFPyHSP90 $\alpha^{\Delta(211-259)}$ on the broken DNA at the second hour post-DNA damage induction, as there was maximum damage at the second hour time point (data not shown). We found no detectable recruitment of GFP-yHSP90 $\alpha^{\Delta(211-259)}$; whereas wild-type GFP-yHSP90 α was detected at the HO cleavage site, 2-h post-HO induction and IgG precipitation acted as a negative control (Figure 10F). Using Western blot analysis, we determined the levels of the wild type and the mutant protein in the immunoprecipitated samples of the 2-h post-HO induction and didn't observe any noticeable difference (Figure 10F, lower panel). We repeated the chromatin immunoprecipitation assay thrice with these two strains and quantified the occupancy of the wild type and the CL-deleted protein at the HO cleavage site. We found that the mutant protein was severely defective in its recruitment compared with the WT protein (Figure 10G). To determine the specificity of the CL domain for the nuclear import we have investigated the effect of an ATPase dead mutant, hsp82T1011 (Nathan and Lindquist, 1995), that also affects the amino-terminal association of yHSP90 α (Prodromou et al., 2000). We exposed the mutant strain and the isogenic wild-type strain to MMS and observed that the nuclear import of the mutant protein showed a similar trend as that of the wild-type yHSP90 α (Figure 10H). We have estimated the levels of yHSP90 α and Rad51 from the P82a and mutant strain and presented them graphically (Figure 10I). We observed that both yHSP90 α and yHSP90 α^{T1011} showed a nearly twofold increased level in the nucleus. However, as expected and reported earlier (Suhane et al., 2014), the level of Rad51 was highly reduced in the mutant strain, although it showed similar fold upregulation in the nucleus upon MMS treatment. Thus using two separation-of-function mutants of yHSP90 α our study reveals that the CL domain of yHSP90, which is responsible for the Aha1-mediated conformational rearrangement but not the N-terminal ATPase domain, is required for the nuclear import of yHSP90 α .

Loss of nuclear translocation of yHSP90 α is correlated with increased sensitivity to MMS

An earlier study in our laboratory demonstrated that the mutant yHSP90 $\alpha^{\Delta(211-259)}$ displays extreme MMS sensitivity and a drastic reduction in Rad51-mediated gene targeting efficiency in yeast (Suhane et al., 2014). Our present study shows that this mutant is defective in DNA damage-induced nuclear import. To study whether DNA damage-induced nuclear import of yHSP90 α is directly linked to the protection against MMS-induced cell death, we measured the MMS sensitivity of the mutant yHSP90 $\alpha^{\Delta(211-242)}$ and compared it with the isogenic wild-type and yHSP90 $\alpha^{\Delta(211-259)}$ strains. We observed that the yHSP90 $\alpha^{\Delta(211-242)}$ strain showed similar viability as that of the wild-type strain in the presence of 0.03% MMS (Figure 11), whereas the larger CL-deleted mutant yHSP90 $\alpha^{\Delta(211-259)}$ showed a significant reduction in cell survivability. Hence our study establishes that DNA damage-induced enhanced nuclear accumulation of yHSP90 α is a major determinant for providing protective activity against genotoxic stress.

The absence of Aha1 sensitizes the cells to DNA-damaging agents

To further ascertain the importance of Aha1 in DNA repair, we determined the sensitivity of the Δaha1 strain toward various DNA-damaging agents. The WT and the $\Delta aha1$ strains were exposed to 0.03% MMS. We found that the absence of Aha1 led to the reduction of cell survivability to 30%, whereas the wild-type strain showed 80% viability (Figure 12A). However, the sensitivity was reversed with the episomal expression of AHA1 (Figure 12B). We next exposed the WT and the $\Delta aha1$ strains to two different doses of zeocin, namely, 5 and 15 µg/ml. Zeocin, belonging to the bleomycin family of the glycopeptide antibiotic, induces DSB in the chromosome. Our study showed that the absence of Aha1 made the strain more susceptible to zeocin in a dose-dependent manner compared with the isogenic wild-type strain (Figure 12C). However, the sensitivity of zeocin could be reversed by the overexpression of AHA1 in the Δaha1 strain (Figure 12D). Together, this study suggests a direct link between the Aha1 and the genomic stability in the budding yeast.

DISCUSSION

This study has demonstrated for the first time that yHSP90 α displays a noncanonical nuclear function during DNA repair in yeast. We observe that cytoplasmic $yHSP90\alpha$ is redistributed to the nucleus in response to DNA damage and this phenomenon is essential for maintaining genome stability. We analyzed two well-characterized CL deletion mutants of yHSP90 α that are different by the presence of 17 amino-acid stretches in the linker region (Hainzl et al., 2009). The mutant yHSP90 $\alpha^{\Delta(211-242)}$ shows wild type-like survivability upon MMS treatment and displays an increase in cytoplasm to nuclear accumulation under similar treatment. However, the mutant yHSP90 $\alpha^{\Delta(211-259)}$ fails to get accumulated in the nucleus and displays a fourfold reduction in cell survivability compared with the mutant yHSP90 $\alpha^{\Delta(211-242)}$. This suggests an essential nuclear function of yHSP90 α during DNA damage. Comparing the kinetics of the DSB repair and extent of its recruitment, we conclude that yHSP90 α may not be involved in the maintenance of the assembly of protein complexes that are recruited immediately after generation of DSB. In our assay, yHSP90α didn't show its immediate association at the first hour, even when the majority of the DNA was broken. Rather, its binding during the second and third hours indicates its probable function during DNA repair. Furthermore, at those time points, yHSP90α shows a significant association up to 4 kb distal position from the cleavage site in a manner similar to that of Rad51. In HRmediated DSB repair, a long resection occurs at the broken ends that produces a 3' single-stranded tail region in which the Rad51 protein is coated (Singh et al., 2008). We could detect yHSP90 α and Rad51 to the furthest region from the broken side even at a time when 50% breaks still remain unrepaired. As it was previously shown that yHSP90 α is physically associated with Rad51 (Suhane et al., 2014), we propose that $yHSP90\alpha$ might play a role in the initiation and maintenance of the Rad51 nucleoprotein filament formation. To establish that further, we studied the extent of chromatin association of the mutant GFP-yHSP90 $\alpha^{\Delta(211-259)}$. We find that this mutant is completely defective in its recruitment to the DSB ends. It is noteworthy that this mutant displays a significant reduction in the MMSinduced Rad51 foci formation and shows a severe defect in Rad51mediated gene targeting efficiency (Suhane et al., 2014). Hence we conclude that the nuclear import of yHSP90 α , followed by its recruitment to the broken ends of DNA, is a prerequisite for effective DNA repair via HR-mediated DNA repair pathway failure of which it can significantly reduce Rad51 nucleoprotein filament formation. It is noteworthy that $yHSP90\alpha$ does not have any DNA binding domain, so it probably associates with chromatin via some unidentified proteins.

It is noteworthy that we didn't determine the kinetics of yHSP90 α recruitment at the donor DNA (3' end of the URA3) locus, which is 3 kb away toward the right side of the cleavage junction. The resultant

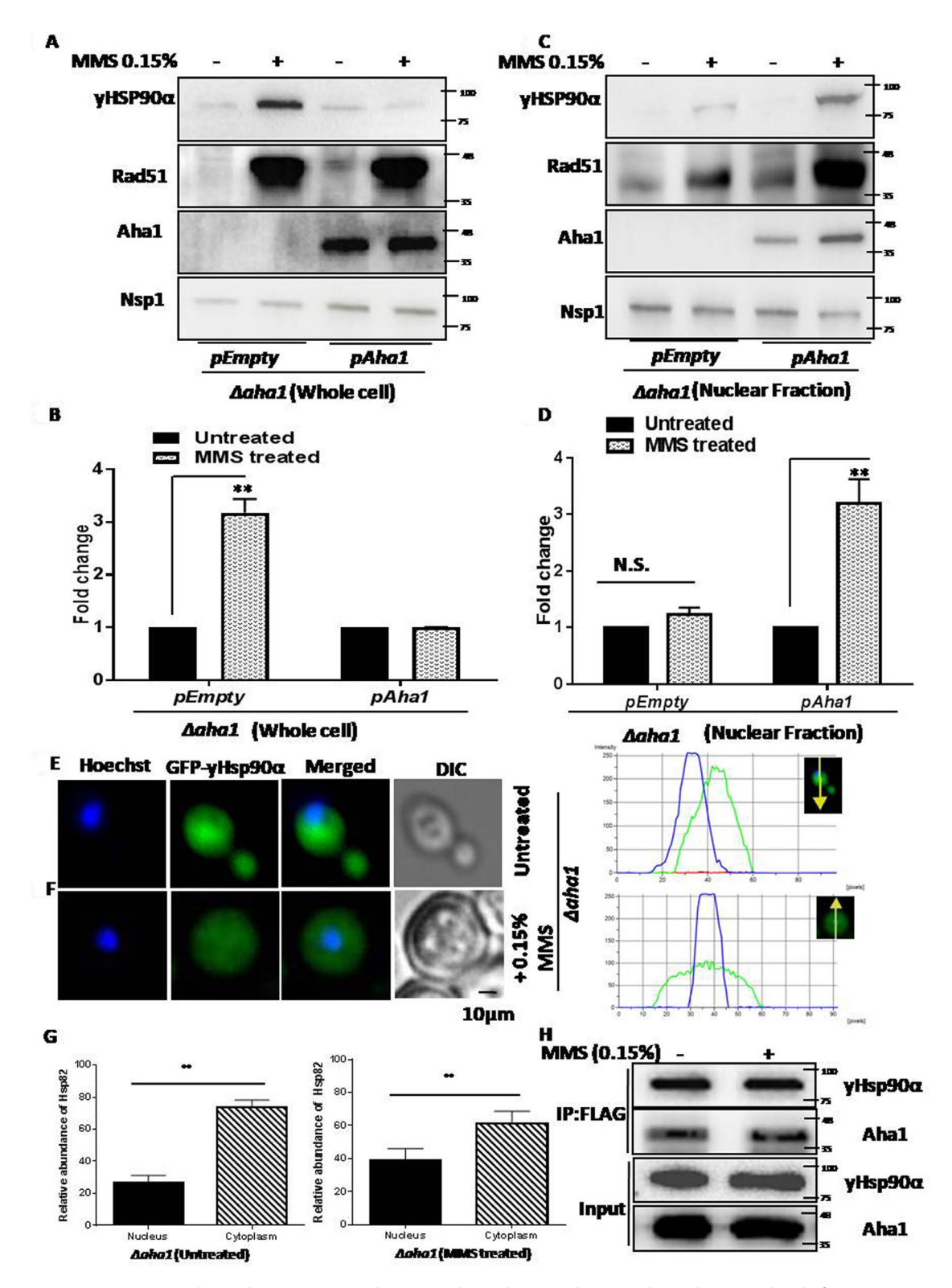


FIGURE 7: yHSP90 α transport to the nucleus upon DNA damage is dependent on Aha1. (A) The endogenous level of yHSP90 α is induced in $\Delta aha1$ cells upon 0.15% MMS treatment. There is no difference in its expression between untreated and treated condition upon ectopic expression of *AHA1*. (B) The experiment was repeated multiple times and yHSP90 α level was estimated from independent experiments and plotted, *P* values were calculated using the two-tailed Student's t test (**P < 0.01; N.S., not significant). (C) Negligible accumulation of yHSP90 α occurs in the nucleus of $\Delta aha1$ cells upon 0.15% MMS treatment, whereas a marked increase was observed upon ectopic expression of *AHA1* in $\Delta aha1$ cells under similar conditions. (D) The experiment was repeated multiple times, the nuclear level of yHSP90 α was estimated from independent experiments and presented, and *P* values were calculated using the two-tailed Student's t test (**P < 0.01; N.S., not significant). (E) Fluorescence images showing the distribution of GFP-yHsp90 α (green) in the whole cell of $\Delta aha1$ untreated cells. (F) Fluorescence images showing the distribution of GFP-yHsp90 α (green) in the

12 | N. Fangaria et al. Molecular Biology of the Cell

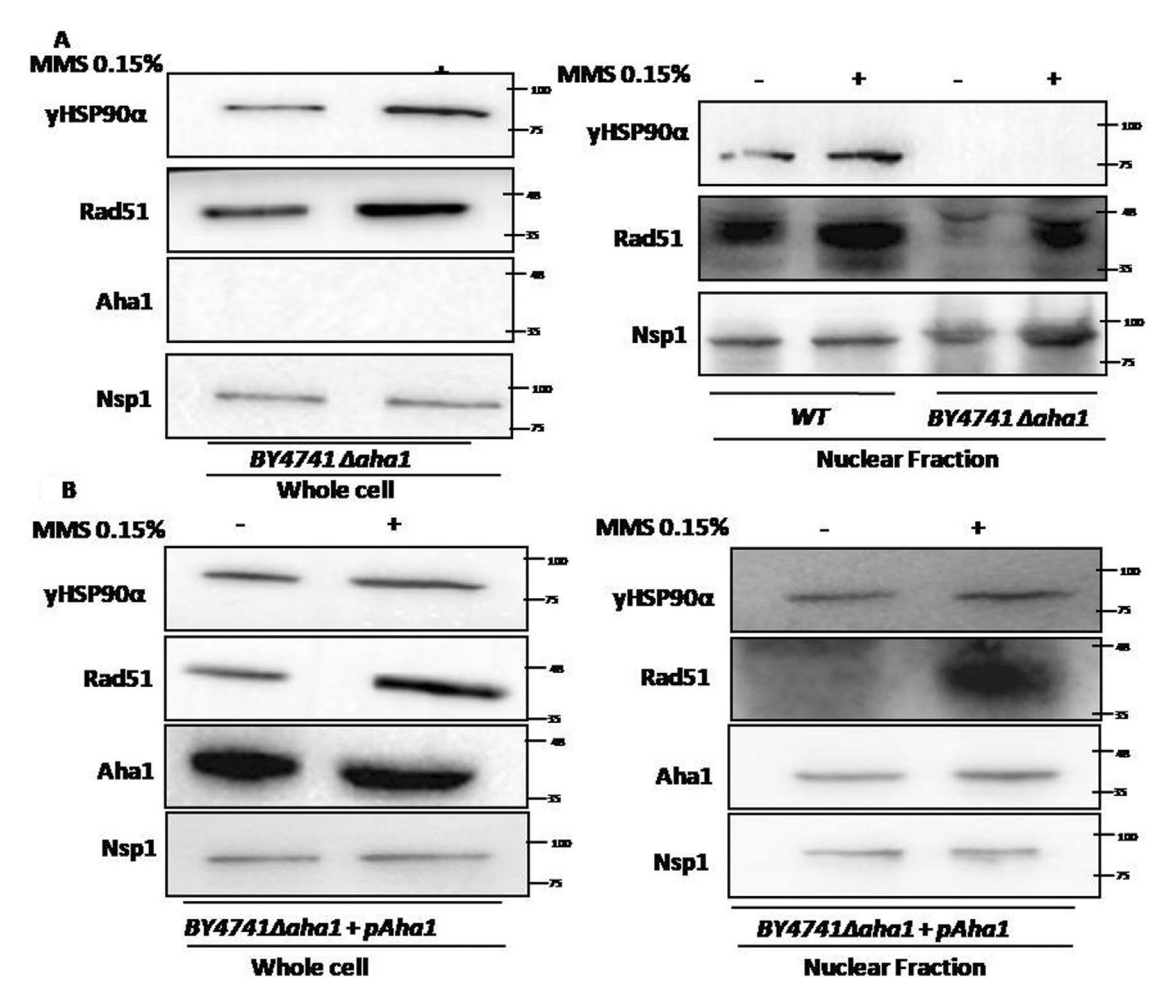


FIGURE 8: yHSP90 α transport to the nucleus upon DNA damage is dependent on Aha1 in BY4741 strain. (A) Western blot analysis shows significant induction of endogenous levels of yHSP90 α upon 0.15% MMS treatment in BY4741 Δ aha1 strain (left panel). The increased nuclear accumulation of yHSP90 α was observed in the WT strain but no signal of yHSP90 α was traced in the BY4741 Δ aha1 strain upon 0.15% MMS treatment (right panel). (B) The left panel represents the expression of respective proteins in the whole-cell extract of BY4741\(Delta\) aha1 strain harboring AHA1 expression plasmid. The right panel displays that ectopic expression of AHA1 rescued the defect in nuclear accumulation of yHSP90 α in the BY4741 Δ aha1 strain. In all the experiments Rad51 served as a control for DNA damage and Nsp1 acted as a loading control.

amplicon during ChIP analysis may be ambiguous as the donor sequence is also identical to that present in the 3' end of the mutant ura3. Hence it will be difficult to delineate the recruitment of yHSP90 α between the proximal and distal ends of HO cleavage site.

In this study we have identified the structural determinant of yHSP90 α that enables its nuclear translocation. yHSP90 α adopts multiple conformational changes in its chaperone cycle, one of them being mediated by the ATPase stimulator Aha1 that regulates yHSP90 α 's allosteric timing. However, how these conformational changes alter its physiological function remains obscure. An earlier biochemical study showed that the conformational flexibility within the amino-terminal and MD of yHSP90 α is essential for Aha1-mediated acceleration of ATP hydrolysis of yHSP90 α (Hainzl et al., 2009). We speculate that the initial step of Aha1-mediated partially closed conformational rearrangement of yHSP90 α could be essential for its nuclear import (Wolmarans et al., 2016). First, the absence of Aha1 completely abrogates the nuclear import of yHSP90 α in two different strain backgrounds which are completely reversed on ectopic expression of Aha1. Second, the conformationally rigid CL deletion mutant yHSP90 $\alpha^{\Delta(211-259)}$, which has a 2.5-fold reduction in Aha1dependent ATPase activity, is fully defective in its nuclear accumulation, although the smaller CL deletion mutant that has wild type-like Aha1-dependent ATPase activity is fully competent in nuclear import. Last, the yHSP90 α^{T101I} mutant, which is ATPase-dead mutant

whole cell of Δaha1 cells treated with 0.15% MMS. The nucleus (blue) was stained with Hoechst dye. Intensity profiles were derived for all fluorescence experiments using NIS elements AR software. Isogenic WT control are presented in Figure 1, C and D. (G) Relative fluorescence intensities of GFP-yHSP90 α in the nucleus and cytoplasm were quantified and the mean values (±SD) were plotted using GraphPad Prism. P values were calculated using the two-tailed Student's t test (*P < 0.05; **P < 0.01; N.S., not significant). (H) Western blot showing coimmunoprecipitation of Aha1-FLAG with Hsp90 in the wild-type strain from the untreated and cells treated with 0.15% MMS. Pull down was done using anti FLAG antibody.

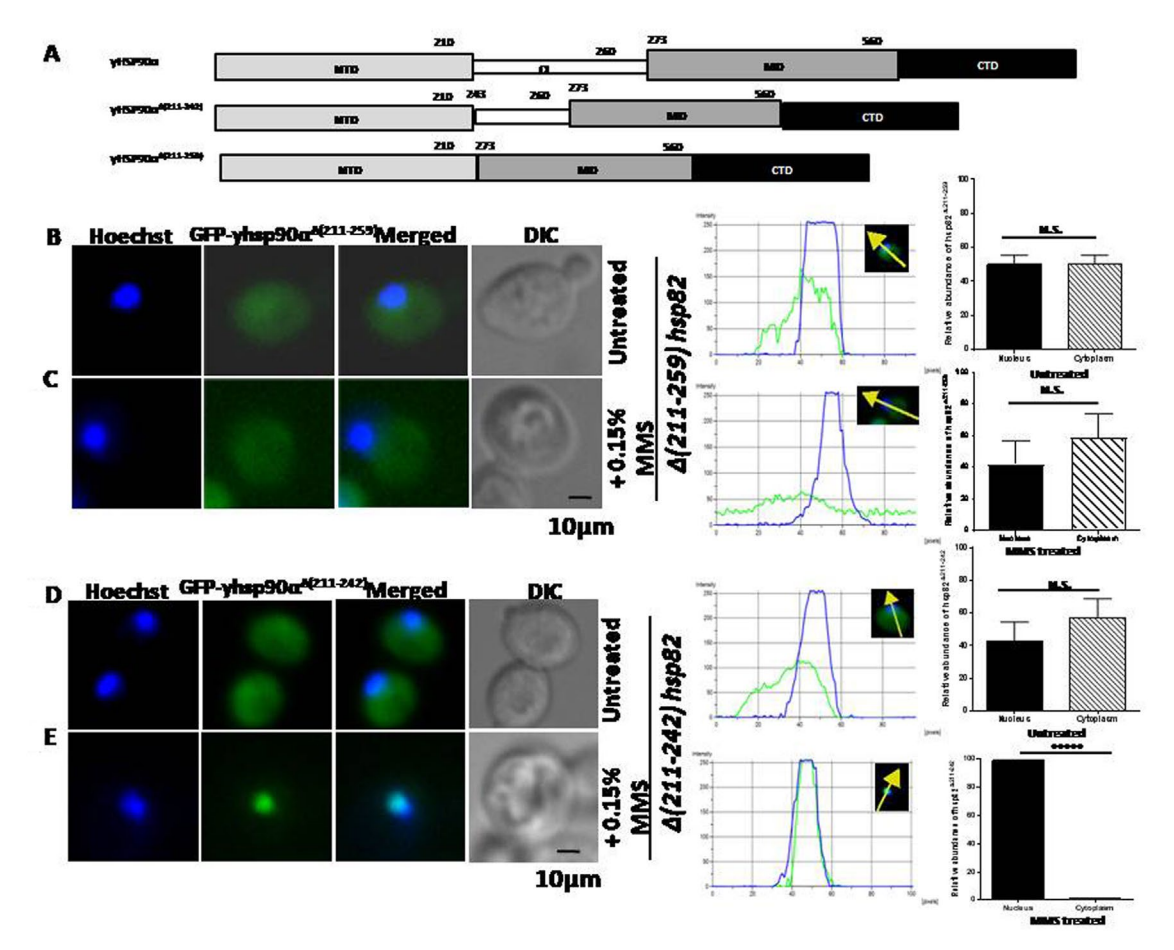


FIGURE 9: The domain responsible for the conformational flexibility between the amino terminal and the MD of yHSP90α is essential for its nuclear translocation upon DNA damage. (A) Schematic representation of wild-type and two CL deletion mutants of yHSP90α. (B) Fluorescence images showing the distribution of GFP-yHsp90α $^{\Delta(211-259)}$ (green) in the whole cell both in the untreated and (C) in the 0.15% MMS-treated condition. (D) Fluorescence images showing the distribution of GFP-yHsp90α $^{\Delta(211-242)}$ (green) in the whole cell in the untreated condition but (E) nuclear localization in the 0.15% MMS-treated condition. Intensity profiles were derived for all fluorescence experiments using NIS elements AR software; relative fluorescence intensities of GFP-yhsp90α mutants in the nucleus and cytoplasm were quantified and the mean values (±SD) were plotted using GraphPad Prism. P values were calculated using the two-tailed Student's t test (*****P < 0.00001; N.S., not significant).

with reduced amino-terminal association, shows no defect in nuclear translocation.

While our earlier study (Suhane et al., 2014) demonstrated that the cytoplasmic function of $yHSP90\alpha$ is essential for DNA repair, our present study illustrates that the nuclear function of yHSP90 α is also an important determinant for effective DNA repair. It is noteworthy that although the nuclear import of vHSP90α does not depend on its canonical ATPase activity, as seen in the case of T101lhsp82, being an ATPase dead mutant, Rad51 stability is greatly reduced in this mutant background. In our earlier study we reported that this mutant shows severe sensitivity to DNA-damaging agents (Suhane et al., 2014). Thus using two separation-of-function mutants, namely, the T101Ihsp82 and CL deletion mutant, we demonstrate that the N-terminal domain and the CL domain have distinct functions in DNA repair: while the N-terminal domain is required for the functional stability of the client proteins belonging to the HR pathway, the CL domain is required for the nuclear import of yHsp90, which is a prerequisite for its nuclear role at the time of DSB repair.

It was earlier reported by two independent studies that DNA-PK (Quanz et al., 2012) and ATM (Elaimy et al., 2016) are responsible for the Thr-5/7 phosphorylation of human HSP90 α in response to DNA

damage. Both enzymes are members of the phosphatidylinositol 3-kinase-like protein kinase (PIKK) family that are the sensors of DNA damage. However, an ortholog of DNA-PK is absent in yeast. Besides, the first 14 amino acids are also absent from yHSP90 α . It was never addressed whether there is an increase in the nuclear level of HsHSP90 α in response to DNA damage or whether T7/5 phosphorylation is essential for its nuclear import as well as chromatin recruitment. Using human HSP90 α and its mutant (T7-A) we have shown that in yeast the nuclear translocation of HsHSP90 α is independent of T7 phosphorylation. Further, the ChIP analysis confirms that the association of yHSP90 α to the damaged chromatin is independent of the presence of the first 14 amino-acid residues (including T-7). This kind of stress-induced nuclear translocation of yHSP90 α was also reported earlier in budding yeast under the condition of glucose starvation (Tapia and Morano, 2010).

We have established for the first time that Aha1 is an important regulator for DNA repair pathway. We observed that AHA1 was transcriptionally up-regulated in response to DNA damage and showed about a threefold up-regulation in protein level. Using two different strain backgrounds of $\Delta aha1$, we showed that Aha1 regulates the nuclear import of yHSP90 α . The absence of nuclear

14 N. Fangaria et al. Molecular Biology of the Cell

accumulation of yHSP90 α in $\Delta aha1$ strain was fully restored with ectopic expression of AHA1. Last, Aha1 deletion shows sensitivity toward genotoxic agents. Although enhanced accumulation of Aha1 was observed into the nucleus under MMS treatment as well as upon induction of single DSB in the genome, its nuclear function during DNA repair has not been addressed in this study. It did not escape our notice that our findings indicate an Aha1-mediated protein homeostasis of yHSP90 α under a DNA-damaging condition. The underlying molecular mechanism or its implications need to be explored in future.

In this study we observed that yHSP90 α and two of its cochaperones, Sba1 and Aha1, behaved differently upon MMS treatment. yHSP90 α is not induced but is redistributed to the nucleus upon DNA damage. Although both Aha1 and Sba1 are induced upon DNA damage, in the case of Aha1, a concomitant increase in its nuclear level was observed, whereas no such increase in the nuclear level of Sba1 was found. We currently do not know the significance of this finding. It could be possible that Aha1 has both nuclear and cytoplasmic roles, whereas Sba1 has a cytoplasmic role during DNA repair.

Presently, it is not understood how a genotoxic stress condition triggers an increase in the nuclear import of yHSP90α. Intriguingly, we find that Hsp90 and Aha1 remain physically associated with each other under normal and DNA-damaging conditions. It is yet to be determined whether some post-translational modifications of yHSP90 α and/or Aha1 are necessary for this phenomenon.

We speculate that in a mammalian system also such Aha1-assisted nuclear import of $Hsp90\alpha$ might exist, which needs to be explored in the future. Our finding is very significant as it may open new avenues of research to target Aha1 for arresting HR-mediated DSB repair in cancer cells. Besides, it has been reported earlier in Drosophila and mammals that $HSP90\alpha$ occupies the promoter regions of several coding and noncoding genes and regulates the gene expression in response to external stimuli (Khurana and Bhattacharyya, 2015; Sawarkar et al., 2012). If the Aha1 dependence for the nuclear import of $HSP90\alpha$ is universally conserved in higher eukaryotes, then inhibition of Aha1 can be used as a tool to decipher the nuclear function of HSP90 α .

MATERIALS AND METHODS

Yeast strains

Strains used in this study have been tabulated in Supplemental Table S1. In W303a yeast background, SBA1 and CDC37 genes were MYC tagged by HR using HIS cassettes (Longtine et al., 1998) flanked by 40 bp homologous sequence of the upstream and downstream regions of the stop codons of the respective genes to create the MYC tagged SBA1 and CDC37 strains, namely, NFY14 and NFY15, respectively. For creating the NFY14 strain, the homologous sequence was added in the primers (OSB389 and OSB390) used for amplifying the HIS cassette from the pFA6a-His-Myc plasmid. This cassette was then transformed into the W303a strain and the cells were grown in a histidine drop-out medium. The MYC tagging of SBA1 was confirmed by PCR using the primer pairs OSB391 and OSB390. For creating the NFY15 strain, the homologous sequence was added in the primers (OSB398 and OSB399) used for amplifying the HIS cassette from the pFA6a-His-Myc plasmid. This cassette was then transformed into the W303a strain and the cells were grown in a histidine drop-out medium. The MYC tagging of CDC37 was confirmed by PCR using the primer pairs OSB400 and OSB399. P82a harboring wild-type HSP82 expressing vector (TRP) was transformed with centromeric pHCA-hsp82Δ(211-242) plasmid and the transformed strain was grown in histidine drop-out complete medium to

generate the KRAY16 strain, where the HSP82 was replaced by the mutant by plasmid shuffling. In the W303a yeast background, AHA1 gene was knocked out by HR using a HIS cassette (Longtine et al., 1998) flanked by a 40 bp homologous sequence of the upstream and downstream regions of the AHA1 gene to create the strain NFY24. The homologous sequence was added in the primers (OSB273 and OSB274) used for amplifying the HIS cassette from the pFA6a-His plasmid. This cassette was then transformed into the W303a strain and the cells were grown in a histidine drop-out medium. The knockout was confirmed by PCR using the primer pairs OSB275 and OSB274. We used another Δaha1 strain which was in the BY4741 background, purchased from Open Biosystems. Plasmids: Sequences of all the primers used in this paper are tabulated in Supplemental Table S2. Full-out HSP82, AHA1, and RAD51 were amplified using the primer pairs OSB21/OSB22, OSB215/OSB216, and OMKB90/OMKB88, respectively, and individually cloned in the 2-μ vector pTA between the BamH1 and the Sal1 restriction sites to create pTA-HSP82, pTA-AHA1, and pTA-RAD51, respectively. We purchased the mammalian expression vector pcDNA3.1+/C-(K)-DYK from GenScript, USA, which harbors full-out human HsHSP90α with C-terminal FLAG tag. We amplified HsHSP90α-FLAG using the primer pairs OSB531/OSB539 and subcloned in the centromeric pHCA vector (Laskar et al., 2011) between the BamHI and the Sall restriction sites. Two mutants of HsHsp90 α , namely, $hsp90\alpha T7A$ and the CL deletion mutant $hsp90\alpha\Delta$ (224-279) were generated by splice overlap extension (SOE) and ultimately subcloned in pHCA with Cterminal FLAG tag. The CL deletion mutant hsp82∆(211-259) was amplified using the genomic DNA isolated from the HH1a-p2HG/ hsp82Δ(211-259) strain (Louvion et al., 1996; Suhane et al., 2014) with the primer pairs OSB21/OSB22. It was subsequently subcloned into the pTA vector within the BamHI and Sall restriction sites. Hsp82 deletion mutant hsp82\(\Delta(211-242)\) was generated by SOE and subsequently subcloned in pHCA within the BamHI and Sall restriction sites. To create the GFP-Hsp82 fusion constructs, GFP was first amplified from the plasmid, p2U/S65T, using the primer pair OSB517/ OSB518 and subcloned within the BamH1 restriction site, which is present in the N-terminal end of HSP82, hsp82Δ(211-259), and hsp82∆(211-242). The orientation of GFP was checked using Pstl digestion to create pTA-GFPhsp82, pTA-GFPhsp82Δ(211-259), pHCA-GFPHSP82, pHCA-GFPhsp82Δ(211-259), and pHCA-GFPhsp82Δ(211-242) fusion constructs, where GFP is fused at the N-terminal end of Hsp82 in all the cases. DNA sequencing (Eurofins) was done to confirm the cloning.

Fluorescence imaging

GFP fluorescence imaging was done using the strains NFY31, NFY32, NFY33, and NFY35 as described earlier (Tapia and Morano, 2010). Typically, the cells were grown until 0.5 OD₆₀₀ in selective media. Half batch of cells were treated with 0.15% of MMS and grown for 2 h along with the untreated batch of cells. NFY31 was additionally treated with 15 µg/ml nocodazole (Cell Signaling Technology) for 2 h. Nocodazole-induced cell cycle arrest at G2/M was confirmed by visualization of a large number of dumbbell-shaped budding cells under the microscope. Subsequently, the cells were harvested and washed with Milli-Q water. The cells were then treated with 70% ethanol for 1 min at 30°C with shaking and were again washed with water. The cells were resuspended in 100 µl of water and the nuclei of the live cells were stained using Hoechst 33342 (Thermo Fisher Scientific) stain at a concentration of 20 µg/ml for 10 min. The cells were mounted on glass slides using 25% glycerol and were visualized under the 100x objective using a Nikon Eclipse (Ni-E AR) upright fluorescence microscope. The images were

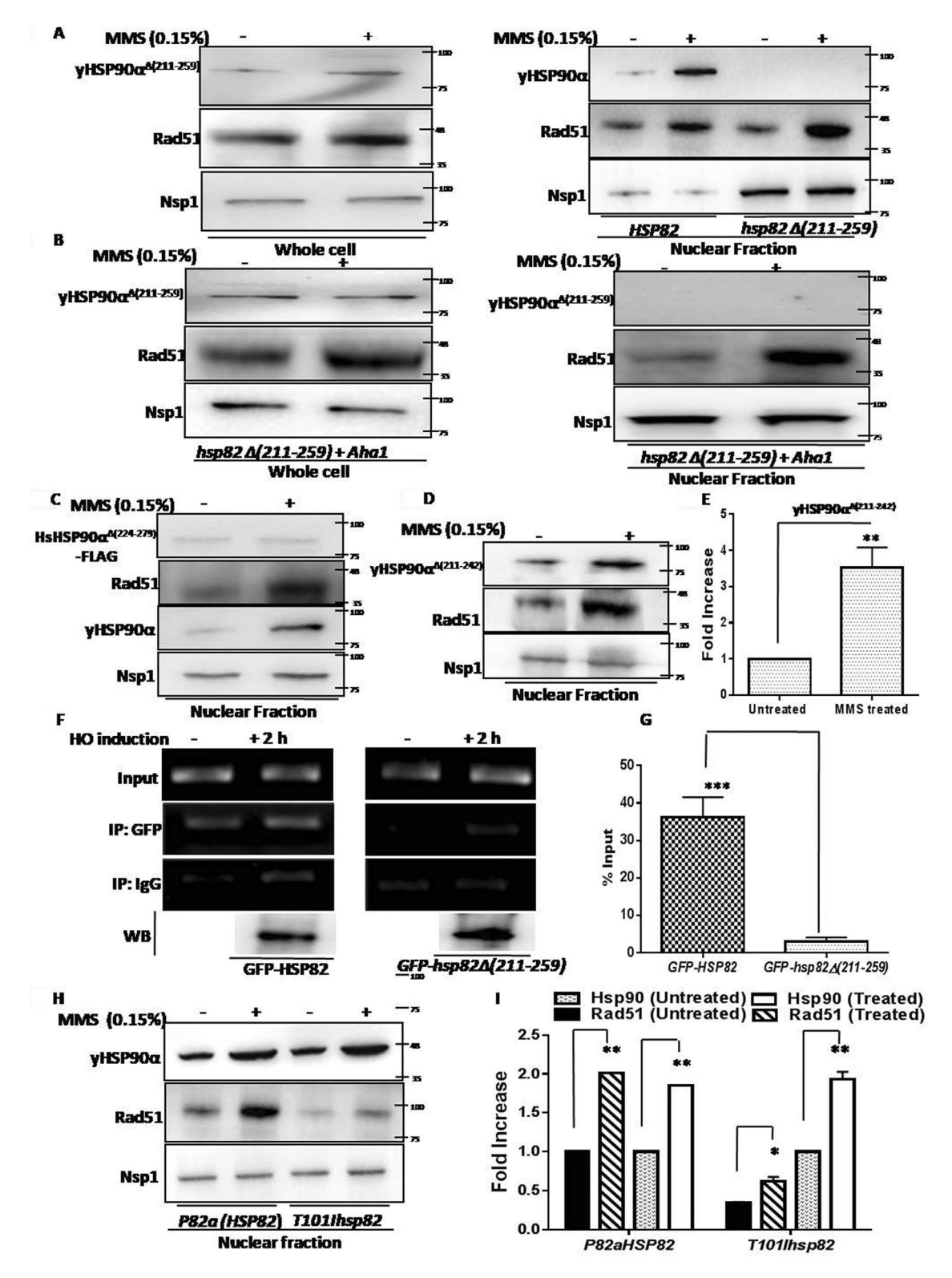


FIGURE 10: The subcellular fractionation of various mutants of yHSP90α in response to DNA damage. (A) Western blots showing the endogenous levels of yHSP90α $^{\Delta(211-259)}$ in whole-cell extract in the presence and absence of MMS treatment (left panel). Increased nuclear accumulation of yHSP90α MT but no nuclear accumulation of yHSP90α $^{\Delta(211-259)}$ upon 0.15% MMS treatment was observed (Right panel). (B) Endogenous levels of yHSP90α $^{\Delta(211-259)}$ in whole-cell extract (left panel) and in nucleus (right panel) shows that no nuclear accumulation of yHSP90α $^{\Delta(211-259)}$ upon 0.15% MMS treatment even if AHA1 was overexpressed in the cells. (C) Western blot showing no nuclear accumulation of FLAG tagged HsHSP90α $^{\Delta(224-279)}$ upon 0.15% MMS treatment. (D) Western blot showing increased nuclear accumulation of yHSP90α $^{\Delta(211-242)}$ upon 0.15% MMS treatment. (E) The experiment was repeated and the quantification of the Western blots showed a fourfold increase in the nuclear level of the mutant yHSP90α $^{\Delta(211-242)}$ upon MMS treatment. Error bars indicate SD; P values were calculated using the two-tailed Student's t test (**P<0.01). (F) Chromatin

16 N. Fangaria et al. Molecular Biology of the Cell

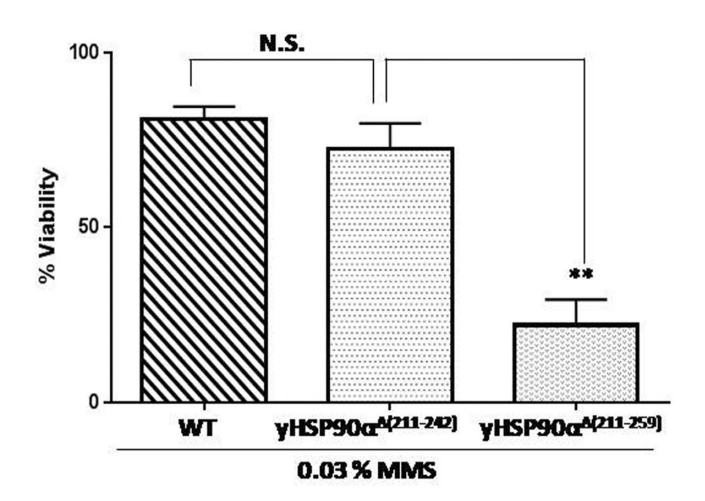


FIGURE 11: Loss of nuclear translocation of yHSP90 α is correlated with increased sensitivity to MMS. Percent survivability of yHSP90 $\alpha^{\triangle(211-259)}$, yHSP90 $\alpha^{\triangle(211-242)}$ and isogenic wild-type strains were determined after exposure to 0.03% MMS for 2 h. Error bars indicate \pm SD (n = 3); P values were calculated using the two-tailed Student's t test (NS: not significant; **P < 0.01).

captured using a monochrome camera (Andor), which were subsequently processed and deconvoluted using NIS elements Advanced Research software (Towa Optics Private Limited). We have performed three independent sets of experiments and analyzed more than 100 cells per condition. The results represent mean \pm SD. P values were calculated using the two-tailed Student's t test.

Indirect immunofluorescence assay

The W303a strain was grown in YPD media until 0.5 OD_{600} and a half batch of cells was treated with 0.15% MMS and both batches were grown for an additional 2 h. The cells were washed and fixed using 4% formaldehyde for 2 h; 10^7 – 10^8 cells were taken and washed with 1× phosphate-buffered saline (PBS, containing 1 mM dithiothreitol [DTT] and 0.5 mM PMSF). The cells were resuspended in spheroplast buffer (18.2% sorbitol, 1% glucose, 0.2% yeast nitrogen base, 0.2% casamino acids, 25 mM HEPES, pH 7.4, 50 mM Tris, 1 mM DTT) containing YPDS (YPD, 1 M sorbitol) and lyticase. The cells were then incubated for 1.5 h at 30°C with gentle shaking for spheroplasts to form. The slides were meanwhile prepared by coating each well with 0.1% poly-L-lysine and incubated for more than 20 min at room temperature. Extra liquid was removed by aspiration and the wells were dried completely. The fixed yeast spheroplasts were then loaded into each well and allowed to settle for 20 min. Extra liquid was aspirated and the wells were washed with 1× PBS for 5 min. Permeabilization of the cell membrane of the fixed yeast cells was done with a 1:3 mixture of acetone and methanol for 15 min. After washing with 1× PBS, the wells were blocked using 3% bovine serum albumin (BSA) for 1.5 h. The liquid was aspirated and a 1:50 dilution of rabbit anti-Aha1 primary antibody (Invitrogen) diluted in 3% BSA was added to each well and incubated at 37°C for 1 h. After incubation, the extra liquid was aspirated and the wells were washed subsequently with $1 \times PBS$, $1 \times PBST$, and $1 \times PBS$ for 15 min each at 37°C. To each well, a 1:250 dilution of the secondary antibody, Goat anti-Rabbit IgG (H+L) Cross-Adsorbed Secondary Antibody, Alexa Fluor 488 (Life Technologies) was diluted in 3% BSA along with 10 µg/ml Hoechst 33342 vital stain (Thermo Fisher Scientific), and the slides were incubated at 37°C for 45 min. All the liquid was then aspirated and the slides were allowed to dry completely after which the samples were mounted using gold antifade (Thermo Fisher Scientific), and the slides were visualized under a 100× objective using a Nikon Eclipse (Ni-E AR) upright fluorescence microscope. The images were captured using monochrome camera (Andor), which were subsequently processed and deconvoluted using the NIS elements Advanced Research software (Towa Optics Private Limited). We have performed three independent sets of experiments and analyzed more than 100 cells per condition. The results represents mean \pm SD. P values were calculated using the twotailed Student's t test.

Site-directed mutagenesis

The CL deletion mutants, $hsp82\Delta(211-242)$ and human $hsp90\alpha\Delta(224-242)$ 279)-FLAG, were created using splice overlap extension PCR. To generate the hsp82Δ(211-242) deletion mutant, yeast genomic DNA was used as a template, and the full-length gene was amplified in two fragments to delete the desired region. For amplifying the first and second fragments, primer sets OSB21/OSB537 and OSB538/OSB22 were used, respectively. Finally, hsp82Δ(211-242) deletion was generated by annealing the first two PCR products followed by a third PCR using the primer set OSB21/OSB22. To generate the human $hsp90\alpha\Delta(224-279)$ deletion mutant, the full-length gene was amplified as two fragments, one using the primer set OSB531/OSB533 and the other using the OSB534/OSB539 primer pair. The two PCR products were denatured, allowed to hybridize with each other, and subsequently amplified using the primer pair OSB531/OSB539 to create the human $hsp90\alpha\Delta(224-279)$ deletion. To create the human T7Ahsp90α mutant by site-directed mutagenesis, the pcDNA3.1+/C-(K)-DYK vector was used as a template along with the primer set OSB535/OSB539. The codon ACC was changed to GCT within the primer OSB535 to create the human T7Ahsp90a mutant. All the mutants were confirmed by sequencing.

immunoprecipitation (ChIP) assay were done using NA14 strain harboring either GFP tagged yHSP90 α vector or GFP tagged CL-deleted mutant y $hsp90\alpha$ vector. Anti GFP antibody was used to pull down WT and CL-deleted mutant yHSP90 α from uninduced and 2 h HO induced samples. The pellet fraction was PCR amplified; the recruitment of GFP tagged yHSP90 α^{WT} was detected at 2 h of HO induction while the recruitment of the mutant protein was not detected. The samples were normalized with respect to input. The lower panel shows the Western blotting of the IP sample, which detects the presence of comparable amount of the wild-type and the mutant protein in the +2 h galactose treated samples. (G) The ChIP assay was repeated twice (n = 2) and the occupancy of the GFP-Hsp82^{WT} and the GFP- $Hsp82^{\Delta(211-259)}$ at the HO cleavage site were plotted. Error bars indicate SD; P values were calculated using the twotailed Student's t test (***P < 0.001) (H) Western blot showing increased nuclear accumulation of $yHSP90\alpha$ in P82a strain as well as in an isogenic hsp82T101I strain upon 0.15% MMS treatment. Rad51 levels were very less in the hsp82T101I strain as expected, nonetheless it shows significant up-regulation upon MMS treatment. (I) Quantification of the Western blots from multiple experiments shows significant increase in the nuclear level of both yHSP90 α and Rad51 in the WT and the mutant strain. Error bars indicate SD; P values were calculated using the two-tailed Student's t test (**P < 0.01; *P < 0.05).

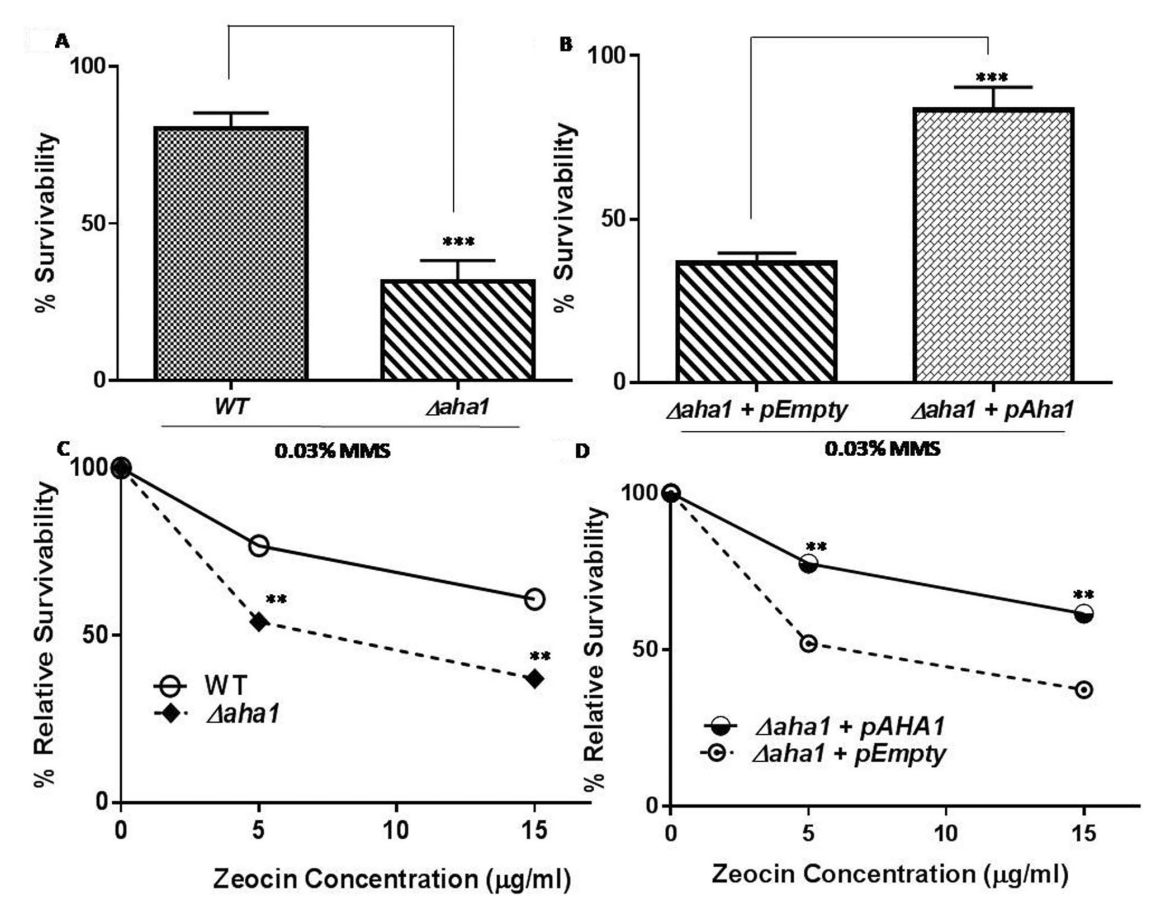


FIGURE 12: Aha1 deletion sensitizes the cells to DNA-damaging agents. (A) Return to growth experiments were conducted with the wild-type and isogenic $\Delta aha1$ strain. Percentage survivability upon 0.03% MMS treatment were plotted relative to that of untreated cells. (B) Return to growth experiments were conducted with the $\Delta aha1$ cells harboring AHA1 expressing vector or empty pTA vector upon exposure to 0.03% MMS. Each treatment was repeated three times, and the mean value (\pm SD) was plotted; P values were calculated using the two-tailed Student's t test (****P < 0.0001; ****P < 0.001). (C) WT and $\Delta aha1$ strains were exposed to two doses of zeocin (5 µg/ml and 15 µg/ml) and their relative survivability was plotted. $\Delta aha1$ strain showed greater susceptibility toward zeocin compared with the WT strain. The experiment was repeated three times and the mean values were plotted; P values were calculated using the two-tailed Student's t test (**P < 0.01). (D) Zeocin sensitivity of $\Delta aha1$ strain harboring empty plasmid was reversed in AHA1 expressing $\Delta aha1$ strain. The mean values were plotted (n = 3); P values were calculated using the two-tailed Student's t test (**P < 0.01).

Cellular fractionation

The nuclear fractionation was done with wild-type, NA14 (Agmon et al., 2009), $\Delta sba1$ (SLY6), $\Delta aha1$ (NFY24), and tscdc37S14A strains (grown at restrictive temperature 37°C). Similar fractionations were also performed with the strains carrying wild-type HsHsp90α-FLAG (KRAY15) and those carrying the human hsp90αT7A-FLAG (KRAY17) and human $hsp90\alpha\Delta$ (224-279)-FLAG (KRAY18). To measure whether the nuclear level of yHSP90 α depends on Aha1, we did nuclear fractionation of $\Delta aha1$ strain carrying empty plasmid (NFY26) and that carrying AHA1 overexpression plasmid (NFY27). Finally, various mutants of hsp82, namely, HH1a-p2HG/hsp82 Δ (211-259), T101Ihsp82, and $hsp82\Delta(211-242)$ (KRAY16), and the isogenic control strain P82a were also subjected to nuclear fractionation. Typically, cells were grown until $0.5~{\rm OD}_{600}$ in selective media. A half batch of cells were treated with 0.15% of MMS and continuously grown at 30°C for 2 h along with the untreated batch of cells. In the NA14 strain, DNA damage was induced as a specific double-strand DNA break at an HO restriction site by inducing HO endonuclease within the cell using 3% galactose (Agmon et al., 2009). After DNA damage, 100 OD₆₀₀ cells were harvested and washed with PBS containing DTT and PMSF. In each case, cells were then incubated with spheroplast buffer (18.2% sorbitol, 1% glucose, 0.2% yeast nitrogen base, 0.2% casamino acids, 25 mM HEPES, pH 7.4, 50 mM Tris, 1 mM DTT) for 15 min at 30°C with gentle shaking. After incubation, cells were resuspended in spheroplast buffer containing YPDS (YPD, 1 M sorbitol) and lyticase enzyme. It was then allowed to grow at 30°C with gentle shaking for 1.5 h. Again, YPDS was added into spheroplast and spun at 4000 rpm for 10 min. Washing of the spheroplast was performed with ice-cold YPDS followed by spinning at 4000 rpm for 5 min. Spheroplast was resuspended in ice-cold sorbitol and spun at 4000 rpm for 5 min. Ultimately the spheroplast was resuspended in 5 ml of buffer N (25 mM K_2SO_4 , 30 mM HEPES, pH 7.6, 5 mM MgSO₄, 1 mM EDTA, 10% glycerol, 0.5% NP40, 3 mM DTT, 1% protease inhibitor cocktail) and homogenized by giving 20 strokes under chilled conditions. The homogenized spheroplast was spun at 2000 rpm at 4°C for 15-20 min to pellet down the cell debris. We pelleted down the nuclei at 6000 rpm for 25 min at 4°C. This nuclear fraction sample was then resuspended in 50 µl of buffer N. The sample was then boiled for 10 min and used for the Western blotting analysis.

18 | N. Fangaria et al. Molecular Biology of the Cell

Coimmunoprecipitation

The KRAY29 strain was grown in the selective media without tryptophan until 0.5 at OD_{600} . A half batch of cells was treated with 0.15% of MMS and grown at 30°C for 2 h along with the untreated batch of cells. Cells were harvested and the pull down was done by using anti-FLAG antibody as described previously (Suhane et al., 2019). After coimmunoprecipitation, the relative association of Hsp90 with Aha1 was analyzed by Western blotting.

Western blotting

Western blot was done to study protein levels in whole-cell protein samples or nuclear fractions. Protein samples were loaded onto a SDS polyacrylamide gel. Polyvinylidene difluoride membrane was used for the Western blot as described earlier (Laskar et al., 2011). The primary antibodies used were mouse anti-Act1 antibody (Abcam), rabbit anti-Rad51 (Abcam), mouse anti-Hsp82 antibody (Calbiochem), rabbit anti-Aha1 antibody (Invitrogen), mouse Anti-DDDDK tag antibody (Abcam), and rabbit anti-GFP antibody (Abcam) at 1:5000 dilutions. For subcellular fractionation, we used mouse anti-Nsp1 antibody (Abcam) as loading control at 1:5000 dilution. For secondary antibodies, horseradish peroxide-conjugated anti-rabbit antibody (Promega) and antimouse antibody (Promega) were used at 1:10,000 dilution. The Western blots were developed using chemiluminescent detection system (Thermo Fisher Scientific). Every experiment was repeated at least three times and band intensities were quantified by using ImageJ software. Mean relative densities were plotted using GraphPad Prism.

Repair kinetics of a single double-strand DNA break

NA14 cells (Agmon et al., 2009) were grown in YPD media in the presence of 3% glycerol until 0.3 at OD₆₀₀; 60 OD of cell were harvested (untreated or 0 h) and the remaining cells were treated with 3% galactose for different time points (1, 2, 3, and 4 h). At each time point, 5 OD₆₀₀ of cells were harvested. The yeast cells were disrupted using 0.3 g glass beads and 200 µl breaking buffer (2% Triton X-100, 1% SDS, 10 mM NaCl, 10 mM Tris [pH 8], 1 mM EDTA [pH 8]). The genomic DNA was subsequently extracted from the yeast cells using PCIA. The extracted genomic DNA was treated with RNase and resuspended in 30 μl 1× Tris-EDTA solution. The kinetics of a single double-stranded break repair at the HO restriction site were monitored by PCR using the primers OSB289 and KanB1 which are specific to the upstream and downstream regions of the HO restriction site.

Chromatin immunoprecipitation

The strains, NFY21, NFY22, NFY23, NFY25 and KRAY19, were grown in the selective media without tryptophan until 0.3 at OD₆₀₀ in the presence of 3% glycerol; 60 OD of cell were taken out and treated with 1% formaldehyde for 15 min (untreated or 0 h) and the remaining cells were treated with 3% galactose for different time points (1, 2, 3, and 4 h). At each time point, 60 OD_{600} of cells were taken out and treated with 1% formaldehyde for 15 min each. Formaldehyde-mediated protein cross-linking was stopped using 2.5 M glycine. After formaldehyde treatment, each set of cells was harvested and washed with 1× PBS. ChIP assay was performed for each set of cells as described earlier (Laskar et al., 2014). Pull down was done with each set using 10 µg anti-Hsp90 antibody (Calbiochem), 10 µg anti-Rad51 antibody (Abcam), 10 µg anti-Aha1 antibody (Abcam), and 10 μg anti-GFP antibody (Abcam) to precipitate HSP90 α , Rad51, Aha1, and GFP bound DNA fragments, respectively, at each time point. Recruitment of HSP90 α , Rad51, and Aha1 was then

monitored at the HO cleavage proximal site and up to -5 kb distal position by PCR using the immune precipitate and input DNA samples for each time point. Recruitment near the broken region was studied by subjecting the samples to PCR using the primers OSB519 and OSB520 while recruitment to the 1, 2, 3, 4, and 5 kb away from the HO cleavage side toward the left direction was measured using the primers OSB567/OSB568, OSB569/OSB570, OSB571/OSB572, OSB573/OSB574, and OSB575/OSB576, respectively. Samples were subjected to electrophoresis on 2% agarose. For a negative control, ChIP was performed with IgG antibody. We amplified 300 bp at the 3' end of ACT1 using OSB14 and OSB16 (Laskar et al., 2011), which was used as a normalization control.

MMS sensitivity assay

W303a, NFY24, NFY26, and NFY27 strains were tested for MMSinduced DNA damage sensitivity. All strains were grown in YPD medium overnight at 30°C. The next day, secondary culture was grown until 0.5 OD_{600} at 30°C . After OD_{600} reached to 0.5, the culture was divided into two sets. One set of cells was treated with 0.03% (vol/ vol) of methyl-methane-sulfonate (MMS) (Sigma Aldrich) and grown at 30°C for 2 h and another set was continuously grown at 30°C for 2 h without MMS. After that, the cells were washed twice and serially diluted, and 1000 cells of each culture were spread on respective selective media or YPD plates. The plates were incubated at 30°C for 40 h and the colonies obtained were counted in both treated and untreated conditions. Subsequently, the percentage survivability was calculated using the following formula: % survivability = [(number of cells grown on MMS plate)/(number of cells grown on untreated plate)] *100.

Zeocin sensitivity assay

W303a, NFY24, NFY26, and NFY27 strains were tested for zeocininduced DNA damage sensitivity. All strains were grown in YPD medium for overnight at 30°C. The next day, secondary culture was grown until 0.5 OD₆₀₀ at 30°C. After OD₆₀₀ reached 0.5, the culture was divided into two sets. One set of cells was treated with 5 µg/ml or 15 µg/ml zeocin (Invitrogen) and grown at 30°C for 1 h, and another set was continuously grown at 30°C for 1 h without zeocin. After that the cells were washed twice and serially diluted and 1000 cells of each culture were spread on respective selective media or YPD plates. The plates were incubated at 30°C for 40 h, the colonies obtained were counted, and the percentage survivability was calculated.

Real-time RT-PCR

The W303lpha strain was grown at 30°C until the OD₆₀₀ reached to 0.5. It was subsequently exposed to 0.15% MMS for 2 h. Total RNA was isolated from the untreated and MMS-treated cells using the acid phenol method as described previously (Suhane et al., 2014). Further cDNA was synthesized using reverse transcriptase (Omni Script; Qiagen, Hilden, Germany) as described previously (Suhane et al., 2014). The primer pair, OSB 14 and OSB 16, was used to amplify 307 bp at the 3' end of ACT1 transcript. To amplify 326 bp at the 3' end of RAD51, the primer pair OSB 44 and OSB 45 was used. Similarly, to amplify 291 bp at the 3' end of the AHA1 transcript, the primer pair OSB 216 and OSB 394 was used. Finally, to amplify 276 bp at the 3' end of SBA1, the primer pair OSB 391 and OSB 445 was used. For real-time RT-PCR, cDNA was diluted (1:50) and used for PCR using a Takara TB Green RT-PCR kit as described earlier (Suhane et al., 2014). The mean values (±SD) from three independent experiments were plotted using GraphPad Prism 6 software.

ACKNOWLEDGMENTS

The authors thank Mrinal K Bhattacharyya, University of Hyderabad, for critical reading of the manuscript. N.F. was supported by the Senior Research Fellowships from Council for Scientific and Industrial Research (CSIR), India. K.R. and P.S. were supported by the Senior Research Fellowships from Council for Scientific and Industrial Research (CSIR), India. The plasmid p2U/S65T.Hsp82 was a kind gift from Didier Picard, University of Geneva. The $\Delta aha1$ strain (BY4741 background) and the temperature-sensitive strains cdc37S14A were a kind gift from Atin K. Mandal, Bose Institute, Kolkata.

REFERENCES

- Agmon N, Pur S, Liefshitz B, Kupiec M (2009). Analysis of repair mechanism choice during homologous recombination. Nucleic Acids Res 37, 5081–5092
- Ali MMU, Roe SM, Vaughan CK, Meyer P, Panaretou B, Piper PW, Prodromou C, Pearl LH (2006). Crystal structure of an Hsp90-nucleotide-p23/ Sba1 closed chaperone complex. Nature 440, 1013–1017.
- Andriuskevicius T, Kotenko O, Makovets S (2018). Putting together and taking apart: assembly and disassembly of the Rad51 nucleoprotein filament in DNA repair and genome stability. Cell Stress 2, 96–112.
- Aylon Y, Kupiec M (2004). DNA repair: the yeast paradigm. DNA repair 3, 797–815.
- Caplan AJ, Ma'ayan A, Willis IM (2007). Multiple kinases and system robustness: a link between Cdc37 and genome integrity. Cell Cycle 6, 3145–3147.
- Echtenkamp FJ, Zelin E, Oxelmark E, Woo JI, Andrews BJ, Garabedian M, Freeman BC (2011). Global Functional Map of the p23 Molecular Chaperone Reveals an Extensive Cellular Network. Mol Cell 43, 229–241.
- Elaimy AL, Ahsan A, Marsh K, Pratt WB, Ray D, Lawrence TS, Nyati MK (2016). ATM is the primary kinase responsible for phosphorylation of $Hsp90\alpha$ after ionizing radiation. Oncotarget 7, 82450–82457.
- Hainzl O, Lapina MC, Buchner J, Richter K (2009). The Charged Linker Region is an important regulator of Hsp90 function. J Biol Chem 284, 22559–22567.
- Khurana N, Bhattacharyya S (2015). Hsp90, the concertmaster: tuning transcription. Front Oncol 5, doi:10.3389/fonc.2015.00100.
- Kimura Y, Rutherford SL, Miyata Y, Yahara I, Freeman BC, Yue L, Morimoto RI, Lindquist S (1997). Cdc37 is a molecular chaperone with specific functions in signal transduction. Genes Dev 11, 1775–1785.
- Laskar S, Bhattacharyya MK, Shankar R, Bhattacharyya S (2011). HSP90 controls SIR2 mediated gene silencing. PLoS One 6, e23406.
- Laskar S, Sheeba K, Bhattacharyya MK, Nair AS, Dhar P, Bhattacharyya S (2014). Heat stress induced Cup9 dependent transcriptional regulation of Sir2. Mol Cell Biol 35, doi: 10.1128/MCB.01046-14.
- Li J, Soroka J, Buchner J (2012). The Hsp90 chaperone machinery: Conformational dynamics and regulation by co-chaperones. Biochim Biophys Acta 1823, 624–635.
- Li X, Heyer WD (2008). Homologous recombination in DNA repair and DNA damage tolerance. Cell Res 18, 99–113.
- Longtine MS, Mckenzie A, Demarini DJ, Shah NG, Wach A, Brachat A, Philippsen P, Pringle JR (1998). Additional modules for versatile and

- economical PCR-based gene deletion and modification in Saccharomyces cerevisiae. Yeast 14, 953–96.
- Louvion JF, Warth R, Picard D (1996). Two eukaryote-specific regions of Hsp82 are dispensable for its viability and signal transduction functions in yeast. Proc Natl Acad Sci 93, 13937–13942.
- Lundin C, North M, Erixon K, Walters K, Jenssen D, Goldman ASH, Helleday T (2005). Methyl methanesulfonate (MMS) produces heat-labile DNA damage but no detectable in vivo DNA double-strand breaks. Nucleic Acids Res 33, 3799–3811.
- Mader SL, Lopez A, Lawatscheck J, Luo Q, Rutz DA, Hernandez APG, Sattler M, Buchner J, Kaila VRI (2020). Conformational dynamics modulate the catalytic activity of the molecular chaperone Hsp90. Nat Commun 11, https://doi.org/10.1038/s41467-020-15050-0.
- Nathan DF, Lindquist S (1995). Mutational analysis of Hsp90 function: interactions with a steroid receptor and a protein kinase. Mol Cell Biol 15, 3917–3925.
- Prodromou C, Panaretou B, Chohan S, Siligardi G, O'Brien R, Ladbury JE, Roe SM, Piper PW, Pearl LH (2000). The ATPase cycle of Hsp90 drives a molecular 'clamp' via transient dimerization of the N-terminal domains. EMBO J 19, 4383–4392.
- Quanz M, Herbette A, Sayarath M, Koning LD, Dubois T, Sun JS, Dutreix M (2012). Heat shock protein 90α (Hsp 90α) is phosphorylated in response to DNA damage and accumulates in repair foci. J Biol Chem 287, 8803–8815.
- Sawarkar R, Sievers C, Paro R (2012). Hsp90 globally targets paused RNA polymerase to regulate gene expression in response to environmental stimuli. Cell 149, 807–818.
- Siligardi G, Panaretou B, Meyer P, Singh S, Woolfson DN, Piper PW, Pearl LH, Prodromou C (2002). Regulation of Hsp90 ATPase activity by the co-chaperone Cdc37p/p50cdc37. J Biol Chem 277, 20151–20159.
- Singh TR, Ali AM, Busygina V, Raynard S, Fan Q, Du CH, Andreassen PR, Sung P, Meetei AR (2008) BLAP18/RMI2, a novel OB-fold-containing protein, is an essential component of the Bloom helicase—double Holliday junction dissolvasome. Genes Dev 22, 2856–2868.
- Suhane T, Bindumadhavan V, Fangaria N, Nair AS, Tabassum W, Muley P, Bhattacharyya MK, Bhattacharyya S (2019). Glu-108 in ScRad51 is critical for DNA damage induced nuclear function. mSphere 4, doi: 10.1128/ mSphere.00082-19.
- Suhane T, Laskar S, Advani S, Roy N, Varunan S, Bhattacharyya D, Bhattacharyya S, Bhattacharyya MK (2014). Both charged linker region and ATPase domain of Hsp90 are essential for Rad51 dependent DNA repair. Eukaryot Cell 14, 64–77.
- Sun L, Prince T, Manjarrez JR, Scroggins BT, Matts RL (2012). Characterization of the interaction of Aha1 with components of the Hsp90 chaperone machine and client proteins. Biochimica et Biophysica Acta 1823, 1092–1101.
- Tapia H, Morano KA (2010). Hsp90 nuclear accumulation in quiescence is linked to chaperone function and spore development in yeast. Mol Biol Cell 21, 63–72.
- Tsutsumi S, Mollapour M, Prodromou C, Lee CT, Panaretou B, Yoshida S, Mayer MP, Neckers LM (2012). Charged linker sequence modulates eukaryotic heat shock protein 90 (Hsp90) chaperone activity. Proc Natl Acad Sci USA 109, 2937–2942.
- Wolmarans A, Lee B, Spyracopoulos L, LaPointe P (2016). The Mechanism of Hsp90 ATPase Stimulation by Aha1. Sci Rep 6, doi:10.1038/srep33179.

20 | N. Fangaria et al. Molecular Biology of the Cell





Glu-108 in Saccharomyces cerevisiae Rad51 Is Critical for DNA **Damage-Induced Nuclear Function**

Tanvi Suhane, a Vijayalakshmi Bindumadhavan, b Nupur Fangaria, a Achuthsankar S. Nair, b Wahida Tabassum, c Poorvaja Muley,^a Mrinal K. Bhattacharyya,^c Sunanda Bhattacharyya^a

ABSTRACT DNA damage-induced Rad51 focus formation is the hallmark of homologous recombination-mediated DNA repair. Earlier, we reported that Rad51 physically interacts with Hsp90, and under the condition of Hsp90 inhibition, it undergoes proteasomal degradation. Here, we show that the dynamic interaction between Rad51 and Hsp90 is crucial for the DNA damage-induced nuclear function of Rad51. Guided by a bioinformatics study, we generated a single mutant of Rad51, which resides at the N-terminal domain, outside the ATPase core domain. The mutant with an E to L change at residue 108 (Rad51^{E108L}) was predicted to bind more strongly with Hsp90 than the wild-type (Rad51WT). A coimmunoprecipitation study demonstrated that there exists a distinct difference between the in vivo associations of Rad51WT-Hsp90 and of Rad51E108L-Hsp90. We found that upon DNA damage, the association between Rad51WT and Hsp90 was significantly reduced compared to that in the undamaged condition. However, the mutant Rad51^{E108L} remained tightly associated with Hsp90 even after DNA damage. Consequently, the recruitment of Rad51^{E108L} to the double-stranded broken ends was reduced significantly. The E108Lrad51 strain manifested severe sensitivity toward methyl methanesulfonate (MMS) and a complete loss of gene conversion efficiency, a phenotype similar to that of the $\Delta rad51$ strain. Previously, some of the N-terminal domain mutants of Rad51 were identified in a screen for a Rad51 interaction-deficient mutant; however, our study shows that Rad51^{E108L} is not defective either in the self-interaction or its interaction with the members of the Rad52 epistatic group. Our study thus identifies a novel mutant of Rad51 which, owing to its greater association with Hsp90, exhibits a severe DNA repair defect.

IMPORTANCE Rad51-mediated homologous recombination is the major mechanism for repairing DNA double-strand break (DSB) repair in cancer cells. Thus, regulating Rad51 activity could be an attractive target. The sequential assembly and disassembly of Rad51 to the broken DNA ends depend on reversible protein-protein interactions. Here, we discovered that a dynamic interaction with molecular chaperone Hsp90 is one such regulatory event that governs the recruitment of Rad51 onto the damaged DNA. We uncovered that Rad51 associates with Hsp90, and upon DNA damage, this complex dissociates to facilitate the loading of Rad51 onto broken DNA. In a mutant where such dissociation is incomplete, the occupancy of Rad51 at the broken DNA is partial, which results in inefficient DNA repair. Thus, it is reasonable to propose that any small molecule that may alter the dynamics of the Rad51-Hsp90 interaction is likely to impact DSB repair in cancer cells.

KEYWORDS DNA repair, Hsp90, homologous recombination, Hsp90-Rad51 interaction, Rad51 recruitment to chromatin, molecular chaperone

Citation Suhane T, Bindumadhavan V, Fangaria N, Nair AS, Tabassum W, Muley P, Bhattacharyya MK, Bhattacharyya S. 2019. Glu-108 in Saccharomyces cerevisiae Rad51 is critical for DNA damage-induced nuclear function. mSphere 4:e00082-19. https://doi.org/10.1128/ mSphere.00082-19.

Editor Aaron P. Mitchell, Carnegie Mellon

Copyright © 2019 Suhane et al. This is an open-access article distributed under the terms of the Creative Commons Attribution 4.0 International license.

Address correspondence to Sunanda Bhattacharyya, sdeb70@gmail.com.

Received 1 February 2019 Accepted 28 February 2019 Published 20 March 2019



^aDepartment of Biotechnology and Bioinformatics, School of Life Sciences, University of Hyderabad, Hyderabad, India

^bDepartment of Computational Biology and Bioinformatics, University of Kerala, Thiruvanthapuram, India

^cDepartment of Biochemistry, School of Life Sciences, University of Hyderabad, Hyderabad, India



henever cells are exposed to DNA-damaging agents, the family of DNA repair proteins must relocate to the nucleus and be recruited to the damaged chromatins to elicit a DNA damage response and to ensure efficient repair of damaged DNA (1-3). These groups of proteins include DNA damage signaling proteins (Mre11, ATM, ATR, and DNA-PKcs), cell cycle checkpoint effectors (Chk1 and Chk2), and DNA processing enzymes (Mre11, Exol, Sae2, Rad51, Rad52, Rad54, BRCA1/2, BLM, Ku70/80, ligase IV, etc.) (4). The sequential assembly and disassembly of DNA repair proteins at DNA broken ends depend on reversible protein-protein interactions. Rad51, a central player of homology-directed double-strand break (DSB) repair, remains in the cytoplasm under normal conditions. DNA damage leads to the redistribution of Rad51 from the cytoplasm to the nucleus and its loading onto the broken ends of DNA. It is reasonable to propose that insufficient recruitment of Rad51 onto the chromatin is likely to have a severe impact on homologous recombination (HR) efficiency. Earlier reports demonstrated that in a human cell line, BRCA1 promotes the localization of BRCA2 to damage foci through the BRCA2 binding protein PALB2 (5-8). BRCA2 interacts with RAD51 and promotes RAD51 assembly onto single-stranded DNA (ssDNA) (9-11). However, BRCA2 is absent in lower eukaryotes, where HR is the predominant pathway for DNA repair. It is reported that in Saccharomyces cerevisiae, Rad52 promotes Rad51 filament assembly (12) by interacting with RPA. Rad52 is thought to replace RPA bound to ssDNA with Rad51 or provide a seeding site within the RPA-bound ssDNA for subsequent binding of Rad51 (13).

Our previous study revealed that Rad51 is a direct client of Hsp90 and is dependent upon Hsp90 for its maturity and activity (14). Apart from merely providing maturity to the client proteins, Hsp90 also assists in the translocation of proteins to different cellular compartments (15). Previous reports have established that the Hsp90 chaperone machinery not only escorts steroid hormone receptors (SHRs) to the nucleus but is also responsible for the recycling of the receptor on chromatin and stabilizing the DNA-binding properties of the receptor (16). Two cochaperones of Hsp90, p23 and Bag-1L, are found to modulate steroid hormone receptor function by controlling receptor binding to chromatin (16).

Our earlier study demonstrated that the charged linker deletion mutant of yHsp90 ($\Delta 211$ -259hsp82) inhibits effective Rad51 focus formation in the nucleus upon DNA damage (14). This finding was positively correlated with severe methyl methanesulfonate (MMS) sensitivity (comparable to that for the Δrad51 strain) and with the complete loss of Rad51-dependent gene targeting function. We demonstrated that the charged linker deletion (Δ211-259hsp82) mutant strain is strikingly different than the wild-type strain in the distribution of Rad51 foci upon MMS treatment. Although there was only a 20% overall reduction in the Rad51 focus formation, the number of nuclei having multiple foci was drastically reduced in the mutant strain. This clearly indicates that in mutant nuclei, effective Rad51 levels may be low. Since the charged linker region is responsible for providing structural flexibility between amino and carboxyl-terminal domains of Hsp90 (17), an optimum interaction between Rad51 and Hsp90 may be compromised in the mutant. Hence, we hypothesize that effective Hsp90 and Rad51 interaction may be crucial for nuclear function of Rad51. To prove this, we utilized a bioinformatics approach to design a point mutant with an E to L change at residue 108 (Rad51^{E108L}), which has a stronger affinity toward Hsp90. Our data reveal that there exists a dynamic equilibrium between the association of wild-type Rad51 (Rad51WT) and Hsp90 under a normal condition and dissociation under DNA-damaging conditions. In the case of Rad51^{E108L}, due to tighter association, the interaction between Hsp90 and mutant Rad51 becomes irreversible; hence, even under DNA-damaging conditions, the mutant Rad51 protein does not proficiently dissociate from Hsp90. As a result, the mutant Rad51^{E108L} is not recruited to the broken DNA ends as efficiently as wild-type Rad51. Hence, the E108L-rad51 strain shows extreme sensitivity toward DNA-damaging agents and poor gene conversion activity. This study points out that the DNA damage-induced reversible protein-protein interaction between Rad51 and Hsp90 plays a critical role in Rad51 function.



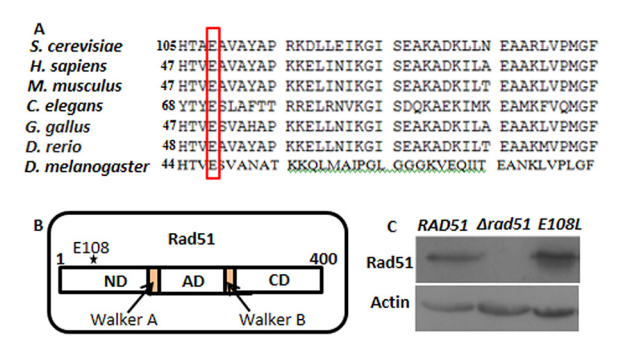


FIG 1 Generation of *RAD51* mutant strain. (A) Multiple sequence alignment of Rad51 (N-terminal domain) protein sequences of *S. cerevisiae* (yeast) with *Homo sapiens* (human), *Mus musculus* (mouse), *Gallus gallus* (bird), *Danio rerio* (zebrafish), *Caenorhabditis elegans* (nematode), and *Drosophila melanogaster* (fruit fly). The conserved glutamic acid residues among various organisms are represented by the red box. (B) Schematic representation of Rad51 domains demonstrating boundaries of N-terminal, ATPase (AD), and C-terminal domains along with the Walker A and Walker B motifs. The star depicts the approximate location of E108 in the N-terminal domain of Rad51. (C) Western blot was performed using protein extracts from wild-type, $\Delta rad51$, and E108L-rad51 strains. Actin was used as a loading control.

RESULTS

Generation of RAD51 mutant strain based on the molecular docking studies between yHsp90 and Rad51. Earlier studies in our lab demonstrated that yHsp90 and Rad51 can physically interact (14). Unlike other chaperones, there is no specific binding pocket present in Hsp90 through which it binds to the client proteins. Hence, in order to understand the point of contacts between yHsp90 and Rad51, we employed a bioinformatics approach. To that end, Rad51 proteins (PDB identifier [ID] 1SZP) having various combinations of monomers, dimers, and hexamers were allowed to dock with yHsp90 (PDB ID 2CG9) using the fully automated web-based program ClusPro 2.0 (18), which employs the improved fast Fourier transform (FFT)-based rigid docking program PIPER (19). Thirty models of the protein-protein complex for each type of interaction, namely, balanced, electrostatic favored, hydrophobic favored, and van der Waal's plus electrostatic, were generated for each docking. It was found that a hydrophobicfavored interaction showed the lowest energy scores; hence, the corresponding protein complex model with the largest cluster was chosen. The surface view of the threedimensional structure of Rad51 displays a characteristic pocket in each of the monomers into which the yHsp90 is found to dock. The docked complex models showed that the N-terminal residue of the Rad51 E chain, Glu 108 (1.88 Å), has the shortest bond distance with yHsp90 C-terminal residues. We conducted a multiple-sequence alignment of Rad51 (Fig. 1A) and found that E108, which is predicted to have the strongest association with Hsp90, is evolutionarily conserved. In Rad51, the amino acid residue E108 is present in the N-terminal domain of Rad51, which lies outside its catalytic domain (Fig. 1B). To explore whether the Hsp90 and Rad51 association mediates Rad51 nuclear function under DNA-damaging conditions, one approach may be the generation of a Rad51 mutant with a reduced affinity for Hsp90. However, as Rad51 is a client of Hsp90, we reasoned that any mutant of Rad51 that fails to interact with Hsp90 due to a low affinity would be unstable in the cell. Hence, we designed a strong-affinity mutant to establish our hypothesis. By in silico mutation, we created four single mutants of Rad51 where the glutamic acid at the 108th position was replaced by neutral residues (glycine, alanine, leucine, and isoleucine). Table 1 displays a comparison of the parameters of yHsp90 docking with the wild-type and mutant Rad51 based on ClusPro results. Our study shows that the mutant Rad51E108L and Hsp90 docked complex results in a maximum increase in cluster size of 139 compared to 71 for the wild type. This implies a greater probability of the receptor-ligand complex being found in that specific conformation. Furthermore, there is a decrease in the energy score from -1,407.2 to -1,512.6 between the wild-type and Rad51^{E108L} mutant, respectively, which points to an increased stability of the protein complex. The rad51 mutant was



TABLE 1 ClusPro results depicting cluster sizes and energy scores of yHsp90 (2CG9A) with wild-type and mutant Rad51

	Hydrophobic-favored	Hydrophobic-favored interaction			
Rad51 (1SZP ABCDEF) strain	Cluster size	Energy score			
Wild-type (E108)	71	-1,407.2			
E108G	117	-1,534.0			
E108A	117	-1,518.4			
E108I	113	-1,543.3			
E108L	139	-1,512.6			

subsequently cloned into a yeast 2μ expression vector pTA (20) having the GPD promoter. As the Rad51 and Hsp90 interaction is essential for the stability of Rad51, we determined the stability of Rad51 mutant proteins by Western blot analysis. For this, we generated yeast strains NRY1, NRY2, and TSY17 by transforming empty vector (pTA), pTA-RAD51, and pTA-E108L-rad51 vectors into a null rad51 yeast strain. The steady-state level of the mutant Rad51 was comparable to that of the wild type (Fig. 1C).

Rad51^{E108L} shows a stronger association with Hsp90 than the wild-type Rad51. To investigate the interaction between Rad51 and yHsp90, we performed coimmunoprecipitation experiments under normal as well as MMS treatment conditions. To capture a detectable association between yHsp90 and Rad51, we overexpressed both yHSP90 and RAD51 (or its mutant version) from two 2μ vectors, each having a GPD promoter. The yHsp90-Rad51 complex was coimmunoprecipitated from the whole-cell extract with an anti-Rad51 antibody, followed by detection on a Western blot using an anti-Hsp82 antibody (Fig. 2A and B). Under normal conditions, in the wild-type strain, a small fraction of Hsp90 was associated with Rad51, whereas, in the case of the mutant strain, a significantly larger fraction of Hsp90 was associated with Rad51. Quantification of the several experimental repeats showed that the relative association between Hsp90 and Rad51^{E108L} was almost double the association found between Hsp90 and Rad51WT. This signifies a stronger association of Hsp90 with Rad51E108L than with Rad51WT. In the presence of MMS, Hsp90 and Rad51 association was reduced in the wild-type strain. On the other hand, in the E108L-rad51 strain, even in the presence of MMS, there was no detectable reduction in the association between Hsp90 and

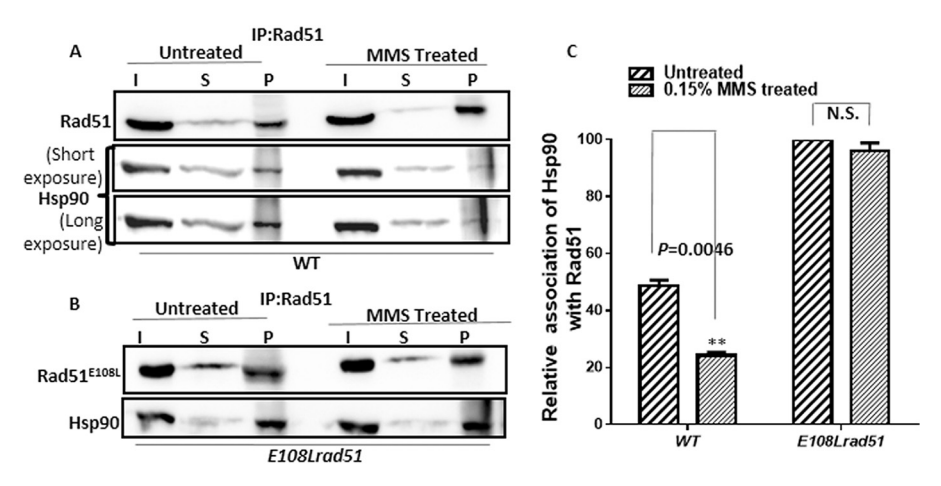


FIG 2 Rad51^{E108L} shows a stronger association with Hsp90 than the wild-type Rad51. (A) Western blot showing coimmunoprecipitation of Rad51 with Hsp90 from whole-cell extracts of wild-type strain and cells treated with 0.15% MMS for 2 h. I, input; S, supernatant; P, pellet. (B) Western blot showing coimmunoprecipitation of Rad51E108L with Hsp90 from whole-cell extracts of E108L-rad51 mutant strain untreated and treated with 0.15% MMS for 2 h. Immunoprecipitation (IP) was performed using an anti-Rad51 antibody. An anti-Hsp90 antibody was used for Western blotting. (C) Relative association of Hsp90 with Rad51 was calculated from at least three independent experiments, and standard deviations are plotted for both wild-type and mutant strains. P values were calculated using the two-tailed Student's t test. **, P = 0.0046; N.S., not significant.



Rad51^{E108L}. We repeated this experiment three times and calculated the relative association of Hsp90 with Rad51 in the presence and absence of MMS. Our analysis shows that approximately 50% dissociation of the Rad51^{WT}-Hsp90 complex occurs upon MMS treatment, whereas no significant dissociation of the Rad51^{E108L}-Hsp90 complex was observed under similar conditions (Fig. 2C). Thus, from this experiment, we conclude that there is a dynamic equilibrium between Rad51-Hsp90 complexes: in the presence of DNA damage, the equilibrium is shifted toward the dissociation of Rad51-Hsp90. However, this dynamic interaction is absent in the *E108L-rad51* strain, and the complex remains in the associated form even in the presence of the DNA-damaging agent.

HO-induced Rad51 recruitment to the broken DNA ends is compromised in the E108L-rad51 strain. During homologous recombination-mediated DNA repair, Rad51 is recruited to the ssDNA overhangs. It searches for the homologous DNA and, once found, facilitates the repair by performing a strand exchange reaction. The recruitment of Rad51 to the broken ends is the hallmark of DNA repair. Our previous observations suggest that the E108L-rad51 mutant is defective in dissociating from Hsp90 upon DNA damage. This defect may cause inadequate recruitment of Rad51 mutants to the broken DNA. To study the recruitment of mutant Rad51 to the DSB, we employed chromatin immunoprecipitation (ChIP) assays. To that end, we used NA14 strains (21) harboring null rad51. We modified the NA14 strain and generated three strains, namely, TSY20, TSY21, and TSY22, where native RAD51 is knocked out, and into those backgrounds, the empty plasmid, wild-type RAD51, and the mutant rad51 were transformed, respectively. These strains have a cassette inserted in chromosome V with two copies of URA3, separated by 3 kb, of which one ura3 copy is inactivated by the insertion of an HO endonuclease restriction site (Fig. 3A). The KANMX gene is incorporated within the two URA3 genes. HO endonuclease is expressed in the strain by a galactose inducible promoter. A double-strand break (DSB) is generated in the ura3 gene upon induction of HO endonuclease. We pulled down the Rad51-bound DNA segments from uninduced and HO-induced samples and subsequently compared the recruitment of mutant Rad51 protein to the donor URA3 locus (22). This experiment was repeated three times, and representative data from one of these are presented (Fig. 3B). To ensure the specificity of Rad51 recruitment to the broken locus, we probed its recruitment at the ACT1 locus, which does not contain an HO cut site. We did not detect any band at the ACT1 locus. We quantified the extent of recruitment of Rad51 proteins by measuring the ratio of amplification in the pellet sample with respect to the amplification observed in the input. To confirm the specificity of Rad51 recruitment to the DSB, we performed ChIP with IgG, which does not result in any amplification with the precipitated sample (Fig. 3B). Although there was no recruitment of Rad51 in the HOuninduced condition, upon HO induction, the recruitment of Rad51E108L was only 40% of that for the wild type (Fig. 3C). To ensure that the defect in the recruitment of the mutant Rad51 to the DSB was not due to the inefficiency of galactose-induced DSB, we probed the HO endonuclease recognition site in the presence and absence of HO induction. To that end, we amplified the HO site flanking the ura3 region using a forward primer, which is 20 bp upstream of the HO site, and a reverse primer, which is complementary to the middle part of KANMX gene. We observed the amplification of the target region in a galactose-untreated sample; however, after 1 h of galactose induction, the amplicon disappeared, indicating the successful generation of DSBs in all the strains (Fig. 3D). Overall, from these experiments, we conclude that the effective concentration of the Rad51^{E108L} mutant at broken DNA ends is less than that of the wild-type Rad51.

Mutation at the E108 position of Rad51 sensitizes the cells to MMS and renders them deficient in gene conversion. In *S. cerevisiae*, homologous recombination is the preferred pathway for repairing DSBs, in which Rad51 plays a central role. To understand the effect of *rad51* mutation, we performed the return-to-growth assay upon DNA damage. This was conducted by exposing the strains to 0.03% MMS (methyl methanesulfonate) for 2 h. Subsequently, treated and untreated cells were serially



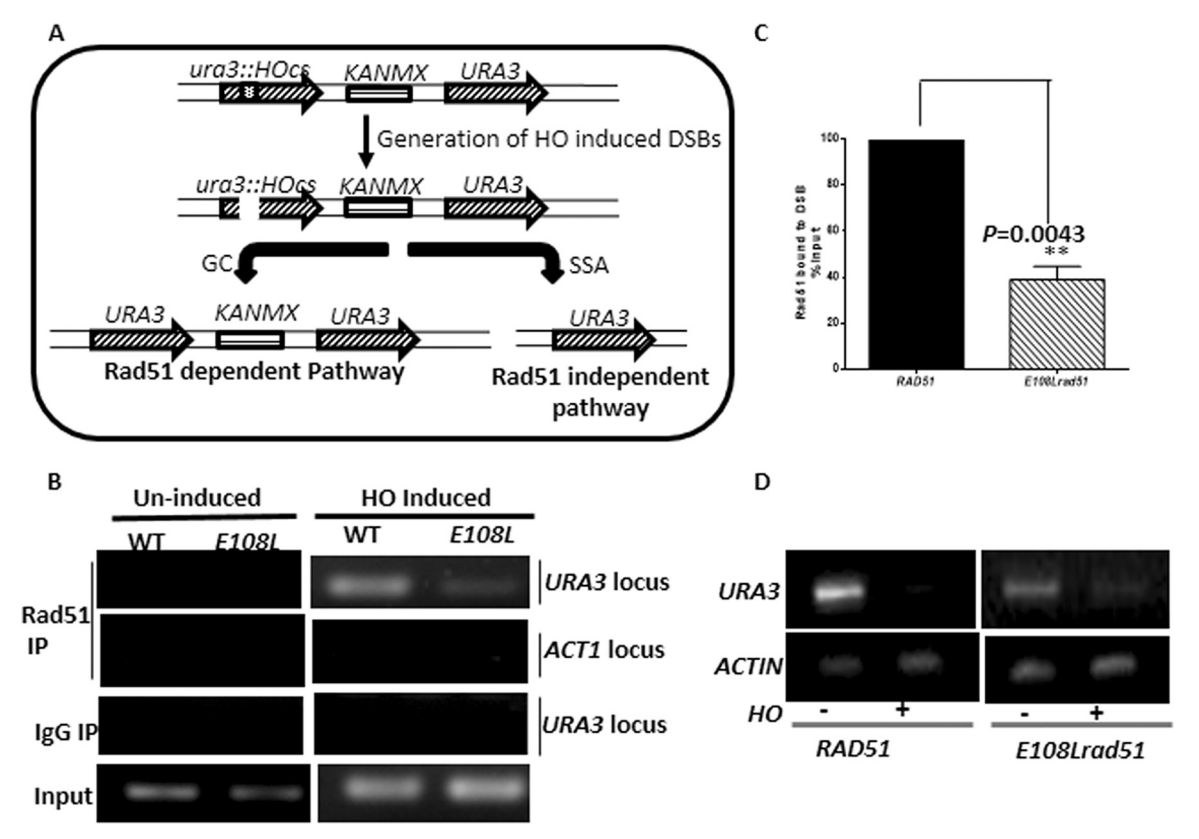


FIG 3 HO-induced Rad51 recruitment to the broken DNA ends is severely compromised in E108L-rad51 mutant. (A) Schematic diagram of a cassette incorporated in the strain used for studying gene conversion efficiency. It harbors two copies of URA3, one of which is mutated by the insertion of an HO endonuclease site. Induction with galactose creates single DSB in the mutated ura3, repair of which takes place in either a Rad51-dependent or Rad51-independent manner. KANMX cassette will be retained only if repair happens via the Rad51-dependent manner. (B) Chromatin immunoprecipitation (ChIP) of strains expressing wild-type Rad51 and E108L-rad51. Gel image showing one of the representative PCR products of input and precipitated samples using URA3 donor-specific primer and ACT1-specific primer. Immunoprecipitation was performed using anti-Rad51 and IgG antibodies. Input represents the total amount of DNA in the sample. (C) Each set was repeated three times, and the band intensities of the recruited samples upon HO induction were quantified using ImageJ software; comparative recruitment of Rad51 and Rad51^{E108L} is plotted with respect to the input. Error bars indicate standard deviations (SDs); n = 3 (P values were calculated using the two-tailed Student's t test). **, P < 0.01. (D) Semiquantitative reverse transcriptase PCR (RT-PCR), representing the amplification of DNA around the DSB site in ura3 before and after HO endonuclease induction. Lower intensity of band in HO-induced sample indicates the DSB generation in strains having wild-type Rad51 and E108L-rad51. Actin was used as a loading control.

diluted by 10-fold as presented in Fig. 4A and spotted on selective medium. We observed that the E108L-rad51 strain showed a slow growth phenotype compared to that of the wild type and $\Delta rad51$ strains. The survivability of the cells was positively correlated with the efficiency of DNA repair. We observed that E108L-rad51 cells were highly sensitive to MMS-induced DNA damage, similar to that observed in $\Delta rad51$ cells. The mechanism of homologous recombination involves repairing the DSBs by utilizing a homologous sequence from the genome. If the genome contains repetitive sequences and a double-strand break is created in any one of the repeats, it can be repaired by gene conversion, which is Rad51 dependent. We examined the gene conversion efficiency of the Rad51 mutant in the yeast strain NA14 (21). The DSB can be repaired by either of the two HR pathways (gene conversion or single strand annealing), and the repair products are easily distinguishable. If repaired by the Rad51-dependent gene conversion pathway, the strain behaves as G418 sulfate resistant; if it is repaired by the Rad51-independent single-strand annealing (SSA) pathway, the strain will be G418 sulfate sensitive (Fig. 3A) (21). The percent gene conversion was scored by growing cells on G418 sulfate-containing plates after galactose induction. Our experimental data indicate that there was no significant change in the gene conversion (GC) efficiency of the wild type (near 40%). However, the GC score for the



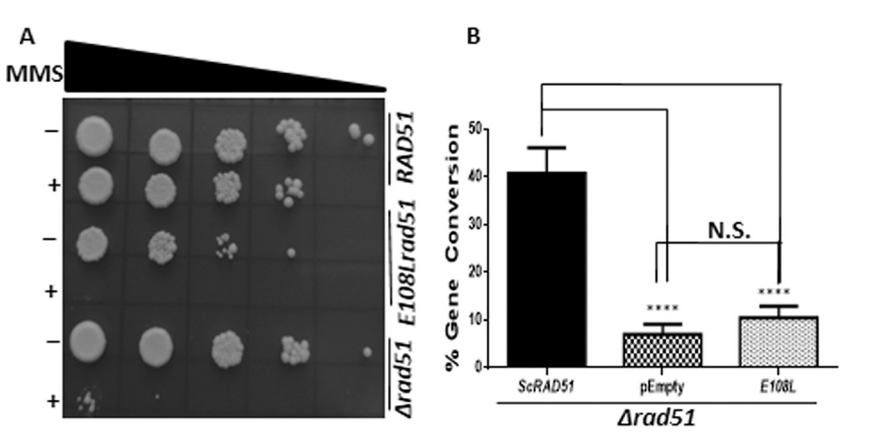


FIG 4 Mutation at E108 position of Rad51 sensitizes the cells to MMS and renders them deficient in gene conversion. (A) Pictorial representation of return-to-growth assay upon MMS treatment. Cells were spotted after serial dilution of treated and untreated cells for wild-type and mutant strains. First lane for each strain shows untreated and second lane shows treated cells. (B) Graph showing the percentages of gene conversion. Cells were spread on galactose-containing plates and subsequently obtained colonies were patched on G418 sulfate plates. Percentage was determined by calculating the number of colonies grown on G418 sulfate plate versus number of colonies obtained on galactose plate. Error bars indicate SDs; n = 3; P values were calculated using the two-tailed Student's t test. *****, P < 0.0001; N.S., not significant.

E108L-rad51 mutant (10.5%) was comparable to that of the Δ rad51 strain (7%) (Fig. 4B). Overall, we conclude from our experimental data that the E108L-rad51 mutant behaved as a complete loss-of-function mutant of Rad51 in our assay.

Rad51^{E108L} can form homodimers and interacts efficiently with the Rad52 epistasis group of proteins. It has been established that to execute the nuclear function, Rad51 interacts with itself. Also, Rad52 and Rad54 modulate the catalytic activity of Rad51 via direct physical interaction. We wanted to test whether Rad51^{E108L} has any defect in self-association or association with Rad52 and Rad54. To that end, we used a yeast two-hybrid assay to measure the protein-protein interaction between Rad51^{E108L} and the Rad52 epistasis group. Figure 5 (top) shows the results with wild-type Rad51, which acts as a positive control in our study. The bottom of Fig. 5 shows that Rad51^{E108L}

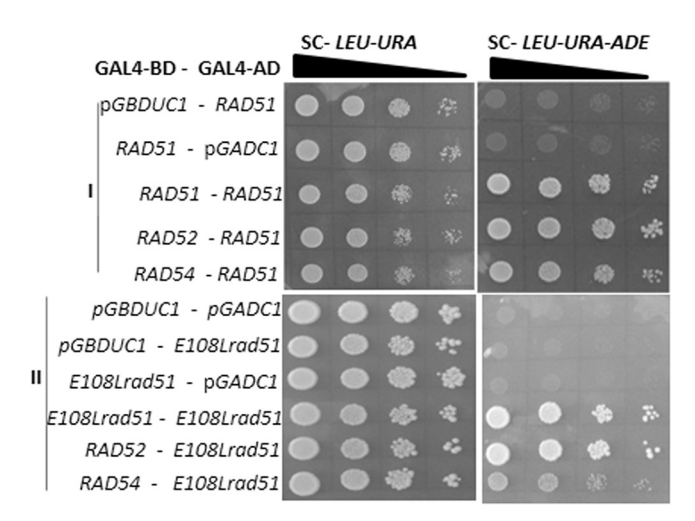


FIG 5 Rad51^{E108L} can form homodimers and bind efficiently to the Rad52 epistasis group of proteins. Yeast two-hybrid analysis depicting the interaction of *RAD51/rad51* mutants with Rad52 epistasis group. Various strains harboring bait and prey vectors are represented on the left. Cells of each strain were grown to an ${\rm OD}_{\rm 500}$ of 0.5 and serially diluted before spotting. To monitor the interaction between proteins, diluted cells were spotted on medium lacking Leu and Ura (left panel) as well as on medium lacking Leu, Ura, and Ade. Homodimerization as well as interaction of Rad51 (positive control) (I) and Rad51^{E108L} (II) with Rad52 and Rad54 was unaltered.



interacted efficiently with itself as well as with Rad52 and Rad54. We verified that Rad52 and Rad54 do not cause self-activation of a reporter gene (data not shown). No growth in a triple-drop-out plate for the strains PMY11 and PMY14 indicated that there was no self-activation for the indicative strains.

DISCUSSION

Rad51 protein, which facilitates homologous strand exchange, is the central player for HR in mammalian cells. Disruption of this gene is associated with embryonic lethality in mice (23). It is reported that haploinsufficiency of this gene is linked with defects in human neurodevelopment (24, 25). The Rad51 focus formation in response to DNA damage is one of the regulatory events in HR.

Previously, we established that besides providing stability to the Rad51 protein, Hsp90 also controls its nuclear function, i.e., DNA damage-induced focus formation. Taking that study further, we show that the dynamic interaction between Hsp90 and Rad51 can influence the nuclear function of Rad51. We are reporting for the first time that DNA damage triggers the dissociation of Rad51 and Hsp90, which could be a prerequisite for the nuclear function of Rad51. Due to a stronger association with Hsp90, the Rad51^{E108L} protein probably remains locked with Hsp90; hence, the recruitment of Rad51^{E108L} to the broken DNA ends, even at a very high MMS concentration (0.15%), is considerably defective. This is evident by 10.5% GC efficiency and complete loss of cell survivability in the E108L-rad51 mutant cells under DNA-damaging conditions. Thus, our study shows that there is a positive correlation between the extent of Hsp90-Rad51 dissociation after DNA damage and Rad51 nuclear activity. It appears that in the case of E108L-rad51, a major portion of the Hsp90 pool is associated with Rad51, which might result in an insufficient availability of free Hsp90 for other cellular functions. This is supported by our observation that the E108L-rad51 mutant strain showed a slow growth phenotype compared to that of the wild-type strain. However, it is possible that the constitutive form of yHsp90, namely, Hsc82, might be sufficient for the essential cellular function of Hsp90, ensuring the survivability of the mutant strain.

A defect in recruitment to the damaged DNA may result from a defect in DNA binding or defects in its interactions with other nuclear proteins. An earlier report showed that glycine at the 103rd position of Rad51 is crucial for DNA binding (26). Another report showed that valine at 328, proline at 339, and isoleucine at 345 are also involved in DNA binding (27). Although there is no report available regarding the DNA binding capacity of the mutant used in our study, we do not anticipate any defect in DNA binding, as the mutant was recruited to the chromatin DNA albeit at lesser extent, probably due to the lesser availability of free Rad51^{E108L} proteins. In the case of the Rad51^{E108L} mutant, despite its apparent defect in reversible dissociation from Hsp90 under DNA-damaging conditions, its 40% recruitment confirms that it is not defective in DNA binding.

In our study, we expressed *RAD51* and *E108L-rad51* from episomal plasmids in a $\Delta rad51$ background and compared their phenotypes. Thus, it is important to ensure that the observed phenotypes were not due to overexpression. In an earlier study, it was observed that overexpression of Rad51 does not have any effect on MMS sensitivity or repair of a single DSB in wild-type cells. However, it sensitizes $\Delta srs2$ and $\Delta ku70$ strains toward MMS (28). It was also observed that a high level of Rad51 reduces the frequency of but does not eliminate HR (28). In our study, the steady-state levels of Rad51^{WT} and Rad51^{E108L} were comparable. Thus, the severe DNA repair defects observed in the *E108L-rad51* strain compared to that in *RAD51* cells are not due to overexpression but rather to the point mutation.

It did not escape our notice that nearly 50% less recruitment of Rad51 in the E108L-rad51 strain had a profound effect on DNA repair. It is not unexpected, as our earlier study demonstrated that an only 20% reduction of Rad51 focus formation in the $\Delta 211$ -259hsp82 strain led to severe sensitivity to MMS and UV treatment (14). These



findings prompted us to conclude that 20% to 50% less occupancy of Rad51 at the broken DNA ends is sufficient to perturb DSB repair.

The E108 residue of Rad51 that is in close proximity to Hsp90 resides outside the ATPase domain of Rad51 and is evolutionary conserved. The N-terminal domain of Rad51 is implicated in the monomer-monomer interaction as well as the interactions with the members of the Rad52 epistasis group (27, 29). Although the mutation is present in the N-terminal domain, it was not previously identified in Rad51 interactiondeficient mutants (30). The yeast two-hybrid assay confirms that the ability of Rad51^{E108L} for self-association as well as for associations with Rad52 and Rad54 are comparable to that of wild-type Rad51. As Rad51 recruitment to the broken DNA ends is an upstream event, the defect will be dominant over any other defects. Thus, the drastic phenotype found in the E108L-rad51 strain is likely to be one of the primary causes for the loss-of-function phenotype in the mutant strain.

It is known that Hsp90 shows a variable degree of association with its clients. Hsp90 clients such as kinases are primarily associated with Hsp90 through transient interactions, and once chaperoned, they are readily released from Hsp90 as functional proteins. On the other hand, clients such as steroid hormone receptors remain associated with Hsp90 to maintain their functional forms. Also, the extent of association between Hsp90 and its client can alter the cellular function of its client. For example, the single point mutations in the epidermal growth factor receptor (EGFR^{L858R}) and B-Raf kinase (B-Raf^{V600E}) promote tumor formation. It was observed that these point mutants have enhanced levels of association with Hsp90 compared to those of their wild-type counterparts (31, 32). While binding with its clients, Hsp90 exhibits specificity toward the hydrophobic residues of proteins (33). The incorporation of leucine at the 108th position of Rad51 increases the hydrophobic stretch on Rad51 (107 to 113 amino acids). We speculate that such an increase in hydrophobicity might result in a tighter binding between Hsp90 and mutant Rad51 protein.

Collectively, our work establishes the importance of Hsp90 in the HR pathway, where it appears to regulate the stability and functions of Rad51. Increasing lines of evidence suggest that the functions of several DNA repair proteins, such as BRCA1, BRCA2, Chk1, DNA-PKcs, FANCA, and the Mre11/Rad50/NBS, are likely to be dependent on Hsp90 (34). A recent report showed that overexpression of Hsp90 leads to genomic instability through a negative regulation of the checkpoint kinase RAD53 (22). Our work along with these reports embarks on the relationship of Hsp90 with DNA repair. Currently, DNA repair along with the Hsp90 inhibitor is being targeted in many cancer studies. Understanding the detailed regulation of HR will be beneficial for further knowledge in the field.

There are many reports which show that in response to various signals, Hsp90/ Hsp82 gets posttranslational modifications (PTMs), and such PTMs help the release of the client protein (35–37). Currently, it is not known whether such PTM of Hsp90 occurs due to MMS treatment and that causes the decrease in association between Rad51WT and Hsp90. It is also unclear how the stronger association between Rad51E108L and Hsp90 was not overcome during the DNA damage response (DDR). These questions are interesting but beyond the scope of this report, and future studies might unravel the mechanism underlying the dissociation of Rad51 from Hsp90 upon DNA damage.

MATERIALS AND METHODS

Plasmids. The sequences of all the primers used in this paper are tabulated in Table 2. The RAD51 mutant (E108L-rad51) was cloned in 2 \mu yeast expression vector pTA (20) between the BamH1 and Pst1 restriction sites to generate the pTA-E108L-rad51 plasmid. pTA-RAD51 was used as a positive control in our study (20). Full-length RAD51 and E108L-rad51 were subcloned into prey vector pGADC1 and bait vector pGBDUC1 from pTA-RAD51 and pTA-E108L-rad51, respectively. Thus, the plasmids pGADC1/ RAD51, pGBDUC1/RAD51, pGADC1/E108L-rad51, and pGBDUC1/E108L-rad51 were generated. Full-length RAD52 was amplified using the OSB330/OSB331 primer set and cloned into pGBDUC1 vector between EcoRI and Sall restriction sites to create the pGBDUC1/RAD52 plasmid. To generate the pGBDUC1/RAD54 plasmid, RAD54 was amplified using the OSB332/OSB333 primer set and cloned into pGBDUC1 vector between EcoRI and Sall restriction sites.



TABLE 2 Primer list

Primer	Sequence (5'→3')	Purpose
OMKB90	GGATCCATGTCTCAAGTTCAAGAAC	Forward primer to amplify full-length RAD51
OMKB88	CTGCAGCTACTCGTCTTCTC	Reverse primer to amplify full-length RAD51
OMKB149	GTCGACCTCGTCTTCTTCTGG	Reverse primer used to clone E108L-rad51 into pET22b vector
OSB305	CTCGGATCCATGTCTCAAGTTCAAGAACAAC	Forward primer used to amplify full-length rad51 mutants
OSB293	GTCGTCGACCTCGTCTTCTTCTCTGGGG	Reverse primer used to amplify full-length rad51 mutants
OSB315	AGTGGGCTTCACACTGCTTTGGCGGTAGCA	Forward primer to create rad51 E108L mutation
OSB314	TCTGGGAGCATATGCTACCGCCAAAGCAGTG	Reverse primer to create rad51 E108L mutation
OSB278	CATGCAAGGGCTCCCTAGC	Forward primer used to amplify URA3 region for ChIP
OSB279	CAACCAATCGTAACCTTCATCT	Reverse primer used to amplify URA3 region for ChIP
OSB289	GTTAGTTGAAGCATTAGGTCC	Forward primer used to confirm HO digestion
KanB1	TGTACGGGCGACAGTCACAT	Reverse primer used to confirm HO digestion
OSB21	GACGGATCCATGGCTAGTGAAACTTTTGAATTTC	Forward primer to amplify full-length hsp82
OSB22	CGGGTCGACCTAATCTACCTCTTCCATTTCGG	Reverse primer to amplify full-length hsp82
OSB16	TGACCAAACTACTTACAACTCC	Forward primer to amplify 307 bp of 3' end of ACT1
OSB14	TTAGAAACACTTGTGGTGAACG	Reverse primer to amplify ACT1
OSB330	CATGAATTCATGAATGAAATTATGGATATCGATG	Forward primer to amplify RAD52
OSB331	CATGTCGACTCAAGTAGGCTTGCGTGCATG	Reverse primer to amplify RAD52
OSB332	CATGAATTCATGGCAAGACGCAGATTACC	Forward primer to amplify RAD54
OSB333	CATGTCGACTCAATGTGAAATATATTGAAATGC	Reverse primer to amplify RAD54

Site-directed mutagenesis. Point mutations were introduced in RAD51 by using the splice overlap extension (SOE) PCR technique. A primer set was designed to incorporate the required mutation in RAD51 at the desired location. Yeast genomic DNA was used as a template, and the full-length gene was amplified in two segments in order to insert the point mutation. For amplifying the first and second segments to generate the E108L-rad51 mutation, primer sets OSB305/OSB314 and OSB315/OSB293 were used, respectively. Full-length RAD51 containing the E108L mutation was then amplified by using the first two segments along with primer set OMKB90/OMKB88. The rad51 mutant was then cloned into the pTA 2μ yeast expression vector using the sites BamH1 and Pstl. After successful cloning, the pTA-E108L-rad51 construct was sequenced to confirm the desired mutation. To create the E108L-rad51 mutant, we changed the codon GAA to TTG.

Yeast strains. The strains used in this study are tabulated in Table 3. LS402 $\Delta rad51$ was transformed with empty vector (pTA), pTA-RAD51, and pTA-E108L-rad51 to generate NRY1, NRY2, and TSY17, respectively. For the gene conversion assay, pTA-RAD51 and pTA-E108L-rad51 were transformed into NA14 $\Delta rad51$ (21) to generate TSY21 and TSY22. For a negative control, the NA14 $\Delta rad51$ strain was transformed with pTA empty vector to generate TSY20. To perform the yeast two-hybrid analysis, empty pGADC1 and pGBDUC1 vectors were transformed into a pJ694a parent strain to generate the PMY3 yeast strain. To study the interaction of wild-type Rad51 with itself and with Rad52 and Rad54 proteins, PMY8, PMY9, and PMY10 were created by transforming prey-RAD51 plus bait-RAD51, prey-RAD51 plus bait-RAD52, and prey-RAD51 plus bait-RAD54 constructs, respectively, into the pJ694a strain. Similarly, to study the interaction of Rad51^{E108L} with itself and with Rad52 and Rad54, strains TSY10, PMY12, and PMY13 were generated by transforming prey-E108L-rad51 plus bait-E108L-rad51, prey-E108L-rad51 plus bait-RAD52, and prey-E108L-rad51 plus bait-RAD54 constructs, respectively. Strains PMY4, PMY7, PMY14, and PMY11 were utilized as controls. These strains were generated by transforming empty prey plus bait-RAD51, prey-RAD51 plus empty bait, empty prey plus bait-E108L-rad51, and prey-E108L-rad51 plus empty bait vectors, respectively, into the pJ694a strain.

Yeast two-hybrid analysis. Yeast two hybrid analysis was performed as described earlier (20). The strains PMY3, PMY8, PMY9, PMY10, TSY10, PMY12, PMY13, PMY4, PMY7, PMY14, and PMY11 were grown in SC-Ura-Leu medium until logarithmic phase. They were then diluted serially as shown in Fig. 5 and spotted on SC-uracil (Ura)-Leu and SC-Ura-Leu-adenine (Ade) medium. The plates were kept at 30°C for 3 to 4 days. The strain PMY3 was used as the negative control in our study.

MMS sensitivity assay. NRY1, NRY2, and TSY17 were tested for DNA damage sensitivity. All strains were grown in tryptophan dropout synthetic medium overnight at 30°C. The next day, a secondary culture was grown to an optical density at 600 nm (OD_{600}) of 0.5 at 30°C. The culture was then divided into two sets. One set of cells was treated with 0.03% (vol/vol) of methyl methanesulfonate (MMS) (Sigma-Aldrich) and grown at 30°C for 2 h, and the other set was continuously grown at 30°C for 2 h without MMS. After that, the cells were serially diluted as mentioned, spotted on selective medium, and incubated at 30°C for 2 to 3 days.

Gene conversion assay. TSY20, TSY21, and TSY22 strains were generated by transforming pTA (empty vector), pTA-RAD51 and pTA-E108L-rad51, respectively, into the NA14 Δrad51 strain. The transformed cells were initially patched on a plate containing glycerol as a sole carbon source. Next, equal numbers of cells were counted and spread on two different plates, one containing glycerol and other containing galactose as a carbon source, and incubated at 30°C for 3 to 5 days. Cells which survived on galactose plates were then patched on another plate containing G418 sulfate and incubated at 30°C for 36 h in order to determine the percentage gene conversion. Cells grown on G418 sulfate-containing plates utilize the Rad51-mediated gene conversion pathway for repair as they retain KANMX6. The ratio of the number of cells grown on the G418 sulfate plate to the number of cells grown on the galactose



Strain Genotype Source or refer NRY1 MATa leu2-3,112 trp1-1 can1-100 ura3-1 ade2-1 his3-11,15 [phi ⁺] RAD51:::LEU2 pTA-RAD51 20 NRY2 MATa leu2-3,112 trp1-1 can1-100 ura3-1 ade2-1 his3-11,15 [phi ⁺] RAD51:::LEU2 pTA-RAD51 20 NRY2 MATa leu2-3,112 trp1-1 can1-100 ura3-1 ade2-1 his3-11,15 [phi ⁺] RAD51:::LEU2 pTA-E108L-rad51 This study 1SY17 MATa leu2-3,112 trp1-1 can1-100 ura3-1 ade2-1 his3-11,15 trp1-1 can1-100 RAD51::LEU2 pTA-RAD51 This study 1SY20 MATa inc ura3-HOcs lys::ura3-HOcs-inc ade3::GALHO ade2-1 leu2-3,112 his3-11,15 trp1-1 can1-100 RAD51::LEU2 pTA-RAD51 This study 1SY21 MATa inc ura3-HOcs lys::ura3-HOcs-inc ade3::GALHO ade2-1 leu2-3,112 tri3-1 can1-100 RAD51::LEU2 pTA-RAD51 This study 1SY21 MATa inc ura3-HOcs lys::ura3-HOcs-inc ade3::GALHHIS3 GAL2-ADE2 met2::GAL7-dac2 pGADC1/RAD51 This study PNW3 MATa trp1-901 leu2-3,112 ura3-52 his3-200 ga14A ga180A LYS::GALHHIS3 GAL2-ADE2 met2::GAL7-lac2 pGADC1/RAD52 This study PNW10 MATa trp1-901 leu2-3,112 ura3-52 his3-200 ga14A ga180A LYS::GALHHIS3 GAL2-ADE2 met2::GAL7-lac2 pGADC1/RAD54 This study PNW10 MATa trp1-901 leu2-3,112 ura3-52 his3-200 ga14A ga180A LYS::GALHHIS3 GAL2-ADE2 met2::GAL7-lac2 pGADC1/RAD54 This study PNW14 MATa trp1-901 leu2-3,112 ura3-52 his3-200	I ABLE 3 reast strains	east strains	
MATa leu2-3,112 trp1-1 can1-100 ura3-1 ade2-1 his3-11,15 [phi+] RAD51::LEU2 pTA-RAD51 MATa leu2-3,112 trp1-1 can1-100 ura3-1 ade2-1 his3-11,15 [phi+] RAD51::LEU2 pTA-RAD51 MATa leu2-3,112 trp1-1 can1-100 ura3-1 ade2-1 his3-11,15 [phi+] RAD51::LEU2 pTA-E108L-rad51 MATa inc ura3-HOcs lysz:ura3-HOcs-inc ade3::GALHO ade2-1 leu2-3,112 his3-11,15 trp1-1 can1-100 RAD51::LEU2 pTA-RAD51 MATa inc ura3-HOcs lysz:ura3-HOcs-inc ade3::GALHO ade2-1 leu2-3,112 his3-11,15 trp1-1 can1-100 RAD51::LEU2 pTA-RAD51 MATa inc ura3-HOcs lysz:ura3-HOcs-inc ade3::GALHO ade2-1 leu2-3,112 his3-11,15 trp1-1 can1-100 RAD51::LEU2 pTA-RAD51 MATa inc ura3-HOcs lysz:ura3-HOcs-inc ade3::GALHO ade2-1 leu2-3,112 his3-11,15 trp1-1 can1-100 RAD51::LEU2 pTA-RAD51 MATa trp1-901 leu2-3,112 ura3-52 his3-200 ga14Δ ga180Δ LYS2::GALHHIS3 GAL2-ADE2 met2::GAL7-lac2 pGADC1/RAD57 pGBDUC1/RAD52 MATa trp1-901 leu2-3,112 ura3-52 his3-200 ga14Δ ga180Δ LYS2::GALHHIS3 GAL2-ADE2 met2::GAL7-lac2 pGADC1/ScRAD51 pGBDUC1/RAD54 MATa trp1-901 leu2-3,112 ura3-52 his3-200 ga14Δ ga180Δ LYS2::GALHHIS3 GAL2-ADE2 met2::GAL7-lac2 pGADC1/ScRAD51 pGBDUC1/RAD54 MATa trp1-901 leu2-3,112 ura3-52 his3-200 ga14Δ ga180Δ LYS2::GALHHIS3 GAL2-ADE2 met2::GAL7-lac2 pGADC1/RAD51 MATa trp1-901 leu2-3,112 ura3-52 his3-200 ga14Δ ga180Δ LYS2::GALHHIS3 GAL2-ADE2 met2::GAL7-lac2 pGADC1/RAD51 MATa trp1-901 leu2-3,112 ura3-52 his3-200 ga14Δ ga180Δ LYS2::GALHHIS3 GAL2-ADE2 met2::GAL7-lac2 pGADC1/RAD51 MATa trp1-901 leu2-3,112 ura3-52 his3-200 ga14Δ ga180Δ LYS2::GALHHIS3 GAL2-ADE2 met2::GAL7-lac2 pGADC1 pGBDUC1/RAD51 MATa trp1-901 leu2-3,112 ura3-52 his3-200 ga14Δ ga180Δ LYS2::GALHHIS3 GAL2-ADE2 met2::GAL7-lac2 pGADC1 pGBDUC1/RAD51 MATa trp1-901 leu2-3,112 ura3-52 his3-200 ga14Δ ga180Δ LYS2::GALHHIS3 GAL2-ADE2 met2::GAL7-lac2 pGADC1 pGBDUC1/RAD51 MATa trp1-901 leu2-3,112 ura3-52 his3-200 ga14Δ ga180Δ LYS2::GALHHIS3 GAL2-ADE2 met2::GAL7-lac2 pGADC1 pGBDUC1/RAD51 MATa trp1-901 leu2-3,112 ura3-52 his3-200 ga14Δ ga180Δ LYS2::GALHHIS3 GAL2-ADE2 met2::GAL7-lac2 pGADC1 pGBDUC1/RAD51 MATa trp1-	Strain	Genotype	Source or reference
MATa leu2-3,112 trp1-1 can1-100 ura3-1 ade2-1 his3-11,15 [phi+] RAD51::LEU2 pTA-F108L-rad51 MATa leu2-3,112 trp1-1 can1-100 ura3-1 ade2-1 his3-11,15 [phi+] RAD51::LEU2 pTA-F108L-rad51 MATa leu2-3,112 trp1-1 can1-100 ura3-1 ade2-1 his3-11,15 [phi+] RAD51::LEU2 pTA-F108L-rad51 MATa inc ura3-HOcs lys2::ura3-HOcs-inc ade3::GALHO ade2-1 leu2-3,112 his3-11,15 trp1-1 can1-100 RAD51::LEU2 pTA-RAD51 MATa inc ura3-HOcs lys2::ura3-HOcs-inc ade3::GALHO ade2-1 leu2-3,112 his3-11,15 trp1-1 can1-100 RAD51::LEU2 pTA-RAD51 MATa inc ura3-HOcs lys2::ura3-HOcs-inc ade3::GALHO ade2-1 leu2-3,112 his3-11,15 trp1-1 can1-100 RAD51::LEU2 pTA-F108L-rad51 MATa trp1-901 leu2-3,112 ura3-52 his3-200 ga14A ga180A LYS2::GALHHIS3 GAL2-ADE2 met2::GAL7-lac2 pGADC1/RAD51 pGBDUC1/RAD54 MATa trp1-901 leu2-3,112 ura3-52 his3-200 ga14A ga180A LYS2::GALLHIS3 GAL2-ADE2 met2::GAL7-lac2 pGADC1/RAD51 pGBDUC1/RAD54 MATa trp1-901 leu2-3,112 ura3-52 his3-200 ga14A ga180A LYS2::GALLHIS3 GAL2-ADE2 met2::GAL7-lac2 pGADC1/RAD51 pGBDUC1/RAD54 MATa trp1-901 leu2-3,112 ura3-52 his3-200 ga14A ga180A LYS2::GALLHIS3 GAL2-ADE2 met2::GAL7-lac2 pGADC1/R108L-rad51 pGBDUC1/RAD54 MATa trp1-901 leu2-3,112 ura3-52 his3-200 ga14A ga180A LYS2::GALLHIS3 GAL2-ADE2 met2::GAL7-lac2 pGADC1/R108L-rad51 pGBDUC1/RAD54 MATa trp1-901 leu2-3,112 ura3-52 his3-200 ga14A ga180A LYS2::GALLHIS3 GAL2-ADE2 met2::GAL7-lac2 pGADC1/RAD51 pGBDUC1/RAD54 MATa trp1-901 leu2-3,112 ura3-52 his3-200 ga14A ga180A LYS2::GALLHIS3 GAL2-ADE2 met2::GAL7-lac2 pGADC1 pGBDUC1/RAD51 MATa trp1-901 leu2-3,112 ura3-52 his3-200 ga14A ga180A LYS2::GALLHIS3 GAL2-ADE2 met2::GAL7-lac2 pGADC1 pGBDUC1/R108L-rad51 pGBDUC1 MATa trp1-901 leu2-3,112 ura3-52 his3-200 ga14A ga180A LYS2::GALLHIS3 GAL2-ADE2 met2::GAL7-lac2 pGADC1 pGBDUC1/R108L-rad51 pGBDUC1	NRY1	MATa leu2-3,112 trp1-1 can1-100 ura3-1 ade2-1 his3-11,15 [phi+] RAD51::LEU2 pTA	20
MATa leu2-3,112 ttp1-1 can1-100 ura3-1 ade2-1 his3-11,15 [phi ⁺] RAD51::LEU2 pTA-E108L-rad51 MATa inc ura3-HOcs lys2::ura3-HOcs-inc ade3::GALHO ade2-1 leu2-3,112 his3-11,15 ttp1-1 can1-100 RAD51::LEU2 pTA-RAD51 MATa inc ura3-HOcs lys2::ura3-HOcs-inc ade3::GALHO ade2-1 leu2-3,112 his3-11,15 ttp1-1 can1-100 RAD51::LEU2 pTA-RAD51 MATa inc ura3-HOcs lys2::ura3-HOcs-inc ade3::GALHO ade2-1 leu2-3,112 his3-11,15 ttp1-1 can1-100 RAD51::LEU2 pTA-RAD51 MATa inc ura3-HOcs lys2::ura3-HOcs-inc ade3::GALHO ade2-1 leu2-3,112 his3-11,15 ttp1-1 can1-100 RAD51::LEU2 pTA-E108L-rad51 MATa inc ura3-HOcs lys2::ura3-S2 his3-200 ga14D ga180D LYS2::GALHIS3 GAL2-ADE2 met2::GAL7-lac2 pGADC1/RAD57 pGBDUC1/RAD57 MATa inc leu2-3,112 ura3-52 his3-200 ga14D ga180D LYS2::GALHIS3 GAL2-ADE2 met2::GAL7-lac2 pGADC1/RAD57 pGBDUC1/RAD54 MATa inc leu2-3,112 ura3-52 his3-200 ga14D ga180D LYS2::GALHIS3 GAL2-ADE2 met2::GAL7-lac2 pGADC1/E108L-rad57 pGBDUC1/RAD57 MATa inc leu2-3,112 ura3-52 his3-200 ga14D ga180D LYS2::GALHIS3 GAL2-ADE2 met2::GAL7-lac2 pGADC1/E108L-rad57 pGBDUC1/RAD54 MATa inc leu2-3,112 ura3-52 his3-200 ga14D ga180D LYS2::GALHIS3 GAL2-ADE2 met2::GAL7-lac2 pGADC1/E108L-rad57 pGBDUC1/RAD54 MATa inc leu2-3,112 ura3-52 his3-200 ga14D ga180D LYS2::GALHIS3 GAL2-ADE2 met2::GAL7-lac2 pGADC1 pGBDUC1/RAD57 MATa inc leu2-3,112 ura3-52 his3-200 ga14D ga180D LYS2::GALHIS3 GAL2-ADE2 met2::GAL7-lac2 pGADC1 pGBDUC1/R08-rad57 MATa inc leu2-3,112 ura3-52 his3-200 ga14D ga180D LYS2::GALHIS3 GAL2-ADE2 met2::GAL7-lac2 pGADC1/E108L-rad57 MATa inc leu2-3,112 ura3-52 his3-200 ga14D ga180D LYS2::GALHIS3 GAL2-ADE2 met2::GAL7-lac2 pGADC1/E108L-rad57 MATa inc leu2-3,112 ura3-52 his3-200 ga14D ga180D LYS2::GALHIS3 GAL2-ADE2 met2::GAL7-lac2 pGADC1/E108L-rad57 MATa inc leu2-3,112 ura3-52 his3-200 ga14D ga180D LYS2::GALHIS3 GAL2-ADE2 met2::GAL7-lac2 pGADC1/E108L-rad57 MATa inc leu2-3,112 ura3-52 his3-200 ga14D ga180D LYS2::GALHIS3 GAL2-ADE2 met2::GAL7-lac2 pGADC1/E108L-rad57 MATa inc leu2-3,112 ura3-52 his3-200 ga14D ga180D LYS2::GALHIS3 GAL2-ADE2 met2	NRY2	MATa leu2-3,112 trp1-1 can1-100 ura3-1 ade2-1 his3-11,15 [phi+] RAD51::LEU2 pTA-RAD51	20
MATa inc ura3-HOcs lys2::ura3-HOcs-inc ade3::GALHO ade2-1 leu2-3,112 his3-11,15 trp1-1 can1-100 RAD51::LEU2 pTA-RAD51 MATa inc ura3-HOcs lys2::ura3-HOcs-inc ade3::GALHO ade2-1 leu2-3,112 his3-11,15 trp1-1 can1-100 RAD51::LEU2 pTA-RAD51 MATa inc ura3-HOcs lys2::ura3-HOcs-inc ade3::GALHO ade2-1 leu2-3,112 his3-11,15 trp1-1 can1-100 RAD51::LEU2 pTA-F108L-rad51 MATa trp1-901 leu2-3,112 ura3-52 his3-200 ga14Δ ga180Δ LYS2::GAL1-HIS3 GAL2-ADE2 met2::GAL7-lacZ pGADC1/RAD51 MATa trp1-901 leu2-3,112 ura3-52 his3-200 ga14Δ ga180Δ LYS2::GAL1-HIS3 GAL2-ADE2 met2::GAL7-lacZ pGADC1/RAD51 pGBDUC1/RAD51 MATa trp1-901 leu2-3,112 ura3-52 his3-200 ga14Δ ga180Δ LYS2::GAL1-HIS3 GAL2-ADE2 met2::GAL7-lacZ pGADC1/SCRAD51 pGBDUC1/RAD54 MATa trp1-901 leu2-3,112 ura3-52 his3-200 ga14Δ ga180Δ LYS2::GAL1-HIS3 GAL2-ADE2 met2::GAL7-lacZ pGADC1/F108L-rad51 pGBDUC1/RAD54 MATa trp1-901 leu2-3,112 ura3-52 his3-200 ga14Δ ga180Δ LYS2::GAL1-HIS3 GAL2-ADE2 met2::GAL7-lacZ pGADC1/RAD51 MATa trp1-901 leu2-3,112 ura3-52 his3-200 ga14Δ ga180Δ LYS2::GAL1-HIS3 GAL2-ADE2 met2::GAL7-lacZ pGADC1/RAD51 MATa trp1-901 leu2-3,112 ura3-52 his3-200 ga14Δ ga180Δ LYS2::GAL1-HIS3 GAL2-ADE2 met2::GAL7-lacZ pGADC1/RAD51 MATa trp1-901 leu2-3,112 ura3-52 his3-200 ga14Δ ga180Δ LYS2::GAL1-HIS3 GAL2-ADE2 met2::GAL7-lacZ pGADC1/F108L-rad51 pGBDUC1/F108L-rad51	TSY17	MATa leu2-3,112 trp1-1 can1-100 ura3-1 ade2-1 his3-11,15 [phi+] RAD51::LEU2 pTA-E108L-rad51	This study
MATa inc ura3-HOcs lys2::ura3-HOcs-inc ade3::GALHO ade2-1 leu2-3,112 his3-11,15 trp1-1 can1-100 RAD51::LEU2 pTA-E108L-rad51 MATa inc ura3-HOcs lys2::ura3-HOcs-inc ade3::GALHO ade2-1 leu2-3,112 his3-11,15 trp1-1 can1-100 RAD51::LEU2 pTA-E108L-rad51 MATa trp1-901 leu2-3,112 ura3-52 his3-200 ga14∆ ga180∆ LYS2::GALHHIS3 GAL2-ADE2 met2::GAL7-lac2 pGADC1/RAD51 pGBDUC1/RAD51 MATa trp1-901 leu2-3,112 ura3-52 his3-200 ga14∆ ga180∆ LYS2::GALHHIS3 GAL2-ADE2 met2::GAL7-lac2 pGADC1/RAD51 pGBDUC1/RAD52 MATa trp1-901 leu2-3,112 ura3-52 his3-200 ga14∆ ga180∆ LYS2::GALHHIS3 GAL2-ADE2 met2::GAL7-lac2 pGADC1/ScRAD51 pGBDUC1/RAD54 MATa trp1-901 leu2-3,112 ura3-52 his3-200 ga14∆ ga180∆ LYS2::GALHHIS3 GAL2-ADE2 met2::GAL7-lac2 pGADC1/E108L-rad51 pGBDUC1/RAD54 MATa trp1-901 leu2-3,112 ura3-52 his3-200 ga14∆ ga180∆ LYS2::GALHHIS3 GAL2-ADE2 met2::GAL7-lac2 pGADC1/E108L-rad51 pGBDUC1/RAD54 MATa trp1-901 leu2-3,112 ura3-52 his3-200 ga14∆ ga180∆ LYS2::GALHHIS3 GAL2-ADE2 met2::GAL7-lac2 pGADC1/RAD51 MATa trp1-901 leu2-3,112 ura3-52 his3-200 ga14∆ ga180∆ LYS2::GALHHIS3 GAL2-ADE2 met2::GAL7-lac2 pGADC1/F108L-rad51 pGBDUC1 MATa trp1-901 leu2-3,112 ura3-52 his3-200 ga14∆ ga180∆ LYS2::GALHHIS3 GAL2-ADE2 met2::GAL7-lac2 pGADC1 pGBDUC1 MATa trp1-901 leu2-3,112 ura3-52 his3-200 ga14∆ ga180∆ LYS2::GALHHIS3 GAL2-ADE2 met2::GAL7-lac2 pGADC1 pGBDUC1 MATa trp1-901 leu2-3,112 ura3-52 his3-200 ga14∆ ga180∆ LYS2::GALHHIS3 GAL2-ADE2 met2::GAL7-lac2 pGADC1 pGBDUC1 MATa trp1-901 leu2-3,112 ura3-52 his3-200 ga14∆ ga180∆ LYS2::GALHHIS3 GAL2-ADE2 met2::GAL7-lac2 pGADC1 pGBDUC1 MATa trp1-901 leu2-3,112 ura3-52 his3-200 ga14∆ ga180∆ LYS2::GALHHIS3 GAL2-ADE2 met2::GAL7-lac2 pGADC1/F108L-rad51 pGBDUC1	TSY20	MATa inc ura3-HOcs lys2:ura3-HOcs-inc ade3::GALHO ade2-1 leu2-3,112 his3-11,15 trp1-1 can1-100 RAD51::LEU2 pTA	This study
MATa inc ura3-HOcs lys2::ura3-HOcs-inc ade3::GALHO ade2-1 leu2-3,112 his3-11,15 trp1-1 can1-100 RAD51::LEU2 pTA-E108L-rad51 MATa trp1-901 leu2-3,112 ura3-52 his3-200 ga14∆ ga180∆ LYS2::GALI-HIS3 GAL2-ADE2 met2::GAL7-lac2 pGADC1/RAD51 pGBDUC1/RAD51 MATa trp1-901 leu2-3,112 ura3-52 his3-200 ga14∆ ga180∆ LYS2::GALI-HIS3 GAL2-ADE2 met2::GAL7-lac2 pGADC1/RAD51 pGBDUC1/RAD52 MATa trp1-901 leu2-3,112 ura3-52 his3-200 ga14∆ ga180∆ LYS2::GALI-HIS3 GAL2-ADE2 met2::GAL7-lac2 pGADC1/SCRAD51 pGBDUC1/RAD54 MATa trp1-901 leu2-3,112 ura3-52 his3-200 ga14∆ ga180∆ LYS2::GALI-HIS3 GAL2-ADE2 met2::GAL7-lac2 pGADC1/SCRAD51 pGBDUC1/RAD52 MATa trp1-901 leu2-3,112 ura3-52 his3-200 ga14∆ ga180∆ LYS2::GALI-HIS3 GAL2-ADE2 met2::GAL7-lac2 pGADC1/E108L-rad51 pGBDUC1/RAD54 MATa trp1-901 leu2-3,112 ura3-52 his3-200 ga14∆ ga180∆ LYS2::GALI-HIS3 GAL2-ADE2 met2::GAL7-lac2 pGADC1/F108L-rad51 pGBDUC1/RAD54 MATa trp1-901 leu2-3,112 ura3-52 his3-200 ga14∆ ga180∆ LYS2::GALI-HIS3 GAL2-ADE2 met2::GAL7-lac2 pGADC1 pGBDUC1/RAD51 MATa trp1-901 leu2-3,112 ura3-52 his3-200 ga14∆ ga180∆ LYS2::GALI-HIS3 GAL2-ADE2 met2::GAL7-lac2 pGADC1 pGBDUC1/F108L-rad51 MATa trp1-901 leu2-3,112 ura3-52 his3-200 ga14∆ ga180∆ LYS2::GALI-HIS3 GAL2-ADE2 met2::GAL7-lac2 pGADC1 pGBDUC1/F108L-rad51 MATa trp1-901 leu2-3,112 ura3-52 his3-200 ga14∆ ga180∆ LYS2::GALI-HIS3 GAL2-ADE2 met2::GAL7-lac2 pGADC1/F108L-rad51 pGBDUC1	TSY21	MATa inc ura3-HOcs lys2:ura3-HOcs-inc ade3::GALHO ade2-1 leu2-3,112 his3-11,15 trp1-1 can1-100 RAD51::LEU2 pTA-RAD51	This study
MATa trpl-901 leu2-3,112 ura3-52 his3-200 ga14Δ ga180Δ LYS2::GALI-HIS3 GAL2-ADE2 met2::GAL7-lacZ pGADC1 pGBDUC1/RAD51 MATa trpl-901 leu2-3,112 ura3-52 his3-200 ga14Δ ga180Δ LYS2::GALI-HIS3 GAL2-ADE2 met2::GAL7-lacZ pGADC1/RAD51 pGBDUC1/RAD51 MATa trpl-901 leu2-3,112 ura3-52 his3-200 ga14Δ ga180Δ LYS2::GALI-HIS3 GAL2-ADE2 met2::GAL7-lacZ pGADC1/RAD51 pGBDUC1/RAD52 MATa trpl-901 leu2-3,112 ura3-52 his3-200 ga14Δ ga180Δ LYS2::GALI-HIS3 GAL2-ADE2 met2::GAL7-lacZ pGADC1/SCRAD51 pGBDUC1/RAD52 MATa trpl-901 leu2-3,112 ura3-52 his3-200 ga14Δ ga180Δ LYS2::GALI-HIS3 GAL2-ADE2 met2::GAL7-lacZ pGADC1/E108L-rad51 pGBDUC1/RAD54 MATa trpl-901 leu2-3,112 ura3-52 his3-200 ga14Δ ga180Δ LYS2::GALI-HIS3 GAL2-ADE2 met2::GAL7-lacZ pGADC1/RAD51 MATa trpl-901 leu2-3,112 ura3-52 his3-200 ga14Δ ga180Δ LYS2::GALI-HIS3 GAL2-ADE2 met2::GAL7-lacZ pGADC1/F108L-rad51 pGBDUC1 MATa trpl-901 leu2-3,112 ura3-52 his3-200 ga14Δ ga180Δ LYS2::GALI-HIS3 GAL2-ADE2 met2::GAL7-lacZ pGADC1 pGBDUC1 MATa trpl-901 leu2-3,112 ura3-52 his3-200 ga14Δ ga180Δ LYS2::GALI-HIS3 GAL2-ADE2 met2::GAL7-lacZ pGADC1 pGBDUC1 MATa trpl-901 leu2-3,112 ura3-52 his3-200 ga14Δ ga180Δ LYS2::GALI-HIS3 GAL2-ADE2 met2::GAL7-lacZ pGADC1/F108L-rad51 pGBDUC1	TSY22	MATa inc ura3-HOcs lys2:ura3-HOcs-inc ade3::GALHO ade2-1 leu2-3,112 his3-11,15 trp1-1 can1-100 RAD51::LEU2 pTA-E108L-rad51	This study
MATa trpl-901 leu2-3,112 ura3-52 his3-200 ga14Δ ga180Δ LYS2::GALI-HIS3 GAL2-ADE2 met2::GAL7-lacZ pGADC1/RAD51 pGBDUC1/RAD51 MATa trpl-901 leu2-3,112 ura3-52 his3-200 ga14Δ ga180Δ LYS2::GALI-HIS3 GAL2-ADE2 met2::GAL7-lacZ pGADC1/RAD51 pGBDUC1/RAD52 MATa trpl-901 leu2-3,112 ura3-52 his3-200 ga14Δ ga180Δ LYS2::GALI-HIS3 GAL2-ADE2 met2::GAL7-lacZ pGADC1/ScRAD51 pGBDUC1/RAD54 MATa trpl-901 leu2-3,112 ura3-52 his3-200 ga14Δ ga180Δ LYS2::GALI-HIS3 GAL2-ADE2 met2::GAL7-lacZ pGADC1/F108L-rad51 pGBDUC1/RAD52 MATa trpl-901 leu2-3,112 ura3-52 his3-200 ga14Δ ga180Δ LYS2::GALI-HIS3 GAL2-ADE2 met2::GAL7-lacZ pGADC1/RAD51 pGBDUC1/RAD54 MATa trpl-901 leu2-3,112 ura3-52 his3-200 ga14Δ ga180Δ LYS2::GALI-HIS3 GAL2-ADE2 met2::GAL7-lacZ pGADC1 pGBDUC1/RAD51 MATa trpl-901 leu2-3,112 ura3-52 his3-200 ga14Δ ga180Δ LYS2::GALI-HIS3 GAL2-ADE2 met2::GAL7-lacZ pGADC1 pGBDUC1/RAD51 MATa trpl-901 leu2-3,112 ura3-52 his3-200 ga14Δ ga180Δ LYS2::GALI-HIS3 GAL2-ADE2 met2::GAL7-lacZ pGADC1 pGBDUC1/F108L-rad51 MATa trpl-901 leu2-3,112 ura3-52 his3-200 ga14Δ ga180Δ LYS2::GALI-HIS3 GAL2-ADE2 met2::GAL7-lacZ pGADC1 pGBDUC1/F108L-rad51	PMY3	MATa tτpl-901 leu2-3,112 ura3-52 his3-200 ga14Δ ga180Δ LYS2::GAL ⁺ HIS3 GAL2-ADE2 met2::GAL7-IacZ pGADC1 pGBDUC1	This study
MATa trpl-901 leu2-3,112 ura3-52 his3-200 ga14Δ ga180Δ LYS2::GALI-HIS3 GAL2-ADE2 met2::GAL7-lac2 pGADC1/RAD51 pGBDUC1/RAD52 MATa trpl-901 leu2-3,112 ura3-52 his3-200 ga14Δ ga180Δ LYS2::GALI-HIS3 GAL2-ADE2 met2::GAL7-lac2 pGADC1/ScRAD51 pGBDUC1/RAD54 MATa trpl-901 leu2-3,112 ura3-52 his3-200 ga14Δ ga180Δ LYS2::GALI-HIS3 GAL2-ADE2 met2::GAL7-lac2 pGADC1/F108L-rad51 pGBDUC1/F108L-rad51 MATa trpl-901 leu2-3,112 ura3-52 his3-200 ga14Δ ga180Δ LYS2::GALI-HIS3 GAL2-ADE2 met2::GAL7-lac2 pGADC1/F108L-rad51 pGBDUC1/RAD54 MATa trpl-901 leu2-3,112 ura3-52 his3-200 ga14Δ ga180Δ LYS2::GALI-HIS3 GAL2-ADE2 met2::GAL7-lac2 pGADC1/RAD51 MATa trpl-901 leu2-3,112 ura3-52 his3-200 ga14Δ ga180Δ LYS2::GALI-HIS3 GAL2-ADE2 met2::GAL7-lac2 pGADC1/RAD51 pGBDUC1 MATa trpl-901 leu2-3,112 ura3-52 his3-200 ga14Δ ga180Δ LYS2::GALI-HIS3 GAL2-ADE2 met2::GAL7-lac2 pGADC1/F108L-rad51 pGBDUC1 MATa trpl-901 leu2-3,112 ura3-52 his3-200 ga14Δ ga180Δ LYS2::GALI-HIS3 GAL2-ADE2 met2::GAL7-lac2 pGADC1/F108L-rad51 pGBDUC1	PMY8	MATa tτp!-901 leu2-3,112 ura3-52 his3-200 ga14Δ ga180Δ LYS2::GAL!-HIS3 GAL2-ADE2 met2::GAL7-IacZ pGADC1/RAD51 pGBDUC1/RAD51	This study
MATa trpl-901 leu2-3,112 ura3-52 his3-200 ga14Δ ga180Δ LYS2::GALI-HIS3 GAL2-ADE2 met2::GAL7-lac2 pGADC1/ScRAD51 pGBDUC1/RAD54 MATa trpl-901 leu2-3,112 ura3-52 his3-200 ga14Δ ga180Δ LYS2::GALI-HIS3 GAL2-ADE2 met2::GAL7-lac2 pGADC1/E108L-rad51 pGBDUC1/E108L-rad51 MATa trpl-901 leu2-3,112 ura3-52 his3-200 ga14Δ ga180Δ LYS2::GALI-HIS3 GAL2-ADE2 met2::GAL7-lac2 pGADC1/E108L-rad51 pGBDUC1/RAD52 MATa trpl-901 leu2-3,112 ura3-52 his3-200 ga14Δ ga180Δ LYS2::GALI-HIS3 GAL2-ADE2 met2::GAL7-lac2 pGADC1/E108L-rad51 pGBDUC1/RAD54 MATa trpl-901 leu2-3,112 ura3-52 his3-200 ga14Δ ga180Δ LYS2::GALI-HIS3 GAL2-ADE2 met2::GAL7-lac2 pGADC1/RAD51 pGBDUC1 MATa trpl-901 leu2-3,112 ura3-52 his3-200 ga14Δ ga180Δ LYS2::GALI-HIS3 GAL2-ADE2 met2::GAL7-lac2 pGADC1/F108L-rad51 pGBDUC1 MATa trpl-901 leu2-3,112 ura3-52 his3-200 ga14Δ ga180Δ LYS2::GALI-HIS3 GAL2-ADE2 met2::GAL7-lac2 pGADC1 pGBDUC1/F108L-rad51 pGBDUC1	PMY9		This study
MATa trpl-901 leu2-3,112 ura3-52 his3-200 ga14Δ ga180Δ LYS2::GALI-HIS3 GAL2-ADE2 met2::GAL7-lac2 pGADC1/F108L-rad51 pGBDUC1/E108L-rad51 MATa trpl-901 leu2-3,112 ura3-52 his3-200 ga14Δ ga180Δ LYS2::GALI-HIS3 GAL2-ADE2 met2::GAL7-lac2 pGADC1/F108L-rad51 pGBDUC1/RAD52 MATa trpl-901 leu2-3,112 ura3-52 his3-200 ga14Δ ga180Δ LYS2::GALI-HIS3 GAL2-ADE2 met2::GAL7-lac2 pGADC1/F108L-rad51 pGBDUC1/RAD54 MATa trpl-901 leu2-3,112 ura3-52 his3-200 ga14Δ ga180Δ LYS2::GALI-HIS3 GAL2-ADE2 met2::GAL7-lac2 pGADC1/RAD51 pGBDUC1 ma3-52 his3-200 ga14Δ ga180Δ LYS2::GALI-HIS3 GAL2-ADE2 met2::GAL7-lac2 pGADC1/RAD51 pGBDUC1 ma3-52 his3-200 ga14Δ ga180Δ LYS2::GALI-HIS3 GAL2-ADE2 met2::GAL7-lac2 pGADC1 pGBDUC1 pGBDUC1 ma3-52 his3-200 ga14Δ ga180Δ LYS2::GALI-HIS3 GAL2-ADE2 met2::GALI7-lac2 pGADC1 pGBDUC1 pGBDUC1 leu2-3,112 ura3-52 his3-200 ga14Δ ga180Δ LYS2::GALI-HIS3 GAL2-ADE2 met2::GAL7-lac2 pGADC1/F108L-rad51 pGBDUC1	PMY10		This study
MATa trpl-901 leu2-3,112 ura3-52 his3-200 ga14Δ ga180Δ LYS2::GALI-HIS3 GALZ-ADE2 met2::GALZ-lacZ pGADC1/F108L-rad51 pGBDUC1/RAD52 MATa trpl-901 leu2-3,112 ura3-52 his3-200 ga14Δ ga180Δ LYS2::GALI-HIS3 GALZ-ADE2 met2::GALZ-lacZ pGADC1/F108L-rad51 pGBDUC1/RAD54 MATa trpl-901 leu2-3,112 ura3-52 his3-200 ga14Δ ga180Δ LYS2::GALI-HIS3 GALZ-ADE2 met2::GALZ-lacZ pGADC1 pGBDUC1/RAD51 MATa trpl-901 leu2-3,112 ura3-52 his3-200 ga14Δ ga180Δ LYS2::GALI-HIS3 GALZ-ADE2 met2::GALZ-lacZ pGADC1/RAD51 pGBDUC1 MATa trpl-901 leu2-3,112 ura3-52 his3-200 ga14Δ ga180Δ LYS2::GALI-HIS3 GALZ-ADE2 met2::GALZ-lacZ pGADC1 pGBDUC1/F108L-rad51 MATa trpl-901 leu2-3,112 ura3-52 his3-200 ga14Δ ga180Δ LYS2::GALI-HIS3 GALZ-ADE2 met2::GALZ-lacZ pGADC1/F108L-rad51 pGBDUC1	TSY10		This study
MATa trpl-901 leu2-3,112 ura3-52 his3-200 ga14Δ ga180Δ LYS2::GALI-HIS3 GAL2-ADE2 met2::GAL7-lacZ pGADC1/F108L-rad51 pGBDUC1/RAD54 MATa trpl-901 leu2-3,112 ura3-52 his3-200 ga14Δ ga180Δ LYS2::GALI-HIS3 GAL2-ADE2 met2::GAL7-lacZ pGADC1 pGBDUC1/RAD51 MATa trpl-901 leu2-3,112 ura3-52 his3-200 ga14Δ ga180Δ LYS2::GALI-HIS3 GAL2-ADE2 met2::GAL7-lacZ pGADC1/RAD51 pGBDUC1 MATa trpl-901 leu2-3,112 ura3-52 his3-200 ga14Δ ga180Δ LYS2::GALI-HIS3 GAL2-ADE2 met2::GAL7-lacZ pGADC1 pGBDUC1/F108L-rad51 MATa trpl-901 leu2-3,112 ura3-52 his3-200 ga14Δ ga180Δ LYS2::GALI-HIS3 GAL2-ADE2 met2::GAL7-lacZ pGADC1/F108L-rad51 pGBDUC1	PMY12		This study
MATa trpl-901 leu2-3,112 ura3-52 his3-200 ga14Δ ga180Δ LYS2::GALI-HIS3 GAL2-ADE2 met2::GAL7-lacZ pGADC1 pGBDUC1/RA <i>D51</i> MATa trpl-901 leu2-3,112 ura3-52 his3-200 ga14Δ ga180Δ LYS2::GALI-HIS3 GAL2-ADE2 met2::GAL7-lacZ pGADC1/RAD51 pGBDUC1 MATa trpl-901 leu2-3,112 ura3-52 his3-200 ga14Δ ga180Δ LYS2::GALI-HIS3 GAL2-ADE2 met2::GAL7-lacZ pGADC1 pGBDUC1/F108L-rad51 MATa trpl-901 leu2-3,112 ura3-52 his3-200 ga14Δ ga180Δ LYS2::GALI-HIS3 GAL2-ADE2 met2::GAL7-lacZ pGADC1/F108L-rad51 pGBDUC1	PMY13		This study
MATa trpl-901 leu2-3,112 ura3-52 his3-200 ga14Δ ga180Δ LYS2::GALI-HIS3 GAL2-ADE2 met2::GAL7-lacZ pGADC1/RAD51 pGBDUC1 MATa trpl-901 leu2-3,112 ura3-52 his3-200 ga14Δ ga180Δ LYS2::GALI-HIS3 GAL2-ADE2 met2::GAL7-lacZ pGADC1 pGBDUC1/F108L-rad51 MATa trpl-901 leu2-3,112 ura3-52 his3-200 ga14Δ ga180Δ LYS2::GALI-HIS3 GAL2-ADE2 met2::GAL7-lacZ pGADC1/F108L-rad51 pGBDUC1	PMY4		This study
MATa trpl-901 leu2-3,112 ura3-52 his3-200 ga14Δ ga180Δ LYS2::GALI-HIS3 GAL2-ADE2 met2::GAL7-lacZ pGADC1 pGBDUC1/F108L-rad51 MATa trpl-901 leu2-3,112 ura3-52 his3-200 ga14Δ ga180Δ LYS2::GALI-HIS3 GAL2-ADE2 met2::GAL7-lacZ pGADC1/F108L-rad51 pGBDUC1	PMY7		This study
MATa trpl-901 leu2-3,112 ura3-52 his3-200 ga14Δ ga180Δ LYS2::GALI-HIS3 GAL2-ADE2 met2::GAL7-lacZ pGADC1/F108L-rad51 pGBDUC1	PMY14		This study
	PMY11		This study



plate was calculated to determine the percent gene conversion. The assay was performed more than 3 times, and the mean values were plotted using GraphPad Prism.

Chromatin immunoprecipitation. TSY21 and TSY22 were grown in the selective medium to an OD_{600} of 0.3 in the presence of 3% glycerol. Half of the batch of cells was then treated with 3% galactose for 3 h, and other half continued to grow in glycerol medium. The ChIP assay was performed as described earlier (38). One microgram anti-Rad51 antibody was added to the sample to precipitate Rad51-bound DNA fragments. Recruitment of Rad51 was then monitored by PCR with 30 cycles using primer set OSB278/OSB279 in a reaction mixture volume of 50 μ l using the immunoprecipitate and input DNA samples. Samples were subjected to electrophoresis on 2% agarose. For control, ChIP was performed with rabbit IgG antibody. To verify whether a double-stranded break (DSB) was generated by HO digestion in the assay strain, we used OSB289 as a forward primer, which is complementary to the 20 bp upstream of HO cut site (HOcs), and a reverse primer (KanB1) which is complementary to the KANMX gene. We amplified full-length ACT1 using OSB14 and OSB16 as a normalization control.

Western blotting. Western blottin was performed to check Rad51 levels in NRY1, NRY2, and TSY17 strains. Protein samples were loaded on an SDS polyacrylamide gel. A polyvinylidene difluoride (PVDF) membrane was used for the transfer as described earlier (39). The primary antibodies used were mouse anti-Act1 (Abcam), rabbit anti-Rad51 (Santa Cruz), and mouse anti-Hsp82 (Calbiochem) at 1:5,000 dilutions. For subcellular fractionation, we used anti-Pgk1 antibody (Novus Biologicals) and mouse anti-Nsp1 antibody (Abcam) at 1:3,000 and 1:5,000 dilutions, respectively. For secondary antibodies, horseradish peroxide-conjugated anti-rabbit antibody (Promega) and anti-mouse antibody (Santa Cruz Biotechnology Inc., CA, USA) were used at 1:10,000 dilutions. The Western blots were developed using a chemiluminescent detection system (Pierce). Every experiment was repeated at least 3 times, and band intensities were quantified by using Image J software. Mean relative densities were plotted using GraphPad prism.

Protein-protein docking. The protein sequence of Rad51 with entry P25454 and the ATP-dependent molecular chaperone yHsp90 (Hsp82) with entry P02829 of Saccharomyces cerevisiae (strain ATCC 204508/S288c) are publicly available from the central repository of protein sequence and function, UniProt (Universal Protein Resource). The three-dimensional (3D) structures of Rad51 (PDB ID 1SZP) and yHsp90 (PDB ID 2CG9) were retrieved from the RCSB protein data bank. Protein-protein docking was conducted using a fully automated web-based program ClusPro 2.0, which employs an improved fast Fourier transform (FFT)-based rigid docking program PIPER. The program output is a short list of putative complexes ranked according to their clustering properties (18). Biovia Discovery Studio Visualizer is utilized for visualization and analysis of protein complexes. For mutation studies, the sequence of Rad51 protein retrieved from PDB (1SZP ABCDEF) was viewed in the sequence viewer of Biovia Discovery Studio software. The critical amino acids to be mutated were selected in all six chains and replaced. The sulfate ions were removed, and the structure of the protein generated was subjected to clean geometry and energy minimization before using for protein-protein docking. The amino acid Glu108 (E108) was mutated with four different amino acids, namely, leucine (E108L), alanine (E108A), glycine (E108G), and isoleucine (E108I), in chains A, B, C, D, E, and F to generate single mutant hexamers. The mutated Rad51 proteins were again subjected to protein-protein interaction with yHsp90 2CG9A. Protein-protein docking similar to that of the wild type was repeated with the mutant protein against Hsp90 using the online tool ClusPro

Coimmunoprecipitation. Wild-type and E108L-rad51 cells harboring yHsp90 overexpression plasmid (under GPD promoter; 2μ vector) were grown to an ${\rm OD_{600}}$ of 0.5. Ten milliliters of each culture was harvested, resuspended in 1 ml spheroplast buffer (50 mM Tris-HCI [pH 8], 25 mM HEPES [pH 7.4], 0.2% Casamino Acids, 0.2% yeast nitrogen base [YNB], 1% glucose, 18.2% sorbitol) containing dithiothreitol (DTT) and lyticase, and incubated at 30°C for 90 min. Subsequently, glass beads were added and the cells were intermittently vortexed and incubated on ice six times for a period of 30 s each. An anti-Rad51 antibody was added to the supernatant for overnight incubation at 4°C. Protein A agarose (25%; Calbiochem) was added, and the mixture was incubated for 2 h at room temperature. The beads were then spun down for 15 s at 1,000 rpm, and the pellet was washed 3 times with NETNS buffer (20 mM Tris-HCI [pH 8], 1 mM EDTA, 1 M NaCl, 0.5% [vol/vol] NP-40 with protease inhibitor) and twice with NETN buffer (20 mM Tris-HCl [pH 8], 1 mM EDTA, 100 mM NaCl, 0.5% [vol/vol] NP-40 with protease inhibitor). The bound protein was eluted with 4× Laemmli buffer by boiling for 10 min and was further spun down, and the supernatant was collected and used for Western blotting. The proteins in the supernatant were precipitated using 20% trichloroacetic acid, eluted using $4 \times SDS$ loading dye containing dithiothreitol (DTT) and Tris (pH 8.8), and boiled for 10 min. The sample was spun down and the proteins in the supernatant were used for Western blotting. After the coimmunoprecipitation, the relative association of Hsp90 with Rad51 was calculated for each experiment using the following formula: relative association of Hsp90 with Rad51 = (Hsp90 in the pellet/Hsp90 in the input) ÷ (Rad51 in the pellet/Rad51 in the input).

ACKNOWLEDGMENTS

The work was supported by the Council of Scientific and Industrial Research (India), [37(1669)/16/EMR-II] to S.B. T.S. and W.T. were supported by senior research fellowships from the University Grants Commission, India, and N.F. was supported by a junior research fellowship from the Council for Scientific and Industrial Research (CSIR), India. P.M. was supported by an MSc thesis grant, Department of Biotechnology, India.

We declare no conflict of interest.



REFERENCES

- Polo SE, Jackson SP. 2011. Dynamics of DNA damage response proteins at DNA breaks: a focus on protein modifications. Genes Dev 25:409 – 433. https://doi.org/10.1101/gad.2021311.
- Tembe V, Henderson BR. 2007. Protein trafficking in response to DNA damage. Cell Signal 19:1113–1120. https://doi.org/10.1016/j.cellsig.2007 .03.001.
- Reynolds P, Botchway SW, Parker AW, O'Neill P. 2013. Spatiotemporal dynamics of DNA repair proteins following laser microbeam induced DNA damage—when is a DSB not a DSB? Mutat Res 756:14–20. https:// doi.org/10.1016/j.mrgentox.2013.05.006.
- Ciccia A, Elledge SJ. 2010. The DNA damage response: making it safe to play with knives. Mol Cell 40:179–204. https://doi.org/10.1016/j.molcel .2010.09.019.
- Xia B, Sheng Q, Nakanishi K, Ohashi A, Wu J, Christ N, Liu X, Jasin M, Couch FJ, Livingston DM. 2006. Control of BRCA2 cellular and clinical functions by a nuclear partner, PALB2. Mol Cell 22:719–729. https://doi .org/10.1016/j.molcel.2006.05.022.
- Sy SMH, Huen MSY, Chen J. 2009. PALB2 is an integral component of the BRCA complex required for homologous recombination repair. Proc Natl Acad Sci U S A 106:7155–7160. https://doi.org/10.1073/pnas .0811159106.
- Zhang F, Ma J, Wu J, Ye L, Cai H, Xia B, Yu X. 2009. PALB2 links BRCA1 and BRCA2 in the DNA-damage response. Curr Biol 19:524–529. https://doi. org/10.1016/j.cub.2009.02.018.
- Zhang F, Fan Q, Ren K, Andreassen PR. 2009. PALB2 functionally connects the breast cancer susceptibility proteins BRCA1 and BRCA2. Mol Cancer Res 7:1110–1118. https://doi.org/10.1158/1541-7786.MCR-09-0123.
- Jensen RB, Carreira A, Kowalczykowski SC. 2010. Purified human BRCA2 stimulates RAD51-mediated recombination. Nature 467:678–683. https://doi.org/10.1038/nature09399.
- Liu J, Doty T, Gibson B, Heyer WD. 2010. Human BRCA2 protein promotes RAD51 filament formation on RPA-covered single-stranded DNA. Nat Struct Mol Biol 17:1260–1262. https://doi.org/10.1038/nsmb.1904.
- Thorslund T, McIlwraith MJ, Compton SA, Lekomtsev S, Petronczki M, Griffith JD, West SC. 2010. The breast cancer tumor suppressor BRCA2 promotes the specific targeting of RAD51 to single-stranded DNA. Nat Struct Mol Biol 17:1263–1265. https://doi.org/10.1038/nsmb.1905.
- 12. Shinohara A, Ogawa T. 1998. Stimulation by Rad52 of yeast Rad51-mediated recombination. Nature 391:404–407. https://doi.org/10.1038/34943.
- Song B, Sung P. 2000. Functional interactions among yeast Rad51 recombinase, Rad52 mediator, and replication protein A in DNA strand exchange. J Biol Chem 275:15895–15904. https://doi.org/10.1074/jbc .M910244199.
- Suhane T, Laskar S, Advani S, Roy N, Varunan S, Bhattacharyya D, Bhattacharyya S, Bhattacharyya MK. 2015. Both charged linker region and ATPase domain of Hsp90 are essential for Rad51-dependent DNA repair. Eukaryot Cell 14:64–77. https://doi.org/10.1128/EC.00159-14.
- Pratt WB, Toft DO. 2003. Regulation of signaling protein function and trafficking by the hsp90/hsp70-based chaperone machinery 1. Exp Biol Med (Maywood) 228:111–133. https://doi.org/10.1177/153537020322800201.
- Cato L, Neeb A, Brown M, Cato AC. 2014. Control of steroid receptor dynamics and function by genomic actions of the cochaperones p23 and Bag-1L. Nucl Recept Signal 12:e005. https://doi.org/10.1621/nrs.12005.
- Jahn M, Rehn A, Pelz B, Hellenkamp B, Richter K, Rief M, Buchner J, Hugel T. 2014. The charged linker of the molecular chaperone Hsp90 modulates domain contacts and biological function. Proc Natl Acad Sci U S A 111:17881–17886. https://doi.org/10.1073/pnas.1414073111.
- Comeau SR, Gatchell DW, Vajda S, Camacho CJ. 2004. ClusPro: a fully automated algorithm for protein–protein docking. Nucleic Acids Res 32:W96–W99. https://doi.org/10.1093/nar/gkh354.
- Kozakov D, Brenke R, Comeau SR, Vajda S. 2006. PIPER: an FFT-based protein docking program with pairwise potentials. Proteins 65:392–406. https://doi.org/10.1002/prot.21117.
- Roy N, Bhattacharyya S, Chakrabarty S, Laskar S, Babu SM, Bhattacharyya MK. 2014. Dominant negative mutant of Plasmodium Rad51 causes reduced parasite burden in host by abrogating DNA double-strand break repair. Mol Microbiol 94:353–366. https://doi.org/10.1111/mmi.12762.
- Agmon N, Pur S, Liefshitz B, Kupiec M. 2009. Analysis of repair mechanism choice during homologous recombination. Nucleic Acids Res 37: 5081–5092. https://doi.org/10.1093/nar/gkp495.

- Khurana N, Laskar S, Bhattacharyya MK, Bhattacharyya S. 2016. Hsp90 induces increased genomic instability toward DNA-damaging agents by tuning down RAD53 transcription. Mol Biol Cell 27:2463–2478. https://doi.org/10.1091/mbc.E15-12-0867.
- 23. Tsuzuki T, Fujii Y, Sakumi K, Tominaga Y, Nakao K, Sekiguchi M, Matsushiro A, Yoshimura Y, Morita T. 1996. Targeted disruption of the Rad51 gene leads to lethality in embryonic mice. Proc Natl Acad Sci U S A 93:6236–6240. https://doi.org/10.1073/pnas.93.13.6236.
- Depienne C, Bouteiller D, Méneret A, Billot S, Groppa S, Klebe S, Charbonnier-Beaupel F, Corvol JC, Saraiva JP, Brueggemann N, Bhatia K, Cincotta M, Brochard V, Flamand-Roze C, Carpentier W, Meunier S, Marie Y, Gaussen M, Stevanin G, Wehrle R, Vidailhet M, Klein C, Dusart I, Brice A, Roze E. 2012. RAD51 haploinsufficiency causes congenital mirror movements in humans. Am J Hum Genet 90:301–307. https://doi.org/10.1016/j.ajhg.2011.12.002.
- Gallea C, Popa T, Hubsch C, Valabregue R, Brochard V, Kundu P, Schmitt B, Bardinet E, Bertasi E, Flamand-Roze C, Alexandre N, Delmaire C, Méneret A, Depienne C, Poupon C, Hertz-Pannier L, Cincotta M, Vidailhet M, Lehericy S, Meunier S, Roze E. 2013. RAD51 deficiency disrupts the corticospinal lateralization of motor control. Brain 136:3333–3346. https://doi.org/10.1093/ brain/awt258.
- Zhang XP, Lee KI, Solinger JA, Kiianitsa K, Heyer WD. 2005. Gly-103 in the N-terminal domain of Saccharomyces cerevisiae Rad51 protein is critical for DNA binding. J Biol Chem 280:26303–26311. https://doi.org/10.1074/ ibc.M503244200.
- Fortin GS, Symington LS. 2002. Mutations in yeast Rad51 that partially bypass the requirement for Rad55 and Rad57 in DNA repair by increasing the stability of Rad51-DNA complexes. EMBO J 21:3160–3170. https://doi.org/10.1093/emboj/cdf293.
- Paffett KS, Clikeman JA, Palmer S, Nickoloff JA. 2005. Overexpression of Rad51 inhibits double-strand break-induced homologous recombination but does not affect gene conversion tract lengths. DNA Repair (Amst) 4:687–698. https://doi.org/10.1016/j.dnarep.2005.03.003.
- Donovan JW, Milne GT, Weaver DT. 1994. Homotypic and heterotypic protein associations control Rad51 function in double-strand break repair. Genes Dev 8:2552–2562. https://doi.org/10.1101/gad.8.21.2552.
- Krejci L, Damborsky J, Thomsen B, Duno M, Bendixen C. 2001. Molecular dissection of interactions between Rad51 and members of the recombination-repair group. Mol Cell Biol 21:966–976. https://doi.org/ 10.1128/MCB.21.3.966-976.2001.
- Grbovic OM, Basso AD, Sawai A, Ye Q, Friedlander P, Solit D, Rosen N. 2006. V600E B-Raf requires the Hsp90 chaperone for stability and is degraded in response to Hsp90 inhibitors. Proc Natl Acad Sci U S A 103:57–62. https://doi.org/10.1073/pnas.0609973103.
- Shimamura T, Lowell AM, Engelman JA, Shapiro GI. 2005. Epidermal growth factor receptors harboring kinase domain mutations associate with the heat shock protein 90 chaperone and are destabilized following exposure to geldanamycins. Cancer Res 65:6401–6408. https://doi.org/ 10.1158/0008-5472.CAN-05-0933.
- 33. Karagöz GE, Rüdiger SG. 2015. Hsp90 interaction with clients. Trends Biochem Sci 40:117–125. https://doi.org/10.1016/j.tibs.2014.12.002.
- 34. Pennisi R, Ascenzi P, di Masi A. 2015. Hsp90: a new player in DNA repair? Biomolecules 5:2589–2618. https://doi.org/10.3390/biom5042589.
- Kekatpure VD, Dannenberg AJ, Subbaramaiah K. 2009. HDAC6 modulates Hsp90 chaperone activity and regulates activation of aryl hydrocarbon receptor signaling. J Biol Chem 284:7436–7445. https://doi.org/10.1074/jbc.M808999200.
- Kovacs JJ, Murphy PJ, Gaillard S, Zhao X, Wu JT, Nicchitta CV, Yoshida M, Toft DO, Pratt WB, Yao TP. 2005. HDAC6 regulates Hsp90 acetylation and chaperone-dependent activation of glucocorticoid receptor. Mol Cell 18:601–607. https://doi.org/10.1016/j.molcel.2005.04.021.
- Robbins N, Leach MD, Cowen LE. 2012. Lysine deacetylases Hda1 and Rpd3 regulate Hsp90 function thereby governing fungal drug resistance. Cell Rep 2:878–888. https://doi.org/10.1016/j.celrep.2012.08.035.
- Laskar S, Sheeba K, Bhattacharyya MK, Nair AS, Dhar P, Bhattacharyya S.
 2015. Heat stress-induced Cup9-dependent transcriptional regulation of SIR2. Mol Cell Biol 35:437–450. https://doi.org/10.1128/MCB.01046-14.
- Laskar S, Bhattacharyya MK, Shankar R, Bhattacharyya S. 2011. HSP90 controls SIR2 mediated gene silencing. PLoS One 6:e23406. https://doi.org/10.1371/journal.pone.0023406.

00	10	IN I	A 1	ITV	DE	00	TO
UK	100	IINI	AΙ	HY	RE	P(0)	1141

16%

10%

15%

4%

SIMILARITY INDEX

INTERNET SOURCES

PUBLICATIONS

STUDENT PAPERS

PRIMARY SOURCES



Tanvi Suhane, Vijayalakshmi Bindumadhavan, Nupur Fangaria, Achuthsankar S. Nair et al. " Glu-108 in Rad51 Is Critical for DNA Damage-Induced Nuclear Function", mSphere, 2019

5%

/2

Submitted to University of Hyderabad, Hyderabad 3%

Student Paper

3

www.ncbi.nlm.nih.gov
Internet Source

1%

4

Tanvi Suhane, Shyamasree Laskar, Siddheshwari Advani, Nabamita Roy et al. "Both the Charged Linker Region and ATPase Domain of Hsp90 Are Essential for Rad51-Dependent DNA Repair", Eukaryotic Cell, 2015

<1%

5

ec.asm.org

Internet Source

<1%

6

www.unmc.edu

Internet Source

<1%

This is to certify that #1 belongs to her publication and #2 belongs to the 'Material & Method', hence (5+3%) 8% should be deducted from the total score. Hence, the resulting similarity index would be (16-8)% i.e. 8% only. SUNANDA BHATTACHARYYAY Associate Professor

Associate Professor
Dept. of Biotechnology & Bioinformatics
School of Life Sciences